DEVELOPMENT OF TWIN SCREW RHEO EXTRUSION TECHNOLOGY

Thesis submitted to Brunel University for the Degree of
DOCTOR OF PHILOSOPHY

Zen Cassinath

Brunel Centre for Advanced Solidification Technology (BCAST)
School of Engineering and Design
Brunel University
Uxbridge
UB8 3PH
United Kingdom

MARCH 2013

‘The Right to search for truth also implies a duty; one must not conceal any part of what one has recognised to be true’

Albert Einstein 1879-1955

ABSTRACT

Twin Screw Rheo Extrusion (TSRE) is a novel semisolid extrusion process developed at BCAST for producing simple profiles such as rods and wires of light alloys directly from melts with refined microstructures and improved mechanical properties. The process represents a shortened manufacturing route with great savings in investment, energy consumption and operation space. Research was carried out to investigate the feasibility of processing magnesium and aluminum alloys, to obtain the operations for the optimized microstructures and mechanical properties of the final product and to understand the mechanisms governing the evolution of microstructures.

Experiments were conducted using an AZ91D magnesium alloy and several aluminium alloys on two specially made twin screw rheo extrusion machines and a range of conditions were tested. Results showed that the TSRE process was feasible for the AZ91D magnesium alloy and aluminium alloys, although modifications were required for processing aluminium alloys as the twin screw material used was found to react with aluminium. Analysis revealed that the extruded samples of both alloys had a uniform fine microstructure in both transversel and longitudinal directions and liquid segregation was limited, due to the application of intensive shearing during slurry making and extrusion. Low extrusion temperature was found to refine the structure and suppress the formation of the eutectic. The eutectic was easily dissolved upon heat treatment resulting in reasonable mechanical properties. Numerical analysis on thermal management was carried out and the results showed that a steady state thermal profile with a temperature gradient between the slurry feeding point and extrusion die could be established, promoting nucleation and preventing the formed solid particles from extensive growth during extrusion, which was confirmed by microstructural observations.

LIST OF FIGURES & TABLES

LIST OF SYMBOLS

A	the equivalent gap area of the twin screws cross section
A_1	Cross-sectional area of the single thread screw A
A_2	Cross-sectional area of the double threads screw B
As	S-shaped bore volume of the screw casing
α	Overlap angle
B	Axial channel width
C	Contiguity factor
C_p	Specific heat of slurry
D	particle size
D_s	Equivalent diameter of the cylindrical container
d	Nucleating particle size
δ	Flight gap
F	Shape factor
f_s	Solid fraction
f_s^{ch}	the dendrite coherency solid fraction
f_L	Volume fraction of liquid phase
g	Acceleration due to gravity
H	Height of flight
h	Distance between the centreline of the calendar gap to the surfaces of the screws
H_s	Latent heat of the slurry
H_C	height of the slurry container
h_b	Thermal conductivity of the barrel
k	Partition coefficient of the alloy
K_1	Consistency parameter
K_p	Permeability factor
K_v	Kinematic coefficient
K_2	Constant of proportionality in Hallpetch equation
K_3	Constant model parameter
K_4	Constant model parameter
l	Length of the barrel
L_e	Barrel length at which the slurry temperature is equal to the preset extrusion temperature
m	Number of thread starts
μ	Viscosity of liquid phase
N	Screw speed
n	Power law index
$N_{\alpha\alpha}$	Number of intersections per unit length

$N_{\alpha\beta}$	Number of intersections per unit length of the test lines between the primary α phase and the secondarily solidified phases.
N_D	Grain Density
η	Viscosity
σ	Calendar gap width
σ_s	yield strength
σ_0	yield strength of a single crystal
ϕ	Diameter of the extruded rod
P_p	Perimeter of the particles respectively
ρ	Density of the slurry
p	Pressure rise
ρ_L	Density of liquid phase
∇p_L	Pressure gradient applied in a porous solid phase
Q	Volumetric flowrate
Q_{th}	Theoretical output
$\dot{Q}_s$	Slurry heat loss rate during transport
$\dot{Q}_B$	Heat loss rate thorough the barrel wall
Q_{leak}	Backward leakage flow
Q_c	Calendar gap leak
Q_f	Flight gap leak
Q_t	Tetrahedron gap leak
Q_s	Side gap leak
R	Outer diameter of screws
r_o	Outer radius of the barrel
r_i	Inner radius of the barrel
r_s	Equivalent radius of the twin screw
S	Pitch of screw
S_p	Area of the particles respectively
ΔS_V	Entropy of the fusion per unit volume
t_s	Time needed for obtaining the required solid fraction
t_T	time for this convection of material
τ	Shear stress
T_e	Nominal extrusion temperature
T_{PE}	Predicted extrusion temperature
ΔT_{fr}	Freezing range of the alloy
ΔT_{fg}	Free growth undercooling
T_f	Feeding temperature
T_L	Liquidus of the alloy
T_s	Temperature of slurry
T_S	Solidus of the alloy
ΔT	Slurry temperature change
U	Free stream velocity
V	Extrusion speed

V_s	Slurry making rate
V_{1c}	Container velocity
V_c	Total C-chamber volume
V_p	Punch velocity
v	Volumetric displacement by a single revolution of screw B
v_L	Velocity of liquid phase
$\dot{\gamma}$	Shear rate
$\dot{\gamma}_{ch}$	Shear rate in channel
$\dot{\gamma}_0$	Reference shear rate
V_C	Container velocity
w	Wall velocity
y	Boundary layer thickness
Ψ	Flight wall angle

LIST OF PUBLICATIONS

1. Continuous Twin Screw Rheo-Extrusion of an AZ91D Magnesium Alloy- M. Xia, Y. Huang, Z. Cassinath, and Z. Fan. MMTA Volume 43 (2012), Issue 11, pp 4331-4344

2. Rheo-extrusion of AZ91D- M. Xia , Y. Huang, Z. Cassinath and Z. Fan. Solid State Phenomena Vols. 192-193 (2013) pp 470-475

3. Process optimization and microstructure control for twin screw rheo-extrusion of an AZ91D magnesium alloy- Z. Cassinath, M. Xia, Y. Huang, Z. Fan *[Submitted]*

4. Processing of AZ91D Magnesium alloy by Semisolid Rheo Extrusion- Z. Cassinath, M. Xia, Y. Huang, Z. Fan *[Submitted]*

5. Microstructural evolution during Twin screw rheo extrusion in an AZ91D Magnesium alloy Z. Cassinath, M. Xia, Y. Huang, Z. Fan *[Submitted]*

6. Rheo extrusion of Aluminium- Silicon Alloys Z. Cassinath, M. Xia, Y. Huang, Z. Fan *[In preparation]*

7. Eutectic and Intermetallic structures observed in Rheo extruded AZ91D magnesium alloy Z. Cassinath, M. Xia, Y. Huang, Z. Fan *[In preparation]*

CONTENTS

CHAPTER 1

INTRODUCTION

1.1 Light metals today

There are innumerable applications for the use of metals in the transportation industry today and vast quantities of metals are employed in the construction of land, air and sea vehicles. The maximum payload of these vehicles is directly linked to their practicality and a vehicle with less deadweight will be able to carry more freight and be more manoeuvrable. This is exemplified while considering aircraft, when across a standard estimated eight-year depreciation life; the value of a pound saved in weight can exceed £1000.

Structures of vehicles though must be mechanically sound to bear the loads involved so they must have sufficient strength as well as lightness. This leads to the engineering criterion of the strength/weight ratio criterion. The strength to weight ratio suggests that a material of lower strength than another will be more functional if it is much lighter. Therefore it can be shown that weaker and lighter metals, for instance aluminium and magnesium, can compete with stronger heavier steels.

A) Magnesium

Magnesium is the lightest of all structural metals and thence is a relatively straight forward choice for aircraft and other transport concerns. Historically, it owes its rapid increased use in the aviation industry during World War II. Pure magnesium is available at purities of over 99.8% but has little engineering value due to its softness, low corrosion and oxidation resistance, difficulties in cold working, and high cost with respect to other light metals such as aluminium [Polmear, 2006; Greenfield, 1972]. Therefore its use is restricted by its chemical affinity in such devices as flashlights, pyrotechnics and getters in vacuum-tube manufacturing. In spite of this affinity to oxidise, bulk magnesium does not readily ignite below its melting point in the presence of oxygen and it is easy to overcome the fire hazard during melting and machining. Magnesium is the least noble of all structural metals therefore corrosion tends to occur at a higher rate. However, one notable advantage that magnesium alloys display over aluminium alloys are their resistance to corrosion in alkaline conditions since aluminium generally reacts to form aluminates.

Magnesium alloys exhibit high-fatigue properties and a low-elastic modulus, and are therefore chosen to be used in applications that experience vibrational- and shock-loading preferentially over aluminium and steels. The addition of small amounts of alloying elements can improve the properties of magnesium notably and alloys are used to an increased extent in applications previously only known to aluminium and its alloys. Magnesium is commonly alloyed with manganese, aluminium, zinc, rare earth metals, silver and thorium.

Generally, structural magnesium alloys contain up to 10% aluminium as a hardening element. Aluminium is chosen to improve the resistance of the alloy to atmospheric oxidation so as to have the least effect on the overall specific gravity of the alloy. Certain

amounts of zinc are also added to magnesium alloys to form a hardening constituent based around $Mg_3Al_2Zn_3$. These alloys however generally require the addition of manganese to improve the anti-corrosion properties.

B) Aluminium

Aluminium and its alloys have been used extensively by the aircraft and automotive industry since early days due to their low density, high strength (high strength/weight ratio) and durability. Several household uses for this versatile metal were quickly found at the end of World War II when there was a sudden surplus of the metal along with other materials leading to the birth of the global aluminium industry.

The cheapest grade of the material available is the commercial grade aluminium and contains no less than 99% aluminium along with the usual contaminants such as iron, silicon, copper, manganese and zinc. Iron and silicon form a ternary compound with aluminium which is microscopically visible. The metal has a high electrical and thermal conductivity and reflectivity and corrosion resistance. Being a light and malleable metal with a modest melting point of 660ºC suggests that it can undergo fabrication by forging, rolling and extrusion easily.

These properties provide insight into the various applications of the metal. For instance anti-corrosion properties, thermal conductivity and reflectivity contribute to the increase of aluminium usage in kitchenware.

The reflectivity of aluminium is to the tune of approximately 90% for visible radiation and this makes it a very practical choice for use in reflectors of vehicle head lamps. The former accounts for the growing use of aluminium alloys for heat transfer applications such as

cylinder heads and pistons of internal combustion engines. However, the use of the material in the automotive industry is not restricted to engine parts. Owing to the high strength to weight ratio, the average quantity of aluminium used in manufacturing the average car is consistently rising since the initial cost of a vehicle is less important than the ratio of payload/deadload.

In lieu to relative easy fabrication, this grade of aluminium has historically also been used for architectural purposes due to its corrosion resistance properties. Since the commercial grade can be cold reduced 80-90% without inter-annealing, it is used in various tempers in which strength is induced by cold rolling. The most common application of this is foil which is used progressively more in the ever expanding packaging industry.

1.2 Background to semisolid technologies to produce rods

Since its inception in the 1970s[Spencer, et al; 1972] the use of semisolid processing techniques have been greatly increased and used worldwide for metal forming procedures [Fan, 2002; Fan, 2005; Luo et al., 2010]. Semisolid metal (SSM) forming is conducted at temperatures higher than the solidus but lower than the liquidus of the material and its advantages over solid state forming are many. These include reduced forming force, unlimited formability and shortened manufacturing route. Compared to conventional die casting, semisolid technology has advantages of laminar flow during mould filling, reduced solidification shrinkage and lower operating costs [Fan, 2002; Flemings, 1991] . SSM processing offers a noted step change in technique with opportunities to reduce cost energy and resource more than any other novel forming process.

Hot extrusion conventionally achieves a cross-section reduction to form specific profiles by forcing work pieces through a profiled opening or a die. However alloy deformability depends on process temperature [Frost and Ashby, 1983] and material crystal structure [Taylor, 1938]. For instance magnesium being a metal with a low deformability relies on the activation of more slip systems at higher temperatures [Flynn et al., 1961; Obara et al., 1973; Yoo et al., 2001], a finer initial grain size for the extension of non-basal slips [Agnews and Duygulu, 2005; Koike et al., 2003] or grain boundary sliding [Agnews et al., 2003; Koike, 2005] to coordinate along unfavourable orientations or microstructural inhomogenities and surface cracking can be seen to occur in the processing of such hard to deform materials [Cetlin et al.2010].

High processing temperatures causes oxidation and softening of the tooling. Grain refinement on the other hand can be achieved by two main methodologies. The first is severe plastic deformation (SPD) which again is a process dependent on deformability. The second method, chemical addition is limited by the chemical composition of the alloy and makes recycling at a later stage unpractical owing to chemical pollution of the alloy.

The conventional extrusion generally includes the preparation of rods or billets from ingots, homogenisation, preheating and extrusion and is therefore considered to be a complex and prolix process. It relies on high extrusion forces that increase the wear of the equipment.

As an alternative to conventional hot extrusion, since the start of semisolid metal processing [Flemings et al., 1976], semisolid methods [Czerwinski, 2004; Lee et al., 2005; Kim et al., 2007; Pinsky et al., 1984] have been introduced to reduce the microstructural inhomogenities and surface cracking. The majority of these are via the high solid fraction thixo route which is a re-melting slurry making technology [Kopp et al., 1998].

The extrusion pressure and the microstructure of the product will be affected by the morphology and solid fraction of such a slurry [Pinsky et al., 1984] and the slurry making relies on the microstructure of the as-cast billets and re-melting condition. Therefore even though such a process can reduce the extrusion force by increasing the extrusion temperature, the slurry making efficiency [Kopp et al., 1999] and the segregation of phases during extrusion [Pinsky et al., 1984] still hinder the application of semisolid extrusion via the thixo route.

There are several rheo semisolid forming technologies such as gas-induced semisolid rheoextrusion, cooling tube feeding semisolid rheoextrusion, single-screw rheomoulding and twin-screw rheomoulding but since these processes are of a batch nature they have a limited commercial potential.

Continous casting methods such as direct chil casting and direct chill rheocasting have also been used to produce continous profiles fom melts. However it is difficult to cary out such processes at competitive speeds for profiles of suitable dimensions of feedstock for further processing such as rolling and drawing. This limits the applicability of the technology to specific alloys. A continuous casting process based on Conform technology [Guan et al., 2006] is available in industry and has shown some potential to produce continous profiles with desirable properties. However, in the process, solidification takes place before the extrusion which is driven by the friction between the workpiece and the tool and takes place in the solid state. As a result of this the machinery is heavy and complex with high tooling costs and can only process limited alloys based on deformability. Therefore it neither utilises the microstructural or rheological features of semisolid materials to its advantage.

1.3 Objective of the study

Twin-screw rheoextrusion (TSRE) is a novel extrusion process developed at BCAST [Fan and Ji, 2000] and marks a significant progress made in the methods of semi-solid processing and final net shaping to produce continuous extruded bars/rods with a highly refined microstructure. It was developed for the production of high quality and low cost Aluminium and Magnesium wrought products as an alternate process for conventional solid state extrusion by reducing cost and saving energy consumption by combining slurry making and extrusion into one step. The process innovatively adapts the well-established high shear dispersive mixing action of the intermeshing counter-rotating twin-screw extruder to the task of creation of semi-solid metal slurry with fine and spherical solid particles. This is followed by transport and extrusion through a die. It overcomes the disadvantage of severe deformation and internal stresses by conditioning the semisolid metal prior to extrusion in near net shape rod, tube or other complex extruded profiles of high quality.

This technology is loosely based on a counter-rotating twin-screw extruder as used in the polymer industry. The rheoextruder consists of a rotor stator slurry maker, a feeding propeller, two intermeshing counter-rotating screws in a heated barrel that deliver shear to the melt, and a die assembly equipped with a cooling ring. Due to the nature of the flow within the barrel a differential pressure is built up which causes the melt to be pumped out of the barrel and through an extrusion die where it solidifies. During the process,the alloy achieves its designated solid fraction once it is fed into the slurry maker. It is transformed into high quality semisolid slurry and then transferred through the funnel and fed continuously into the extruder which ejects it from the shaped die. By attaching different extrusion dies the rheoextruder can produce rods, tubes and extruded profiles.

The theoretical basis for the development of the microstructure is solidification under forced convection as opposed to conventional casting solidification where nucleation takes place in cooled liquid close to the mould wall. These nuclei have a low survival rate and contribute very little to the final microstructure since they get transferred into the overheated liquid region and get re-melted which leads to a coarse and uneven microstructure. Due to the intensive shearing and mixing actions of the extruder the twin-screw mechanism ensures that the solidifying liquid has a uniform temperature and chemical composition and disperses the emerging nuclei throughout the entire volume of the melt [Fan, 2005; Fan et al., 2005]. Under these conditions nuclei will survive and grow into spherical particles, creating a fine and uniform microstructure [Das et al., 2002, Ji and Fan, 2002].

Its main technical edge is due to the following.

1. First, due to the slurry making by the novel online rotor stator device the process becomes more compact and efficient as the essential high shear conditions for continuous semisolid processing can be achieved.
2. Second, due to the use of the twin-screw mechanism a continuous process can be realised. Furthermore the highly turbulent nature of the flow provided during transport by the screws allows for the forced convection by intensive shearing thereby eliminating the possible dendritic growth. This type of flow is responsible for creating a uniform temperature field and melt chemistry offering an additional measure in microstructural control by controlling the convection intensity and mechanical impact on the slurry.
3. Thirdly thermal scheme allows for the melt to be cooled in the chamber of the extruder which allows for the use of slurry with a higher fluidity and reduces

the preparation time. It also allows for reduced energy consumptions for the extrusion process itself.

The specific aim of the study was

1. To define various process parameters and explore the effect of these process parameters on the microstructure of resultant extrusions.
2. To further develop a new technology to allow continuous rheoextrusion based around a counter-rotating twin-screw extruder design and potentially create a replacement for conventional hot extrusion process.
3. To produce bars of magnesium and aluminium alloys of high quality and refined microstructures.
4. To understand the underlying scientific principles of microstructural refinement offered by the process and to optimise these to help refine the process further.
5. To Evaluate the mechanical properties and heat treatability of the resultant bars.

CHAPTER 2

LITERATURE REVIEW

2.1 Semisolid processing and forming

Semisolid metal processing is an emerging technology for near net-shape production of engineering components, by which alloys are processed as slurries at temperatures above their solidus but below their liquidus. Products of this technology are characterised by non-dendritic microstructure. The main advantages over conventional casting methods include lower operating temperatures, laminar flow while mould filling and reduced solidification shrinkage [Fan, 2002].

2.1.1 Semisolid phenomenon

Spencer's original experiment at MIT that led to the discovery of this processing technology was conducted in 1971. In the experiment he evaluated the viscosity of the partially solidified alloy using a Couette viscometer. In the experiment the dendritic structure of solidifying melt was sheared. He discovered that when the dendritic structure was broken, a partially solidified alloy displays the fluidity of machine oil [Fan, 2002; Spencer et al., 1972]. The measured shear stress at any given temperature was found to be magnitudes lower than that for samples cooled to the same temperature without shear. The material also behaved like a slurry to which a low apparent viscosity could be assigned [Flemings,

1991; Spencer et al., 1972]. Furthermore the achieved grain structure was non-dendritic. Since then a large number of experiments have been carried out relating to the vigorous agitation of semi-solid alloys and confirmed such findings. The new understanding that SSM processing brought about was the ability to control the solidification process which till then had been treated as a natural process. SSM processing allowed scientists to explore new routes to achieve desired microstructures [Fan, 2002; Flemings, 1991].

2.1.2 Rheological behaviour of semisolid slurries

One of the primary advantages of the semisolid phenomenon is the ability to control the viscosity of the slurry and this has several useful applications in various rheo forming methods such as rheocasting [Flemings et al., 1976; Haga and Kapranos, 2002].

The viscosity of a metal alloy in the semisolid state is found to bear a close relationship to the shear rate and cooling rate. These effects are understood in terms of structural evolution since both these actions result in denser, more rounded particles that can move with relatively low hindrance past each other [Spencer et al., 1972; Joly and Meherbian, 1976]. However this does not explain the noticed build-up of structures due to collision and coalescence of particles that are favourably oriented [Fan, 2002], and it is noted that the viscosity of the alloy is dependent on the balance between the continuous build-up and break down of these structures.

In his work Spencer [1976] showed that an agitated SSM Sn-Pb slurry with a solid fraction higher than 0.2 exhibited the properties of a non-Newtonian fluid and displayed values of apparent viscosity that were significantly lower than unstirred dendritic slurry. Later Joly

and Meherabian [1976] demonstrated the rheological phenomena and categorised the different types of behaviour exhibited by semisolid slurries. These are:

1) Behaviour under continuous cooling

When viscosity is observed at a fixed cooling and shear rate it is seen that the apparent viscosity increases with increasing solid fraction: Slowly at low solid fractions and sharply at high solid fractions. In addition, at a fixed solid fraction the apparent viscosity is seen to decrease with increasing the shear rate and lowering the cooling rate as seen in Figure 2.1. This is since both these actions will promote the destruction of dendritic morphology and promote globular morphology.

.

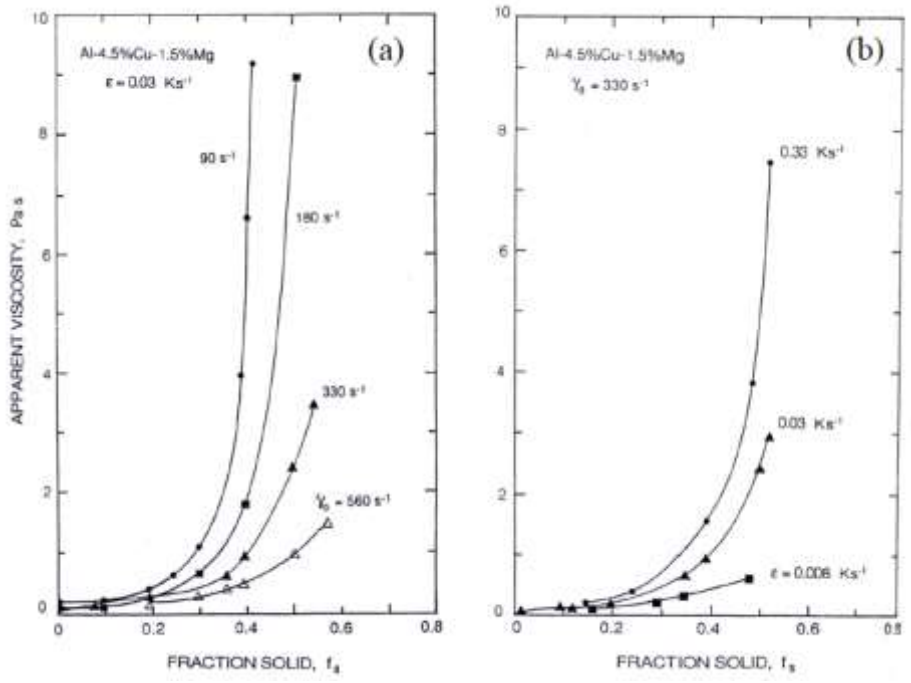

Figure 2.1: (a) and (b) show the effect of shear rate and cooling rate on the apparent viscosity of Al-4.5%Cu-1.5%Mn. *[Flemings, 1991]*

2) Pseudoplastic behaviour

Joly and Mehrebian [1976], saw that if the shear rate was increased then the apparent steady state viscosity would drop to a seemingly asymptotic value. As the shear rate approached infinity the alloy displayed shear thinning or pseudoplastic behaviour. This pseudoplastic behaviour has been confirmed by many other experiments [Leuhy et al., 1985; Kattamis and Piccone, 1991; Taha et al., 1988]. It is noticed that steady state viscosity at a set shear rate is dependent on the agglomeration between solid particles. These arise as a product of the dynamic equilibrium between the formation and the destruction of such agglomerates [Fan, 2002]. Viscosity is measured to be high at lower shear rates. This is partly due to the dendritic form of the grains due to agglomeration [Flemings, 1991]. At higher shear rates the agglomeration decreases and the grains are seen to display a more rosette morphology.

A widely used relation to describe the viscosity of pseudoplastic materials over a range of shear rates is the power law model:

$$\eta = K_1 \dot{\gamma}^{n-1} \tag{2.1}$$

Where η is the viscosity, $\dot{\gamma}$ is the shear rate, n is the power law index and K_1 is the consistency parameter. The smaller the power law index the greater the pseudoplasticity.

3) Thixotropic Behaviour

The time dependency of the steady state viscosity of slurry is defined as its thixotropy. It is observed that if the shear rate changes a new steady state viscosity is attained only after some time. The value of instantaneous viscosity is normally lower than the steady state viscosity. As the forming structure adjusts to the new shear rate over time agglomerates build up and the viscosity approaches the steady state value. The difference between the

curves of instantaneous viscosity and steady state viscosity is a measure of thixotropy of the slurry. Joly and Meherbian [1976] and others [Martin et al., 1994] demonstrated the thixotropic behaviour of slurries by measurement of hysteresis loops during a cyclic shear deformation. It is seen that instantaneous viscosity is much higher at the start of shear. This indicates that there is a build-up of a structure during the rest period. The time required to form this structure is noted to be larger than the time required to break it down. To quantify the kinetics of agglomerates forming and deforming, experimental procedures involving sharp changes to shear rate have been devised to study the structural evolution [Turng and Wang, 1991; Mada and Ajersch, 1996; Taha et al., 1988]. It is noted that a jump in shear rate facilitates the deforming of agglomerates while a drop in shear rate facilitates its forming [Mada and Ajersch, 1996; Modigell and Koke, 1999; Taha et al., 1988].

2.1.3 Deformation behaviour of semisolid slurries

Semisolid slurries with a high solid fraction are observed to have a solid skeleton formed by either partial solidification or partial re-melting. At a critical value of solid fraction defined as the dendrite coherency solid fraction is when the crystals are seen to invade each other's space. This results in a sudden rise in the materials flow resistance [Gourlay and Dahle, 2007]. It has been noted that the dendrite coherency solid fraction is dependent on the size and shape of crystals [Sumitomo et al., 2000; Arnberg et al., 1993; Veldman et al., 2001].
It is noticed that the solid phase responds to the applied hydrostatic pressure macroscopically by particle distribution densification or by deformation at the contacts of solid particles. [Kiuchi and Kopp 2002] Macroscopic deformation consists of microscopic deformation and rotation of individual particles and relative slip among them as seen in Figure 2.2.

In the solid state, mechanical restraints at grain boundaries restrict deformation of particles by interacting with each other and they cannot rotate, deform and move freely. However in semisolid materials these restraints are released as liquid phase is generally found at these grain boundaries. Therefore the rotation and relative slip of grains can occur and the semisolid metal can deform under small external forces. [Kiuchi and Kopp 2002]

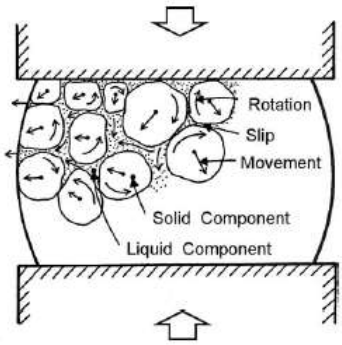

Figure 2.2: Rotation, slipping and movement of solid grains in semisolid metal *[Kiuchi and Kopp 2002]*

Experimental findings of applying various strains to semisolid Sn-15 wt. % Pb structures [Laxmanan and Flemings, 1980; Spencer et al., 1972] have led to the identification of the following deformation characteristics with respect to morphology. In the dendritic material the maximum stress at f_s =0.4 is around 200 kPa, whereas the non-dendritic material displays a lower value at the same solid fraction [Flemings, 1991; Spencer et al., 1972]. This is due to easier deformation due to cooperative grain rearrangement in equiaxed microstructures via sliding and rolling as opposed to dendritic structures where dendritic arms can impede each other's movements [Tzimas and Zavaliangos, 1999].

At higher strain rates liquid phase segregation is found due to pressure built up in the liquid phase by the reduction of interstitial volume.

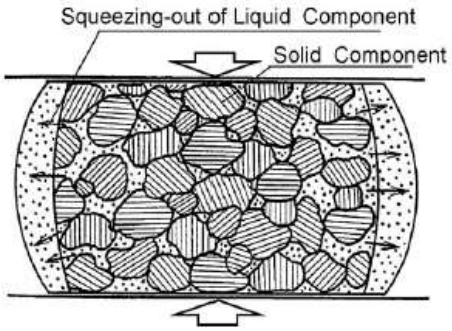

Figure 2.3: Flow of liquid metal in semisolid metal *[Kiuchi and Kopp2002]*

As the semisolid material deforms the liquid phase is seen to flow out through gaps between the solid structures and separates from the solid skeleton as seen in Figure 2.3 and as the fraction of solid decreases this is seen to occur more readily. [Kiuchi and Kopp 2002] Darcy's law that relates the volumetric flow rate of the liquid in a porous solid phase to the pressure gradient applied (∇p_L) on the system is generally used, as follows:

$$f_L v_L = -\frac{K_p}{\mu}(\nabla p_L - \rho_L g) \tag{2.2}$$

where K_p is the permeability factor, g, $v_{L,}$ μ, $f_{L,}$ and ρ_L are the nucleation due to gravity, velocity of the liquid relative to the solid, viscosity of the liquid, volume fraction and the density of the liquid phase respectively [Tzimas and Zavaliangos, 1999]. The permeability is related to the structure of the solid phase and can be described by the modified Carman-Kozeny model, [Bear, 1972].

$$K_p = \frac{D^2 f_L^3}{180(1 - f_L^2)} \tag{2.3}$$

Where, *D* is the average grain size.

It has been found that a high strain rate of deformation, a low dendrite coherency solid fraction and a fine grain size can reduce the quantity of separation of solid-liquid phases during deformation of semisolid materials [Valer et al., 1998; Finke et al., 2000; Chen and Tsao, 1999].

2.1.4 Formation of non-dendritic structures under forced convection

It is observed that under convection and low undercooling in the solidification process a high number of grains occur [Porter and Easterling, 1992]. Literature also shows evidence that such conditions promote the formation of spheroidal particles in agitated slurries. This was also documented by Spencer [1972] who noted when shear was applied to a partially solidified melt dendritic grains broke into smaller spheroidal morphology.

Theories proposed to explain the microstructural evolution in semisolid slurries under shear are discussed below [Fan, 2002; Flemings, 1991].

A) Dendritic breakup and re-melting

It has been suggested by Vogel et al. [1979] that shear forces act upon dendrite arms when stirring is introduced causing them to bend plastically. This strain is accompanied by the production of dislocations. These dislocations can propagate and join to form grain boundaries. At a specific point if the misorientation across a boundary exceeds 20 degrees the grain boundary energy exceeds the solid liquid interface energy causing liquid to seep into the newly formed grain boundary. The grain boundary is then penetrated by wetting causing the arm to separate from the rest of the crystal. This is seen in Figure 2.4

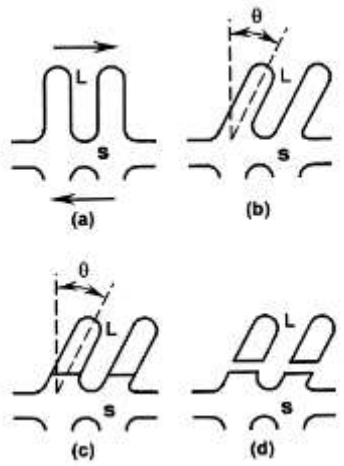

Figure 2.4: Schematic illustration of the dendritic arm fragmentation mechanism (a) un-deformed (b) after bending (c) reorganising or lattice to give grain boundaries(d) $\gamma_{gb}>\gamma_{s/l}$ when grain boundaries have been wetted *[Doherty et al., 1984]*

Initially fragmented arms are not equiaxed and can continue dendritic growth. However due to coarsening or ripening the surface area is reduced and the regions of high curvature are reduced the liquid phase diffusing the solute. This process is directly influenced by the level of the convection of the fluid flow relative to the solid due to enhanced solute transport. This means that continuous shearing will result in evolution of dendritic morphology into rosettes with entrapped liquid and eventually a spheroidal morphology [Fan, 2002].

Hellawell [1996] suggests that the thermal fluctuations caused by stirring of the melt can also be the cause for the induced grain refinement. In such cases thermo solutal convection and solute enrichment will cause the detachment of the secondary dendrite arms to break off from their roots. Here it could be said that re-melting is

- Enhanced by resulting thermal perturbation from turbulent convection.
- Accentuated at the root of the arm due to force from fluid flow at the top.
- Enhanced by high volume of solute in the solid at the dendrite root.

B) Effect of Turbulent Flow and enhanced heterogeneous nucleation by oxide dispersion

The effect of intense turbulent flow on the solidification morphology of Sn-15Pb alloy was studied by Ji and Fan [2001] with the use of a MCAST machine which uses co-rotating twin screws to deliver high levels of shear. They found that under the influence of turbulence the obtained structure was spherical in the initial stages of solidification. Shearing at isothermal conditions revealed that the size shape factor density remained nearly constant with the increase of shearing time and the particle size distribution was found to be similar to that of randomly dispersed mono spheres [Ji et al., 2001]

This theory suggests that at an intermediate shear rate the flow is still essentially laminar up to 1000 s^{-1}. At such levels the fluid is unlikely to interact with secondary dendrite arms to deliver adequate bending forces and these are not expected to experience any fluid motion at the solid liquid interface [Fan, 2002; Ji and Fan, 2002]. However the intensity of the laminar flow can determine the thickness of the diffusion boundary layer around a growing particle and still influence its growth morphology [Fan, 2002; Ji and Fan, 2002]

It has been reported that spheroidisation can usually take up to a few hours in the absence of forced convection whereas it may take a few minutes under laminar flow. Ji and Fan [2002] were able to demonstrate that this process can be accelerated under intensive flow conditions to a few seconds even if the initial structure is fully dendritic.

A systematic study to investigate the growth morphology under various fluid flow conditions using different stirring devices was conducted by Das and Fan [2003]. The findings of such investigations [Ji, 2001; Ji and Fan, 2002; Das and Fan, 2003] were that high levels of turbulence are required to form spherical particles for solidification under forced

convection and rosette and spherical morphologies are growth phenomena under these conditions. A schematic of the morphological transition is seen in Figure 2.5.

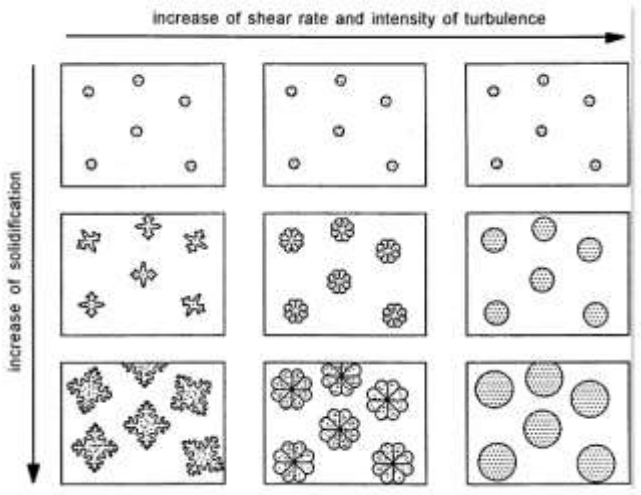

Figure 2.5: Schematic illustration of morphological transition from dendritic to spherical via rosette with increase in shear rate and intensity of turbulence *[Fan, 2002]*

Furthermore by intensive shearing of AZ91 through the MCAST process, it is documented that at the microscopic level oxide films were effectively dispersed into individual particles of 100-200nm in diameter. It was observed that these particles can act as potent sites for nucleation of both primary phase and intermetallics resulting in significant grain refinement. This has been termed as is termed the enhanced heterogeneous nucleation mechanism [Fan et al., 2009a; 2009b; Qian, 2007].

2.1.5 Application of semisolid technology to forming processes

The defining characteristic of products formed by semisolid technologies are their near spherical and non-dendritic grain structure. Compared to conventional casting processes

the key advantages of using a SSM processing technology are lower operating temperatures, laminar flow while mould filling and reduced solidification shrinkage. In addition to this, it also enhances the die life, reduces gas entrapment porosity and tendency towards hot tearing [Fan, 2002]

When Flemings realised that a slurry's viscosity could be controlled [Spencer et al., 1972] the importance of this was almost immediately realised and within a year, industrial trials demonstrating rheoforming and thixoforming had been performed [Fan, 2002].

Thixoforming is used to define the near net shaping of a partially melted non-dendritic alloy within a die. It is referred to as thixocasting if a closed die is used and thixoforging if an open die is used. During slug reheating for thixo forming processes a non-dendritic structure is achieved by isothermal holding of the billet. The driving force for the structural transformation is reduction of the interfacial energy between the solid and liquid phase and refinement occurs through diffusion. The holding time should be long enough to complete the transformation of the morphology but at the same time it should not facilitate excessive grain growth, which in turn is detrimental to mechanical properties.

Rheoforming technologies involve the production of partially solidified non-dendritic slurry that can be transferred immediately to a mould or die for the final shaping process. The slurry can be produced and shaped at relatively low forces due to its pseudoplastic properties. Furthermore as opposed to solid state forming or casting from a liquid state, if intense turbulent mixing is used in a rheoforming process then it can lead to breakdown of dendritic structures and promote the growth of near-spherical particles via rosette morphology. This can effectively control the enhancement of the microstructural and mechanical properties of cast components. The thixotropic property also suggests that the non-dendritic slurry can be produced and held for a period of time without the significant

formation of agglomerates which is useful if the slurry is to be fed into a reservoir for continuous feeding purposes. Available methods to produce slurries include MCAST, cooling plate, Gas induced semisolid, and cooling tube.

2.2 Extrusion Technology to produce bars

Alloy deformability depends on process temperature [Frost and Ashby, 1983] and material crystal structure [Taylor, 1938]. For instance, magnesium being a metal with a low deformability relies on the formation of more slip systems at higher temperatures [Obara et al., 1973; Flynn et al., 1961; Yoo et al., 2001], a finer initial grain size for the extension of non-basal slips [Koike et al., 2003; Agnews and Duygulu, 2005] or grain boundary sliding [Agnews et al., 2003; Koike, 2005] to coordinate along unfavourable orientations or microstructural inhomogenities and surface cracking can be seen to occur in the processing of such hard to deform materials. Extrusion achieves a cross section reduction to form specific profiles by forcing work pieces through a profiled opening or a die and there are technologies several methods incorporated to produce bars.

2.2.1 Solid state methods to produce bars

Extrusion techniques are broadly classified based on process characteristics [Scherba, 1999] and analysis of distinguishing features of the interaction of the billet and elements of the tool. This is in stark contrast to the older classification methods which were based on factors such as extrusion scheme, area of application, design, and type of drive and control systems etc.

The basis of this theme is to analyse the role friction plays in each of these methods and then classify them accordingly. This is because friction plays a major role in extrusion technology as it is the basic boundary condition and affects energy consumption and deformation parameters. Friction can be reduced by several methods including lubrication, but this does not solve the problem entirely. Since a large amount of energy consumed by extrusion technology is in overcoming frictional forces, newer methods to classify extrusion methods are based on analysis of the contact interaction of the billet and the tool.

The methods are classified as

A. Methods that use resistive friction
B. Methods in which friction is absent
C. Methods that use an active friction loading.

A) Methods that use resistive friction loading

Friction creates a resistive loading on the contact surface of the billet. These methods are characterised by their simplicity in execution, the large variety of shapes of extrusions that can be produced and a high surface quality due to a large dead metal zone formed near the die. This keeps most defects of semi-finished product from reaching the surface. It can be executed with or without the use of lubricants and in a semi-continuous or continuous manner. Resistive friction loads create intensive shear strains that replenish layers of metal that form the peripheral regions of the extrudate. Direct extrusion and its variants are typical examples [Somekawa et al., 2008].

A variation of the direct extrusion method is when the metal is allowed to flow laterally by a 90º change in direction. This can rework the structure of the metal when small extrusion

ratios are considered. Greater possibilities are offered by using a semi-continuous variation of this method. In such processes the remainder butt of a billet post extrusion is allowed to remain in the chamber and a new billet is placed. The new billet then welds itself to the previous billet during the extrusion. For the best welds no lubricant is used as this can contaminate the weld. Such methods are utilised in the manufacture of conventional bars, aluminium wire rod and bus bars as well as lead and aluminium used for electrical applications. A lubricated version of this method is generally used to obtain products from metals that do not weld satisfactorily. For such cases conical dies and concave press rings are used to ensure that the joints from successive billets lie in the same plane and that no gap is formed between the die and container in which lubricant can flow. These result in complex die designs that are difficult and costly to manufacture. Generally such methods are made more efficient by subjecting the billet to preliminary heat treatments such as gradient heating and changing contact conditions.

B) Methods where friction is absent

In such technologies friction is absent over much of the contact surface between the container and the billet except for a tiny area just at the entrance of the die. The most common variant of these technologies is reverse extrusion. These methods are characterised by isothermal conditions and constant pressing force that is independent to the length of the billet. This increases the length/diameter ratio of extrudable products and increases the potential of such methods to extrude hard to deform alloys. Uniform deformation of the material is noticed, making the discharge rate 2-3 times more than that of direct extrusions. Furthermore these methods require a lower pressing force (up to 40%

for aluminium). Compared to direct extrusion this can lead to a chamber diameter increase of 15-20% increasing the range of extrudable products.

Hydrostatic or gasostatic extrusions are other variations of this scheme that are used [Perlin and Raitbarg, 1975; Kolpashnikov and Vyalov, 1973]. These methods can be incorporated to extrusion of alloys with a high resistance to deformation but are generally used to deform composites and bimetals.

In such methods extrusions are obtained by the use of a high pressure fluid as opposed to a rigid punch. This high pressure upon the billet is found to greatly improve the ductility during the extrusion and the method is characterised by high strain uniformity. Hydrostatic extrusions have been successfully incorporated to deform high strength alloys without the need of preheating [Perlin and Raitbarg,1975; Kolpashnikov and Vyalov, 1973]. Hot hydrostatic extrusion has several advantages over the cold variant such as lower pressing force which in turn has a positive impact on the life of the tooling. Hydrostatic extrusion of magnesium alloys have led to grain sizes of 3μm [Bohlen et al., 2005].

C) Methods that use an active friction load in the deformation process

Active friction loads are created by having the container move ahead of the punch creating frictional forces in the same direction as the flow in the metal. This increases the rate of longitudinal displacement of the outer layers and reduces the rate of displacement of the axial layers while creating radial flow along the surfaces of the press ring and the die. The interconnected flows create favourable conditions for altering the structure of the billet suppressing mechanisms for the formation of pulls and cracks etc.

These flows are also found to reduce the velocity gradient across the billet near the channel of the die [Berezhnoy, 2000]. The advantages include controlling the distribution of deformation or decreasing its non-uniformity as necessary; controlling the shear component; using the bulk effects of the plastic deformation [Scherba, 1999] for the formation of metal flow within the deformed volume and effective deformation zone; and improved production rates and quality.

Several schemes that use active friction have been developed. Such methods are generally sub categorised by parameters such as the container velocity V_{1c} the punch velocity V_p and the kinematic coefficient K_v that is defined as

$$K_v = V_{1C}/V_p \tag{2.4}$$

The value of K_v for methods that incorporate active friction loading is always greater than unity. The greatest effect in this process would be if the metal was to completely adhere to the wall of the container but this is practically impossible and slip is seen to reduce the active friction load linearly [Berezhnoy 2000].

It has been established experimentally that by changing the value of K_v, extrusion rate and the temperature profile, the character of flow of the metal can be controlled. This leads to being able to control the deformation mechanism actively and the level of mechanical properties of the product i.e. it becomes possible to obtain a product with a desired structure (re-crystallised, un-crystallised and mixed). Thus under certain conditions these methods of extrusion can be utilised to obtain products of superior strength and structural uniformity that significantly exceed the requirements of existing standards as seen in Figure 2.6. Such methods with the most commercial potential are Conform, linex and extrolling processes.

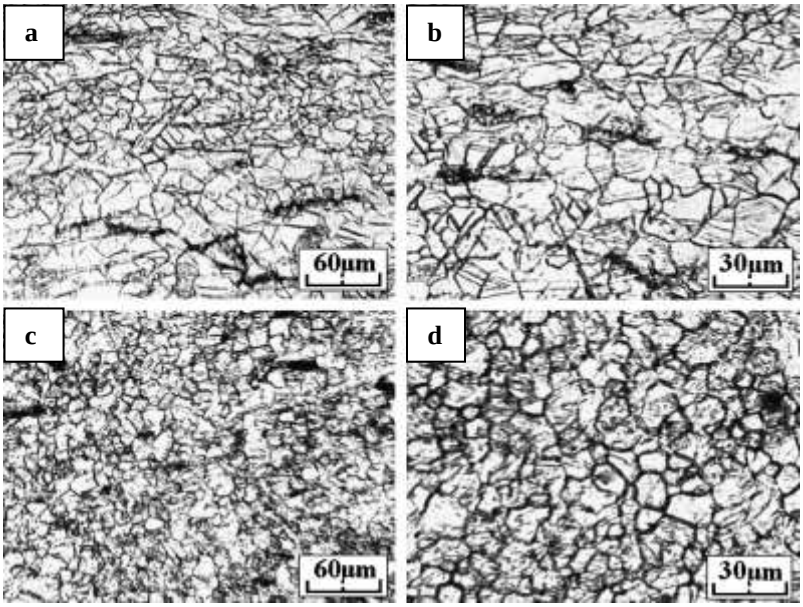

Figure 2.6: Optical microstructures of the as-extruded AZ31 magnesium alloy after: (a & b) conventional direct extrusion process; (c &d) Conform process. *[Zhang et al. 2008]*

2.2.2 Defects and disadvantages of Solid state extrusion technologies

A) Disadvantages of Solid state extrusion

There are several disadvantages to solid state manufacturing of bars. Conventional extrusion generally includes the production of rods or billets, homogenisation, preheating before extrusion [Berezhnoy, 2000].Heavy machinery that can exert a massive quantity of force is required to extrude solid state metals as it relies on friction between the material and the chamber which increases the wear of the equipment. The high levels of force required for deformation is detrimental to the tooling of the machinery which generally require substantial maintenance. In addition, use of elevated temperatures to reduce this force can contribute to the early wear and oxidation of the tooling [Roberts and Fan 2002].

Grain refinement is achieved by two main methodologies. The first is severe plastic deformation (SPD) which again is a process dependent on deformability and may leave severe internal stresses and require downstream processing. Conventionally extruded bars

are observed to have high levels of internal stress due to this. The second method, chemical addition is limited by the chemical composition of the alloy and can make recycling at a later stage difficult owing to chemical pollution of the alloy.

Disadvantages related specifically to methods where friction is present such as direct extrusion include continual change in the contact conditions and the character of the flow which can restrict the speed of the operation; highly non-uniform deformation in hard-to-deform alloys leads to smaller yield of useable product and non-uniform physio-mechanical properties over the volume of the product; limited productivity due to the time taken up by auxiliary operations such as billet changing; and complex die designs [Scherba, 1999].

Disadvantages encountered by methods that utilise methods where friction is absent such as reverse extrusion are poor surface quality requiring further downstream scalping, turning or machining; reduced size of channel through punch – used for products with small cross section; and a limited number of products that can be extruded simultaneously [Scherba, 1999].

B) Defects obtained in solid state extrusion processes [Arif et al., 2002]

An extruded product may be rejected if any of the following factors are encountered

A. Defective/contaminated billets
B. Faulty or incompatible tooling
C. Faults occurring during the extrusion process
D. Flaws from post extrusion operation

This makes extrusions that fail to meet standards and customer specifications which deem it to be rejected, having a significant impact on operational cost. Defects are categorised below based on their cause

1) Metal flow related defects: funnel formation, pipe formation, internal cracking
2) Surface defects: die lines, scoring, pick up and tearing
3) Weld defects: faces contaminated by stray lubricant and oxidised metal.
4) Metallurgical defects: streaking defects due to a difference of microstructure
5) Defects related to temperature and speed: U-shaped crack or hot shortness.
6) Other defects: which include anodising defects and defects arising from equipment and tooling defects

2.2.3 Alternate methods to solid state extrusion to produce continuous profiles

To overcome the disadvantages of conventional solid state extrusion several other methods to produce continuous profiles have been explored. For the purposes of the review they have been classified as

A. Non continuous methods: where a material with a predetermined microstructure is fed into an extrusion system that carries out shaping by conventional means in a similar fashion to injection moulding
B. Continuous methods: based on continuous casting methodology where solidifying alloy is continuously fed and worked upon to create the desired microstructure.

A) Non-continuous methods

Even though the below stated methods can be used to produce extruded materials with enhanced properties, due to the batch nature of utilising a shot sleeve and piston mechanism similar to injection moulding and direct extrusion in the actual shaping process, these methods have little commercial potential to continuously produce bars.

In such methods the desired microstructure is obtained by application of the understanding of semisolid forming technology to reduce the microstructural inhomogeneities and surface cracking. There are two distinct routes namely the thixoforming and the rheoforming route.

i. Thixoforming Route

The majority of extrusion methods that utilise semisolid metal are via the high solid fraction thixo route which is a re-melting slurry making technology [Kopp et al., 1998]. In the thixo route slurry with a high solid fraction is created by isothermal holding of a solid state billet at semisolid temperatures to encourage partial re-melting of the grain boundaries. This is detailed more in the previous section 2.1.5.

The advantage over hot extrusion includes lower pressure, minor friction forces, higher material fluidity and longer tool life. However the extrusion process is generally achieved by methods of direct extrusion as detailed in Figure 2.7 and such methods have their own inherent disadvantages as detailed in Section 2.2.2.

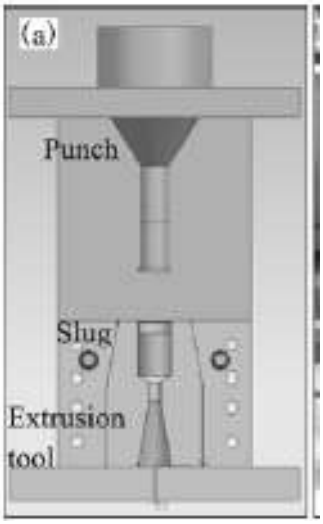

Figure 2.7: Schematic of thixo extrusion *[Forn et al., 2010]*

Compared to solid state extrusion, this process is not very efficient because of the extra step required to reheat the billet which leads to additional cost. The extrusion pressure and the microstructure of the product will be affected by the morphology and solid fraction of such a slurry [Pinsky et al., 1984].

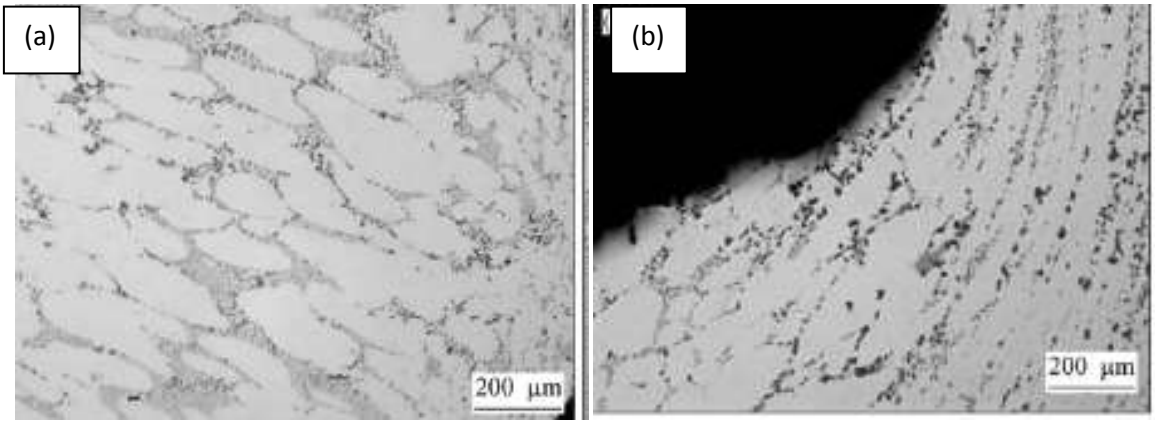

Figure 2.8: Defects observed in thixo extrusion (a) grain elongation (b) segregation *[Forn et al., 2010]*

The slurry microstructure relies on the initial microstructure of the as-cast billets and re-melting conditions. In addition, the effect of the pressing stage leads to anisotropic mechanical properties (grain elongation in press direction, extrusion texture). It is also found that solid particles tend to migrate resulting in segregation. [Forn et al., 2010].

Therefore even though such a process can reduce the extrusion force by increasing the extrusion temperature, the slurry making efficiency and the pressure segregation during extrusion [Pinsky et al., 1984] still hinder the application of semisolid application via the thixo route.

ii. Rheoforming route

In the rheoforming route semisolid slurry is created by cooling the liquid alloy to a desired solid fraction that is generally characterised by its nature of fluidity and can be transferred immediately to a mould or die for the final shaping process usually by methods involving a punch and shot sleeve. Since the viscosity at a given solid fraction can be assigned this makes the rheo route a more controlled means to achieve microstructural refinement. Applications can extend to making metal matrix composites (MMC) using techniques such as extrusion directly following infiltration (EDFI) [Hu et al., 1995] as well as methods of continuous deposition such as solid free form technology where a material is produced layer by layer [Finke and Feenstra, 2002] . The slurry can be produced and shaped at relatively low forces due to its pseudoplastic properties. Refinement of stirred melt occurs through mechanisms of solidification under convection detailed in Section 2.1.4. Such slurries are characterised by uniform non-dendritic morphologies. There are several shaping methods by which slurries have been created to be utilised in rheoforming processes to produce bars such as gas-induced semisolid rheoextrusion, cooling tube and cooling plate feeding

semisolid rheoextrusion single-screw rheomoulding and twin-screw rheomoulding. These are detailed below.

Gas-induced semisolid process extrusion [Rattanochaikul et al., 2010]

Following the work conducted in rheocasting by Wannasin and co-workers [2008] which listed good properties such as low porosity and improved tensile properties, a new method of extrusion has been developed that uses the gas-induced semi-solid (GISS) process to produce the slurry using low solid fractions. By this technology slurry is created by bubbling with an inert gas detailed in Figure 2.9, which is then transported into the shot sleeve of an injection moulding system and the slurry is extruded through a die.

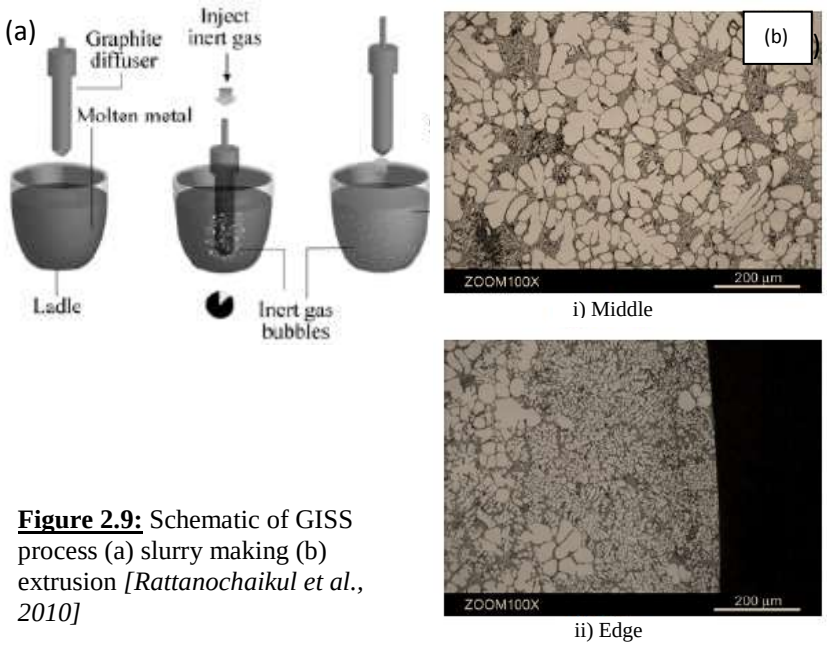

Figure 2.9: Schematic of GISS process (a) slurry making (b) extrusion *[Rattanochaikul et al., 2010]*

Micrographs show that the solid particles are concentrated towards the centre of the obtained bar of the channel during the flow. Furthermore the results suggest that the speed

of the slurry may cause turbulent flow causing surface defects. It is noted that even though processes with a low solid fraction and high punch speed yield longer extrusions the surface quality of these rods were not up to standard and it was observed that high solid fraction and low speeds created favourable surface structures.

Rheomoulding [Czerwinski, 2004; Ji et al., 2001]

Rheomoulding is a shaping process which involves the creation of non-dendritic semisolid slurry by using methods that offer intensive shearing to produce slurry with a fine microstructure. A schematic of this is seen in Figure 2.10a. The two widely used variants of the process are single-screw rheomoulding and twin-screw rheomoulding where the slurry is produced in systems like the MCAST machine. This slurry is then transported to the shot sleeve of an injection moulding system which extrudes the slurry through the die. The properties of rheomoulded products are extremely good and the process takes full advantage of the benefits of semisolid forming technologies and it has been used to produce bars.

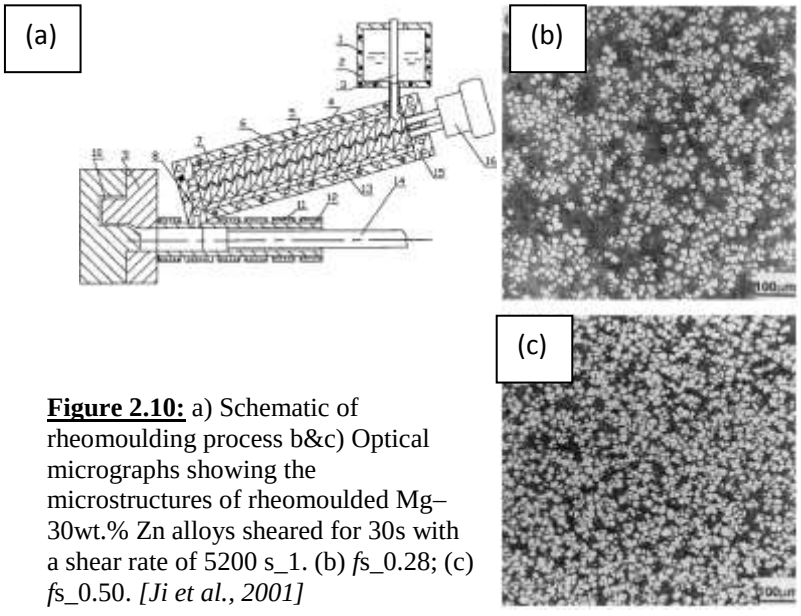

Figure 2.10: a) Schematic of rheomoulding process b&c) Optical micrographs showing the microstructures of rheomoulded Mg–30wt.% Zn alloys sheared for 30s with a shear rate of 5200 s_1. (b) *f*s_0.28; (c) *f*s_0.50. *[Ji et al., 2001]*

Due to the use of a twin-screw mechanism to mix the slurry, high levels of turbulence can be reached. This results in fine and near mono-sized solid particles distributed uniformly in a fine eutectic matrix which makes it advantageous when compared with other existing SSM processing techniques seen in Figure 2.10 b&c. However the one disadvantage that this method has is due to the inherent nature of the co-rotating twin-screw system. Co-rotating screws are ideal devices to deliver shear, however they possess very little transport capability. Therefore the screw extruders used in such purposes always have to be inclined for full discharge of the metal which is also dependent on its fluidity. This means shaping cannot be effectively done while using materials with a higher solid fraction and formed parts will generally have to be subjected to longer heat treatment to dissolve the eutectic phase.

Cooling tube and cooling plate [Nagata et al., 2006]

By this method, melt is introduced to a container as semisolid slurry created by passing alloy through a tube through which heat is extracted. This is similar to the slurry preparation method known as the cooling plate method where slurry is allowed to flow over a plate. The refinement is achieved by changing the rate of movement within the tube and the cooling gradient. Once in the container the melt is extruded by conventional methods. Even though some level of convection is achieved, these methods do not incorporate intense turbulent agitation that is found to be beneficial for the refinement of microstructures.

B) Continuous methods:

Continous casting methods detailed schematically in Figure 2.11 such as direct chill casting and direct chill rheocasting have also been used to produce continous profiles fom melts. However it is found that such methods produce microstructures of inferior properties. Due to the nature of solidification in the casting process columnar, dendritic and uneven structures arising from low nuclei survival rate are observed unless rheo mixed slurry is used, see Figure 2.12.

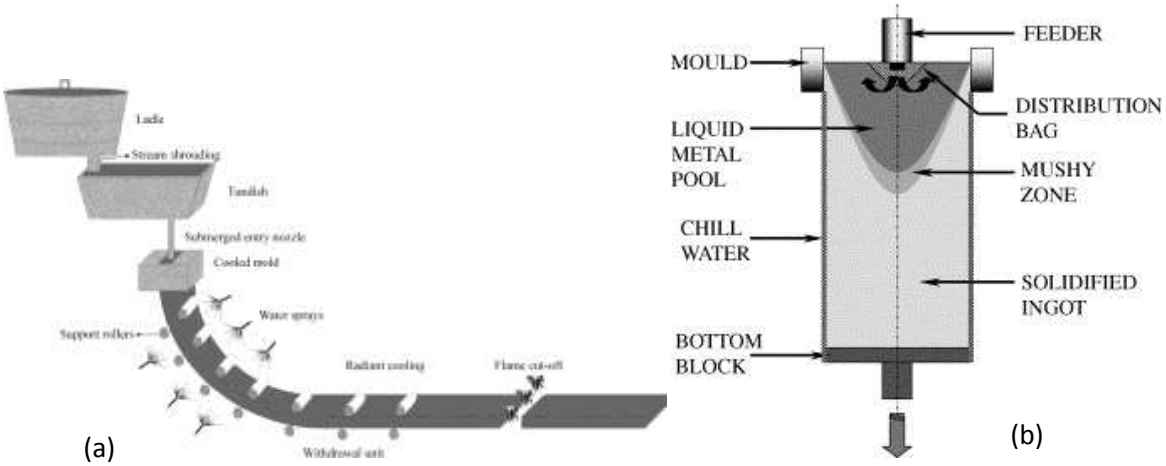

Figure 2.11: Schematic of (a) Continuous casting (b) direct chill casting

The traditional methods of direct chill (DC) casting detailed schematically in Figure 2.11 (b) has long since been used as a method to produce lengthy castings [Haghayegh et al.] of a semi-continuous nature and the more recently developed Ohno continuous casting process is a notable continuous casting process and has been successfully used to create single crystal copper wires [Soda et al., 1995]. However it is difficult to cary out such processes at high speeds to create profiles with suitable dimensions for feedstock for processes such as rolling and drawing. This limits the applicability of the technology to specific alloys.

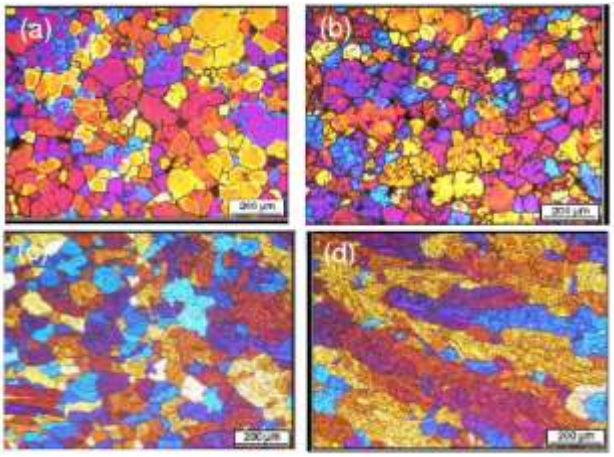

Figure 2.12: Microstructures of DC and MC-DC 7075, a) MC-DC, centre b) MC-DC, edge c) DC, centre d) DC, edge. *[Haghayegh et al.]*

Perhaps the variant of the CC process for manufacturing bars with the most commercial potential is semisolid continuous casting-extrusion and online solutionisation process (CCES) [Zhou et al., 2008]. The process is shown in Figure 2.13.

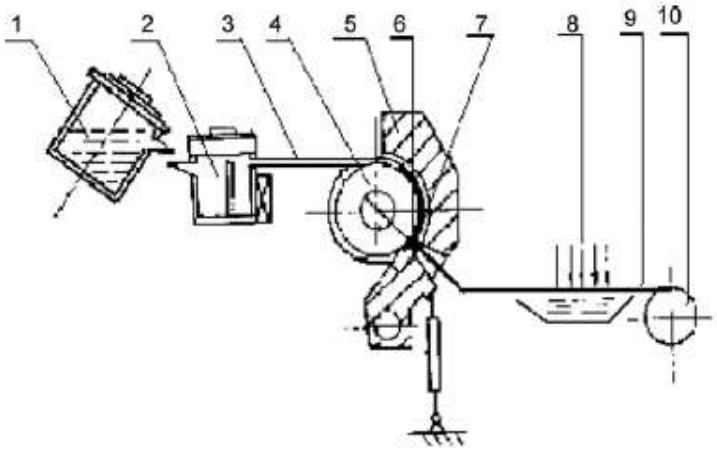

Figure 2.13: Schematic of CCES *[Zhou et al., 2008]*

The melt flows into a tundish (2) and enters the single grooved wheel (4) and shoe (5) for the casting-extrusion via a sluice (3). Cooling is applied on the casting casting-extrusion

wheel where the melt is solidified. This is then turned in the wheel and brought forward to the extrusion die through which it is deformed. Finally the bar is passed through a cooling system which quenches it.

Dendrite arms are crushed into small fragments by the shearing force of the roll, then, the small fragments disperse in the melt and grow as the free grains. The evolution of the microstructure at different points in the rolling shoe is described in Figure 2.14.

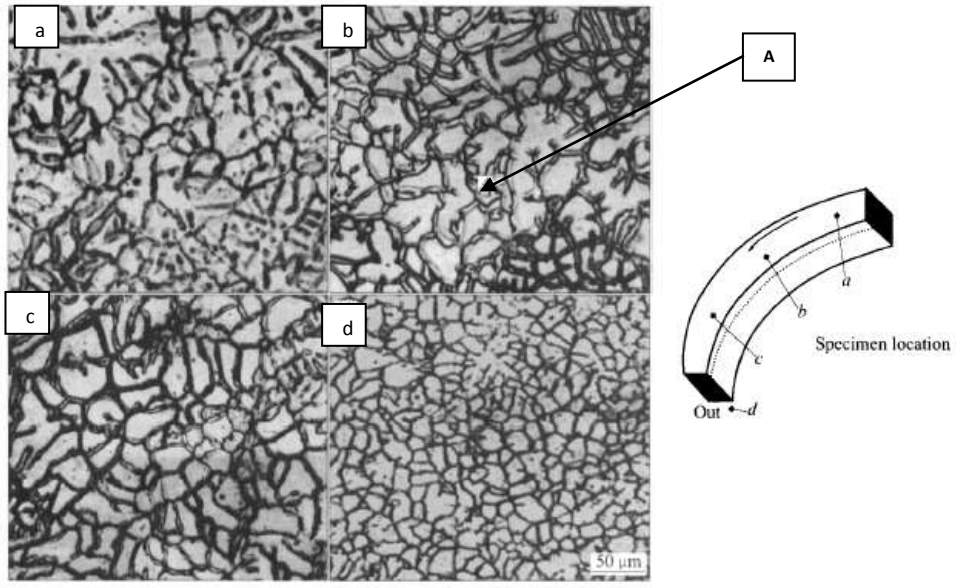

Figure 2.14: Microstructure evolution in and out of roll-shoe gap (right picture shows specimen location) *[Guan et al., 2006]*

The figure suggests as solidification occurs that dendrite arms are sheared due to the large forces and rosette particles are created as seen in Figure 2.14(b). Re-melting of dendrite arms at the root due to ripening can also take place under such shear conditions. This is seen at location 'A' in Figure 2.14(b) where there are lots of deformed arms with the bending angles above 20º. From point (a) to point (b) it can be seen that much refinement has already taken place. It is observed that dendrites have evolved into rosettes and as the

alloy is dragged downwards nearly all of the free grains evolve to spherical or elliptical structures as seen in Figure 2.14(c). By the time the alloy exits the roll shoe, the microstructure is mainly composed of spherical or elliptical structures [Guan et al., 2006]. Microstructural refinement is produced through techniques similar to conform methods. As a result of this, the machinery is heavy, complex, has high tooling costs and can only processes limited alloys based on deformability. Therefore it niether utilises the microstructural or rheological features of semisolid materials to its advantage. Solidification takes place before the extrusion which is driven by the friction between the workpiece and the tool. Furthermore in this method due to the nature of the deformation process high levels of force are required and tight restrictions on the process conditions are needed otherwise defects such as cracks and periodical wave-like surfaces are commonly observed [Guan et al., 2006].

2.3 Twin-screw Extruder Theory

2.3.1 Classification of twin-screw extruders

Based on the rotation direction of the screws relative to each other, twin-screw extruders are classified as co-rotating (screws rotate in the same direction) or counter-rotating (screws rotate in the opposite direction). Based on the interaction of these screws, these categories are subdivided as intermeshing (partially, fully) and non-intermeshing (separated, tangential). Separation between the screw axis in intermeshing extruders is less than the outer screw diameter. Other variants of screw types are conical as well as parallel-screw types. These classifications are detailed in Figure 2.15. The distinguishing feature in parallel-screw extruders is that the external screw diameter and inter-axial distance remain

constant whereas in conical-screw extruders, this is seen to decrease continuously in the direction of the die.

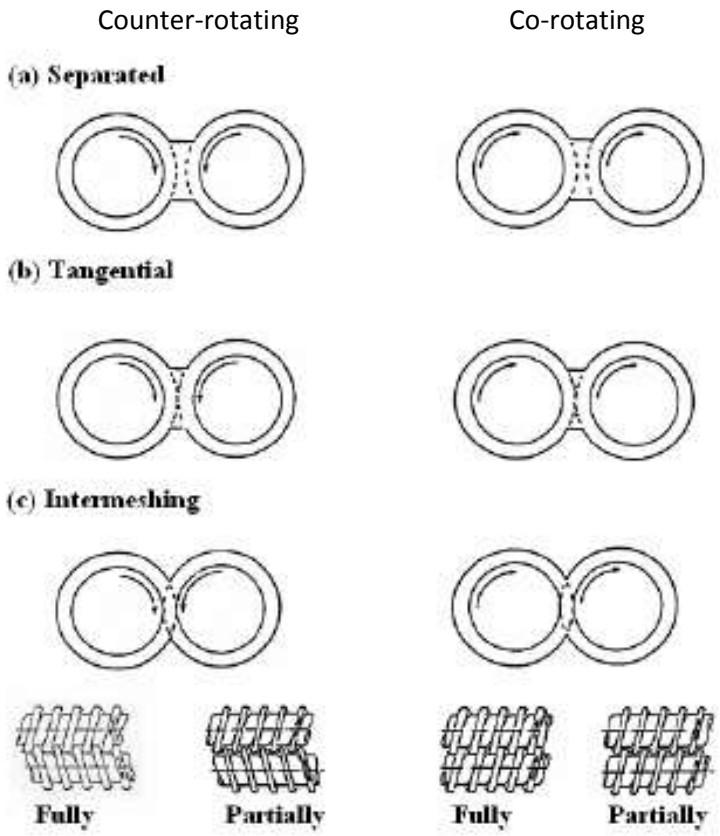

Figure 2.15: Classes of twin-screw extruders *[Hong, 1999]*

2.3.2 Development of extruding application

Thermoplastic extrusion using intermeshing counter-rotating twin-screw extruder has evolved out of twin-screw pumps in the 20th century before which they were mainly used for pumping lubricating oils. The first explicit design of a fully intermeshing counter-rotating twin-screw device for extrusion shown in Figure 2.16 was in an 1874 US patent by Lloyd Wiegland [1879] used for the extrusion of baking dough.

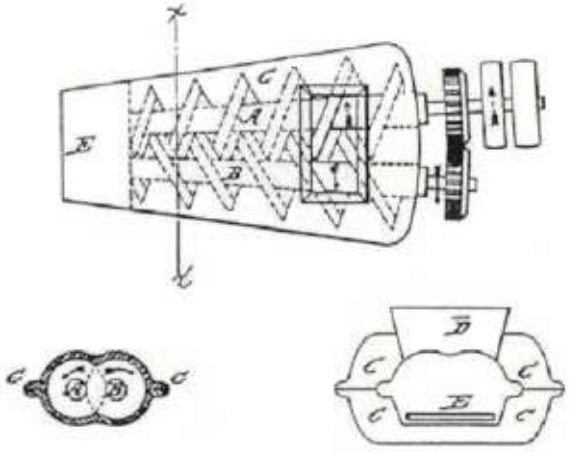

Figure 2.16: Wiegand's 1874 machine for dough sheet *[Wiegand 1879]*

The early description of counter-rotating twin-screw technology is mainly found in patent applications. In 1927 Keisskalt [1927] published the first technical paper followed shortly by Montelius [1933] and summaries of the technology have been given by Janssen [1978] and White [1990].

The greatest advantage offered by the intermeshing counter-rotating twin-screw extruder is the positive displacement mechanism. This refers to the axial displacement of a closed constant volume C-shaped chamber filled with fluid that is being transported. Therefore the throughput can be determined by the geometry and processing parameters like screw speed. The application of these extruders has also extended to rubber compound extrusion due to its advantage in superior output uniformity compared to single-screw extruders. An earlier application using a counter-rotating twin-screw machine in rubber extrusion was described in 1922 in an anonymous patent to the French Olier Company and called the Eddie Moulding Machine shown in Figure 2.17.

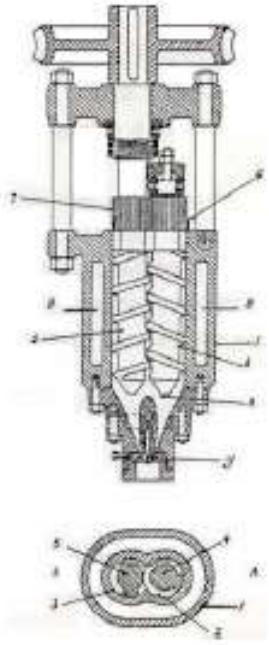

Figure 2.17: Olier intermeshing twin-screw machine *[Olier 1923]*

In 1929 one of the first clear discussions of the C-shaped chamber was provided by the Swedish engineer Montelius [1934] in a patent application. Montelius [1929] also described the dependence of the pumping efficiency on the screw geometry in a 1925 patent application. He argued that the most effective twin-screw pumps were those in which the screws had a different number of thread starts. Thus, a single-threaded screw matched with a double-threaded screw was found to be better than two single-threaded or two double-threaded screws. These machines have been developed for the use of extruding PVC profiles since the 1930s and were commercially developed by Maschinenfabrik Paul Leistritz. Around the same time a new kneading application was also developed for the technology to enhance mixing and compounding and this was mainly applied to coal-oil masses and ceramic masses in addition to rubber compounds. A basic design for this was given by Kiesskalt et al. of IG Farben Industries [Keisskalt et al., 1937; Keisskalt et al., 1939]. It is seen that flight thickness increases along the screw axis as shown in Figure 2.18.

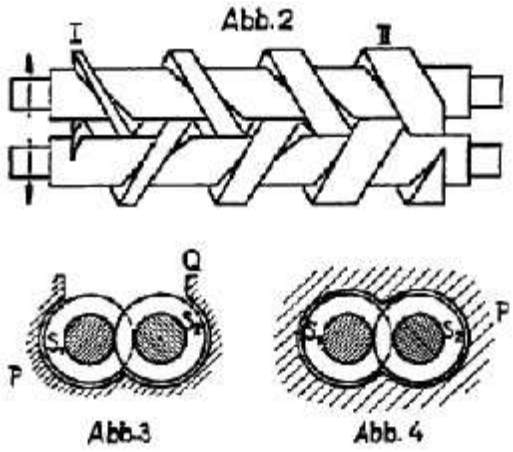

Figure 2.18: Intermeshing twin-screw extruder kneading pump of Kiesskalt et al. *[1937]*

Soon after, modifications to improve the kneading and homogenisation were introduced [Burghauser et al., 1938; Burghauser et al., 1941; Leistritz et al., 1940]. Figure 2.19 shows the modified kneading design by Franz Burghauser and Paul Leistritz of Maschinenfabrik Paul Leistritz [Leistritz et al., 1940]. This machine was designed to lower the C-chamber volume along the pumping direction by steadily decreasing the inter-flight distance causing material to have to move over the flights allowing for increased shear and mixing. Screws with transitions in them such as decreasing inter-flight distance and flight thickness toward the outlet were described by Hartner [1938] and Handle and Maschinenfabrik [1939] and similar tight fitting screw designs are found in patents by Helstrup [1939] and Marshall [1939]. An interesting application for this was patented by Schmitz [1944] to remove carbon disulphide from coagulated cellulose xanthate. In the process the barrel was perforated which entailed liquid phase separated from the additional pressure generated by reducing the C-shape volume could be pushed through the perforations. A continuous intermeshing counter-rotating machine for homogenization of mixtures to produce emulsions was

described by Kiesskalt and Borgwardt [1943] in a 1938 patent. The first commercially produced intermeshing counter-rotating continuous mixer/masticater, called the Knetwolf and used to masticate polyisobutylene, was developed in 1940 and patented in 1941 by W.Ellermann of Friederich Krupp [Anonymous, 1945].

Since the 1950s there has been a significant drive to improve these machines. This is because many new companies began introducing the machine. For instance, the length to diameter ratios in twin-screw extruders increased from 8 to over 30 since then [Schneider, 2005]. Some notable extruders of the time are Schloemann-Siemags Pasquetti Bitruder [Pasquetti, 1952], the Mapre extruder Diekirch [Schutz, 1962], Trudex machine [Baigent, 1956], Kestermann extruder and the Anger conical extruders.

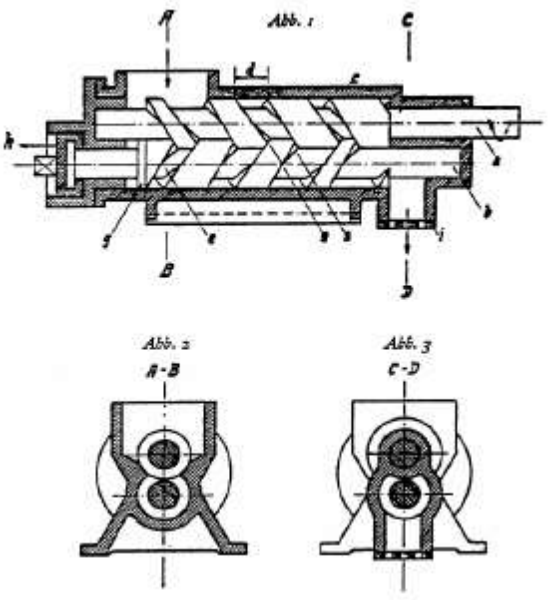

Figure 2.19: Burghauser-Leistritz kneading pump *[Leistritz et al., 1940]*

The first published experiment detailing the extrusion of rigid PVC on a Leistritz machine was given by Tenner [1956] followed by studies of Doboczky [1965a; 1965b] and Tenner and co-workers [Tenner and Kunststoffe, 1987]. In the late 1960s, Tenner also developed a modular

intermeshing counter-rotating twin-screw machine for Maschinenfabrik Paul Leistritz [Tenner, 1963] to compete with the Werner & Pfleiderer modular co-rotating extruder.

In the 1970s, more companies became involved with intermeshing counter-rotating twin-screw machines. Firms like Anger, AGM and Kesterman were absorbed whereas rights to products such as the Bitruder were obtained by various other companies who continued their manufacture [Klenk, 1978]. Around the same time Krauss-Maffei was also seen to enter the market, followed by Japan Steel Works' modular design for extruders in the 1980s [Burger, 1978].

In the 1990s, a new design was developed by Theile [2003] but the full details of the design were never fully disclosed. Modular machines were later applied in de-volatilisation and reactive extrusion processes [Sakai et al., 1987; Dey and Biesenberger, 1987].

An intermeshing counter-rotating twin-screw extruder was utilised as a reactor for modelling both free radial and condensation reaction of several polymerising systems by various groups [Ganzeveld, 1993; Janssen and Ganzeveld, 1963; Ganzeveld et al. 1994]. In these works, C-chambers are modelled as a series of continuous stirred tank reactors moving on a conveyor belt.

A one-step, solvent-free method to form a polyetheramide triblock copolymer was demonstrated by Lee and White [2002]. B.H. Lee and White [Lee and White, 2001] also found that pressurised mixing of twin-screw extruders with proper segments is much higher than the internal mixer.

These days the use of modular counter-rotating twin-screw extruders for compounding is seen to be used in North America whereas the machined shaft variant for polyvinyl chloride pipe and profiles are widely used in Europe and Asia.

2.3.3 Early studies of flow mechanisms

The first appearance of mechanisms of the counter-rotating twin-screw extruders, are found in patents as opposed to scientific literature. The forward pumping of the C-chamber seems to be well understood in the 1894 patent application made by Lloyd Weigand [1879], a 1915 patent application of Holdaway [1917], and the later patent applications of Montelius [1929; 1934]. However a clear mathematical discussion was not presented until the 1925 patent application by Montelius [1929] where he clearly explained the positive displacement pumping action, seen in Figure 2.20.

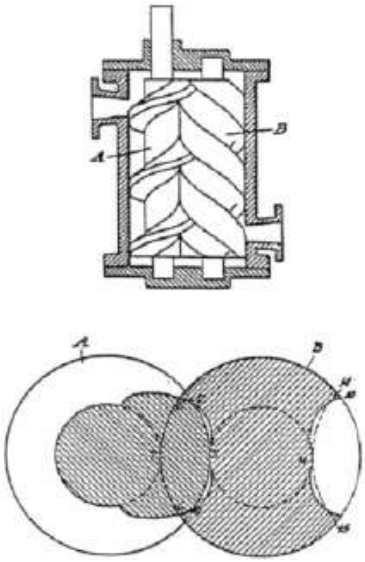

Figure 2.20: Montelius patent drawing for explanation of operating mechanism *[Montelius, 1929]*

The volumetric displacement by a single revolution of screw B is given as,

$$v = S(A_S - A_1 - A_2) \tag{2.5}$$

where A_s is the S-shaped bore volume of the screw casing, A_1 is the cross-sectional area of the single-thread screw A and A_2 is the cross-sectional area of the double-threads screw B.

All of these cross-sections are taken as right angles to the axis, and *S* represents the pitch of screw.

Kiesskalt gave a modified expression for forward pumping capacity as,

$$Q = mV_c - Q_{leak} \tag{2.6}$$

where *m* is the number of thread starts, V_c shows the total C-chamber volume and Q_{leak} is a backward leakage flow. However, a clear development of this and associated quantification only first appeared in 1959 as part of work by Gerhardt Schenkel [1985]. A full view of the C-chamber is shown in Figure 2.21.

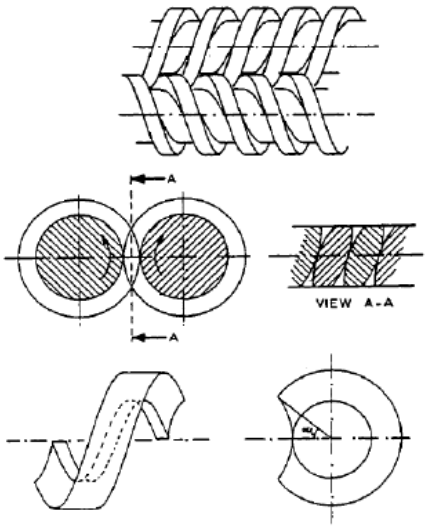

Figure 2.21: Screw geometry of two intermeshing counter-rotating screws *[Rauwendaal, 1986]*

Figure 2.21 details the geometry of two counter-rotating screws and describes the formation of the closed C-shape used in analysis and the extrusion rate is simply the product of the total volume V_c of the C-shaped chambers by the screw rotation rate, i.e.,

$$Q_{th} = 2mNV_c \tag{2.7}$$

Where Q_{th} is the theoretical volumetric throughput, m is the number of the screw thread starts, N is the screw speed and V_c is the associated C-chamber volume per screw. Schenkel [1985] was the first person to give an engineering analysis of the intermeshing counter-rotating screw extruders for thermoplastics in his book in 1959 and later it was Doboczky [1965a; 1965b] who analysed its size.

2.3.4 Experimental studies of screw pumping and mixing

Tenner conducted the first experimental study of the intermeshing counter-rotating twin-screw extruders which he studied axial temperature profiles, polymer distribution and the softening behaviour for PVC profile extrusion.

A later experimental study on pumping characteristics was reported by Doboczky [1965a; 1965b] who concluded that such extruders had about three times the output capacity of a single-screw extruder of the same size and screw speed. Subsequently experimental studies of pressure profiles along the length were published Markhenkel [1965] using PVC. Menges and Klenk [1966] and Klenk [1971a; 1971b] argued that throughput was only dependent on screw speed and found that the range of output is 34-41%, based on experiments with a Schloemann AG Pasquetti Bitruder profile extruder. Janssen and co-workers [1975] confirmed this and showed throughput increased linearly with screw speed. Using a Pasquetti type machine and polypropene they concluded that specific output (*Q/N*) seemed to be independent of pressure developed. They hypothesised that the pressure development was associated more with the level of filling of the machine and the accumulated pressure

rise was lower at higher screw speeds and higher temperatures, due to the lower viscosity obtained at such settings.

A study on the residence time with a Newtonian fluid was presented by Janssen and Smith [1975]. These studies revealed that the transport time in an intermeshing counter-rotating twin-screw extruder were smaller than values obtained by single-screw and other types of twin-screw extruders.

The effect of different modular elements on both the positions of melting and mixing were studied by Lim and White [1994]. Cho and White [1995] compared co-rotating and counter-rotating twin-screw extruders on blending processes of polyethylene and polystyrene and found that melting happened more rapidly in intermeshing counter-rotating than in co-rotating twin-screw extruders.

2.3.5 Modelling flow

The mathematical relationship between flow rates of intermeshing counter-rotating twin-screw extruders is dependent on some basic geometric parameters. In counter-rotating extruders the direction of the threads of each screw are different. The rotation of the screws is such that they diverge above and converge below the intersection plane, seen in Figure 2.22. If they were to be seen in the direction of hopper to die it would be seen that the right screw has a left-hand thread and moves clockwise while the left screw has a right-hand thread and rotates anti-clockwise. This allows for good filling properties as material coming from the hopper is distributed evenly.

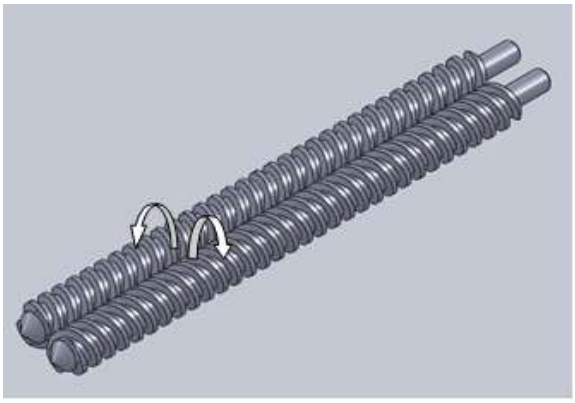

Figure 2.22: Counter rotation twin-screws

a) Basic Parameters

Important dimensions of the screw can be described by height of flight *H*, outer diameter *R* root diameter of the screw (*R*-*H*), the pitch *S*, the flight wall angle Ψ, and the calendar gap width σ schematically illustrated in Figure 2.23.

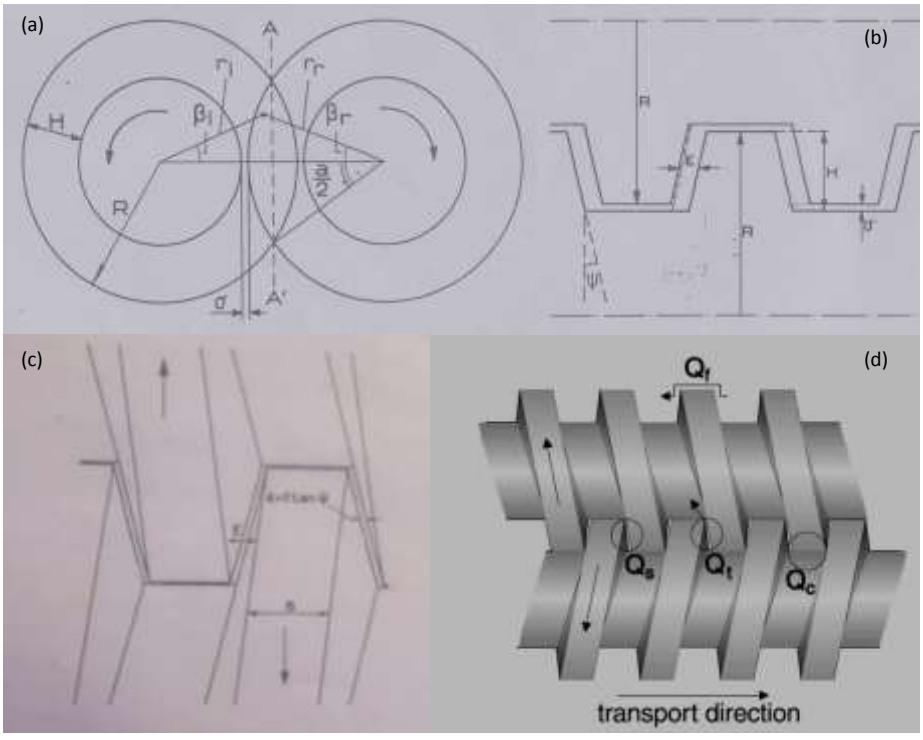

Figure 2.23: Screw Geometry a) front view b) side view c) top view d) Leakage flows from respective gaps

For multi-flighted screws the effective pitch of the screw *P* which is defined as the distance between two adjacent flights is the pitch of the thread divided by the number of flights (*m*). The relationships between different parameters can be described as:

$$P = \frac{S}{m} \tag{2.8}$$

ε is the side clearance given by

$$\varepsilon = \frac{S}{2m} - B - Htan\Psi \tag{2.9}$$

α is the overlap angle defined as

$$\alpha = 2\ tan^{-1}\left[\frac{\sqrt{RH - H^2/4}}{R - H/2}\right] \tag{2.10}$$

b) The chamber volume

The simplest expression for throughput is described in equation 2.6

$$Q_{th} = 2mNV_c$$

The chamber volume is the subtracted volume of a certain length of screw from the volume of the same length of the empty barrel. Carrying out these calculations for one pitch length and one screw only will give the volume of *m* chambers. The volume of one barrel half over one lead length can be found by elementary calculation:

The value of V_c is calculated as

$$V_c = \frac{V_1 - V_2 - mV_3}{m}$$

(2.11)

Where

$$V_1 = \left\{\left(\pi - \frac{\alpha}{2}\right)R^2 + \left(R - \frac{H}{2}\right)\sqrt{RH - \frac{H^2}{4}}\right\}S$$

(2.12)

$$V_2 = \pi(R - H)^2 S$$

(2.13)

$$V_3 = 2\pi\left\{\left(RH - \frac{H^2}{2}\right)B + \left(RH^2 - \frac{2}{3}H^3\right)tan\Psi\right\}$$

(2.14)

c) Axial pressure gradient in the extruder

The pressure change along the axis of the extruder develops from the moving wall and the flows within the chamber itself. The pressure rise along the axis is defined as

$$\frac{dp}{dx} = 6\eta\frac{w}{H^2}$$

(2.15)

where η is the viscosity of slurry and w is the wall velocity in axial direction given by:

$$w = NS$$

(2.16)

where N is the rotational speed in rad/s

The pressure rise due to the moving cylinder wall per flight is defined as

$$\Delta p = 6\eta \frac{w}{H^2}\left(\frac{S}{m} - B\right) \tag{2.17}$$

The theoretical throughput can be described in equation 2.6 as

$$Q_{th} = 2mNV_c$$

However there are several leakage flows that occur in the extruder between the flight and the barrel or between the flights that need to be considered when calculating the throughput of the extruders. This can be seen clearly in Figure 2.23 d.

Flight gap leak is defined as

$$Q_f = (2\pi - \alpha)R\left\{\frac{w\delta}{2} + \frac{\delta^3}{6\eta B}\left[3\eta \frac{w}{H^2}\left(\frac{S}{m} - B\right)\right]\right\} \tag{2.18}$$

Where δ is the flight gap width.

The calendar gap leak is defined as

$$Q_c = \left(\frac{S}{m} - B\right)\left\{-\frac{2}{3}\left(\frac{dp}{dx}\right)h^3 + 2\pi N(R - H)h\right\} \tag{2.19}$$

where *h* is the distance between the centreline of the calendar gap to the surfaces of the screws.

The tetrahedron gap leak is defined as

$$Q_t = 0.0054\Delta p R^3 \left(\frac{H}{R}\right)^{1.8} \left\{\Psi + 2\left(\frac{\varepsilon + \sigma tan\Psi}{H}\right)^2\right\} \tag{2.20}$$

And the side gap leak is defined as

$$Q_s = \frac{\Delta p(H-\sigma)(\varepsilon + \sigma tan\Psi)^3 cos^2\Psi}{12\eta l}\left[1 - 0.63\frac{\varepsilon + \sigma tan\Psi}{H-\sigma}cos^2\Psi + 0.052\left(\frac{\varepsilon + \sigma tan\Psi}{H-\sigma}cos^2\Psi\right)^5\right] \tag{2.21}$$

Where, *l* is the length of the barrel. The total output is therefore defined as

$$Q = Q_{th} - Q_t - 2Q_f - 2m(Q_c + Q_s) \tag{2.22}$$

Concluding Remarks

From the above literature review several thoughts can be concluded. Firstly it is noticed that semisolid technology is an effective means to produce non-dendritic products with a uniform microstructure.

From reviewing the methods available to manufacture bars it can be seen that a continuous rheo method to produce bars has still not been realised. This is mainly because the available technologies still utilise the traditional methods of extrusion during the forming process while working with semi-solid materials as opposed to the utilisation of a method that would be more useful when working with a semisolid material.

Since metal extrusion using a fully intermeshing twin-screw extruder has never been tried before and on analysing the applications and capabilities of such devices it can be concluded that the twin-screw rheoextrusion method is a realisation of a continuous semisolid process as it allows for rods to be produced in a continuous manner while taking full advantage of working with the properties of a semisolid melt such as pseudoplasticity and solidification behaviour under forced convection.

CHAPTER 3

THE TSRE PROCESS

3.1 Description of the Rheo Extrusion Process

Using Twin-Screw Rheo Extrusion (TSRE) it is possible to continuously extrude bars with fine and uniformly distributed microstructures. The process, which was developed and tested in this project, consists of a slurry making and feeding unit, a counter-rotating twin-screw extruder, a die assembly and a central control unit as detailed in Figure. 3.1.

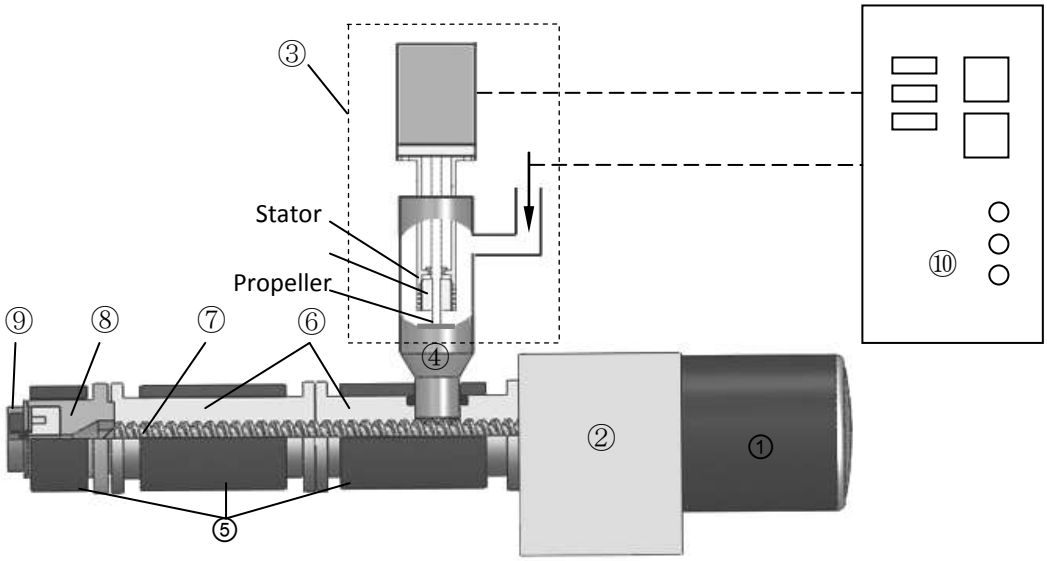

Figure 3.1: Schematic illustrations of the twin-screw rheoextrusion process including the main parts: 1- motor; 2- gear box; 3- rotor-stator high shear slurry maker; 4- funnel; 5- heaters; 6- barrel; 7- screws; 8- die system; 9- water spray cooler; 10- central control panel.

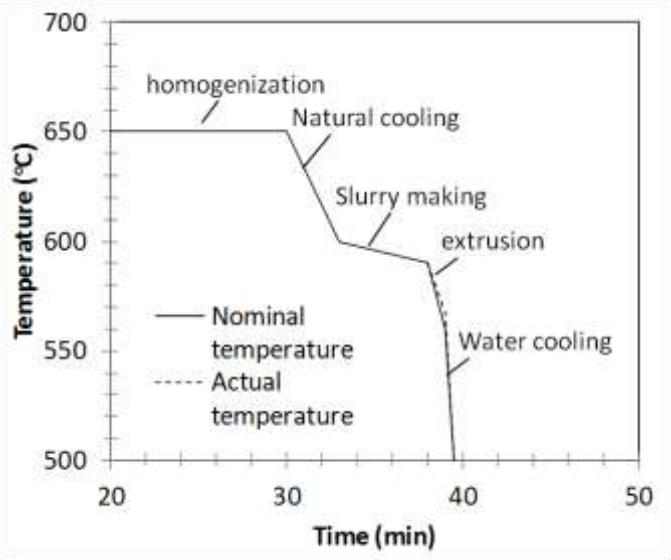

Figure 3.2: A typical thermal scheme for the processing of an AZ91D magnesium alloy: starting from homogenisation at 650°C for 30min followed by natural cooling to 600°C, and then being sheared and cooled in the slurry maker for ~2min to 590°C, and then fed to the extruder at a lower temperature, travelling through the barrel of the extruder for about 15 seconds before being extruded out and water chilled.

Figure 3.2 details the typical thermal scheme for processing an alloy through the TSRE route. During the process, melt is cooled into semisolid slurry with a predetermined solid fraction through an inline slurry maker that is directly attached to the twin-screw extruder. The slurry is intensely mixed in the slurry maker to induce a shear thinning effect and also to minimise the solid liquid segregation. As the melt passes through the slurry maker it passes down a guiding funnel and is fed into the extruder by means of a propeller that is driven by the same axel that drives the slurry maker. As it passes through this propeller it is further sheared. Once in the barrel the melt is subjected to a positive displacement-type pumping action and is transported along the axis of the barrel. During this transport, due to the complex nature of the flow, the melt is subjected to high energy flows characterised by extreme turbulence. This further subjects the melt to shear before it reaches the die. The melt is shaped as it is squeezed out of the profiled die due to the large pumping force that is created by the rotating screws. Once it passes out of the die the shaped semisolid melt is

subjected to water cooling and a solid extrusion is formed. The whole process is continuous and the entire apparatus i.e. the slurry making and feeding unit, the screw extruder and the die assembly temperatures are well controlled within ±1°C. Details of the individual steps of the process are discussed below in section 3.2.

3.2 Details of the Process

3.2.1 Slurry making and feeding

One of the technical difficulties that have been overcome by the TSRE process is the slurry making as it has traditionally been a problem when continuous SSM technologies are considered. This is due to the fact that existing slurry making processes were largely developed for the use of SSM mould casting/forging and are difficult to apply to a continuous process. The only process that is remotely viable is the continuous cooling tube process but due to the volumes of material being extruded this too becomes unviable.

Therefore for the purposes of TSRE a rotor stator mixing device that can process a sufficient amount of slurry is used to provide a high shear rate to the melt at a constant cooling rate. This piece of machinery consists of a rotor and an open cylinder stator with narrow apertures and housed in a heated container.

During the slurry making process the impellor is set at 2000RPM. This causes the melt to be sucked in through the impellor blades and squeezed out of the stator ring. The material flow is characterised by smooth convection. After the melt passes through the stator it is then met by a propeller that is attached to the bottom of the impellor. The propeller is driven by the same shaft and is used to assist the feeding. The feeding speed is related to the extrusion speed (V) which is related to the required slurry making rate (V_s) by

$$V_s = V\left(\frac{\phi}{D_s}\right)^2 \tag{3.1}$$

where ϕ is the diameter of the extruded rod and D_s is the equivalent diameter of the cylindrical container of the slurry maker. The height of the slurry container (H_c) is determined by the product of V_s and the time needed for obtaining the required solid fraction (t_s) at a given cooling rate as

$$H_C = V_s t_s \tag{3.2}$$

3.2.2 Transport and forming

The transport of the melt is governed by the geometry of the extruder screws and barrel along with the rotation speed and viscosity of the material [Ji et al., 2001] as detailed in the literature. The rotation of the screws leads to the creation of a positive displacement type pumping action in a way described in the literature and materials are transported down the axis of the barrel to the die where it is extruded. The time for this convection of material (t_T) is determined by factors such as the extrusion rate and extruder geometry and is calculated as

$$t_T = \frac{4Al}{\pi\phi^2 V} \tag{3.3}$$

where A is the equivalent gap area of the twin-screws cross section that carries the slurry and l is the barrel length of the extruder.

The melt is subjected to large zones of shear force leading to a shear thinning effect and apparent reduced viscosity [Fan, 2002]. This entails that the viscosity of the material can effectively be controlled by choosing an appropriate SSM processing temperature and shearing conditions.

The flow patterns make the machine extremely efficient as a means of conveying mixing at an extremely fine level. The exact scale of the turbulent eddies is difficult to estimate although experimental results from MCAST shearing experiments that utilise co-rotating twin-screws [Fan et al., 2009a] indicate an effect that could reach the nano-scale.

The high shear processing ensures that the growing metal nuclei grow into near-spherical shaped particles rather than dendrites or rosettes [Flemings, 1991]. As the shear rate and intensity of turbulence are increased it is noticed that there is an increased trend in the change of morphology from dendrites to spheres due to changes in the diffusion geometry in the melt around the emergent solid.

This intense melt shearing ensures that the temperature and chemical composition fields display uniformity throughout the melt. This increases the survival rate of emergent nuclei as opposed to conventional methods with uneven temperature distribution where newly formed nuclei can re-melt when moving through areas of higher temperature within the melt. This allows for enhanced heterogeneous nucleation throughout the melt [Fan et al., 2009b] and further microscopic refinement.

At the microscopic level high shear causes oxides to disperse with a fine size and narrow particle size distribution. More importantly since these oxides are completely wetted, they form evenly distributed sites, around which, nuclei of either the primary phase or the intermetallic phase can form by heterogeneous nucleation [Fan et al., 2009a].

3.2.3 Extrusion/Die conditions

The flow enters a narrow channel to be shaped before final extrusion. The solid fraction gets higher as heat extraction from the cooling system pulls energy away from the melt within the die. The structure becomes stronger and rigid and the nature of the material transport turns laminar and the main force acting on the material is surface shear stress by friction. The melt is shaped and compacted with minimal liquid segregated from the melt.

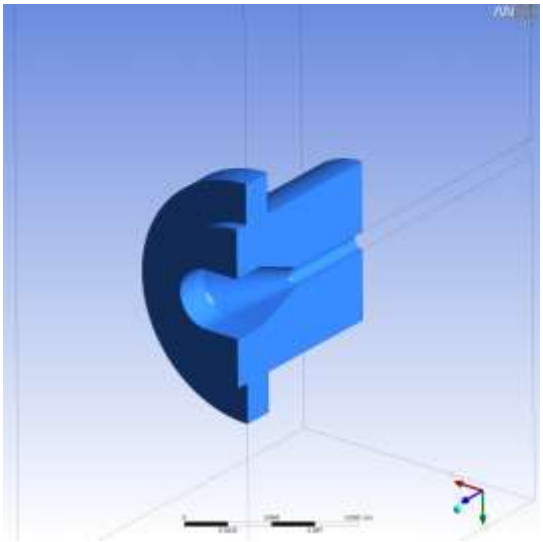

Figure 3.3: Extrusion die CAD model

The pressure built up in the extruder is governed by the geometry and material properties as described in section 2.3. Theoretically, if all the pressure was transferred to the melt with no loss to friction, the die exit velocity would be very high. As this is not observed it can be concluded that a large part of the pressure energy is used to overcome friction. To increase the overall exit velocity friction within the die is reduced to improve the overall output. High die exit temperature causes the surface of the rod to partially melt therefore

reducing the viscosity and overall shear stress which is directly proportional to the viscosity.

$$\tau = \eta \frac{dU}{dy} \tag{3.4}$$

where η is the viscosity, U is the free stream velocity and y is the boundary layer thickness. The die assembly as shown in Figure 3.3 comprises a curved profile into which the conical ends of the screws fit leading to a straight channel that shapes the slurry into the desired circular cross section for making rods. This allows for an even continuous gap between barrel and screws even as the melt leaves the barrel. The temperature at the die is set at the same value as that in the barrel so that minimal temperature drop occurs as the material moves towards the die exit.

3.2.4 Cooling

A brass cooling water ring has been designed specifically for this purpose and its inception has been detailed in section 6.4.4, Evolution of the water cooling system. Figure 3.4 shows the die assembly with the cooling ring used for extrusion. This was developed using a setting at which the melt exits at a near constant temperature. If this steady state temperature is not maintained then the rod will display uneven properties along its axis. From experimental findings and parameter exploration it has been understood that the cooling system needs to achieve sufficient cooling without much deformation of the bar and water cooling must be done just after the die with minimal heat transfer up the rod i.e. it should balance out otherwise the friction is too much for the extruder to pump against.

Cooling must also be done quickly as the bar should have some structural integrity once it hits the trough otherwise it would lead to a build-up of material at the die exit.

Figure 3.4 shows the die assembly. An insert is attached to the die bring the exit of the die forward. To keep the die temperature constant a water cooling system is incorporated on the outside of the exit of the die and is insulated using super wool. The rod is allowed to cool externally before it can be coiled or collected. It is assumed that as the melt shrinks upon solidification it will create a small gap between the material and the die which reduces the frictional forces. However it is seen that contact between the surfaces will inevitably occur causing the reduction of extrusion speed due to frictional forces.

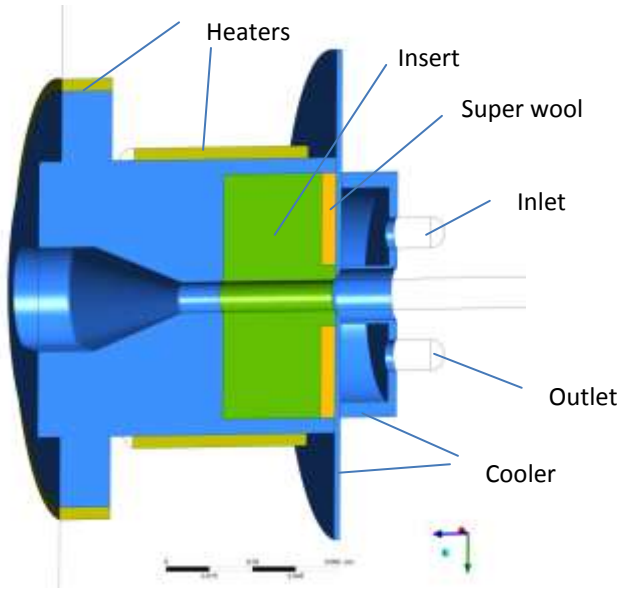

Figure 3.4: Die assembly and cooling system CAD model

CHAPTER 4

EXPERIMENTAL METHODS

4.1 Materials Preparation

Rheoextrusion was carried out on one magnesium alloy and three aluminium alloys. The magnesium alloy used for the study was AZ91D provided by Magnesium Elektron Manchester UK. The aluminium alloys used for the study were AA4043, AA5356 which were prepared in-house and LM24 which was provided by Norton Aluminium. The chemical composition of the magnesium ingots and aluminium alloys used are shown in Table 4.1. Primary studies to understand the processing conditions were conducted on AZ91D due to is good castability and formabiliy as detailed in available literature [Czerwinski, 2004; Czerwinski and Zielinska-Lipiec, 2005; Du and Zhang, 2007; Fan and Liu, 2005; Wang et al., 2006; Zhang et al., 2009] whereas aluminium alloys were used to validate the findings. All alloy compositions are shown in wt. % except when specified otherwise. Compositions were measured using a 'Foundry Master Pro' Arc-spark Optical Emission Spectrometer.

Tables 4.1: Compositions of alloys used

Alloy	Type	Chemical Composition (wt. %)							
		Mg	Al	Be	Cu	Mn	Si	Zn	Others
AZ91D	As received	90.5	8.78	0.001	0.013	0.201	0.0085	0.443	<0.001

Alloy	Type	Chemical Composition (wt. %)							
		Al	Si	Fe	V	Ti	Mg	Zn	Others
4043	Prepared	94.2	5.44	0.185	0.145	0.0129	0.022	0.012	<0.0088

Alloy	Type	Chemical Composition (wt. %)							
		Al	Si	Fe	V	Mn	Mg	Zn	Others
5356	Prepared	94.4	0.214	0.432	0.01	0.0082	4.67	0.13	<0.01

Alloy	Type	Chemical Composition (wt. %)							
		Al	Si	Fe	Cu	Mn	Mg	Zn	Others
LM24	As received	82.3	9.7	1.57	3.68	0.517	0.16	1.54	<0.15

Using a Carbolite VCF 12/23 electric resistance furnace, the alloys were melted in batches of 2kg in a steel crucible for magnesium and a ceramic crucible for aluminium. Melting temperatures of 680ºC (magnesium) and 700ºC (aluminium) were used and the melt was held at 650ºC for half an hour to homogenise.

To avoid severe oxidation and burning when working with AZ91D a protective gas mixture of nitrogen containing 0.5 vol. % sulphur hexafluoride (SF_6) through a narrow tube that delivered 6 litres/minute of nitrogen and 0.025 litres/min SF_6. For aluminium a protective atmosphere of nitrogen was used and the melt was degassed by bubbling nitrogen and through it.

The melt was then stirred to ensure homogenisation of temperature fields and the protective gas was checked at regular intervals to avoid oxidation of the melt.

4.2 Investigations on Slurry Preparation for Feeding

The majority of the slurry experiments were undertaken using aluminium alloys. This is because the need for a slurry feeding device was incepted after the primary investigations had been carried out using the magnesium extruder and the extruder for processing Aluminium had already been delivered.

4.2.1 Determining correct feeding temperature based on performance

To determine the correct pouring temperature based on the fluidity and correct solid fraction, samples of AZ91D and AA5356 slurry that were 0.25cm^3 in volume were quenched in water for less than half a second at different temperatures. These were then cut across the volume at a random plane of orientation and observed by optical microscopy to document the structure prior to feeding.

4.2.2 Validation of degassing

To validate the incorporation of degassing into the slurry preparation procedure the melt was purged with nitrogen and compared to samples prepared without it. Aluminium alloy AA5356 was used for the study. Similarly to the method discussed above, samples of approximately 0.25-0.5cm^3 were quenched for less than half a second. These were then cut across the volume at a random plane of orientation and observed by optical microscopy to see if there was any reduction of porosity.

4.2.3 Comparison of different shearing mechanisms

To compare the effectiveness in breaking agglomerations and promoting non-dendritic growth, different shearing/propelling mechanisms were tested out on AA5356 slurry at different temperatures. Four different types of stirring were tried out and these were a blender (B type), common stirrer (C type), dual-layer (D type), and high shear mixer (H type) as detailed in Figure 4.1.

Figure 4.1: Different types of stirring mechanisms used

In the same way as stated in section 4.1, AA5356 was used for the study. Slurry was continuously mixed and samples of reducing slurry temperature that were 0.25-0.50cm^3 in volume were quenched in water for less than half a second. These were then cut across the volume at a random plane of orientation and observed by optical microscopy to observe the morphology and dispersion of the grains.

4.3 Extrusion Experiments

Two twin screw extruders were specially developed for the purposes of extruding aluminium alloys (Figure 4.2a). magnesium (Figure 4.2b) and The main components of each machine, i.e. the control panel, motor, funnel, barrel and die of each machine have been labelled as C, M, F, B and D respectively.

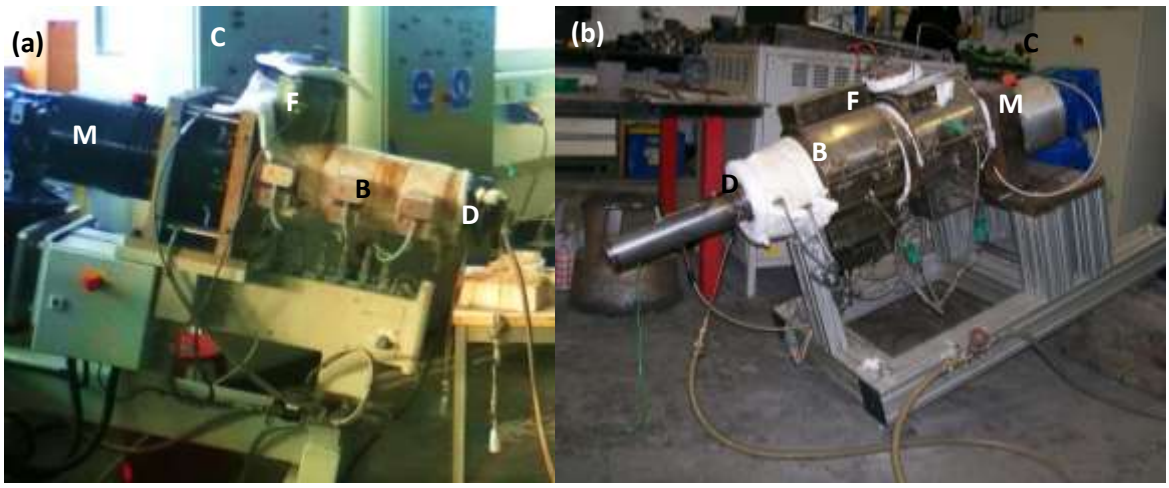

Figure 4.2: a) Aluminium Extruder b) Magnesium Extruder

Although the functioning/operations of the machines remain identical, to improve the transport capabilities dimensions have been modified. These are detailed in table 3.1 and the effects of these changes have been detailed in Chapter 6. Initial experiments were conducted on the magnesium extruder and findings were used to design the aluminium extrusion process. The main difference between the machines is that the magnesium extruder is constructed using steel whereas to minimise chemical attack the aluminium machine was made of molybdenum.

Table 4.2: The basic dimensions extruders

Dimension	Magnesium Extruder	Aluminium Extruder
Outer diameter of the screw (mm)	39.6	53.5
Root diameter of the screw (mm)	27.6	36
Axial channel width (mm)	11	10.9
Axial flight width (mm)	5	4.08
Channel width at the root (mm)	7	4.04
The Depth of a c-shaped chamber (mm)	6	8.75
The number of screw starts	2	2
Centreline distance of screws (mm)	34	45
Calendar gap (mm)	0.5	0.25
Flight gap (mm)	0.5	0.25

Detailed procedure for the extrusion process

1. The machine components were cleaned of residual melt and assembled.
2. To preserve the heaters and to ensure the entire system was at the correct temperature, the extruder heaters were then set to and held at 250°C and 450°C to allow the barrels to soak and to check whether all the heating rings were working properly. The heaters were then set to the final extrusion temperature. The machine was allowed to soak at temperature again.
3. The melt was cooled to the correct pouring temperature and stirred to ensure homogeneity and minimise segregation. Any visible oxide was removed. The screws were then set to the predetermined speed for the experiment.
4. The melt was carefully poured into the feed section of the extruder, cooling water valve to the die on the machine was turned on and a bar was obtained.
5. The motor was turned off and the heaters were set to the liquidus temperature. The die was cooled slightly to form a plug. Once the barrel

temperature was obtained the die temperature was increased and the screw speed increased to maximum to expel the remaining melt in the barrel.

6. Once the liquid had stopped the screw speed was reduced to 20RPM and the heaters were turned off. The screws were turned off once the barrel reached a temperature below 450°C to ensure the mechanism would not be jammed by oxide formation.
7. The die was removed and cleaned of any remaining melt and oxide.

4.3.1 Testing of process variables

The primary investigation into the effect of the process variables on the microstructure was carried out using AZ91D. The settings used in this study are detailed in Table 4.3 below

Table 4.3: Investigated parameters of extruder

	Settings Explored			
Effect of Motor Speed (RPM) *Settings Fixed* Pouring Temperature 610 ºC Barrel Temperature 545 ºC	125	135	145	150
Effect of Pouring Temperature (ºC) *Settings Fixed* Motor Speed 150 RPM Barrel Temperature 548 ºC	595	610	625	640
Effect of Barrel Temperature (ºC) *Settings Fixed* Motor Speed 150 RPM Pouring Temperature 610 ºC	545	548	551	554
Varying the exit Diameter (mm) *Settings Fixed* Motor Speed 150 RPM Pouring Temperature 640 ºC Barrel Temperature 548 ºC	10	8		
Varying Motor Power (kW) *Settings Fixed* Motor Speed 150 RPM Pouring Temperature 640ºC Barrel Temperature 540ºC	3	4		

4.3.2 Exploration of water cooling designs and settings

Experiments to establish the correct methodology of cooling and the level of cooling as detailed in section 6.4.4 were conducted between the range of settings of barrel temperature 570-580ºC pouring temperature 580-590ºC and a fixed motor speed 150RPM at a frequency of 70Hz using AZ91D.

4.3.3 Exploration of different process settings

Magnesium alloy AZ91D was used to determine the effect of varying processing temperature on the microstructure. Settings of successful extrusions used to explore the process temperature using the final cooling system are detailed below in Table 4.4.

A mechanism was developed and tested to feed the slurry at lower temperature. This is detailed in section 6.4.3. Due to experimental constraints in feeding, the parameters of pouring temperature were limited to the lowest possible temperature of the slurry with a workable fluidity as detailed in section 5.1.1 and adjusted between the narrow range of 590-610ºC while the motor speed was set to a fixed 150rpm (50-70 Hz). These parameters can be further explored and are in need of optimising

Table 4.4: Process settings of steady state extrusions explored

Alloy	Process Temperature (ºC)	Pouring Temperature ºC)	Motor Speed (rpm)	Water Cooling Rate (l/min)
AZ91	560	595	150	4
	565	595	150	4
	575	595	150	4
	585	595	150	4

To determine the lowest possible processing temperature of aluminium alloys AA5356 and LM24, melt was extruded at a variety of temperatures and initially quenched to approximately determine the lowest correct process temperature for throughput. Feeding temperature was set as the lowest possible temperature with workable fluidity as determined from the slurry experiments detailed in section 5.1.1. Once within the correct range of temperatures the cooling ring was attached with a fixed flow rate of approximately 4l/min to determine a final lowest processing temperature.

4.4 Characterisation of Extruded Samples

4.4.1 Macroscopic analysis

Several forms of analysis were carried out to judge the experimental settings. On the macro scale this amounted to parameters such as smoothness, surface tearing, and straightness of the extruded bar measured qualitatively.

4.4.2 Microstructural characterisation

A) Sample Preparation

Extruded rods were examined using optical microscopy to reveal the microstructural features as a function of processing parameters. At least three metallurgical samples for each condition were cut from the different lengths of the extrudates in order to investigate the uniformity of the extrudates at cross sections and along the extrusion direction. Both transverse and longitudinal sections were investigated.

The specimens were grinded with 120, 600, 800, 1200, 2500 and 4000 grade silicon carbide abrasive papers on a Beuler, Phoenix 4000 semi-automatic sample preparation system and polished with colloidal Struers OP-S colloidal silica (0.04 μm in grain size).

Magnesium samples were colour-etched for 1-2 seconds using acetic-picral solution etching (4.2g picric acid (conc.), 70ml ethanol, 15ml distilled water and 15ml acetic acid (conc.). Aluminium samples were etched with a sodium hydroxide solution (10% NaOH) for approximately 30 seconds. Samples were washed with ethanol and air dried between grinding, polishing and etching and stored in a sample box containing a desiccant. Samples for SEM were swabbed with Nital (5ml HNO3 (conc.) in 95ml ethanol) for 3-4 seconds.

B) Optical Microscopy

A Zeiss optical microscope, Zeiss Axioskop2 (Zeiss Gmbh, Gottingen, Germany), equipped with a polarised light system was used for the optical microscopy. To record the microstructures, an AxioCam digital camera was used to link the microscope to the PC and was quantified using Axiovision image analysis software. The linear intersect method was applied for the grain size measurement under the standard of ASTM E112-96. The intersect method involves an actual count of the number of grains intercepted by a test line or the number of grain boundary intersections with a test line. This is done by image processing. The values of grain size reported in this study are measured from at least five different test lines. Grain density (N_D) was calculated by marking out an area using the image analysis software and then counting the number of grains within it. For analysis of the slurry, the shape factor of particles in the slurry was estimated by the relation

$$F = 4\pi S_p / P_p^2 \tag{4.1}$$

where S_p and P_p are the average area and perimeter of the particles respectively. The contiguity factor (C) was estimated using the relationship

$$C = 2N_{\alpha\alpha}/(N_{\alpha\alpha} - N_{\alpha\beta}) \tag{4.2}$$

where $N_{\alpha\alpha}$ is the number of intersections per unit length and $N_{\alpha\beta}$ is the number of intersections per unit length of the test lines between the primary α phase and the secondarily solidified phases. Assuming a random distribution of particles, volume fraction of solid particles (f_s) in the slurry was calculated from measured particle size (D) and density by:

$$f_s = \frac{\pi D^2}{6} N_D \tag{4.3}$$

C) Scanning electron microscopy (SEM)

A scanning electron microscope 'Zeiss Supra 35VP', which is an ultra-high performance field emission scanning electron microscope with both high-vacuum and variable operating pressure (VP) capability, was used. The field emission source and Gemini column result in high resolution at high magnifications. The microscope is equipped with a suite of analytical techniques for composition and phase detection including an energy-dispersive x-ray analysis (EDX), back-scattered electron detection (BSE) and an in lens detector. These were used to investigate fracture surfaces, eutectic structures and chemical compositions within the microstructure at high magnification. An accelerating voltage of 20kV was used for the observation at a working distance of 9mm and aperture of 30μm.

4.5 Spectral Analysis

The extrusion die was blocked and aluminium alloy was introduced to the barrel. The melt was held in the machine with the screws rotating so as to simulate shearing. The melt was then expelled after a variety of times and temperatures, collected and cast. The resultant sample was polished using 120, 800 and 2500 silicon carbide papers. The sample was then washed with ethanol and air dried. Spark analysis was carried out on a 'Foundry Master Pro' Arc-spark Optical Emission Spectrometer as seen in Figure 4.3. The machine contains a solid state spark source, a vacuum system, an optical system and an output system (PC). The sample was positioned on the spark stand for chemical composition analysis which was performed at least eight times at different locations for each specimen.

Figure 4.3: 'Foundry Master Pro' Arc-spark Optical Emission Spectrometer

4.6 Mechanical Testing

Tensile specimens were machined out of AZ91D rods into standard dog bone samples of 6.5mm diameter and a gauge length of 25mm of samples extruded at 565ºC and 545ºC to determine the effect of extrusion temperature on the mechanical properties.

The tensile test was conducted at room temperature on an INSTRON 5569 universal test machine as seen in Figure 4.4 at a strain rate of $0.66x10^{-3}s^{-1}$ along with an extensometer. Calculation of tensile strength and elongation to fracture were obtained by the machine.

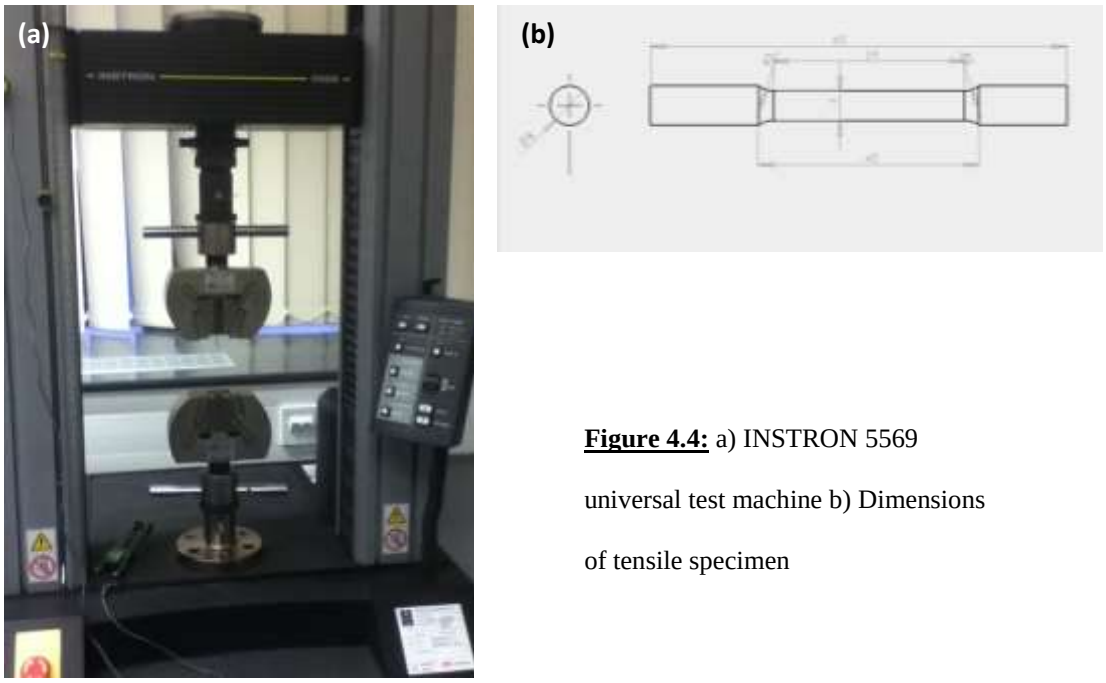

Figure 4.4: a) INSTRON 5569 universal test machine b) Dimensions of tensile specimen

4.7 Thermal Modelling

A model of the aluminium extruder was created on Solid Works and FEM analysis was carried out on it. The model contained 19219 cells and 34327 nodes. The model was a full scale 3D representation of the extruder and was considered to be a thermodynamically

adiabatic system with no overall input or output of heat. This was chosen because the machine was completely insulated with superwool.

Input parameters included, barrel temperature, die temperature, feed section temperature melt temperature. The output temperature of the slurry was measured and compared to solid fraction of quenched melt to compare the validity of the model to the laboratory experiment. The model was also used to simulate the results of the lowest possible extrusion temperature (620ºC) and to determine the process settings that would achieve a desirable solid fraction f_s=0.6.

Details of the analytical approach to heat transfer are detailed in section 6.3.

4.8 Heat Treatment

The AZ91D bar produced at 545ºC from a melt of 590ºC was subjected to a subsequent homogenisation treatment as a preliminary investigation at 370, 390, 410, 420 and 430ºC for two hours (T4) and at 410ºC at extended holding times of 1, 2 and 48 hours to observe precipitation (T6).

The heat treatment procedure was carried out in air with the protection of carbon powder on the surface of the samples using an Elite BSF12/6 chamber furnace with a maximum working temperature of 1200ºC.

CHAPTER 5

RESULTS

5.1 Investigations on slurry preparation

Investigations were conducted to study the microstructural evolution and fluidity of the slurry in order to find the best conditions for slurry making. The flow features of the slurry as a function of temperature were explored to determine the temperature at which the slurry was fed. The observable structure of slurry quenched at different temperatures show globular particles within a secondarily solidified network. The primary phase solid particles formed in the slurry upon shearing were non-dendritic and relatively equiaxed but some dendritic and rosette particles were also observed. This is due to the limited solidification time of about half a second during quenching. As expected, as the slurry temperature decreased both the solid fraction and average particle size increased and more equiaxed particles started appearing. The morphology of these particles was seen to be independent of the slurry making temperature and the creation of this type of semisolid structure was similar to that observed in the normal rheoforming process as described in previous studies by Czerwinski and Flemings [Czerwinski and Zielinska-Lipiec, 2005; Flemings, 1991] . This suggests that if the applied convection produces a sufficient amount of shear, granular particles required for the process will be produced almost instantly. Factors that affect the slurry performance are temperature, entrapped gas and shearing. These have been investigated in the following sections.

5.1.1 Temperature

a) Magnesium Alloy AZ91D

Figure 5.1 shows micrographs obtained from samples quenched from a variety of temperatures within the range 586–670ºC. On reducing the slurry temperature a higher fraction of globular primary α-Mg is observed within a secondarily solidified eutectic network of α-Mg and β-$Mg_{17}Al_{12}$.Workable fluidity for hand mixing was observed to be at approximately 590ºC corresponding to a solid fraction of 0.2.

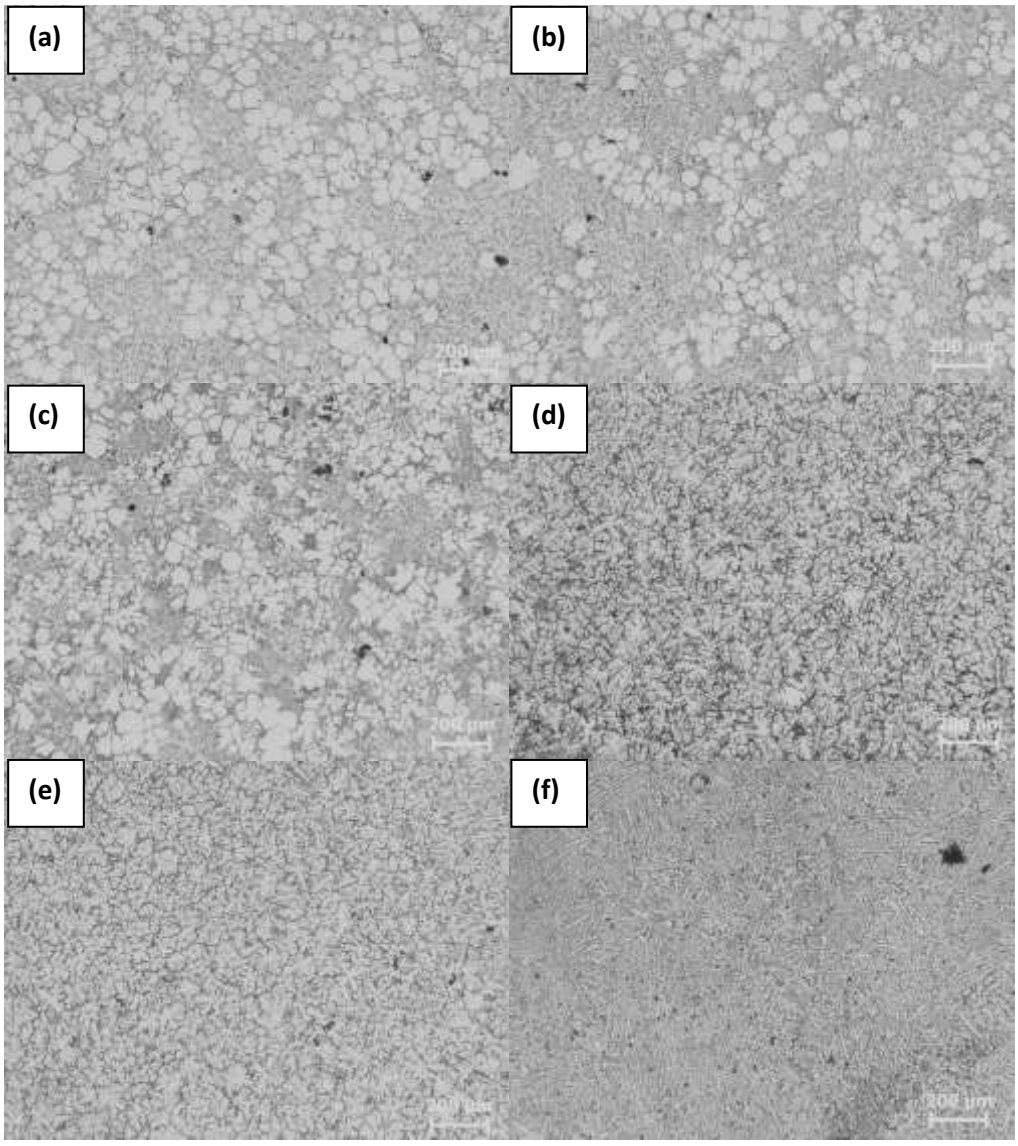

Figure 5.1: AZ91D quenched from (a) 586ºC, (b) 590ºC, (c) 594ºC, (d) 598ºC, (e) 602ºC and (f) 670ºC

b) Aluminium Alloy AA5356

Figure 5.2 shows micrographs obtained from samples quenched from a variety of temperatures within the range 636–624ºC. On reducing the slurry temperature a higher fraction of globular primary α-Al is observed within a secondarily eutectic network of α-Al and β-Al_3Mg_2. Workable fluidity for hand mixing was observed to be at approximately 628ºC corresponding to a solid fraction of 0.2 as per the calculated scheil curve.

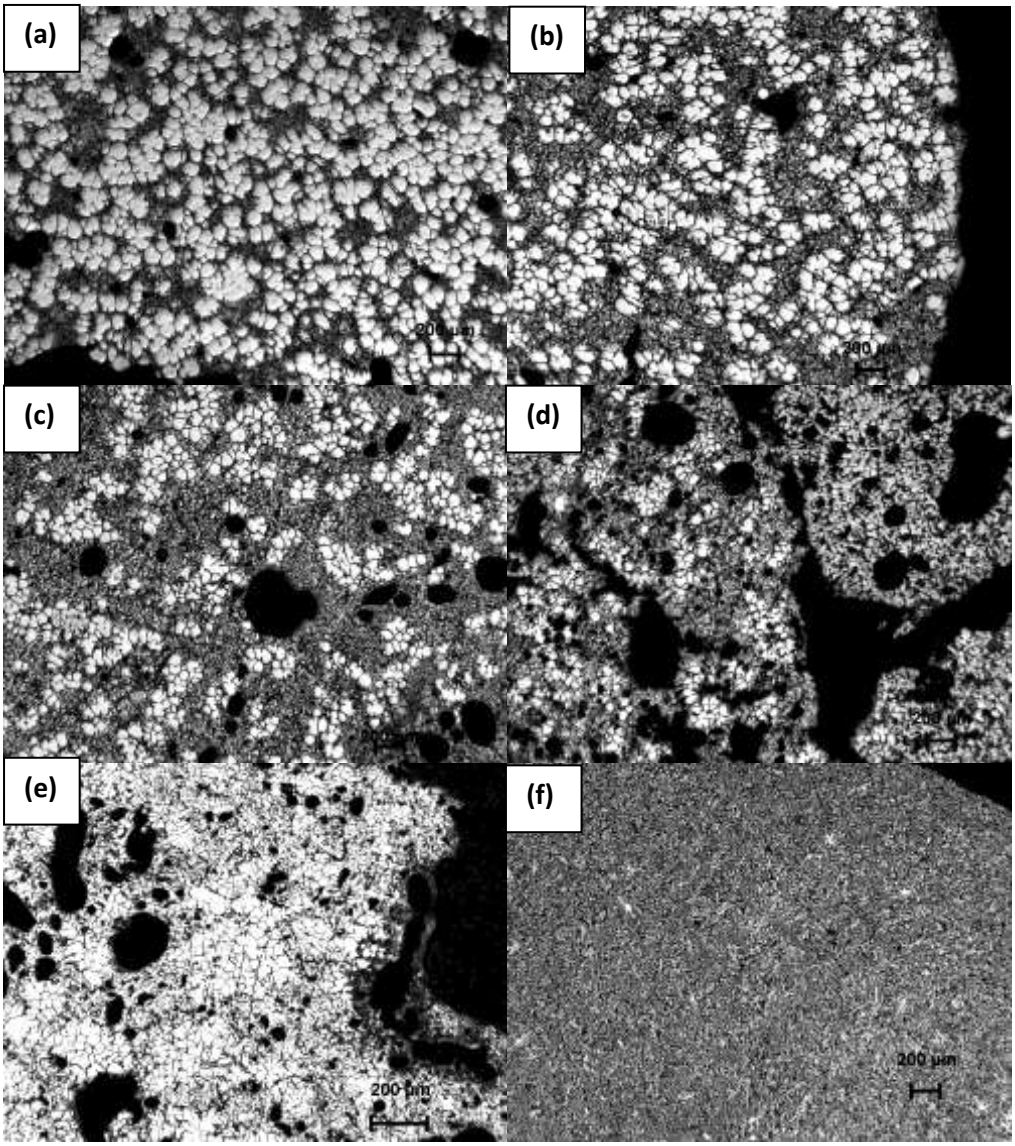

Figure 5.2: AA5356 quenched at (a) 620ºC, (b) 624ºC, (c) 626ºC, (d) 629ºC, (e) 635ºC, and (f) 632 º C

Similar trends in structural evolution were observed in both AA4043 and LM24. For AA4043 the workable temperature of the alloy was observed to be 621ºC which corresponds to a solid fraction of 0.2 as per the calculated scheil curve. On reducing the slurry temperature a higher fraction of globular primary α-Al is observed within a secondary eutectic network of eutectic α-Al and eutectic silicon.

For LM24 the workable temperature of the alloy was observed to be 570ºC which corresponds to a solid fraction of 0.15. On reducing the slurry temperature a higher fraction of globular primary α-Al is observed within a secondary eutectic network of α-Al and eutectic silicon.

5.1.2 Degassing (AA5356)

AA5356 was used for the study to validate the incorporation of degassing into the slurry preparation procedure in which slurry was purged with nitrogen and compared to samples prepared without it. In Figure 5.3 it can be seen qualitatively that the structure of both samples is that of a globular primary solidified phase within a secondarily solidified network. It can also be observed that on purging the slurry with nitrogen, porosity from gas entrapment is seen to reduce. In addition to this the presence of an inert gas like nitrogen can also contribute to the reduced formation of oxides.

However it should be noted that the observed porosity levels and oxides present in quenched samples do not represent the true scale of porosity and feature of oxidation in the real rheo-extrusion process. This is because when considering a small amount of slurry there is a higher level of contact with air during mixing and with water during quenching. These can result in a substantially higher tendency for oxidation and gas entrapment.

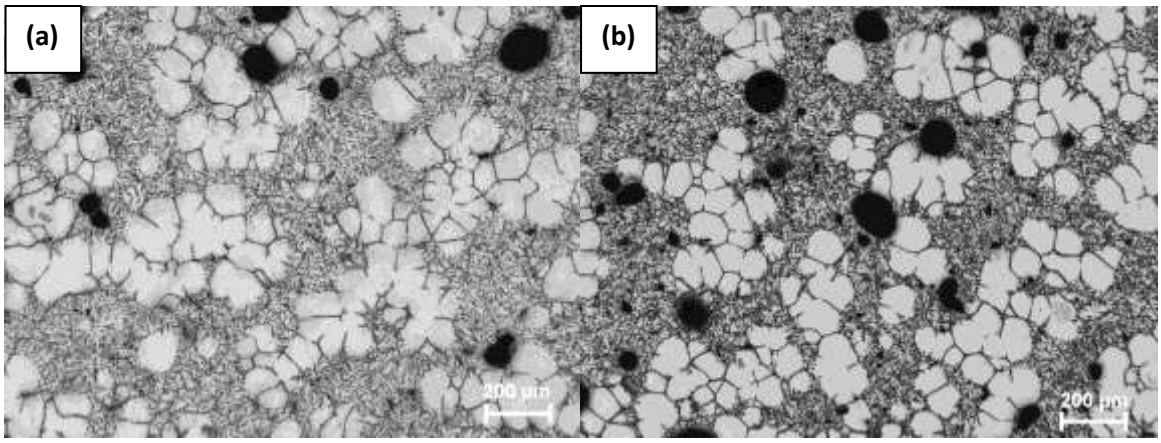

Figure 5.3: Microstructures of AA5356 slurries obtained using a B-type stirrer at 630ºC (a) with nitrogen purging (b) without nitrogen purging

5.1.3 Shearing

Figure 5.4 details microstructures obtained by the use of different stirring mechanisms while solidifying AA5356 alloy. From the micrographs of the quenched samples it can be seen that the presence of forced convection from the different propellers produce smaller equiaxed grains. Comparing the effect of different stirrers by measure of agglomeration must be determined by comparing the contiguity factor of the obtained samples.

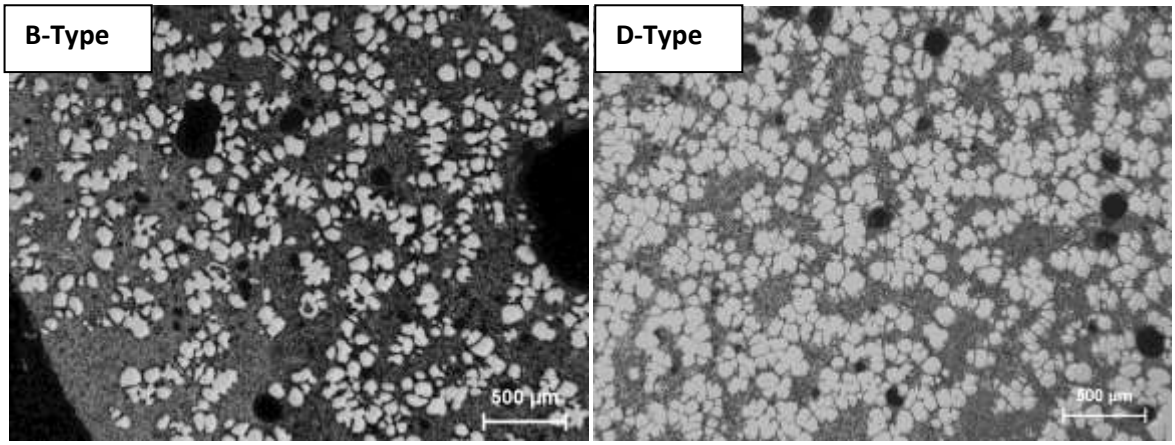

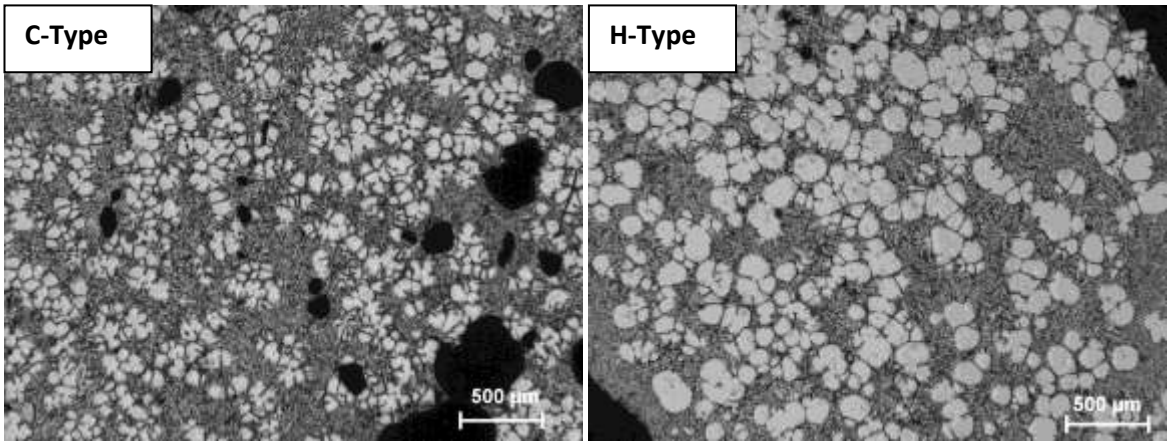

Figure 5.4: Microstructures of AA5356 obtained from different stirring mechanisms

It is observed in Figure 5.5 that the contiguity factor does not show much variance and it can be assumed that sufficient shearing can be reached using either stirrer. It is seen that the B-type mechanism produces a structure that is free of dendrites and agglomerates whereas the D-type mechanism shows agglomerated and dendritic structures and the H-type shows granular and agglomerated structures. This means that even the simplest stirring mechanism as used in the funnel can effectively subdue the formation of the viscosity enhancing agglomerates due to the thixotropic nature of the slurry.

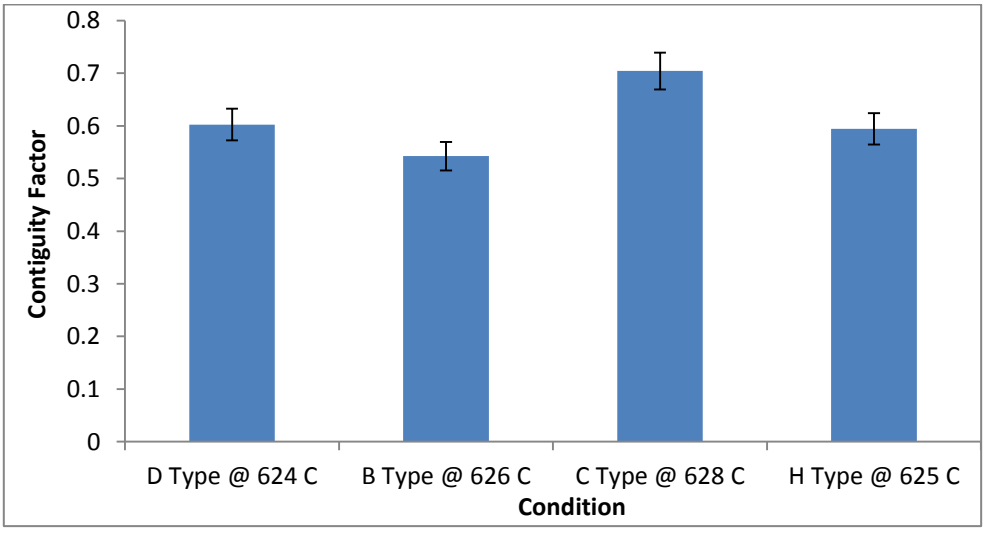

Figure 5.5: Comparison of contiguity factors of AA5356 slurry samples using different stirring mechanisms

The most common oxide in aluminium melts is observed as a bifilm and these inclusions can be local points where stress concentrations can occur. To reduce the overall presence of oxides, slurry was prepared under the atmosphere of nitrogen. Studies have shown that these dispersed oxide particles can act as potential sites for heterogeneous nucleation [Qian, 2007]. The observation of non-dendritic structures therefore signifies that the stirring mechanism may have dispersed oxide particles throughout the melt evenly.

Based on the results presented in Figure 5.5 the H-type mixer was chosen for the purposes of the slurry making. Figure 5.6 compares micrographs obtained from AZ91D slurry hand mixed and sheared using the H-type mixer at 585°C.

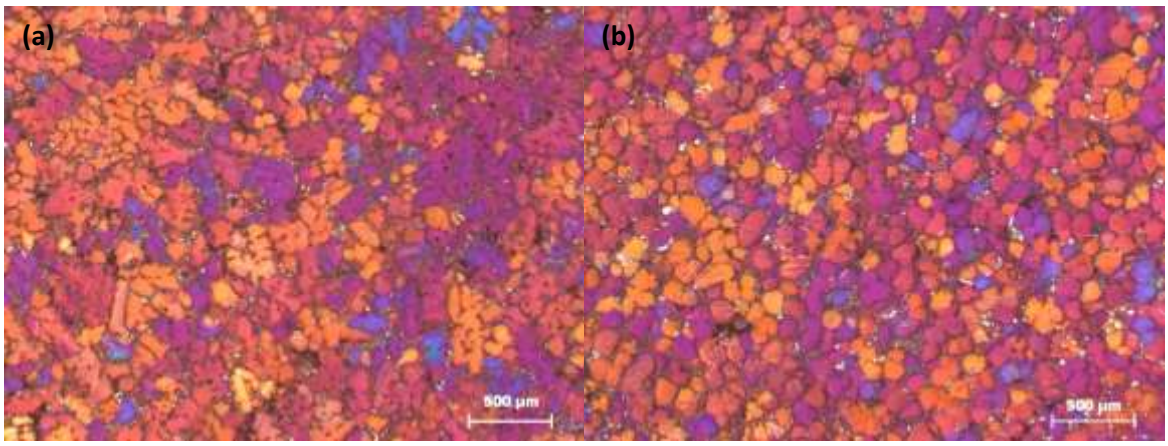

Figure 5.6: AZ91D slurry at 585°C (a) Hand mixed (b) Sheared using a H-type mixer

It can be seen that the primary particles in the slurry sheared at 585°C are globular and equiaxed in morphology whereas the primary particles observed in hand mixed slurry display characteristic dendritic structures. The validation of the C-type mixer for feeding slurry into the extruder has been detailed in Chapter 6 using AA5356.

The dependence of the shape factor on the slurry temperature was studied using AZ91D. The shape factor (*F*) equals to 1 for a perfect spherical structure. For the AZ91D slurries quenched at different temperatures (*F*) was measured about 0.6 at 597ºC and increased steadily with decreasing temperature reaching a value 0.73 at 580ºC. This is detailed in Figure 5.7. Analysis revealed that the value of the contiguity factor was in the range 0.35–0.45 and independent of the temperature indicating there was only limited particle agglomeration. The average error was found to be 0.016.

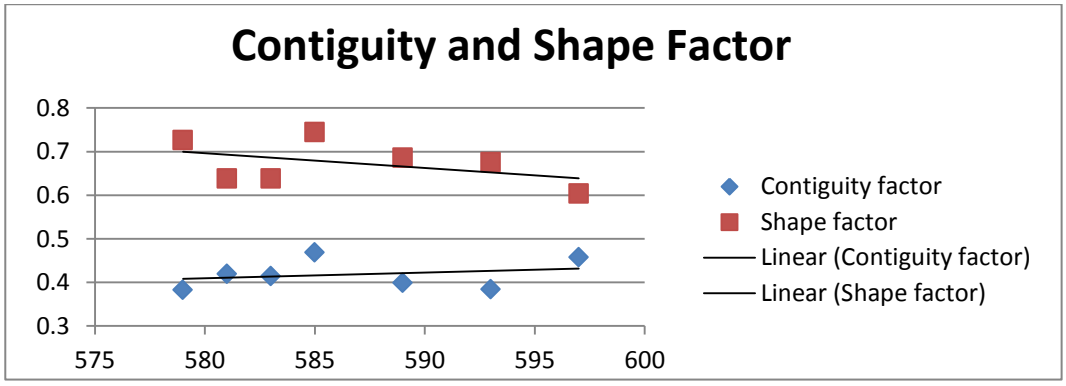

Figure 5.7: Dependence of shape factor on temperature in AZ91D slurry

It is observed that the particle density per unit area of quenched AZ91D slurry samples increases almost linearly as the processing temperature is lowered. It can also be observed that the particle size in the slurry develops quickly from 597ºC to 593ºC and then stays roughly at a constant level with decreasing temperature. These results are looked at more in detail in Figure 5.21. Since decreasing slurry temperature will increase the time for slurry processing and consequently for the solidified particles to grow, the constant particle size suggests that the convection offered by the mixing prevented the solidified particles from extensive growth, although the mechanisms are not clear.

5.2 Twin-Screw Rheoextrusion

Rheoextruded bars of metal produced by the twin-screw extruder had smooth surfaces, and bars of up to 10m were produced continuously. On observation of the microstructure in Figure 5.8, a typical microstructure obtained, it is seen that the samples had a fine uniform and more importantly non-dendritic microstructure in both the cross-section and longitudinal section. Unlike conventional extrudates, no inhomogenities in microstructures such as obvious grain size or morphological fluctuations were observed. Samples from different positions along the extrusion direction showed a reliable consistency of properties. Studies were conducted using magnesium alloy AZ91D primarily.

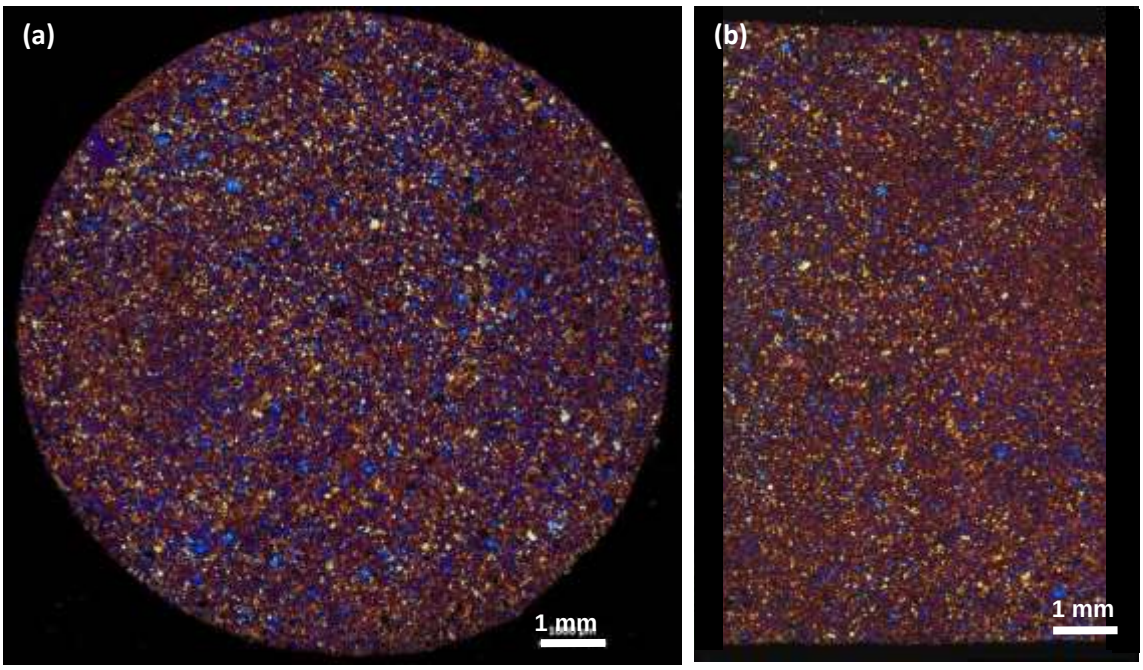

Figure 5.8: Uniform microstructure of rheoextruded AZ91D bar in both (a) transverse and (b) longitudinal sections. Extruder chamber temperature was 545^{o}C, screw rotating speed 150rpm and liquid was feed at 610^{o}C.

It has been theorised that in as-cast structures the process starts by the nucleation of primary α-phase magnesium below the liquidus. This primary phase magnesium can be said to have a dendritic structure with six-fold symmetry. Factors such as cooling conditions, composition and sites for heterogeneous nucleation are important in controlling grain size in the process. Furthermore work by Ohno et al. [2006] suggests that at 642°C the formation of intermetallic compound Al_8Mn_5 act as sites for nucleation of the primary magnesium along with the dispersed oxide.

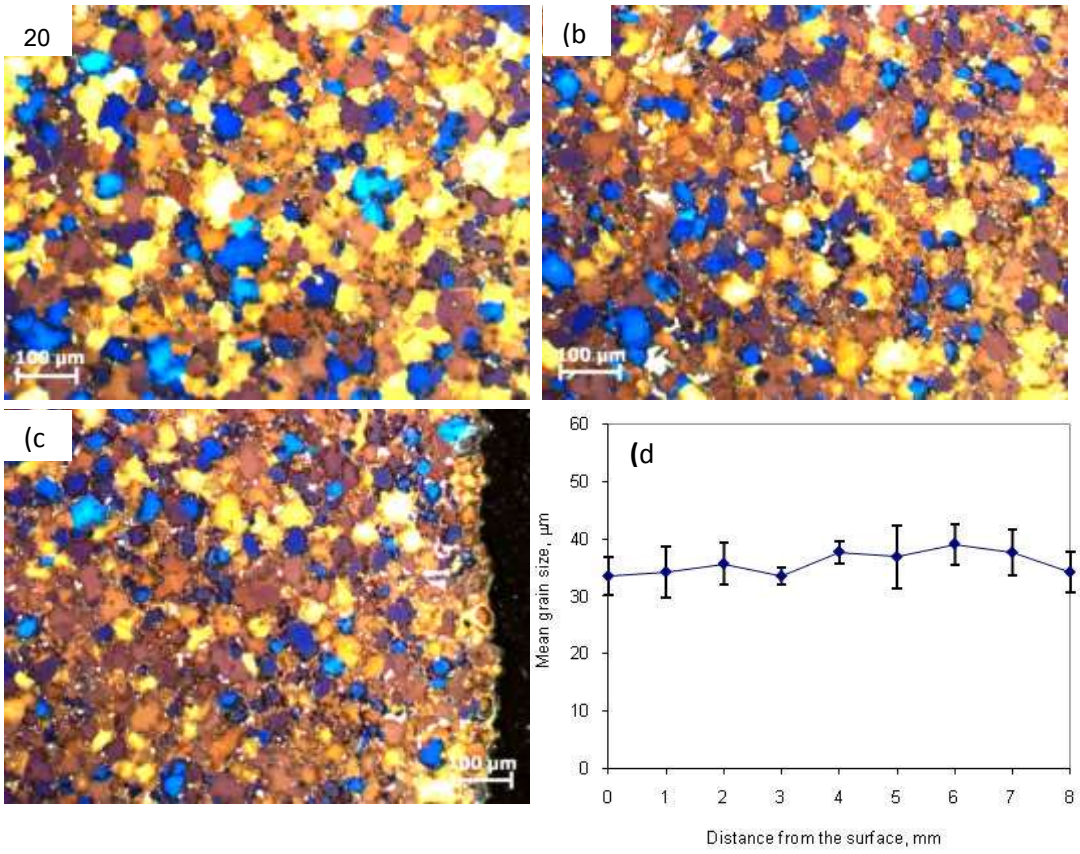

Figure 5.9: Microstructural uniformity of rheoextruded AZ91D alloy compared from (a) centre, (b) ½ radius and (c) edge. The barrel temperature was 525°C; screw rotating speed 180rpm and liquid was fed at 625°C. **(d)** Uniformly fine grain size distribution along diametric direction in rheoextruded AZ91D

Figure 5.9 shows the typical microstructure at different positions from the centre sample of rheoextruded AZ91D displaying a uniform distributed microstructure across the radius with a grain size of around 30-40μm. This is significantly lower than as cast AZ91D which has a grain size of approximately 600μm. There was no significant fluctuation from the edge to the centre which suggests a very even and uniform grain size distribution.

Compared to conventional casting where overheated liquid is poured into a cool mould and heterogeneous nucleation only occurs at the mould walls and the nuclei survival rate is low resulting in coarse uneven microstructures it can clearly be seen that the nuclei survival rate is much higher contributing to the final microstructure.

This can be accredited to the uniform temperature and composition through the volume of the alloy arising from turbulent mixing forces offered by the process that also help to disperse heterogeneous nucleation sites resulting in more effective nucleation. This is discussed more in detail in Section 7.1.

The microstructure is affected by different process parameters. These are detailed below in Section 5.2.1.

5.2.1 Effect of process parameters on the microstructural evolution

a) Screw speed

While keeping both the pouring temperature and barrel temperature constant the screw speed was varied from 125rpm to 150rpm. Figure 5.10 compares the resultant microstructures. The Pouring temperature was set at 610ºC and the barrel temperature was set at 548ºC.

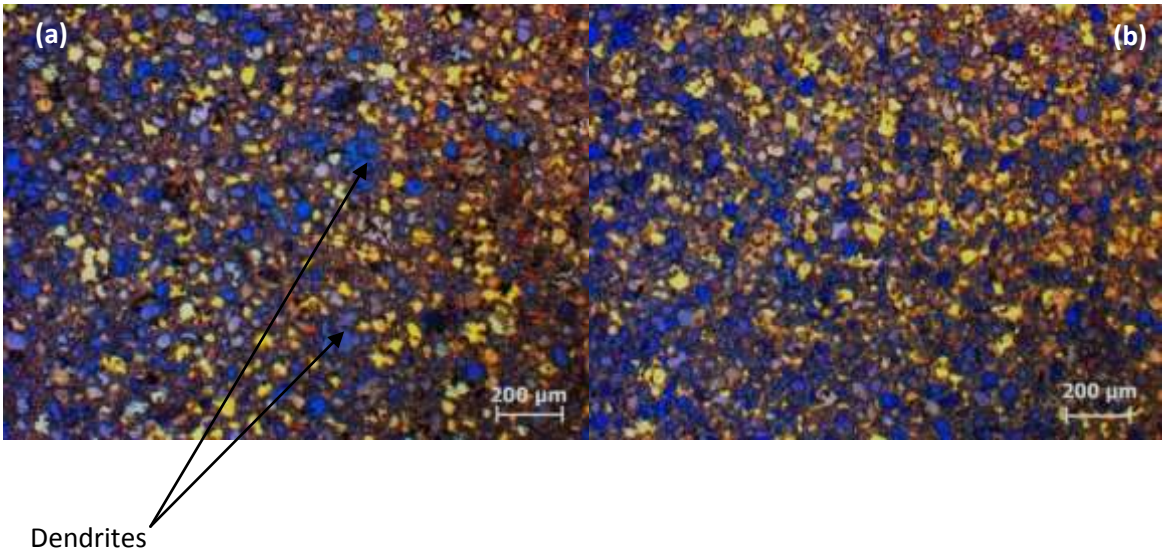

Figure 5.10: Comparison of different screw speed (a) 125rpm (b) 150rpm

From the evolution of the microstructure it can be observed that the α-Magnesium grain structure becomes more equiaxed, refined and compacted. This is because shear rate and pumping force are both directly proportional to the screw speed as detailed in the literature. Since the slurry contains a limited number of dendritic particles the effect of high shear speed is thought to only improve the solute distribution leading to even primary α-magnesium grain growth. It may also cause primarily formed α-magnesium dendrites to fracture and multiply. At 150rpm the observed grain size of AZ91D was 40.3µm. At 125rpm speed minor developed dendrites and coarse grains are observed and the average grain size was measured to be 45.34µm. The refinement of the microstructure in the extruder is down to several possible mechanisms that are detailed in Section 7.1.

b) Pouring temperature

While keeping both the barrel temperature and extrusion speed constant the pouring temperature was varied from 595ºC to 640ºC. Figure 5.11 compares the resultant

microstructures. The barrel temperature was set at 548ºC and the extrusion speed was set at 150rpm.

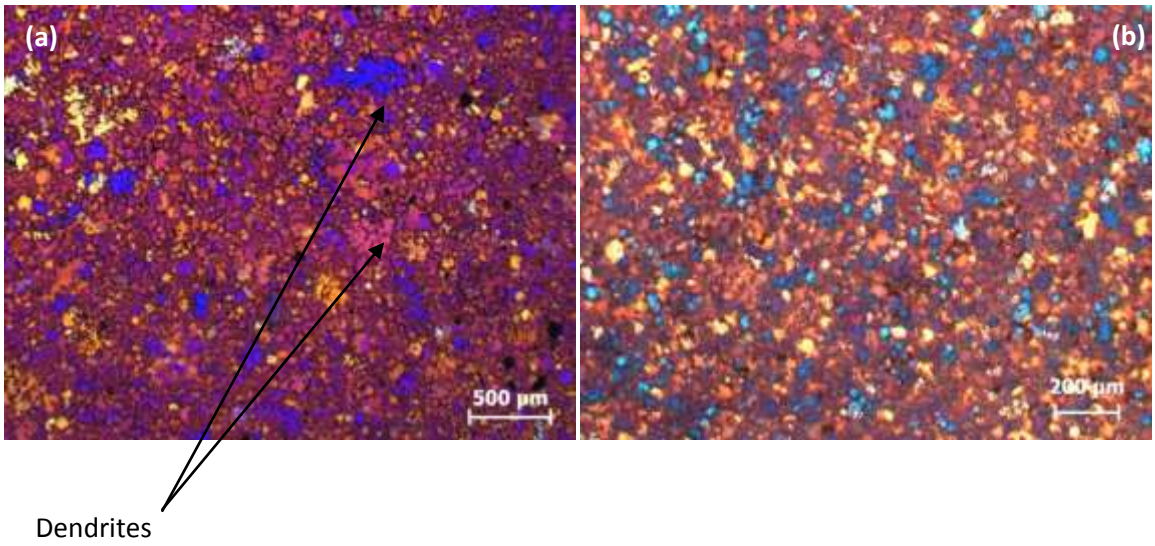

Figure 5.11: Comparison of different pouring temperature (a) 595ºC (b) 640ºC

From the evolution of the microstructure it can be seen that lower pouring temperature can lead to more primary α-magnesium dendrites developing. This can occur because the grains that have already nucleated and slightly developed in the slurry before feeding can be transported down the barrel and develop into larger α-magnesium dendrites. At 595ºC the grain size of α-magnesium was measured to be 76.2µm. This is because the nature of the flow within the extruder is more pressure and transport oriented rather than shearing as in the case of co-rotating screw systems which has limited transport features.

Alternatively, it was observed that higher pouring temperatures cause coarse primary α-magnesium grains with fewer size variations to develop. This is because more nucleation starts within a high shear environment resulting in more spherical primary α-magnesium grains. The grain size corresponding to a pouring temperature of 640ºC was 39.5µm.

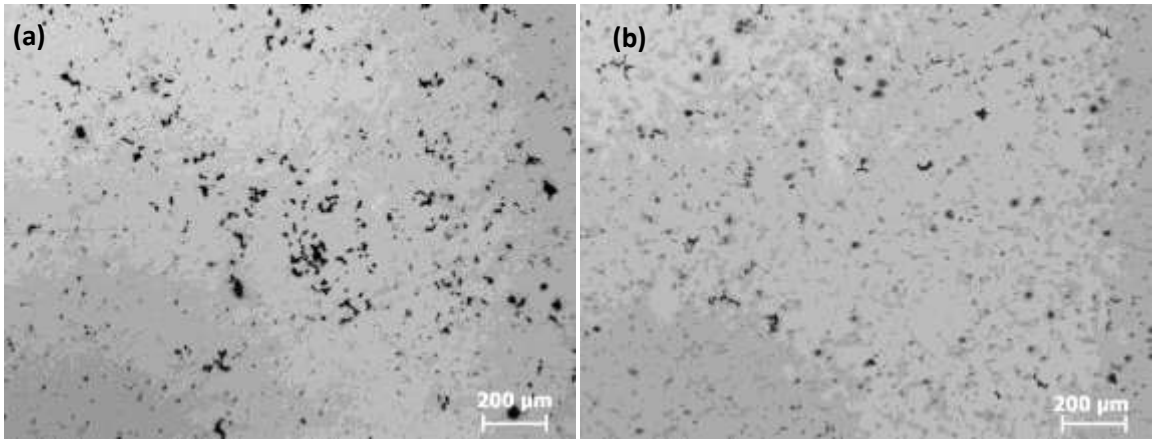

Figure 5.12: Segregation observed at different pouring temperatures (a) 640ºC and (b) 595ºC

It was also observed that porosity is increased at higher pouring temperatures as seen in Figure 5.12 by macrosegregation and shrinkage. This is due to a higher fraction of liquid phase that can be squeezed out of the skeleton of formed solid phase as flight gap leakage due to the pressure built up in the extruder as detailed in the literature[Jansen 1978]. It is therefore deduced to keep the pouring temperature to a minimum to reduce this and incorporate a shearing of the slurry before pouring.

c) Barrel temperature

Finally while keeping the pouring temperature and the extrusion speed constant the barrel temperature was varied from 545ºC to 554ºC. Figure 5.13 compares the resultant microstructures. The pouring temperature was set at 610ºC and the extrusion speed was set at 150rpm.

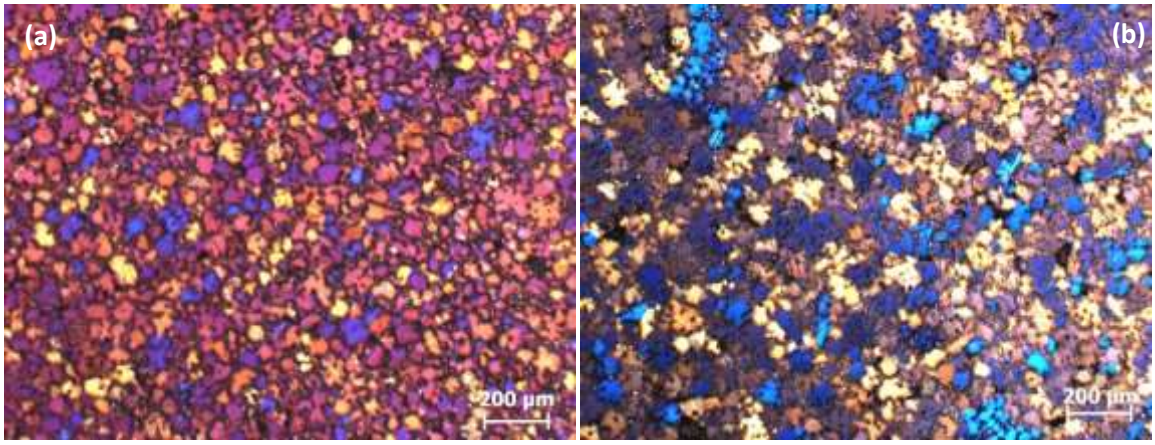

Figure 5.13: Comparison of different barrel temperatures (a) 545ºC (b) 554ºC

At a higher barrel temperature larger but more dendritic α-magnesium grains are observed as the shear effect is reduced due to the high temperature. Since shear stress is directly linked to viscosity and thus temperature, solidification taking place under convection at lower temperatures is more likely to produce spherical particles of primary α-magnesium.

Reducing the chamber temperature also makes primary α-magnesium dendrites more brittle and susceptible to plastic deformation and fragmentation mechanisms.

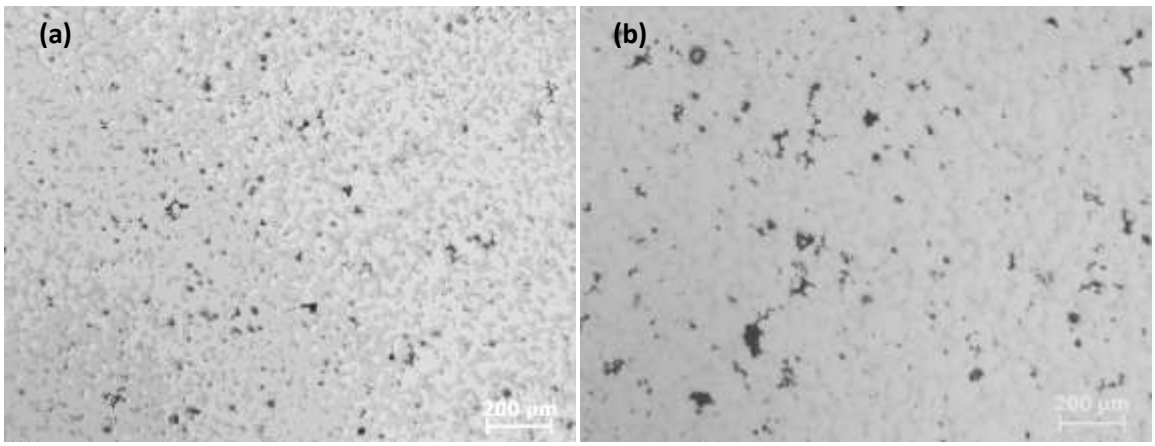

Figure 5.14: Segregation observed at different barrel temperatures (a) 545ºC (b) 554ºC

Figure 5.14 shows that porosity is also observed to increase with the barrel temperature by mechanisms of shrinkage and macrosegregation as there is a higher fraction of available liquid phase that can be squeezed back through gaps in the metal solid skeleton and back into the flight gap as leakage flow as is suggested by the literature. [Jansen 1978].

d) Establishing a stable process temperature to model a continuous process

For the extrusion process to be successful it is necessary that the extruded bar holds its shape in air and under water cooling. This requires a fraction of solid to be present that can form a skeletal structure. Primary studies showed that feeding at a pouring temperature below 590ºC for AZ91D was not feasible as the resultant bar was not smooth due to increased viscosity and entrapped air. However for an isothermal process, if the barrel temperature was also set at this, the solid fraction at this temperature was not sufficient for the strand to hold its shape. To counter this the barrel temperature was set at a temperature lower than the minimal pouring temperature so that the slurry could reach a more desirable solid fraction once inside the extruder. The problem of having a large difference between the pouring temperature and the barrel temperature is the ever changing temperature of the slurry exiting the die. This change in temperature leads to uneven properties along the axis of the extruded bar. This can be seen in Figure 5.15 where samples were taken at different cross-sections of the extruded rod. The evolution of the microstructure clearly shows a morphological change in the primary α-magnesium and its quantity and higher intermetallic phase at the end of the rod compared to a sample obtained approximately 2m in front of it. This suggests that the temperature of the slurry is still changing and is lower at the beginning of the extrusion as there is significantly less primarily solidified alpha

phase. The specimen was extruded at 544°C, fed at 592°C and the screw speed was 150rpm.

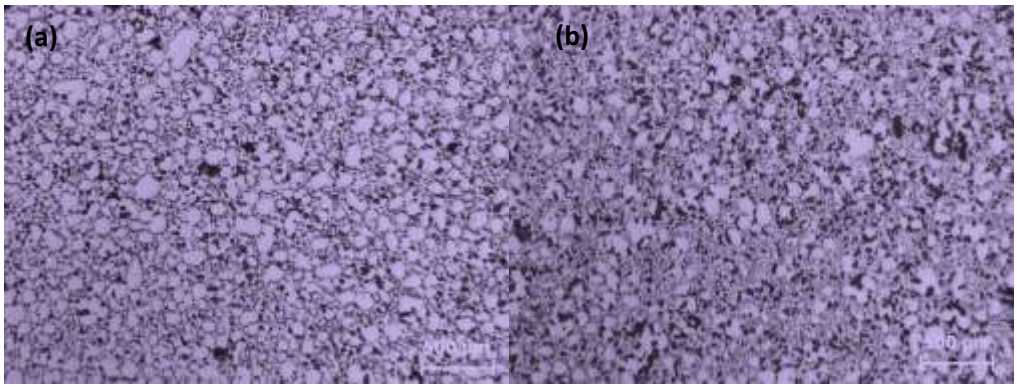

Figure 5.15: Uneven microstructure obtained between (a) Start of the rod (b) at 2m from specimen in 5.15a

Therefore it was deemed that the extruder may not be capable of transferring all the heat from the slurry to the barrel to achieve equilibrium during the narrow window transport process. To achieve a stable process and even microstructure it was important to model a steady condition to understand and develop the process further. The heat transfer is discussed and quantified in Chapter 6.

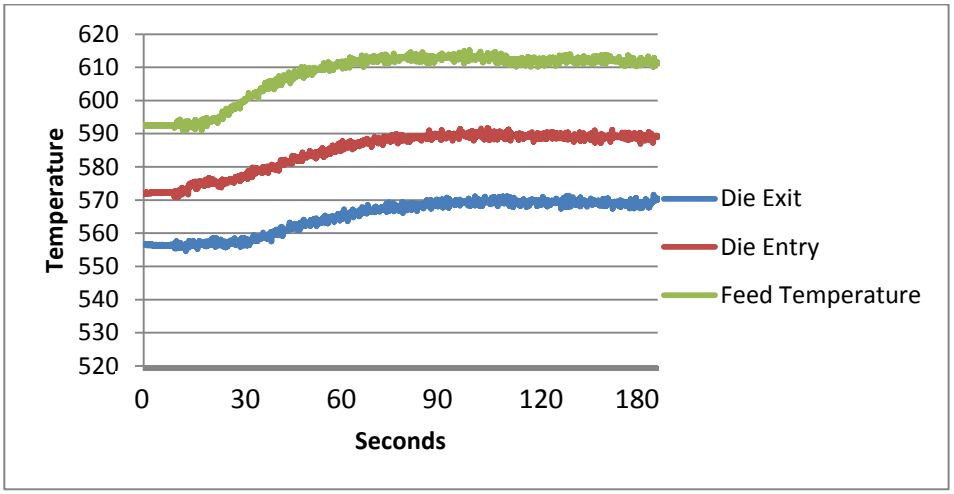

Figure 5.16: Measured temperature rise of the magnesium extruder parts while extruding AZ91D

To determine a barrel temperature setting at which the melt entering the die would have a stable temperature at the die, i.e. heat transfer was sufficiently quick in the time it takes the slurry to move down the barrel, a die with inserted thermocouple sensors was used. It was found that if an AZ91D melt in the vicinity of 610ºC was fed into the magnesium rheoextruder set at 575ºC with the die exit temperature set at 560ºC the temperature of the melt on reaching the die exit would be closer to the desirable steady state at 570ºC corresponding to a solid fraction of 0.5. Figure 5.16 shows that significant temperature changes took place within the first minute but evened out although a steady state temperature would take much longer to be established.

Temperatures around this base standard were used in optimising processing condition settings to study extrusions at various processing temperatures and designing and optimising the water cooling system. Parameters defined are given in Table 5.1.

Table 5.1: Established parameters for steady state and water cooling experiments

Experiment Type	Barrel Temperature (ºC)	Pouring Temperature (ºC)	Motor Speed (RPM)
Water cooling design tests	580	590	150 (50Hz)
Steady state rheoextrusion	560–580	590–610	150 (70Hz)

It should be noted that the parameters of pouring temperature and extrusion speed were limited between this narrow range due to experimental constraints. The interdependence of these parameters can be further explored and are in need of optimising. Microstructures of samples obtained at various steady state conditions have been detailed in Section 5.2.2.

5.2.2 Microstructure evolution under steady state

a) Longitudinal and transverse cross-section analysis

It is observed that the microstructures consisted mainly of globular primary α-Mg particles embedded in a well dispersed secondarily solidified dendritic network with consistent properties along both the longitudinal and transverse cross-sections. This can be seen in Figure 5.17. The α-Mg particles were measured to have an average shape factor of 0.87. The high value of the shape factor suggests that solidification has taken place under intensive turbulence thereby promoting the formation of near-spherical structures which is in accordance with work done by Ji and Fan [2002].

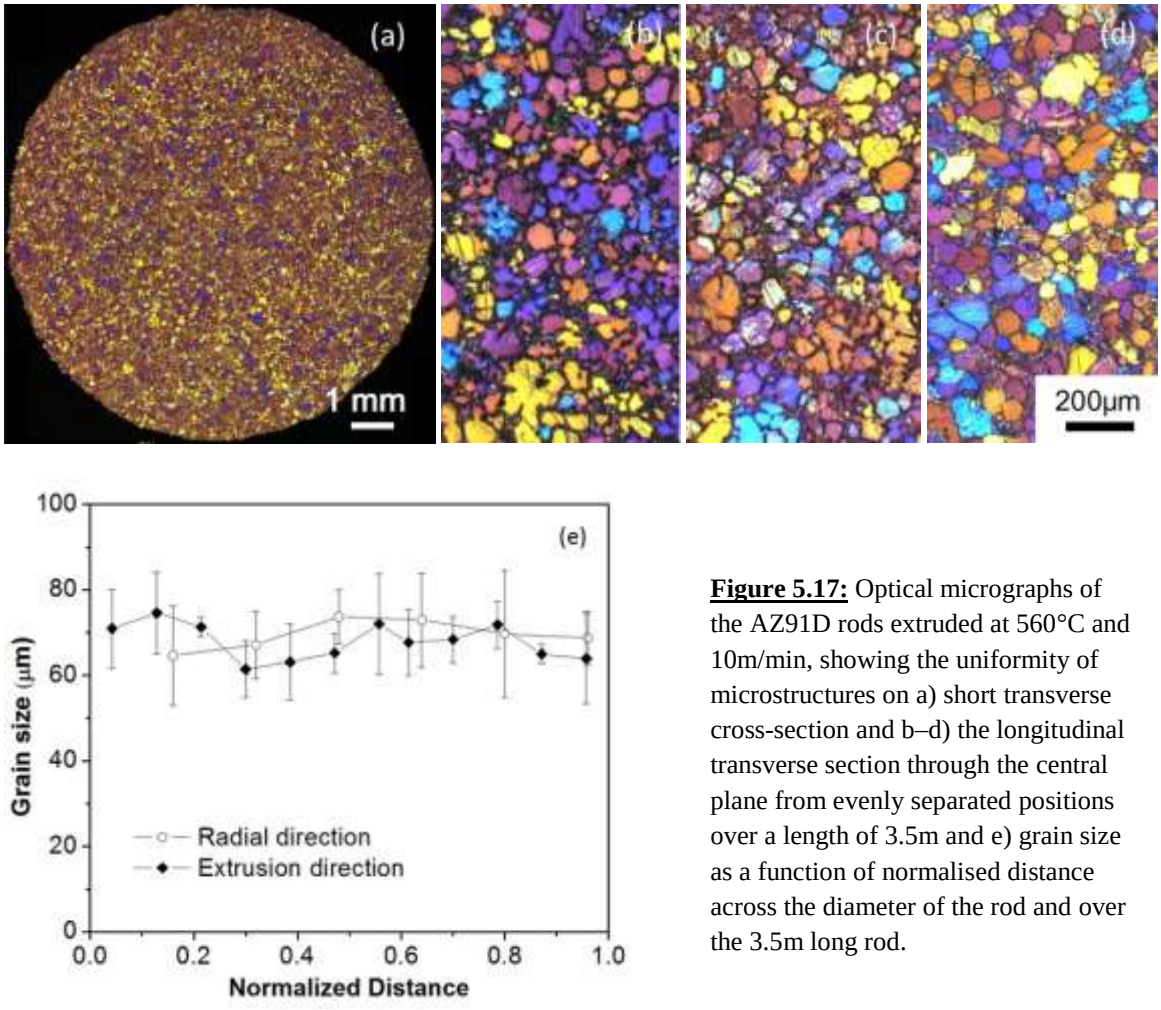

Figure 5.17: Optical micrographs of the AZ91D rods extruded at 560°C and 10m/min, showing the uniformity of microstructures on a) short transverse cross-section and b–d) the longitudinal transverse section through the central plane from evenly separated positions over a length of 3.5m and e) grain size as a function of normalised distance across the diameter of the rod and over the 3.5m long rod.

b) Effect of isothermal process temperature

Figure 5.18 compares micrographs obtained of samples extruded at different temperatures. It is observed that evenly sized primary α-magnesium particles are equiaxed and are embedded in a network of secondarily solidified eutectic phase. It can be seen that as the extrusion temperature decreases, the primary grain size is seen to decrease; whereas the shape and uniformity of the primary α-magnesium can be observed to be more or less constant. The mechanisms and development of non-dendritic solidified structures will bediscussed in Section 7.1.

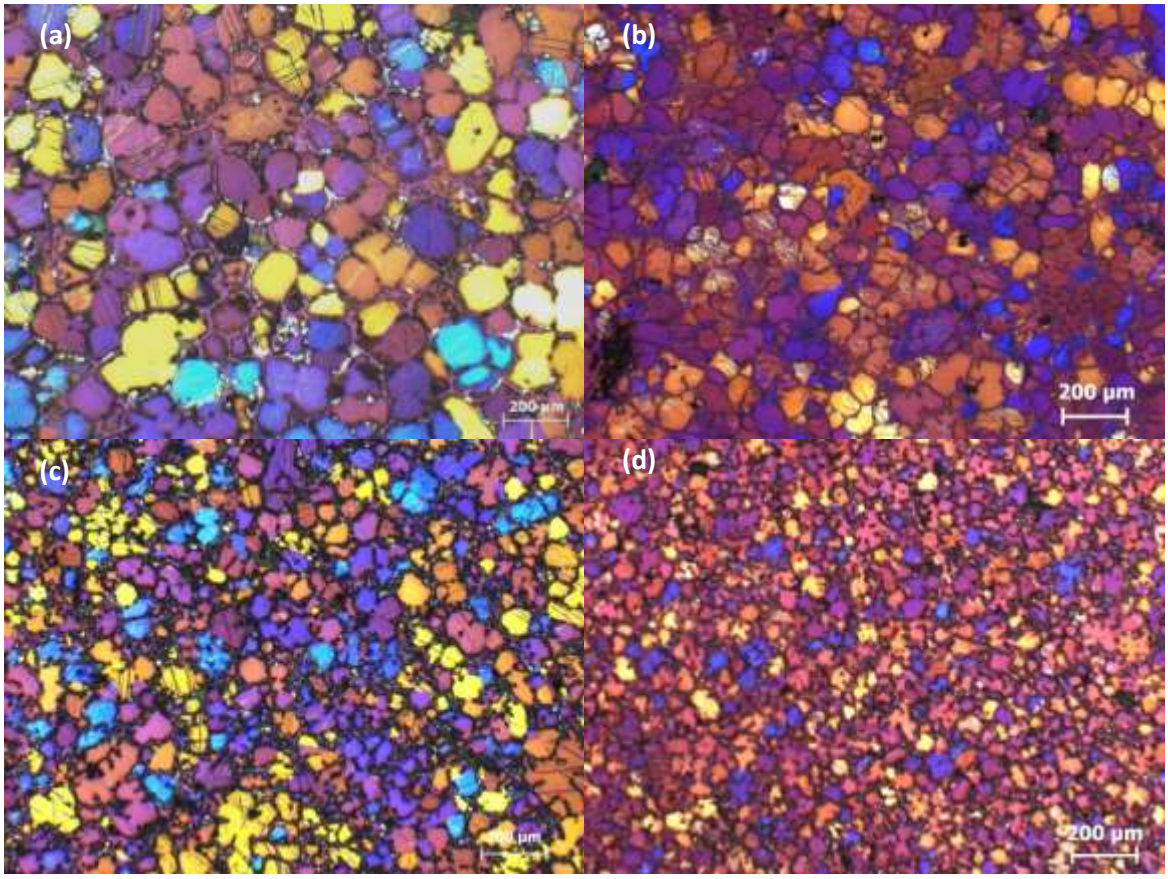

Figure 5.18: Comparison of microstructures at steady state extrusions of AZ91D obtained at a barrel temperature (a) 585ºC (b) 575ºC (c) 560ºC (d) 545°C with a fixed pouring temperature of 610ºC and motor speed of 150rpm

With the AZ91D it was observed that the primary phase grain size reduced gradually along with the decrease in extrusion temperature and there seemed to be a turning point at 560ºC beyond which the grain size reduced at a higher rate. At 545ºC an average alpha particle size of 35μm was obtained which is considerably smaller than reported values for microstructures obtained in semisolid processing of the same material such as thixo moulding done by Czerwinski et al.[2001;2004] and Zhang et al. [2009], rheo die casting done by Fan and Liu [2005] and isothermal holding experiments conducted by Wang et al. [2008].

c) Cooling rate

The cooling rate was observed to play a significant role in the formation of the microstructure. In Figure 5.19 it is observed that when the rod was air cooled the primary grains continued to grow in a spherical shape with very little intermetallic in the intergranular space. However on quenching, the microstructure at elevated temperature is retained and shows smaller grains with a partially dendritic morphology embedded in a thick intermetallic. This suggests that the entire solidification process is not completed in the narrow time window during transport in the barrel and the high cooling rate offered by quenching with the cooling system during final solidification causes the grains to develop slightly dendritically. This suggests that further work needs to be done to optimise the cooling rate and solidification time for the process. Furthermore air-cooling requires a high solid fraction so the slurry can hold its shape on extrusion. This is currently unachievable due to the limitations of the motor.

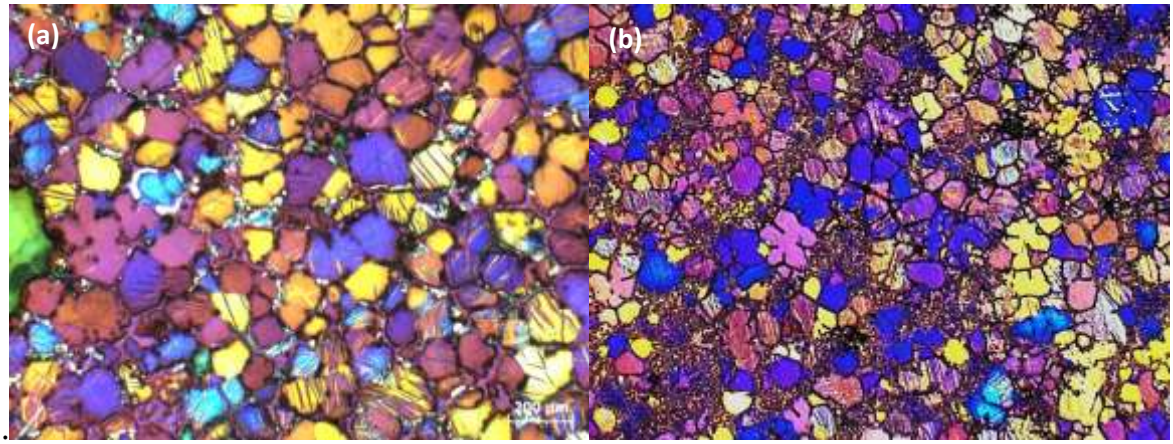

Figure 5.19: Rod extruded at 580°C (a) Air cooled (b) Quenched using BCWR

d) Slurry shearing

It was observed that preconditioning a melt with additional shearing significantly altered the microstructure of the extruded bar. In samples where preconditioning of the slurry was not done, dendritic structures of primary α-magnesium were observed as seen in Figure 5.20(a). On preconditioning the melt more equiaxed primary α-magnesium grains are observed as seen in Figure 5.20(b).

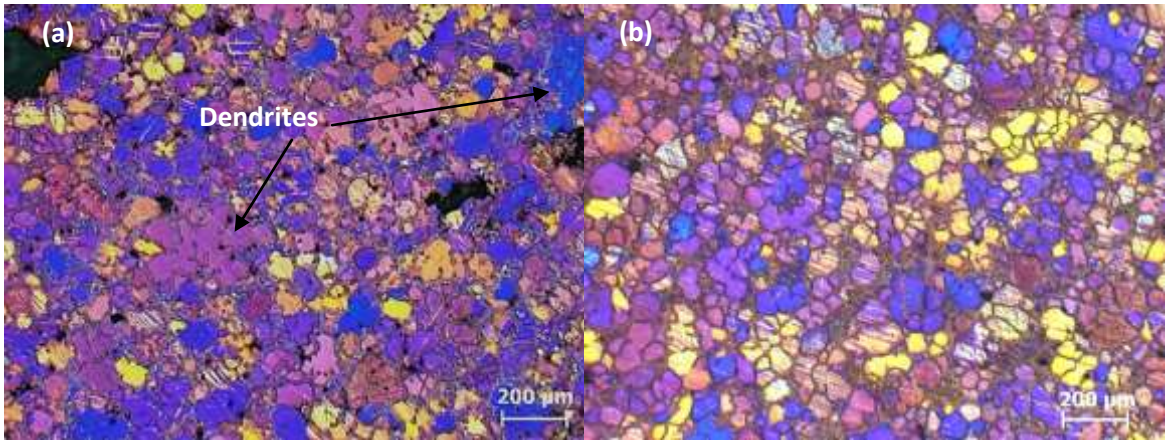

Figure 5.20: AZ91D extruded at barrel temperature 565ºC (a) without shear and (b) with shear

It is known that the shear offered by the flow mechanisms of the twin-screw extruder also offer some level of grain refinement and non-dendritic formation. The mechanism for this refinement is detailed in Section 7.1. Furthermore it can be seen that the additional shear suppresses the formation of the intermetallic β-$Mg_{17}Al_{12}$ by distributing the solute. This is seen in Figure 5.20. When compared to the slurry prepared at the same temperature it is observed that the average size of the primary phase is clearly smaller confirming that the shear offered by the twin-screw extrusion process clearly creates a grain refining effect and this is quantified in Figure 5.21(a).

The parameters obtained from the results of the grain size and grain density per unit area of slurry samples and extruded rods processed at different temperatures were compared quantitatively to observe the microstructural development at different processing conditions. The results are presented in Figure 5.21.

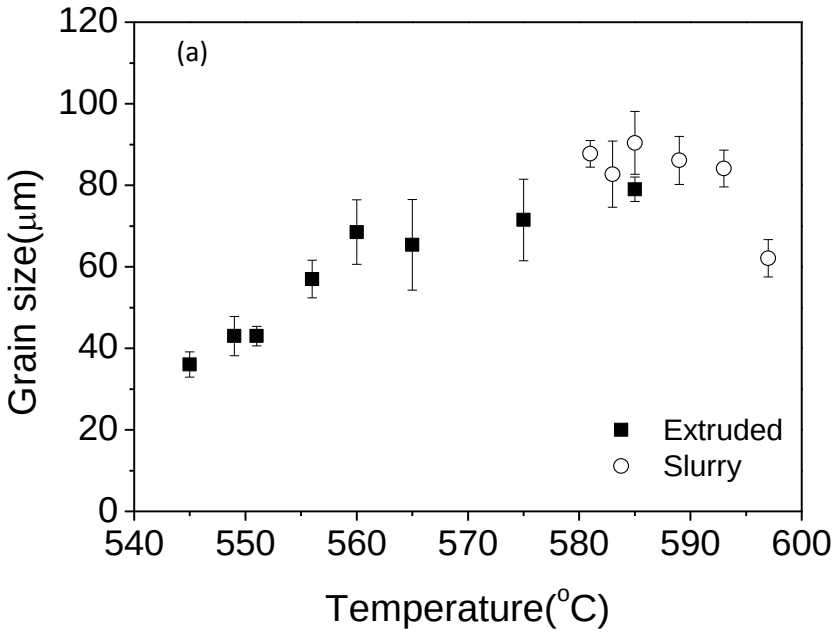

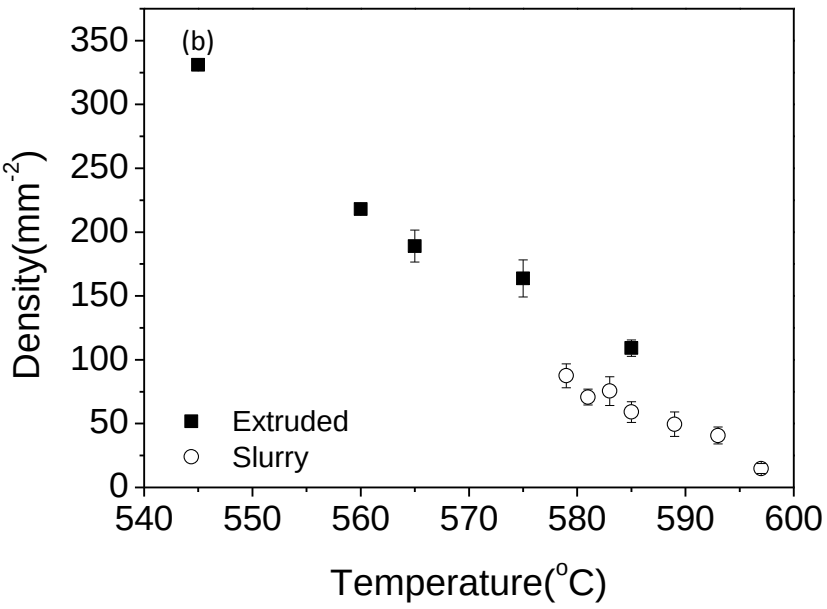

Figure 5.21: Microstructural parameters of the AZ91D slurry and extrusion as a function of extrusion temperature: a) primary particle size, b) density

e) Deformation of grains

Twins and dislocation cells were observed in some extruded AZ91 samples even after a level of dynamic recovery had taken place due to working at semisolid temperatures. This indicates that grain size refinement at lower temperatures could be because of plastic deformation.

During the final stages of the extrusion process, slurry with a higher fraction is fully compacted in the die chamber and squeezed through a narrow die opening, where primary particles could have coordinated with each other by grain boundary sliding or deformation.

It is observed in Figure 5.22 that at lower extrusion temperatures plastic deformation occurs by twinning and dislocation slip that split orientation of grains which may explain the faster decrease in grain size between 560ºC and 545ºC. However the plastic

deformation is more than likely limited as there is no significant change in particle shape in response to deformation across the range of extrusion temperature.

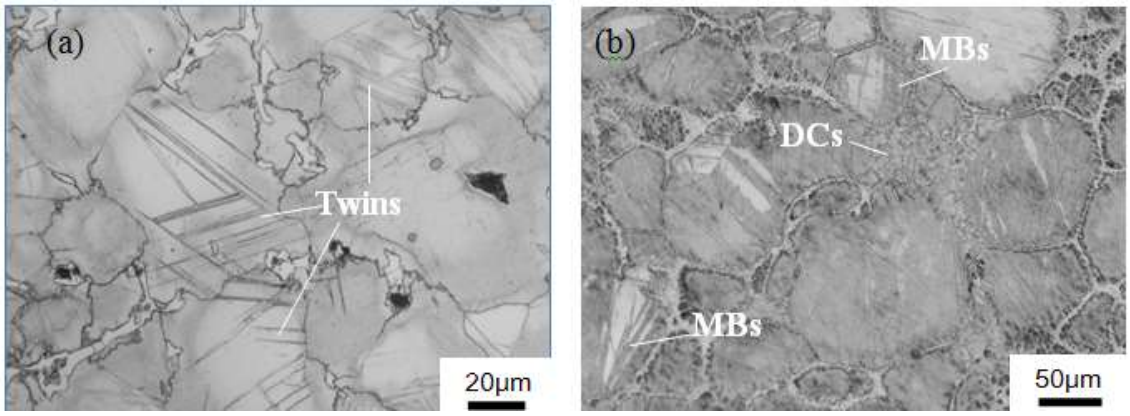

Figure 5.22: Optical micrographs of the extruded AZ91D rods, showing features of plastic deformation at barrel temperatures of a) 560°C and b) 545°C.

Figure 5.22 shows that in AZ91D for higher temperatures the main evidence of deformation are twins where as at lower temperatures dislocation cells (DC) and micro bands (MB) are also present. In addition to this, shear bands cutting through more than one primary phase particle were not observed indicating that the deformation only occurred due to local stresses.

The microstructure of rheoextruded AZ91D alloys therefore reveals both, high temperature deformation characters as well as a smooth spherical semisolid character with continuously thin eutectic films [Spencer et al., 1972].

f) Eutectics

At 431°C the eutectic phase formation of Mg-$Mg_{17}Al_{12}$ is observed [Dahle et al., 2001]. It is believed that the formation of this phase occurs when the aluminium content is around 13wt%, although it has been observed that in non-equilibrium cooling conditions the eutectic phase can even occur in alloys containing only 2wt% Aluminium [Polmear, 2006]. Figure 5.23 compares micrographs of structures obtained at different temperatures for AZ91D extrusions.

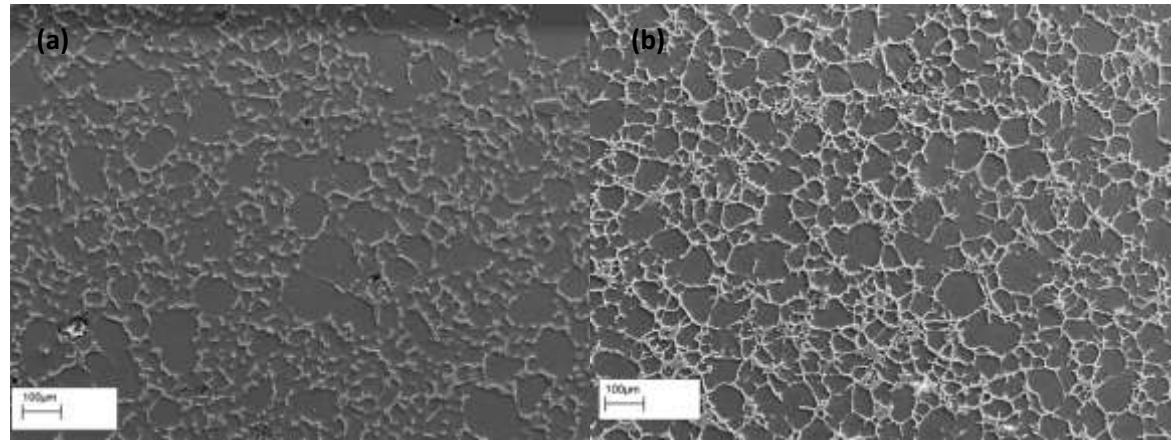

Figure 5.23: Optical micrographs showing a thick continuous intermetallic network for a sample obtained at a barrel temperature of (a) 545ºC for AZ91D compared to a thin and broken intermetallic as obtained at a barrel temperature of (b) 575ºC (c) Quantified qualitative rise of intermetallic phase with respect to process temperature extracted from micrographs of samples taken at 20X

It can be seen from the micrographs that at higher processing temperatures the intermetallic phase formed by secondary solidification at the grain boundary has a higher volume fraction and is thick and relatively consistent whereas the thinning of the intermetallic networks can be observed as the extrusion temperature is decreased. This is because as process temperature is increased more liquid phase is squeezed in between the primarily formed alpha particles and this microstructure is retained after cooling.

Higher magnification of the samples reveals the evolution of the morphology of the eutectic structure as the process temperature is increased. In the sample obtained at 550°C a fully divorced eutectic morphology consisting of totally divided phases with a single β-phase $Mg_{17}Al_{12}$ particles surrounded being by eutectic α-magnesium is observed. This is seen in Figure 5.24(a). At a higher processing temperature of 580°C partially divorced structures are seen as observed in Figure 5.24(b).

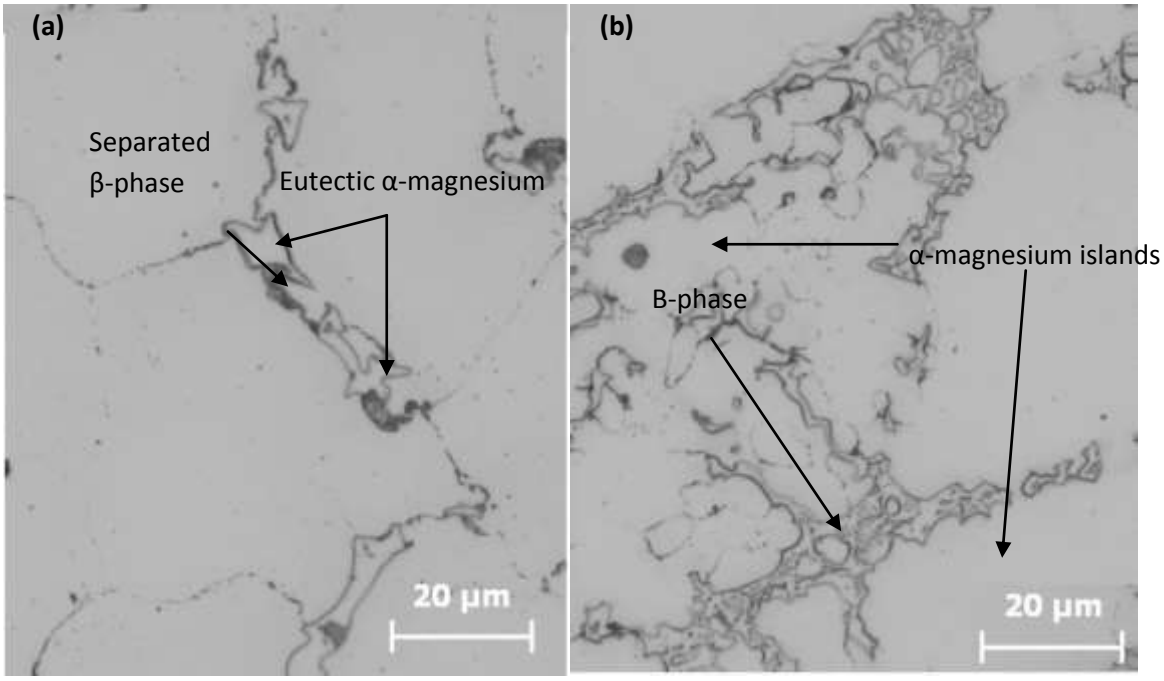

Figure 5.24: Detail observation of intermetallic morphology (a) 550°C (b) 580°C

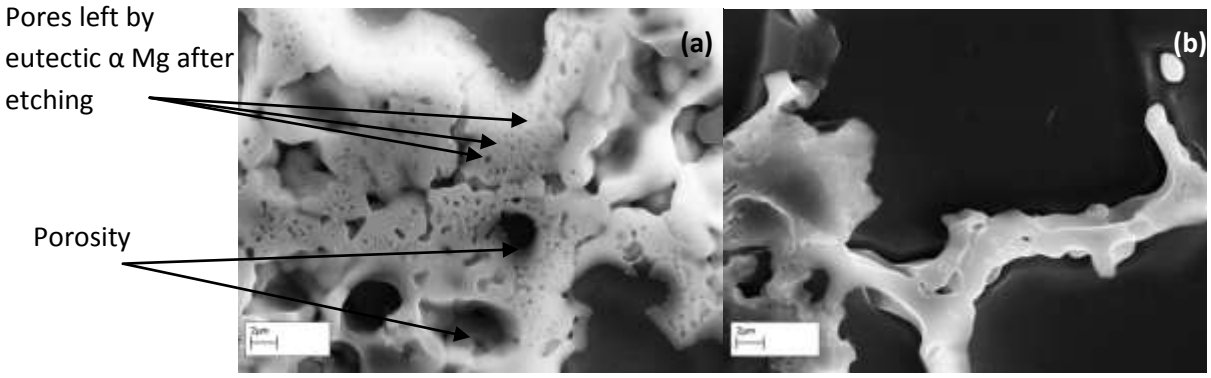

Figure 5.25: Structure of eutectic in (a) Large cell displaying porosity obtained at 560°C (b) Tiny cell displaying continuity obtained at 545°C

SEM reveals that the size of the eutectic cell plays a significant part in its structure. Larger eutectic pockets from extrusions carried out at high temperatures were seen to contain microporosity whereas the structure of smaller pockets was characterised by a continuous and relatively porosity-free structure as seen in Figure 5.25. Another morphology observed in the eutectic was the formation of magnesium islands within eutectic cells as seen in Figure 5.26. The morphology of these structures was characteristically different when compared to magnesium surrounded by eutectic in partially divorced structures. The reasons for its formation are detailed in Section 7.2.

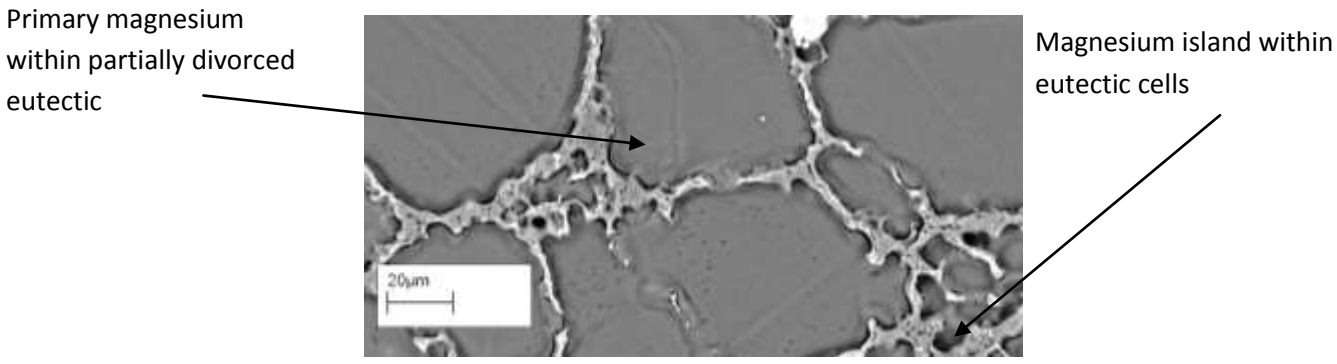

Figure 5.26: Morphological difference between in partially divorced eutectics and observed islands

g) Intermetallics

Several intermetallic structures with different morphologies were observed in the rheoextruded samples as can be seen in Figure 5.27. SEM analysis was used to analyse the composition of striking features. From Table 4.1 it can be seen that the major alloying metallic elements in AZ91D are copper and Manganese. Out of these the most prominent intermetallic structures were formed with manganese.

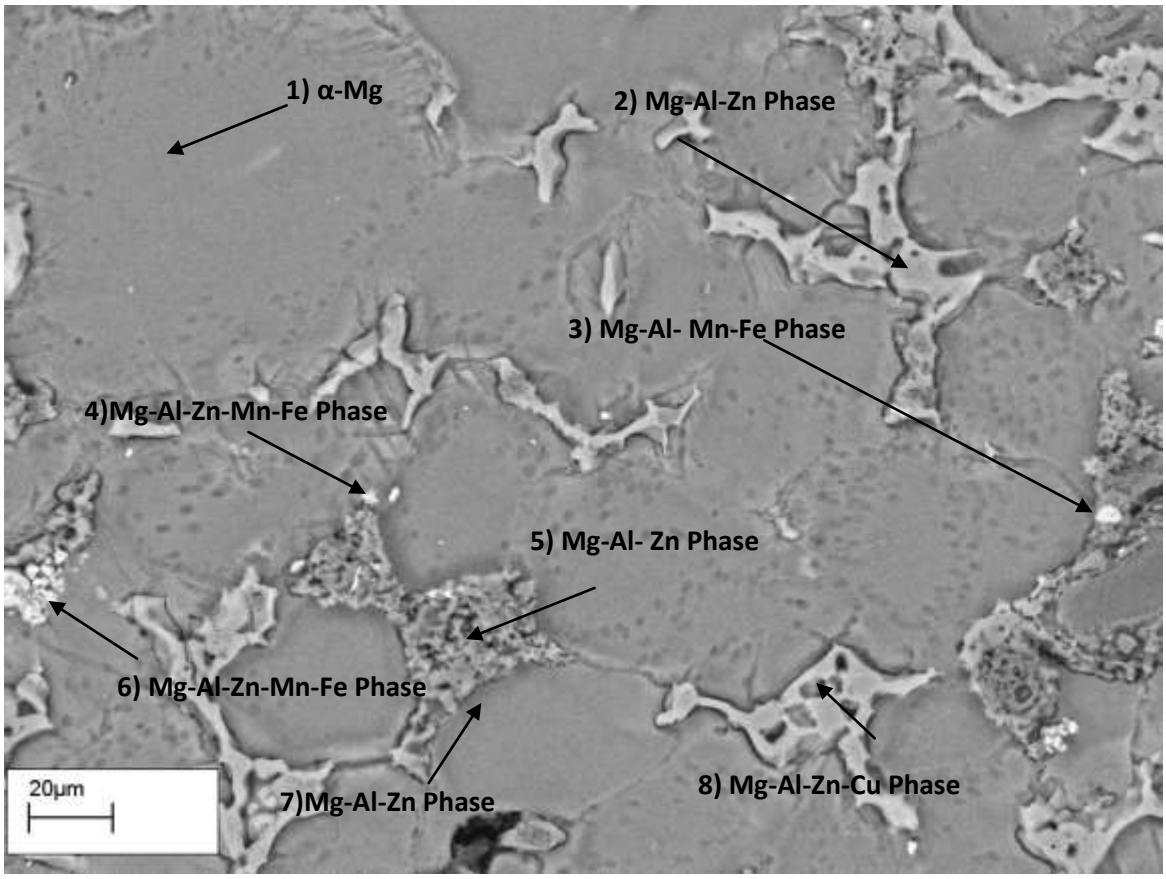

Figure 5.27: A representative area showing a variety of intermetallic structures

Iron is an impurity picked up through the extrusion process and tends to have an affinity towards manganese. The morphology of intermetallic particles with manganese is very

diverse and is dependent on its position within the alloy. Figure 5.28(a) shows larger crystals observed in the centre of primary magnesium. Due to their position and their size, these are thought to be sites upon which nucleation might have taken place as suggested by Ohno et al. [2006]. Another position at which manganese-rich intermetallic was seen to deposit was at the grain boundaries. The size of these crystals was seen to be smaller than their counterparts within the primary magnesium. This can be seen in Figure 5.28(b).

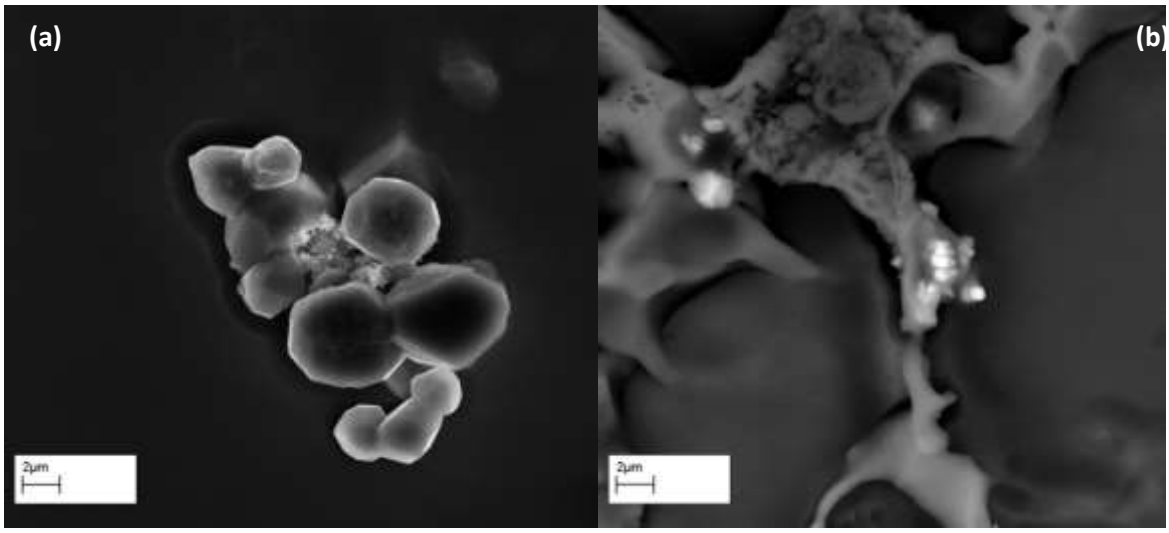

Figure 5.28: Morphology of manganese-rich intermetallic particles (a) in the centre of primary magnesium (b) at the grain boundary in samples extruded at 560°C

The finest morphology of intermetallic was observed to be evenly distributed within the eutectic with concentration at boundaries of porosity within the eutectic phase. This is detailed in Figure 5.29. It is seen that these deposits are no more than 100nm in size and therefore their composition could not be accurately determined due to beam spread. The evolution of the intermetallic is detailed more in Section 7.3.

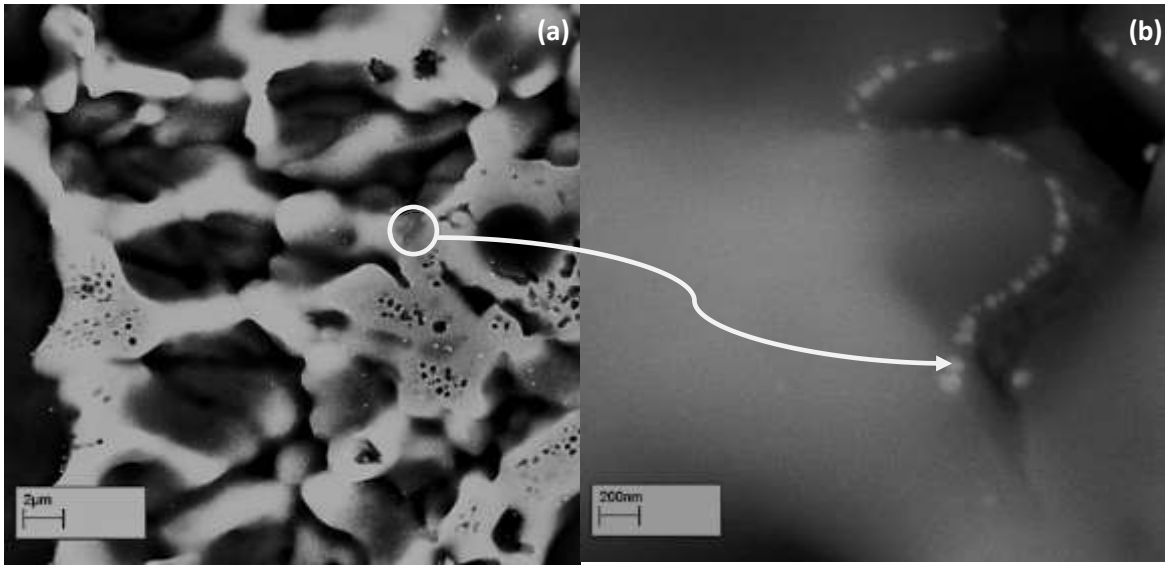

Figure 5.29: (a) Fine dispersed intermetallics observed within the eutectic in samples extruded at 560°C (b) accumulation of very fine intermetallic at boundaries of porosity within eutectic structure

5.2.3 Defects

a) Casting defects

To maximise refinement of the grain structure and the mechanical properties of the extruded bar, the lowest achievable process temperature of the extruder was explored. The pouring temperature was minimised to the lowest allowable value for each alloy as determined by the observation of the lowest workable fluidity from the slurry experiments as detailed in Section 5.1 and water flow rate and the motor speed was kept constant at 150rpm. The next section details the parameters explored using different alloys and the macroevolution of the bar

.

1) AZ91D Mg Alloy

Figure 5.30 shows bars produced over a range of extrusion temperatures keeping the pouring temperature constant at 590ºC. It can be seen that at a barrel temperature of 585ºC the rod barely holds its shape under water cooling but as the extrusion temperature decreases, the quality of the rod improves continuously. At 565ºC the rod can be said to have a good surface finish. The lowest possible temperature extrusion achieved was at 545ºC, below which it was not possible to extrude the AZ91D as the material tended to stick within the die causing the process to jam in the die assembly.

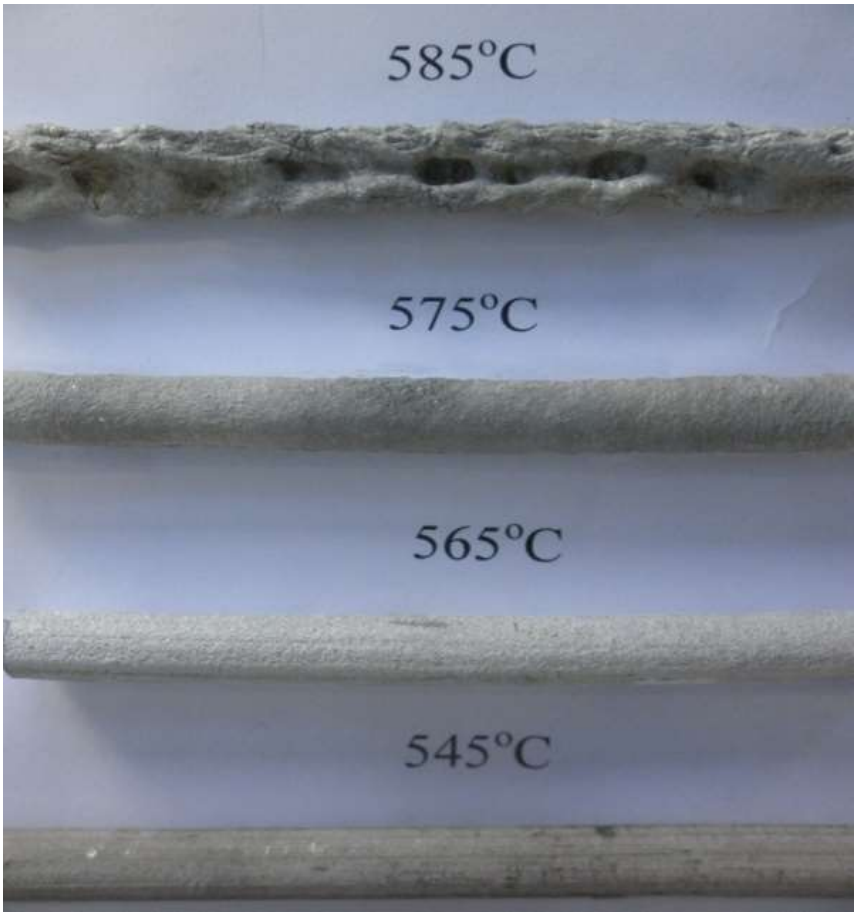

Figure 5.30: Evolution of extruded AZ91D bar at various barrel temperatures. The water flow rate was kept constant at 4.5l/min

2) LM24 Al alloy

Figure 5.31 shows bars produced over a range of extrusion temperatures keeping the pouring temperature constant at 570ºC. It can be seen that at a barrel temperature of 565ºC the rod barely holds its shape under water cooling but as the extrusion temperature decreases, the quality of the rod improves continuously. At 560ºC the rod can be said to have a good surface finish. The lowest possible temperature extrusion achieved was at 557ºC, below which it was not possible to extrude the LM24 as the material tended to stick within the die causing the process to jam in the die assembly.

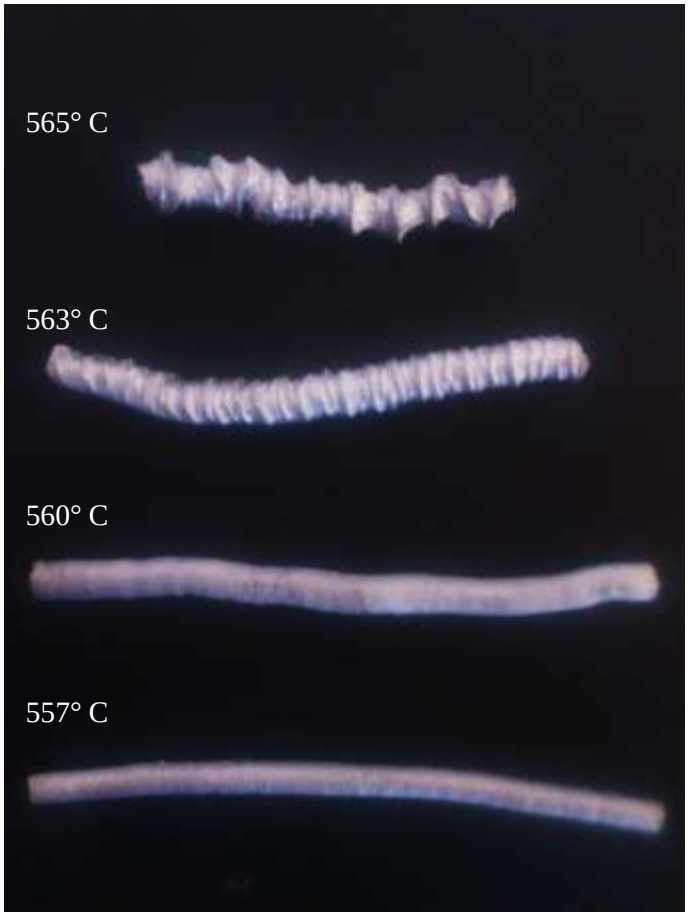

Figure 5.31: Evolution of extruded LM24 bar at various barrel temperatures. The water flow rate was kept constant at 3l/min

3) AA4043 Al alloy

Figure 5.33 shows bars produced over a range of extrusion temperatures keeping the pouring temperature constant at 621ºC. It can be seen that at a barrel temperature of 620ºC the diameter of the extruded rod is not constant but as the extrusion temperature decreases, the quality of the rod improves continuously. At 612ºC the rod can be said to have a good surface finish. The lowest possible temperature extrusion achieved was at 610ºC, below which it was not possible to extrude the AA4043 as the material tended to stick within the die causing the process to jam in the die assembly.

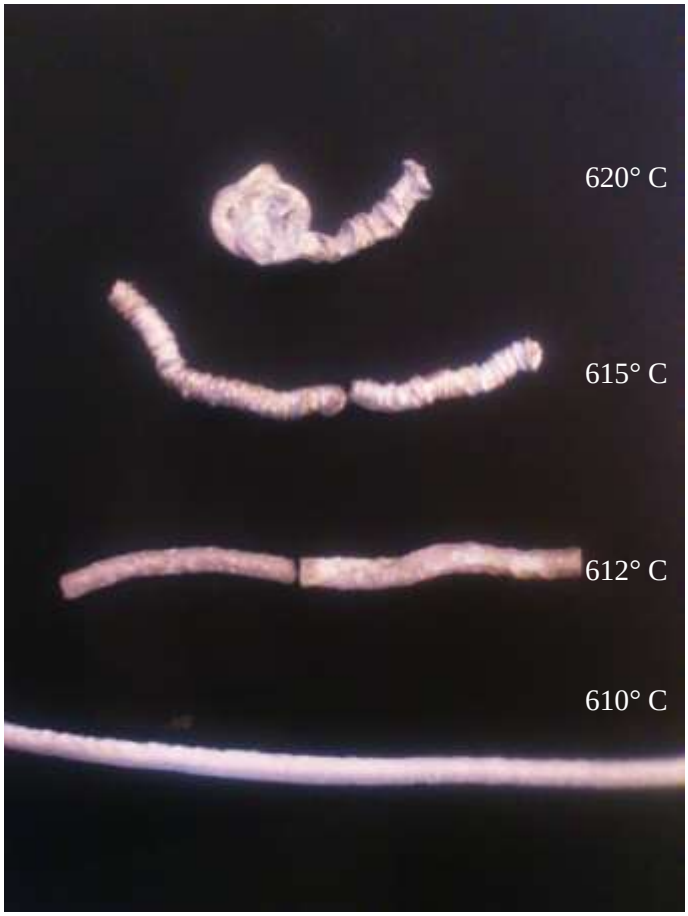

Figure 5.32: Evolution of extruded AA4043 bar at various barrel temperatures. The water flow rate was kept constant at 4l/min

4) AA5356 Al alloy

Figure 5.32 shows bars produced over a range of extrusion temperatures keeping the pouring temperature constant at 628ºC. It can be seen that at a barrel temperature of 625ºC the diameter of the extruded rod is not constant but as the extrusion temperature decreases, the quality of the rod improves continuously. At 622ºC the rod can be said to have a good surface finish. The lowest possible temperature extrusion achieved was at 620ºC, below which it was not possible to extrude the AA5356 as the material tended to stick within the die causing the process to jam in the die assembly.

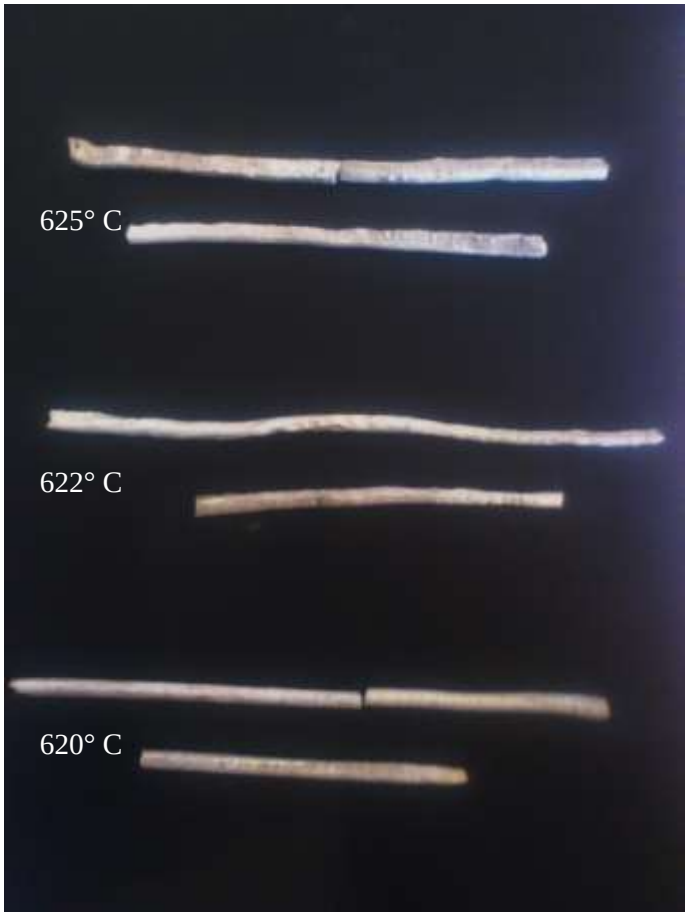

Figure 5.33: Evolution of extruded AA5356 bar at various barrel temperatures. The water flow rate was kept constant at 4l/min

b) Porosity

Large porosities from entrapped gas as seen in Figure 5.34(a&b) were continuously observed in the extruded microstructure of both magnesium and aluminium alloys due to the inherent nature of the machinery and process. Some level of solidification shrinkage was also observed at the grain boundaries in both magnesium and aluminium as seen in Figure 5.34(c&d). The causes of these are discussed in detail in Section 7.4.2.

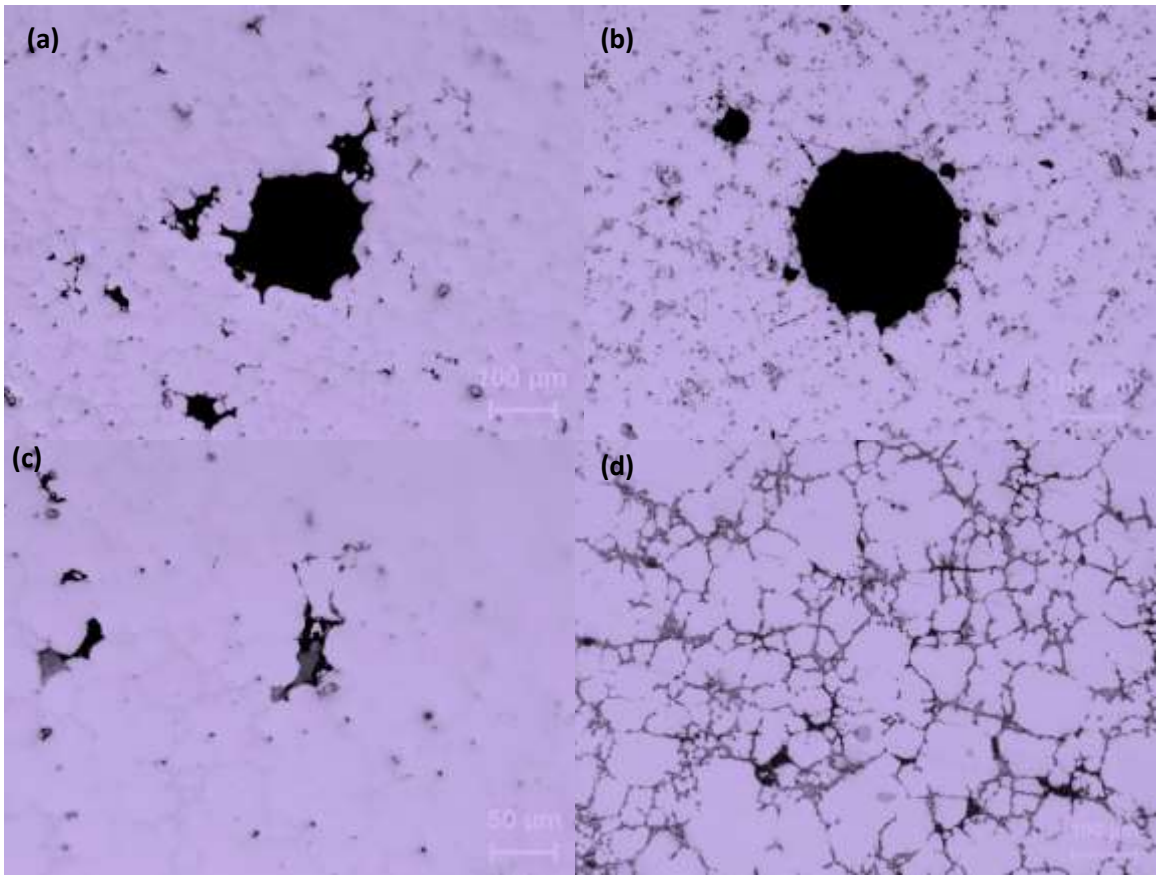

Figure 5.34: Porosity from entrapped air in rheoextruded a) AZ91D and b) AA5356. c) Porosity arising from shrinkage in AZ91D and d) AA5356

orosity arising from hot tearing as seen in Figure 5.35 was mainly observed in LM24. The reasons for this have also been addressed in Section 7.4.3. The effect of such porosities on the mechanical properties is discussed in Section 7.6.

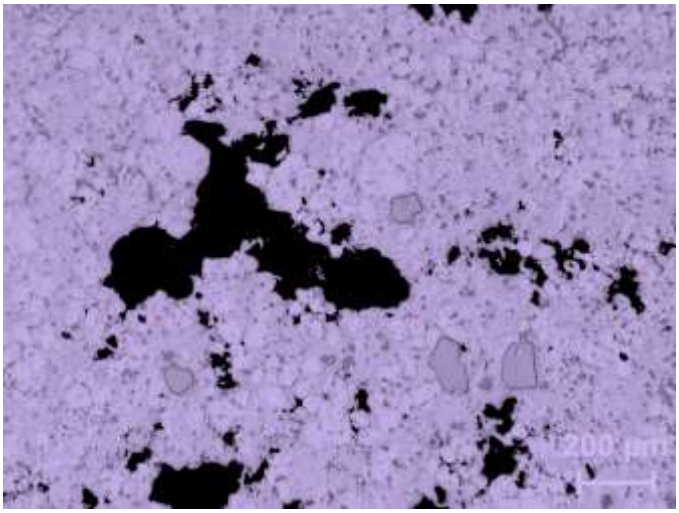

Figure 5.35: Hot Tearing observed in LM24

c) Chemical separation in Al-Si alloys

In the course of the study silicon containing aluminium alloys were explored since the silicon content formed a protective coating of $MoSi_2$ and reduced the chemical attack of aluminium on the machinery. However a large amount of phase separation was observed in Al-Si alloys tested. Phase separation was linked to the process temperature and to the content of the silicon in the system as seen in Figure 5.36. Separation was severe when high-content silicon alloys and high process temperatures were used. Solidified structures show a vast amount of primarily solidified silicon which is in stark contrast to the expected eutectic structure which was obtained using AA5356 with lower silicon content. This is discussed more in detail in Section 7.5.2.

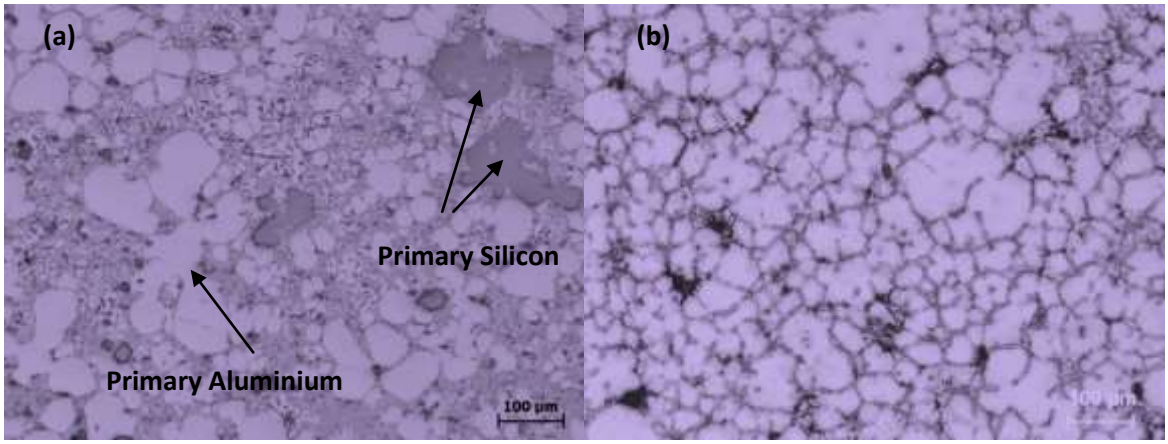

Figure 5.36: Optical micrographs showing (a) large segregated concentrations of silicon and uneven eutectic at 565ºC for LM24 compared to (b) No primary silicon in rheoextruded AA5356

5.3 Heat Treatment

The presence of the eutectic can be solved if the rods are heat treated. Simple heat treatment investigation of rheoextruded bars was carried out to validate in line instant solutionisation but further work needs to be done in this area particularly on bars that would be achieved at a steady state thermal condition. Treatment of AZ91D manufactured through rheocasting have been said to greatly improve both microstructure and mechanical properties as demonstrated by Wang et al. [2006].

Discontinuous cells and pockets of eutectic were seen to greatly reduce on solutionisation. Heat treatment was carried out in an electronic resistance furnace for two hours. The sample was immediately quenched into water to seize the microstructure. The microstructure of the heat treated sample is shown in Figure 5.37. From the microstructural observation, the quantity intermetallics and eutectic phase was dramatically reduced on increase of the solutionisation temperature.

The solvus for AZ91D in the Mg-Al system is 430°C and at this temperature the binary phase diagram of the Mg-Al system predicts that in an alloy with the aluminium content of AZ91D all the intermetallic phase should dissolve back into the matrix. However a range of solutionising temperatures were investigated to see whether the processing conditions played a part in reducing the solutionising temperature.

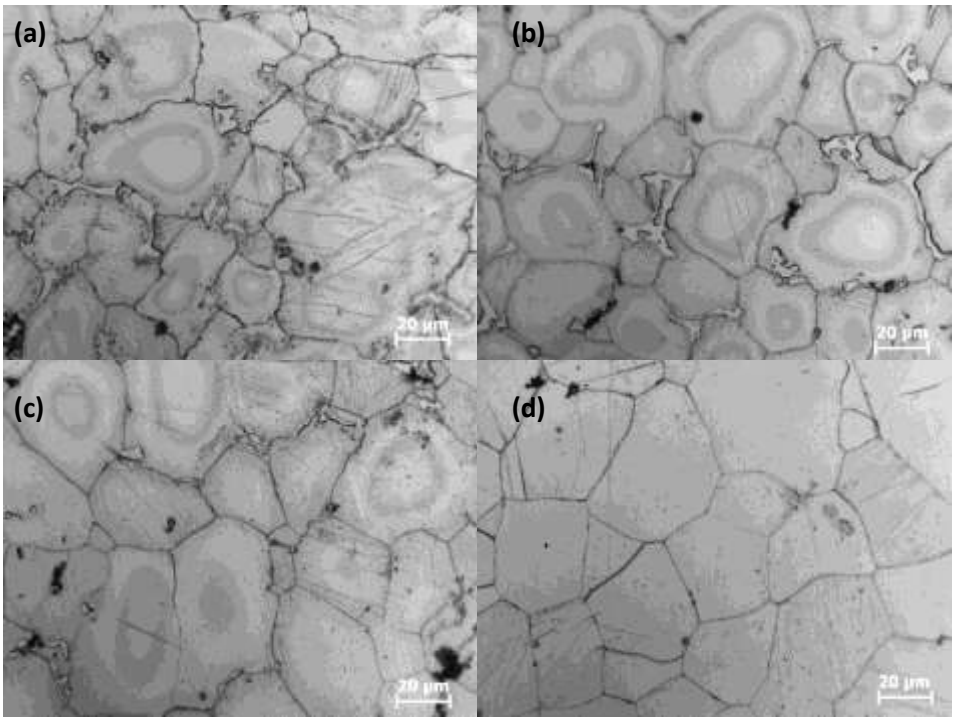

Figure 5.37: AZ91D extruded at 545°C solutionisation heat treatment for 2 hours (a) 370°C (b) 390°C (c) 410°C (d) 430°C

From Figure 5.37(a) it can be seen that at 370°C a large amount of intermetallic still exists along the grain boundary. This is seen to dissolve into the primary α-Mg grains at higher holding temperatures. At 430°C nearly all the intermetallic has re-dissolved into the matrix as seen in Figure 5.37(d).

Based on the above results a solutionising temperature of 430°C was chosen to be explored further. Figure 5.38 compares the microstructures obtained of samples heat treated over a range of holding times. It can be seen that the eutectic phase eventually dissolves into the α-Mg grains.

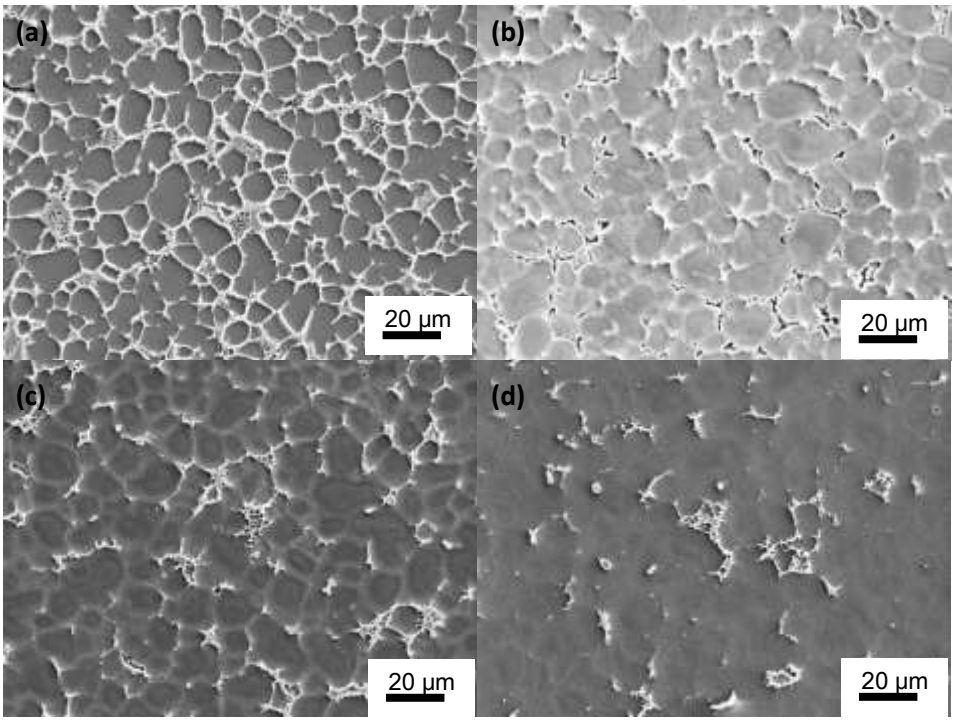

Figure 5.38: AZ91D extruded at 545°C held at 430°C for (a) 0 hours (b) 1 hour (c) 2 hours (d) 4 hours

Samples heat treated at 430°C for three hours were then aged at 215°C for a variety of holding times to observe precipitation of the intermetallic. Each sample was immediately quenched into water to seize the microstructure. Figure 5.39 shows the micrograph obtained after one, three and 48 hours of ageing. By discontinuous or cellular precipitation, the supersaturated solid solution decomposes into a solute-depleted matrix and a precipitate phase. This type of reaction was observed in the Mg-Al system and it can

be described as grain-boundary precipitation with simultaneous boundary migration [Findik, 1998] .A fine precipitated intermetallic phase can be seen to develop as the sample is aged.

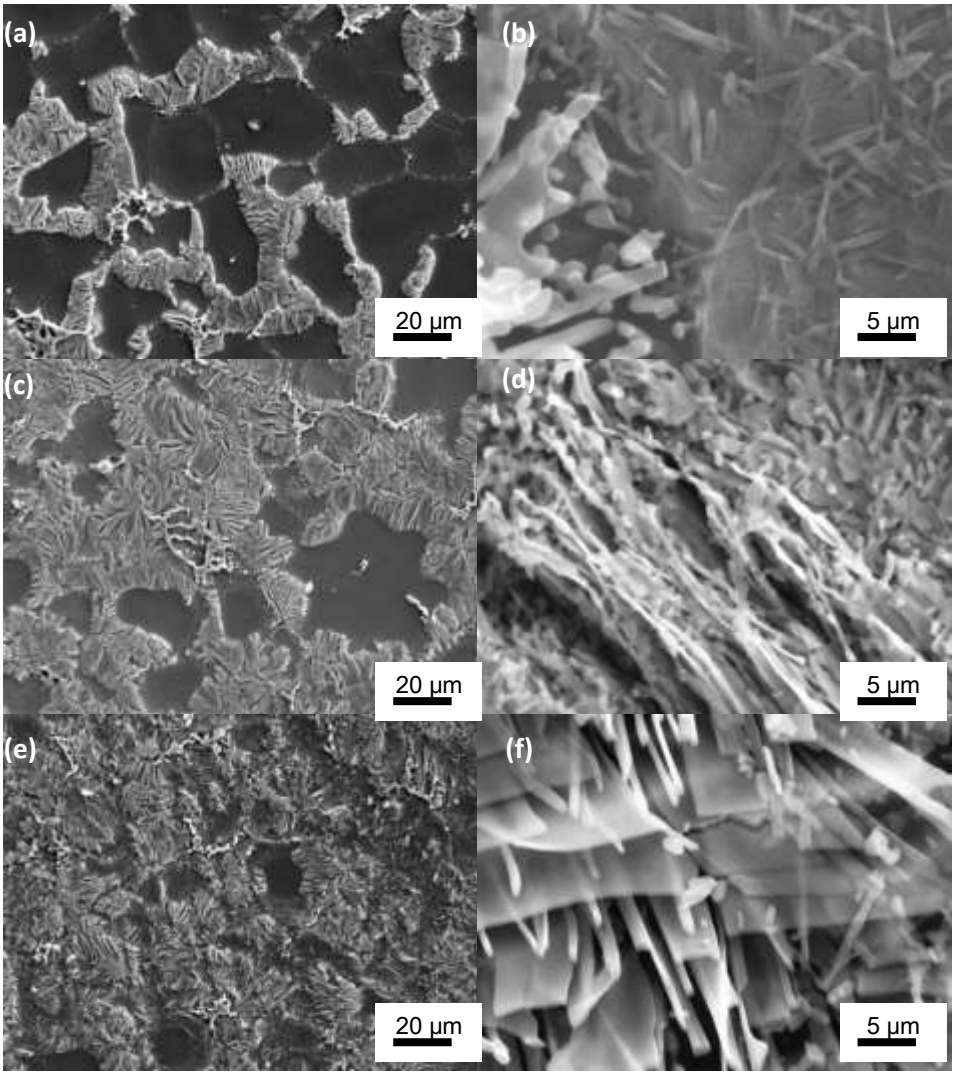

Figure 5.39: Precipitation of intermetallic observed at (a) 1 hour (b) details of intermetallic precipitated for 1 hour (c) 3 hours (d) details of intermetallic precipitated for 3 hours (e) 48 hours (f) details of intermetallic precipitated for 48 hours

Growth was observed to begin near the grain boundaries. Growth begins as tiny fibrous crystals that are observed to intermesh. As growth proceeds the morphology is observed to

be a dense accumulation of longer fibres. Upon further precipitation the fibres are observed to evolve into plate-like structures.

5.4 Mechanical Testing

Mechanical properties of AZ91D bars extruded at 560ºC and 545ºC were measured. An average elongation of 6.1% and average yield strength of 87MPa and UTS of 186MPa was obtained from specimens extruded at 545ºC. Both samples were heat treated at 430ºC for two hours to dissolve the intermetallic phase. It was observed that the ductility decreased with extrusion temperature to 1.8% at 560ºC while the Youngs modulus was observed to remain approximately the same as detailed in Figure 5.40.

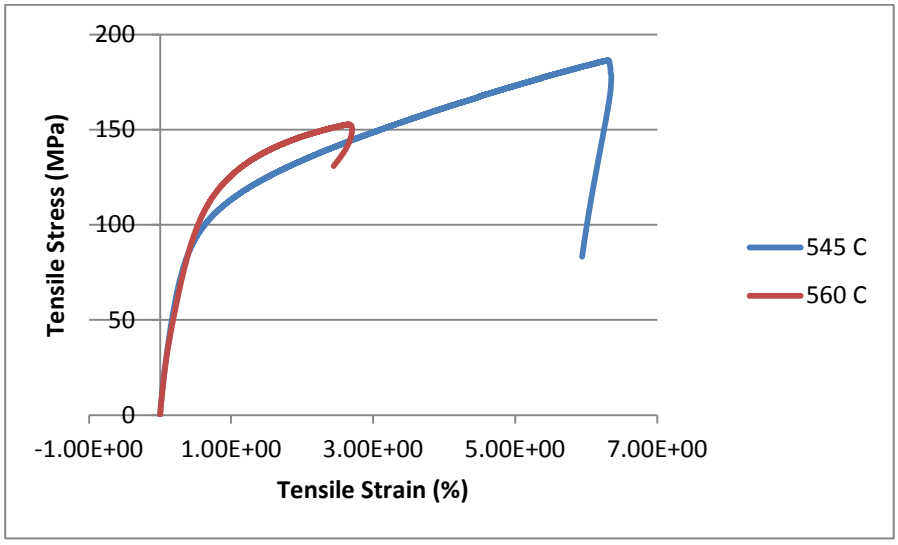

Figure 5.40: Typical tensile stress-strain curves for the AZ91D samples extruded at 560°C and 545°C

It is observed that the grain size is dependent on the processing temperature. Based purely on this observation, the relationship of yield strength on the grain size is in accordance to

the Hall-Petch equation. This said the lower values of yield strength observed in the 560ºC extrusion could also be attributed to other factors detailed in Section 7.6. However the overall performance of the rod, detailed in Table 5.2, was comparable to values obtained from work on rheomoulding and rheodiecasting products in separate works obtained by others [Czerwinski et al., 2001; Du and Zhang, 2007; Zhang et al., 2009].

Table 5.2: Mechanical Properties of AZ91D

Type	Yield Strength	UTS	Elongation	Reference
As-sandcast	95	135	2	[Polmear 2006]
As-chill cast	100	170	2	[Polmear 2006]
Rheoextruded 545	87	186	6.1	Present work
Rheoextruded 560	114	150	1.8	Present work
Rheomoulding	156	217	2.3	[Du and Zhang 2007]
Rheodiecasting	145	248	7.4	[Fan 2005]

Analysis of the fracture surface reveals that the nature of the fracture is intergranular i.e. it occurs along the grain boundaries as opposed to travelling through the grain itself. This implies that the fracture occurs in the weaker, more brittle eutectic phase validating post extrusion processes such as heat treatment. This is detailed in Figure 5.41.

Upon high magnification it can clearly be seen that the fracture follows the curved shape of the grain. On macro-examination of the fracture surface, defects such as porosity were clearly observable. It is believed that the presence of such defects within the secondarily solidified eutectic contributed to areas of stress concentrations within the weak intermetallic phase. This allowed for cracks to propagate easily. This has been discussed in more detail in Section 7.6.

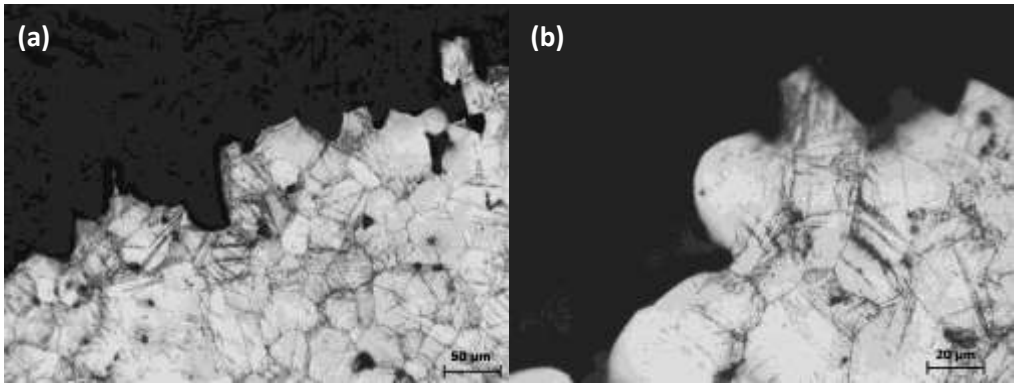

Figure 5.41: Tensile test fracture surface details of sample extruded at 545°C

5.5 Thermal Simulation

From obtained results it is observed that a microstructure obtained at higher solid fraction generally has better properties and the ideal condition would be to get the solid fraction to a maximum value without compromising the advantage of low forming force. Due to experimental constraints some parameters could not be further explored. To overcome this, simulation of the thermal conditions for rheo extruding AA5356 was carried out using finite element analysis (FEM) . Input parameters included barrel temperature, die temperature, feed section temperature, melt temperature. To validate the model, the exit temperature was measured and compared to solid fraction of quenched melt. At this point experimentation had already started on the aluminium machine to be delivered so it was deemed prudent to carry out FEM simulation on just the aluminium rheoextruder.

5.5.1 Validating the model at steady state conditions

FEM results used to simulate steady state extrusion show that there will be no overall heat loss in the melt at the process conditions described below

- Pouring temperature set at the minimal allowable temperature 633ºC into
- Feed section temperature is 650ºC
- Barrel temperature is 630ºC
- Die temperature is 650ºC

Simulation suggests for these process settings the temperature of the melt at the exit remains at 633ºC with a corresponding solid fraction of 0.18. This result was verified experimentally with analysis of the quenched microstructure showing a solid fraction of 0.21 corresponding to an exit temperature of 631ºC which is a result in acceptable limit of error thereby validating the steady state prediction of the model. The results are detailed below in Figure 5.42.

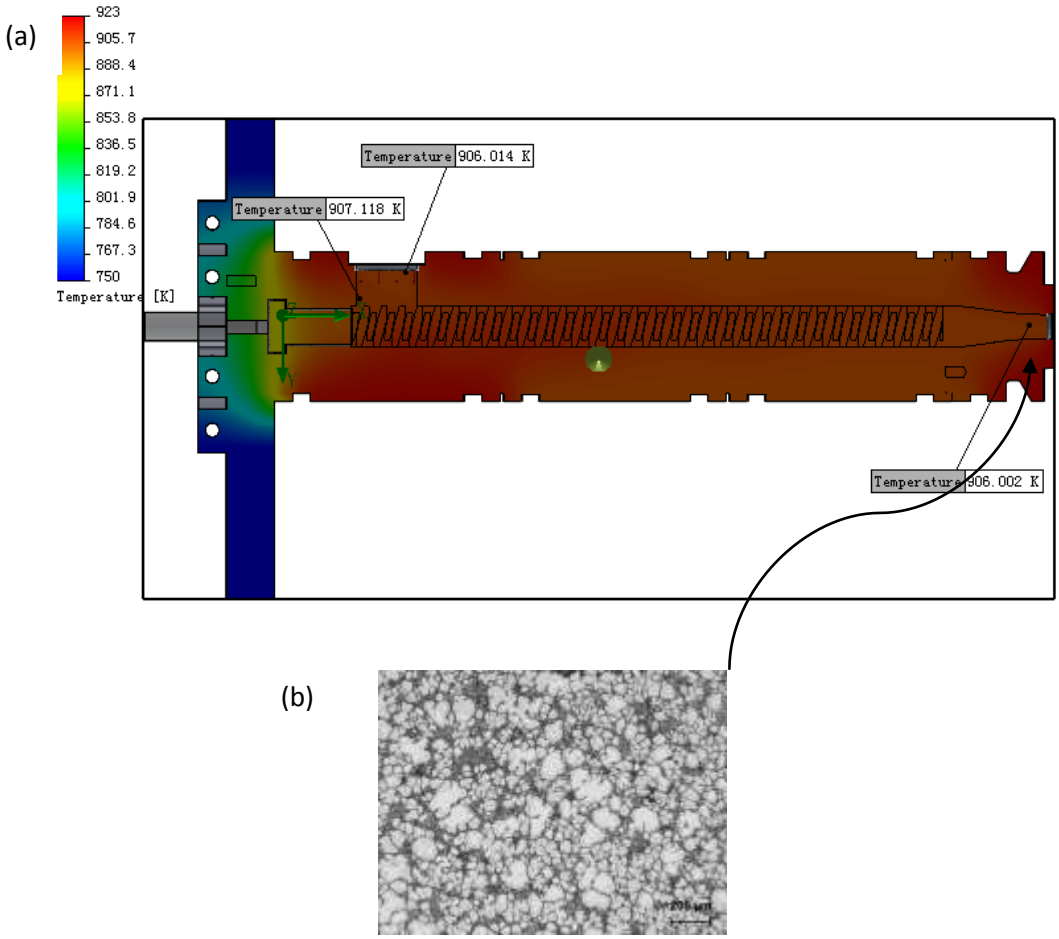

Figure 5.42: (a) Result of extrusion simulation at 630ºC (b) water quenched sample of obtained result

5.5.2 Using the model to identify transient results

To test the validity of a resultant microstructure similar simulations were run for the conditions with a barrel temperature of 620ºC which was the lowest achievable extrusion process temperature for aluminium alloy AA5356. The model revealed that at the steady state the temperature of the melt exiting the die would be 625ºC corresponding to a solid fraction of 0.37. This value is found to be higher than the value obtained by experimentation thereby showing that the result obtained in the laboratory experiment was in the transient state and had not yet reached steady state. This indicates that more than the used 2.5kg of aluminium needs to be extruded continuously for steady state conditions to be reached. The results are detailed below in Figure 5.43.

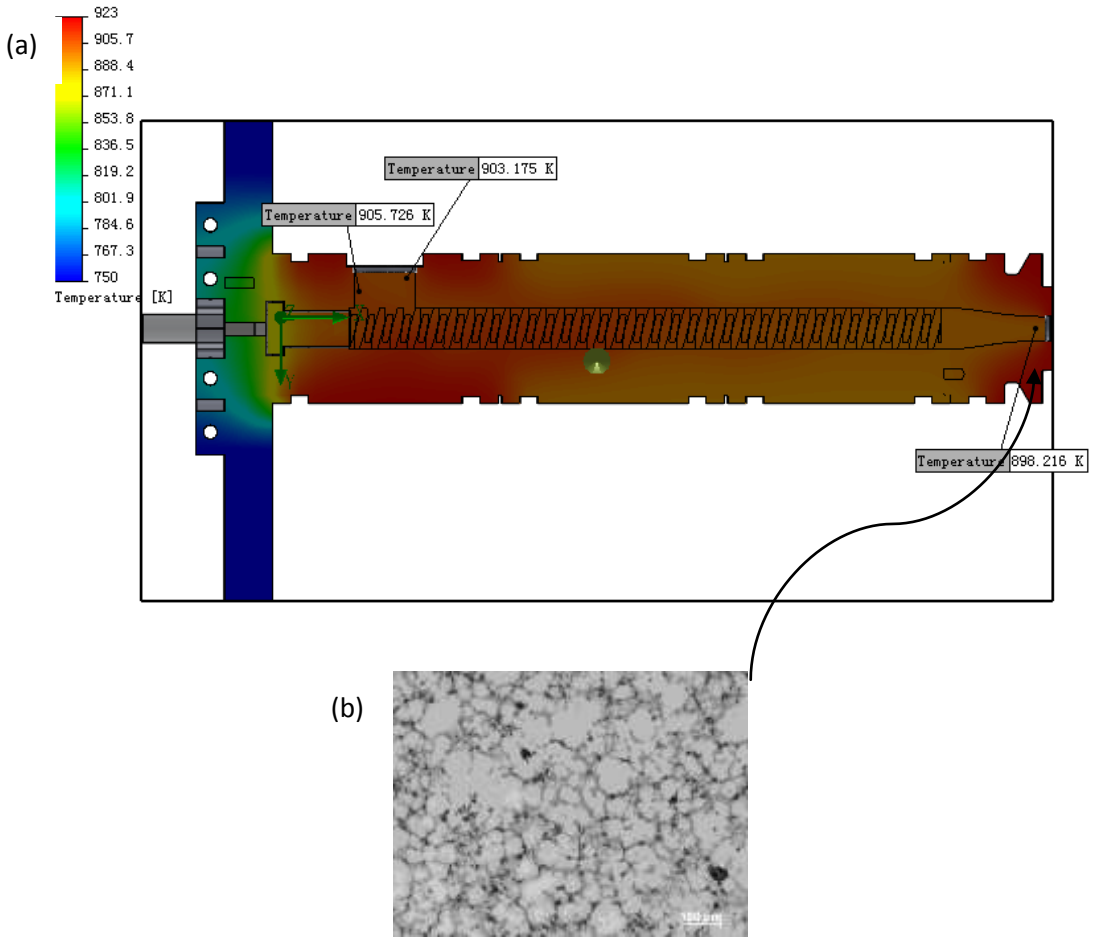

Figure 5.43: (a) Result of extrusion simulation at 620ºC (b) Water quenched sample of obtained result

5.5.3 Prediction for optimal processing conditions

A fully optimised predicted model with a barrel temperature of 610ºC reveals a steady state condition at 612ºC corresponding to a solid fraction of 0.63 which is highly desirable as seen in Figure 5.44. At this solid fraction it is reported that the metal is still relatively formable under low force. However these settings were not achievable in the extruder due to initial metal poured jamming in between the screws as there was not enough power from the motor to break the formed structures formed by the high solid fraction of the melt at the transient state temperature.

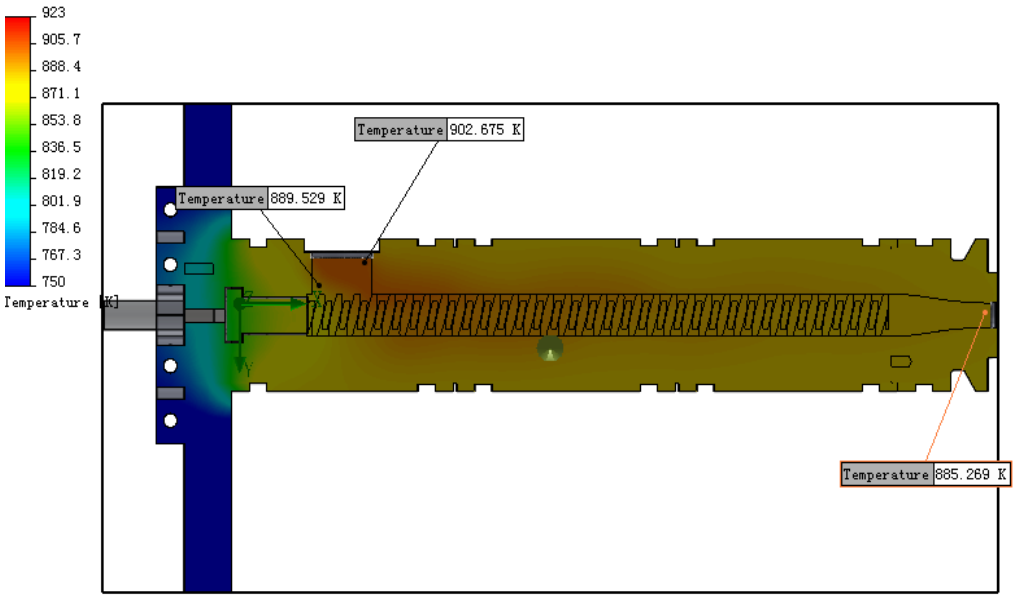

Figure 5.44: Simulation result at 610º C

Summary

The twin-screw rheoextrusion displayed several advantages over existing semisolid forming technologies:

1) High efficiency and productivity due to high speed and continuous processing;

2) Slurry making and semisolid forming are incorporated as an integrated process;

3) The semisolid slurry containing a predetermined fraction of non-dendritic globular primary phase particles displayed typical flow dynamic during forming with excellent fluidity and formability;

4) The continuous shearing by the twin-screw during extrusion not only prevented the slurry from growth but also refined the microstructure in conjunction with the thermal scheme adopted that the barrel temperature was set to be lower than the feeding temperature, which promoted nucleation as the slurry temperature decreased;

5) The shearing by the twin screws during extrusion also helped develop a uniform field of temperature and chemistry in the slurry and offered an additional measure in microstructure control by changing convection intensity and mechanical impact to the slurry.

CHAPTER 6

PROCESS DEVELOPMENT

6.1 Achievement of a One-Step Continuous Process of Semisolid Extrusion

The noted benefits of semisolid forming technologies such as process control, microstructual engineering and property enhancement are yet to be fully realised because of the increased complexity in the process control. This is especially true when one considers the thixo route where pre-processed alloys of non-dendritic microstructures formed by electromagnetic stirring [Brown and Flemings, 1993; Song et al., 2008] or plastic deformation and re crystallisation [Ellias-Boyed et al., 1988; Tzimas and Zavaliangos, 2000; Young et al., 1983] are heated to a semisolid region prior to forming. The pre-processed non-dendritic alloys are expensive and normally subjected to heterogenous heating before forming. This leads to substantial problems in the realisation of the full potential of the semisolid forming. Compared to conventional die casting semisolid metal processing has advantages of laminar flow during mould filling, reduced solidification shrinkage [Fan, 2002; Flemings, 1991] and lower operating costs.

Typically, billets are created in one foundry and then they may be transported to another foundry where they are heat treated before being transported again to the foundry where extrusion is to take place. As a process flow, this is inefficient as it involves detailed

logistical planning and unnecessary operational cost and considered to be a complex and prolix process.

There are several rheo semisolid forming processes in which semisolid slurries are made directly from melts such as gas-induced semisolid rheoextrusion [Rattanochaikul et al., 2010], cooling tube feeding semisolid rheoextrusion [Nagata et al., 2006], single-screw rheomoulding [Czerwinski 2004; Ji et al., 2001] and twin-screw rheomoulding [Ji et al., 2001], however the extrusion employed is similar to injection moulding which is of a batch nature with little commercial potential.

The literature in section 2.3 shows that the intermeshing counter-rotating twin-screw extruder has not yet been applied to the field of metal extrusion. Due to its excellent transport capabilities, turbulent flow and properties as a reactor, it can be successfully applied to continuously extruding metals from the liquid state. The process feature that distinguishes TSRE from continuous casting methods is that a majority of the cooling is done within the machine and the solid fraction steadily rises within the machine before extrusion where as in continuous casting the solidification occurs mainly outside the machine. The theoretical basis for the development of the microstructure is solidification under forced convection as opposed to conventional casting solidification where nucleation takes place in cooled liquid close to the mould wall [Haghayegh et al.], nuclei from continuous castings have a low survival rate and contribute very little to the final microstructure since they get transferred into the overheated liquid region and get re-melted which leads to a coarse and uneven microstructure. Due to the intensive shearing and mixing actions of the extruder the twin-screw mechanism ensures that the solidifying liquid has a uniform temperature and chemical composition and disperses the emerging nuclei throughout the entire volume of the melt [Fan, 2005]. Under these conditions nuclei

will survive and grow into spherical particles, creating a fine and uniform microstructure [Das et al., 2002].

Due to the rheo route taken, the speed of the process is increased by using a pumping mechanism and this is further accentuated since there are no auxiliary operations such as billet changing.

Therefore to have achieved continuous extrusion from semisolid slurry by the rheoextrusion process marks a step increase in technique, offering opportunities to reduce cost, energy and resource more than any other novel forming process. Figure 6.1 compares the process diagram of rheoextrusion to conventional solid state extrusion to demonstrate this.

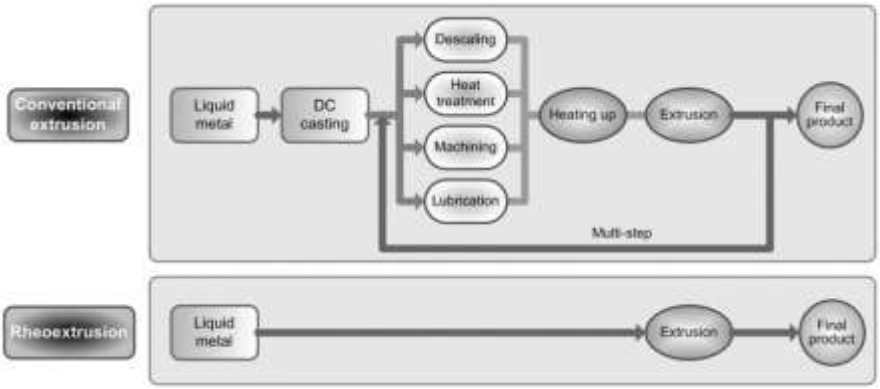

Figure 6.1: Comparison of rheoextrusion with conventional solid state extrusion

6.2 Apparent viscosity

Due to the limitations of technology to measure the viscoscity within the machines an analytical method is adopted. Therefore a simplified model is used to describe the relationship between the viscosity and process parameters. In accordance to work by Ilinka

[2008] the AZ91D alloy has a shear thinning behaviour and the viscosity under a moderate shear rate can be given as

$$\eta = K_3 e^{K_4 f_s} \left(\frac{\dot{\gamma}}{\dot{\gamma}_0}\right)^{-n} \tag{6.1}$$

where K_3 and K_4 are constant model parameters, n is a positive power law coefficient, f_s is the solid fraction of the slurry, $\dot{\gamma}$ is the applied shear rate and $\dot{\gamma}_0$ is a reference shear rate.

The solid fraction of the slurry as a function of temperature is described by the Scheil equation as

$$f_s = 1 - \left(\frac{T_s - T}{T_s - T_L}\right)^{1/1-(k)} \tag{6.2}$$

where T_S and T_L are the solidus and liquidus temperatures of the alloy, T is the slurry temperature, k_0 is the equilibrium partition coefficient.

The slurry is subjected to two different rates depending on its position.

In the barrel shear rate is dependent on the screw rotation speed and the geometrical parameters corresponding to the position [Samilov 1969]. Here shear rate can be expressed as:

$$\dot{\gamma}_{ch} = \frac{\pi R N}{H - 2\sigma} \tag{6.3}$$

where R is the screw diameter, H is the flight height, N is the rotation speed and σ is the calendar gap. The shear rate in the die and the funnel of the fluid was modelled as a Newtonian fluid in a pipe and is expressed as

$$\dot{\gamma} = \frac{Q}{\pi r^3} \tag{6.4}$$

where r is either the radius at the point of measurement and Q is the volumetric flow rate which is determined from the equations in Section 2.3 and the exit Area by the simple expression

$$Q = VA \tag{6.5}$$

6.3 Heat Exchange

To compare the two systems an analytical approach was used. Due to problems associated with feeding at lower temperatures, for the purposes of continuous feeding the feeding temperature was set higher than the extrusion temperature and the melt was allowed to be cooled as it was being transported. The process is therefore started in a transient state and the slurry temperature is observed to cool down while the barrel temperature is thought to increase before reaching a steady state. This steady state extrusion temperature is estimated by a simple thermal analysis as detailed below.

For a given extrusion speed (V) and a slurry temperature drop (ΔT) from the feeding point to the entrance die assembly, the slurry heat loss rate during transport is

$$\dot{Q}_s = \frac{1}{4}\pi\phi^2\rho V\left(C_p\Delta T - H\Delta f_s\right) \tag{6.6}$$

where ϕ is the diameter of the extruded rod, ρ is the material density, C_p is the specific heat capacity of the material, H is the latent heat of solidification and Δf_s is the solid fraction increase corresponding to ΔT.

It is thought that the thermal transfer occurs due to convection between the slurry and the barrel wall and conduction through the barrel wall to the atmosphere. Since the convection coefficient between the slurry and the internal surface of the barrel is much higher than the heat conductivity (3000W/m^{2}K vs. 38W/m^{2}K in the magnesium extruder) of the barrel wall the internal temperature of the barrel wall is assumed to be that of the slurry (T_s). Due to the limited gap size in the radial direction the slurry temperature is assumed to be uniform; and the only heat transfer along the axial direction is thought to contribute to the temperature change of the slurry. The overall heat transfer rate is therefore assumed to be determined by the radial heat conduction through the barrel wall. Figure 6.2 shows the geometry simplified as a solid cylindrical volume in the middle of the barrel. The diameter of the cylinder is determined by the equivalent volume corresponding to the actual structure. The slurry is then assumed to flow in between the screw column and the barrel.

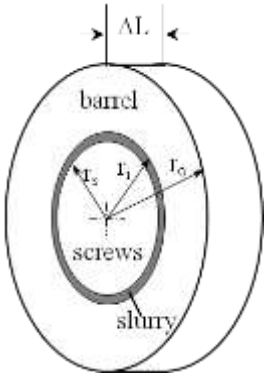

Figure 6.2: Simplified extruder geometry for thermal analysis.

Under this simplified geometry, the heat loss rate of the slurry by radial heat conduction through the walls of the barrel for a length of barrel segment $\Delta l(\Delta \dot{Q}_B)$ is given by

$$\Delta \dot{Q}_B = 2\pi h_b(\Delta l)\frac{T_s - T_{bo}}{ln(r_o/r_i)} \tag{6.7}$$

where T_{bo} is the barrel's outer surface temperature, which is equal to the nominal temperature of extrusion (T_e), h_b is the heat conductivity of the barrel and r_i and r_o are the inner and outer radius of the barrel, respectively. Assuming that T_s decreases linearly along the barrel the integration of equation 3.6 over the full length of the barrel gives the total heat loss rate thorough the barrel wall ($\dot{Q}_B$) as

$$\dot{Q}_B = \pi h_b L\frac{2T_f - 2T_e - \Delta T}{ln(r_o/r_i)} \tag{6.8}$$

where, ΔT is the total slurry temperature drop in the barrel. At steady state $\dot{Q}_s = \dot{Q}_B$ then

$$\Delta T = \frac{8h_b L(T_f - T_e)}{4h_b L + V\rho\phi^2 ln(r_o/r_i)(C_p + H/\Delta T_{fr})} \tag{6.9}$$

using an approximation that $f_s = \Delta T/\Delta T_{fr,}$ where $\Delta T_{fr} = T_L - T_s$ is the freezing range of the alloy where T_L and T_s are the liquidus and solidus of the material respectively.

For the purposes of the analysis the slurry temperature is assumed to be uniform. This is a reasonable assumption since the gap for the slurry to flow is between 0.5-2mm and the nature of the turbulent flow from constant shearing serves to homogenise the slurry temperature. The effect of the screw temperature on the slurry is important during the initial transient stages of the experiment as they can absorb a considerable amount of

energy from the slurry due to their continuous motion. However at steady state without sources of heat generation this value tends towards a negligible amount as they will have the same temperature as the slurry. UParameters for typical magnesium and aluminium extrusions are provided in Table 6.1

Table 6.1: Parameters used for thermal analysis

Symbol	Magnesium Extrusion	Aluminium Extrusion	Description (Unit)
r_o	0.050	0.012	Outer radius of the barrel (m)
r_i	0.028	0.02	Inner radius of the barrel (m)
h_b	38	130	Thermal conductivity of the barrel ($Wm^{-1}K^{-1}$)
ρ	1738	2800	Density of the slurry (kgm^{-3})
C_p	1183	925	Specific heat of slurry ($J\ kg^{-1}K^{-1}$)
H	360000	470000	Latent heat of the slurry ($J\ kg^{-1}$)
T_f	590	628	Feeding temperature (ºC)
T_L	~598	~640	Liquidus of the alloy (ºC)
T_s	~470	~511	Solidus of the alloy (ºC)
T_e	545-585	625-620	Set extrusion temperatures (ºC)

Figure 6.3 shows the predicted extrusion temperature $T_{PE}=T_e - \Delta T$ as a function of the set nominal extrusion temperature (T_e). It can be seen from the figure that for a given feeding temperature (T_f), T_{PE} is proportional to T_e as defined in equation 6.9. The applied thermal conditions (nominal extrusion temp T_e), material parameters (density ρ, heat capacity C_p, and latent heat of fusion H) extruder dimensions (barrel length L, and diameters r_i and r_o) extrusion speed V and diameter of the extruded strand ϕ determine the constant of proportionality

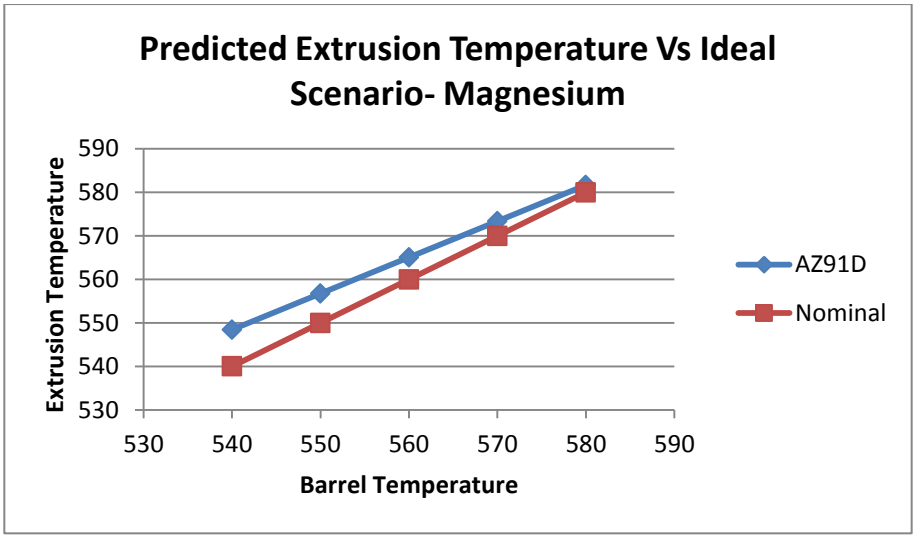

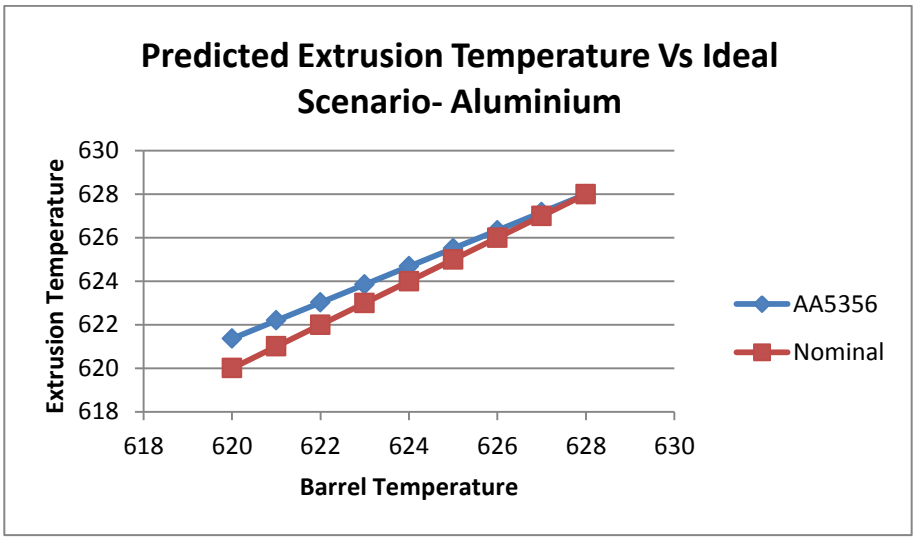

Figure 6.3: Predicted extrusion temperature as comparison with the ideal heat transfer for typical a) Magnesium extrusions b) Aluminium Extrusions

The analysis indicates that for a given TSRE system and product to be processed the actual extrusion temperature can be manipulated by changing the thermal conditions of the barrel and extrusion as Figure 6.4a shows that the measured extrusion die temperatures (T_{ME}) at steady state are close to the predicted T_{PE}.The data can be used to determine the maximum extrusion velocity required for ideal heat exchange.

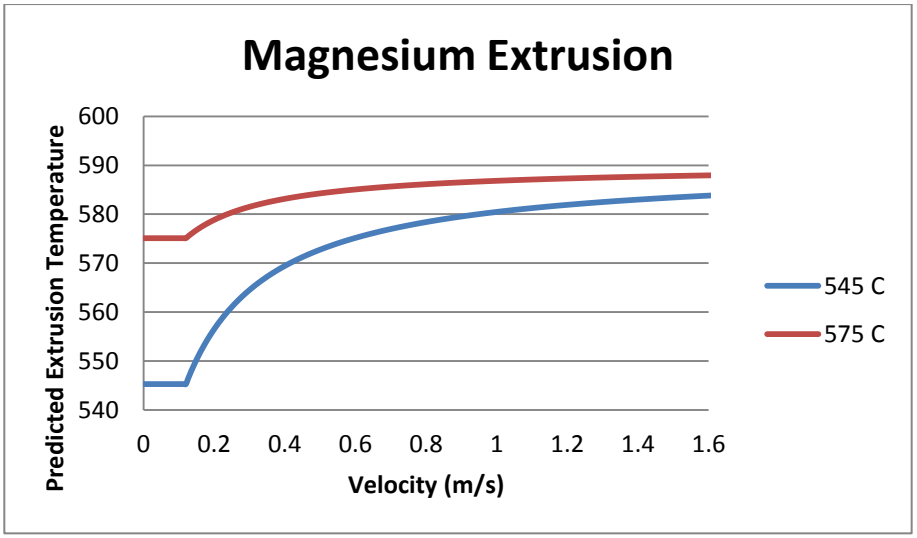

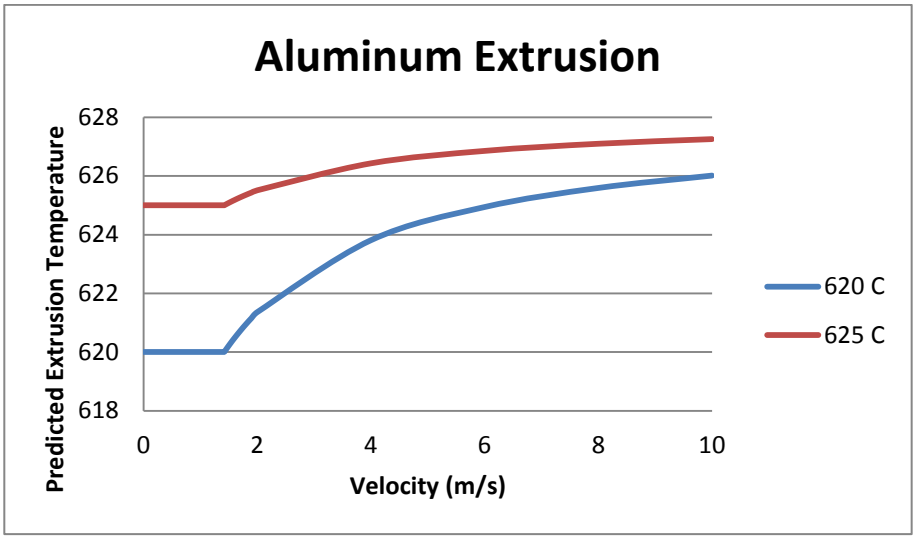

Figure 6.4: Analysis comparing the predicted extrusion temperature with different set barrel temperature as a function of extrusion speed for typical for typical a) Magnesium extrusions b) Aluminium Extrusions

From Figure 6.5 it can be seen that at relatively low extrusion speeds and long barrel size the slurry can be cooled down to the pre-set nominal extrusion temperature. This data can also be used to optimise the minimum length needed for a certain extrusion conditions so that proper heat exchange can take place. The barrel length at which the slurry temperature is equal to the preset extrusion temperature (L_e) is linearly related to the extrusion speed (V) as

$$L_e = \frac{\rho \phi^2 ln(r_o/r_i)\left(C_p + H/\Delta T_{fr}\right)}{4h_b} V$$

(6.10)

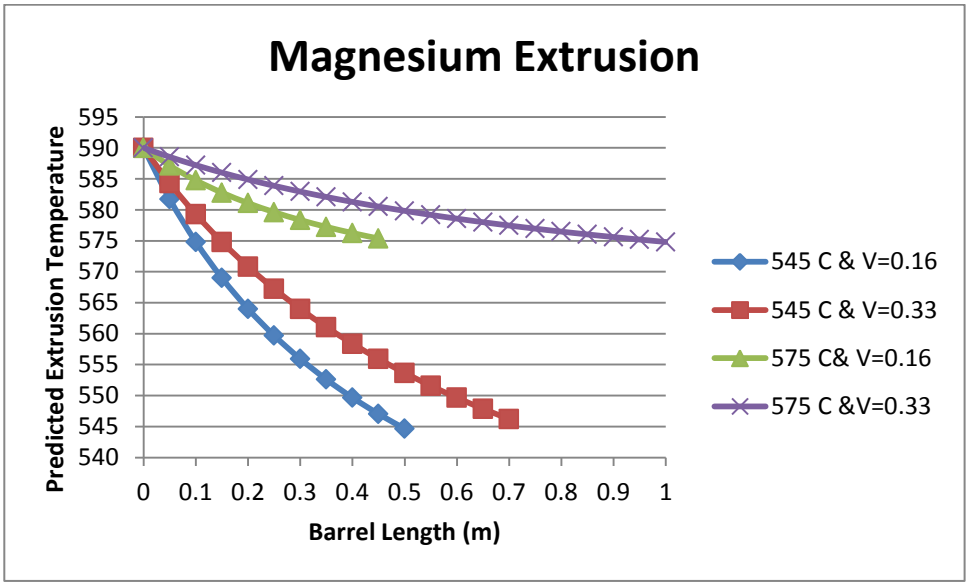

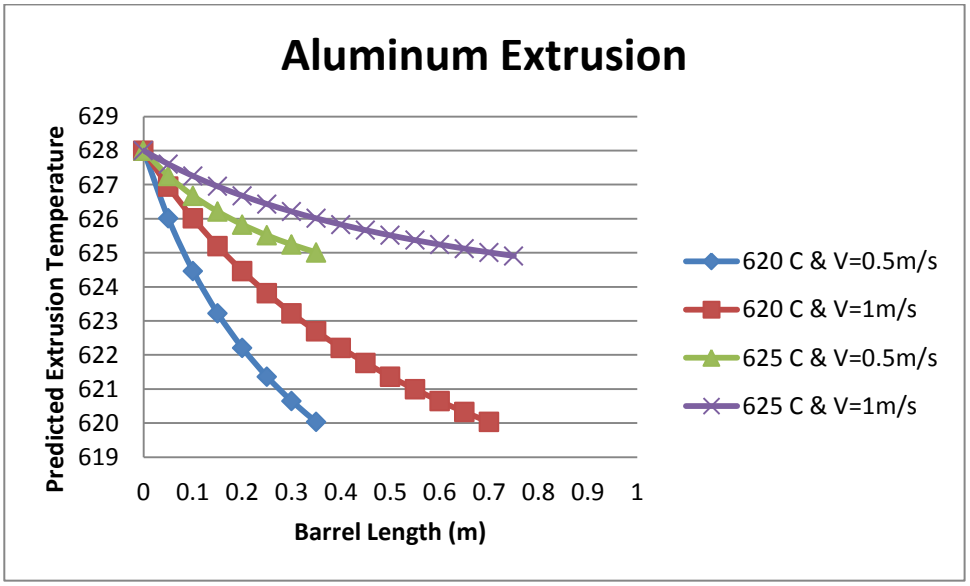

Figure 6.5: Predicted extrusion temperature as a function of barrel length at various extrusion temperatures and velocity for a) Magnesium extrusions and b) Aluminium extrusions

However by Equation 6.5 the diameter of the extruded strand plays a more significant role in achieving the preset extrusion temperature as it is a squared term. Therefore for correct thermal management it is imperative that the correct product size is chosen for the process thermal management.

The limitations of the above analysis is that it cannot predict the time taken to reach a steady state and a more detailed and sophisticated analysis is required that takes into account factors such as the effect of temperature gradient in the axial direction and precise thermal boundary conditions. It is expected that a significant temperature drop in the slurry will occur within a short period of time due to the large ratio of volume between the slurry and the twin screws.

6.4 Machine development

6.4.1 Overcoming transient process difficulties – validation of plate heaters.

Another design flaw of having a narrow gap within a transient thermal system (large difference in pouring and barrel temperatures) is that a dendritic network can form in the narrow gap between the screws in the early stages of extrusion as the solid fraction increases rapidly on contact with the relatively cooler screws. Due to an excessive amount of heat being extracted from the back plate by the cooling system and the excellent thermal conductivity of molybdenum it was observed that the temperature of the screws below the funnel could not be set to a desirable level. This caused the machine to jam on several occasions.

To rectify this specially designed back-plate heaters, as detailed in Figure 6.6 have been attached to the machine. When the block is set to 750ºC a temperature of 610ºC has been achieved at the funnel bottom allowing for even re melting.

Figure 6.6: Back-plate heaters

6.4.2 Improving transport capabilities of extruder

The basic geometry of the extruders is tabulated in Table 3.1. In accordance to equations presented Section 2.3.5 modifications of basic dimensions of the magnesium extruder were undertaken to improve the transport capabilities of the aluminium extruder to allow for more compaction. Comparison of the calculated properties of each extruder is plotted in Figure 6.7. It can be seen that the modification of the extruder geometry allows for improved pressure build up and transport capabilities.

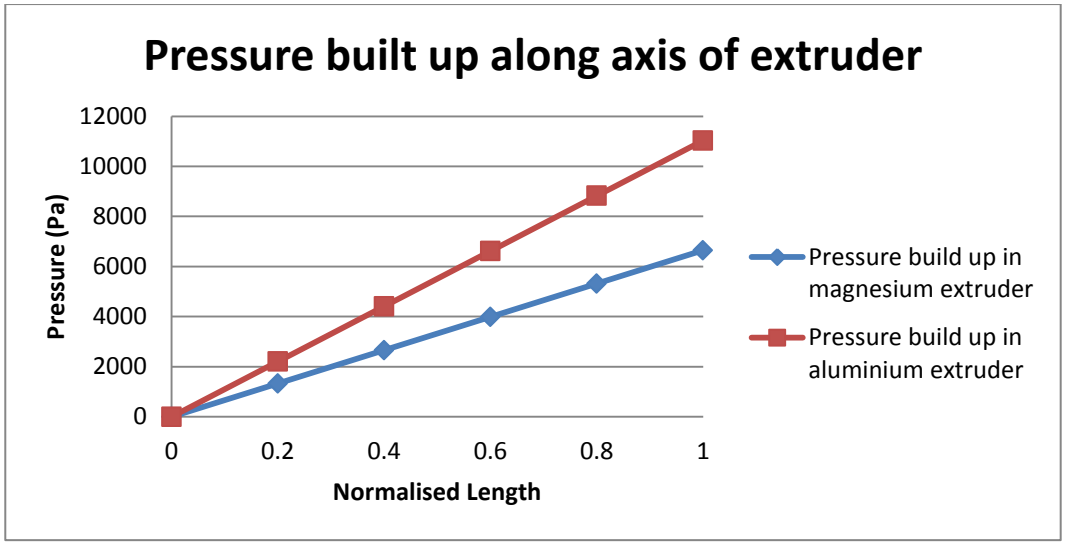

Figure 6.7: Pressure developed by different screw type's extruders across the normalised length

On increasing the power of the motor from 3kW to 4kW more compaction of the melt was observed due to the increased motor speed limit and high-end torque limit. Additional pressure build up is seen to compact the remaining primary particles after the liquid phase has segregated. This in turn was observed to reduce the porosity as detailed in figure 6.8. This modification also entailed that slurries with a higher solid fraction could be transported without the motor jamming.

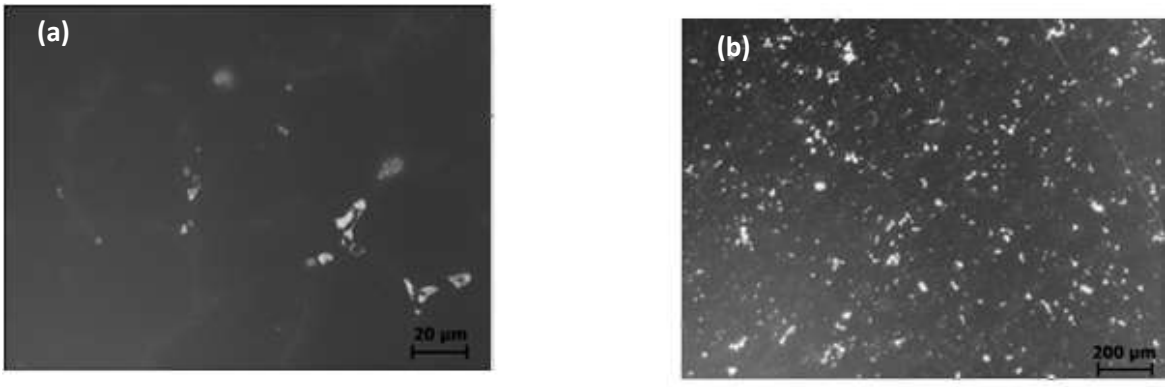

Figure 6.8: Comparison of observed porosity using different power motors (a) 4 kW (b) 3 kW

On reducing the exit diameter using the die insert as detailed in Figure 6.9 below, better surface was observed. This is because on reducing the exit diameter more pressure is built up at the die. This pressure is directly proportional to the exit velocity and therefore shear force on the surface of the semisolid bar as it passes through the passage of the die towards the exit. On reducing process temperature viscosity is increased and less porosity is also observed due to the additional pressure build up. Due to the easy deformability of the semisolid metal a good surface was observed with no signs of pulls or tears.

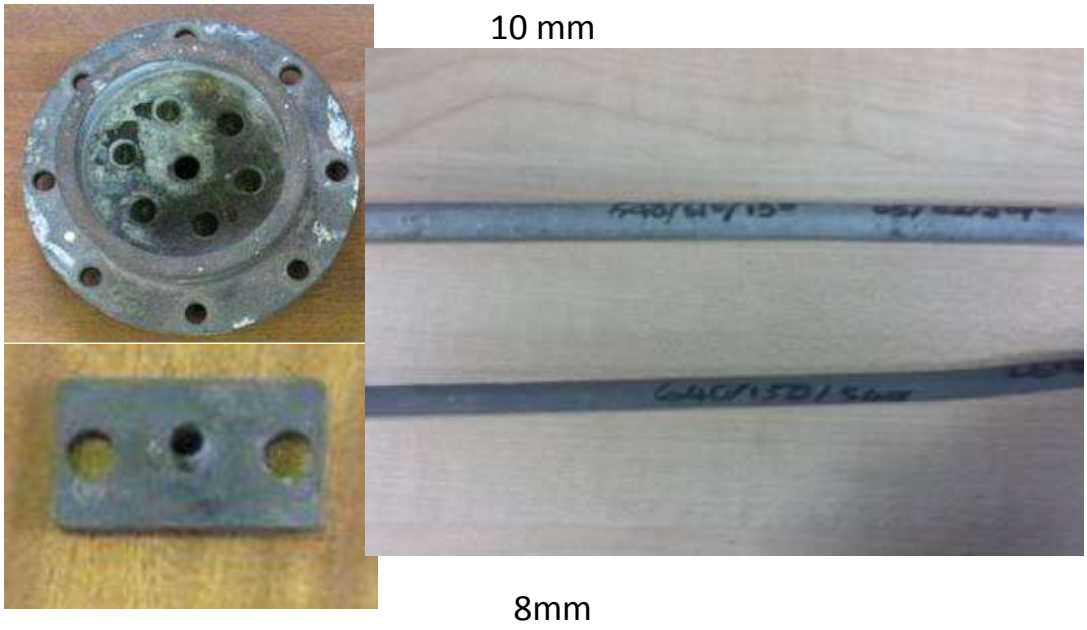

Figure 6.9: Macro comparison of bars obtained with different diameter exits

6.4.3 Solving the problem of reduced fluidity – validation of feeding system

To avoid segregation of the liquid phase it was deemed that the melt introduced into the extruder should be at the lowest allowable temperature. For AZ91D this was around 580ºC. However feeding melt into the extruder at such temperatures is unfeasible as the viscosity

is too high and the resultant bar was not smooth. Furthermore the sinking of the solid phase within the funnel and reformation of the dendritic networks can be problematic as it blocks melt from entering the chamber or gets stuck in between the screws right below the funnel and tends to seize the machine as the dendritic networks grow stronger as detailed in the literature by Fan [2002] and Flemings [1991].

During the alloy exploration process of aluminium alloys it was observed that the lowest workable slurry temperature was 625ºC for AA5356 alloy. Furthermore successful extrusions were carried out in the range of 632-620ºC. Thereby providing a 7ºC window where continuous steady state bars could be processed. However as mentioned above, feeding at these temperatures is problematic and therefore a feeding system was required to be designed.

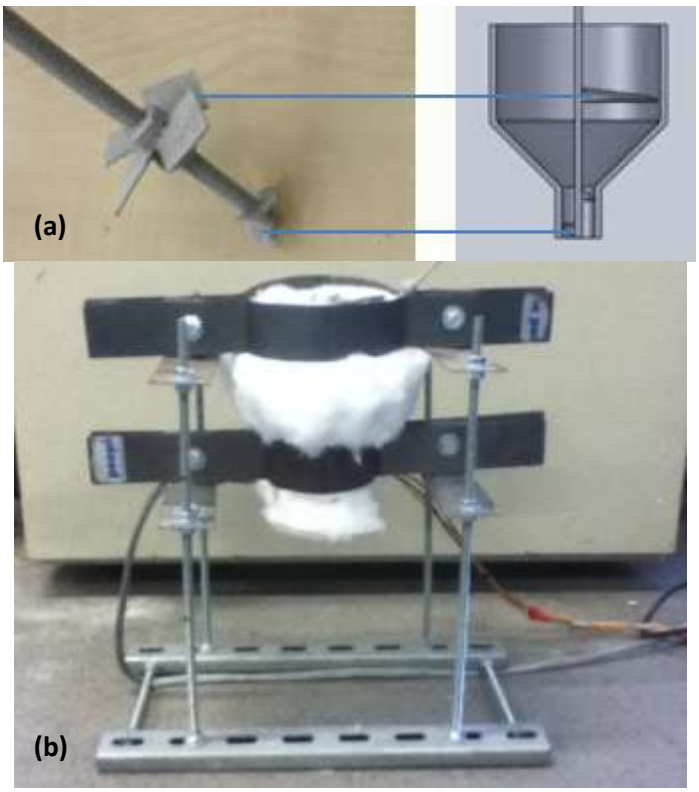

Figure 6.10: Feeding system (a) Duel blade conveyer system (b) Test rig

Due to the nature of flow of the H-type mixer, the fluid is only pushed radially and much of this built up dynamic pressure is useless in conveying the fluid down and into the extruder. Therefore based on the results in Figure 5.5 it was deemed that a C-type propeller be used to convey the slurry into the barrel of the extruder.

A specially designed funnel had been made to simulate the feeding of the slurry as described in Figure 6.10. The rig consisted of an iron funnel coated with boron nitride to prevent erosion from aluminium chemical attack.

It was observed that AA5356 melt at 630ºC could be easily conveyed into the barrel using such a system thereby validating its addition as a stage into the overall process. Slurry was poured into the funnel and a propeller was introduced to test the feasibility of a propeller to push melt into the barrel. Initially melt took the shape of the rig and didn't flow into the crucible below. However, it was observed that the use of a propeller significantly improved the fluidity and transport of the melt through the funnel and it was collected with ease due to the breaking up of dendritic structures upon agitation due to the pseudoplastic behaviour of the semisolid slurry as detailed by Fan [2002] and Flemings [1991 showing that the use of a propeller/ agitation methods is feasible in the feed zone.

6.4.4 Evolution of the water cooling system

1) Simulation results and the optimal thermal profile of the bar at the exit

Figure 6.11(a&b) show the thermal profile of the system without any cooling and the effect of the die exit temperature on the extruded bar. The aim of initial simulations was to investigate the thermal system to determine how to create an optimal thermal profile at the die at steady state. The properties of this optimal profile would be that a semisolid shell

with a level of structural integrity can be formed around the cooling metal as it is extruded. It was also observed that water cooling must be done with minimal heat transfer up the rod, i.e. the position of the solid transition must be outside the die otherwise friction is too much for the extruder to pump against causing the machine to jam and leak. This can be seen in figure 6.11 (a).The modelling used was carried out in collaboration with colleagues at the University of Birmingham.

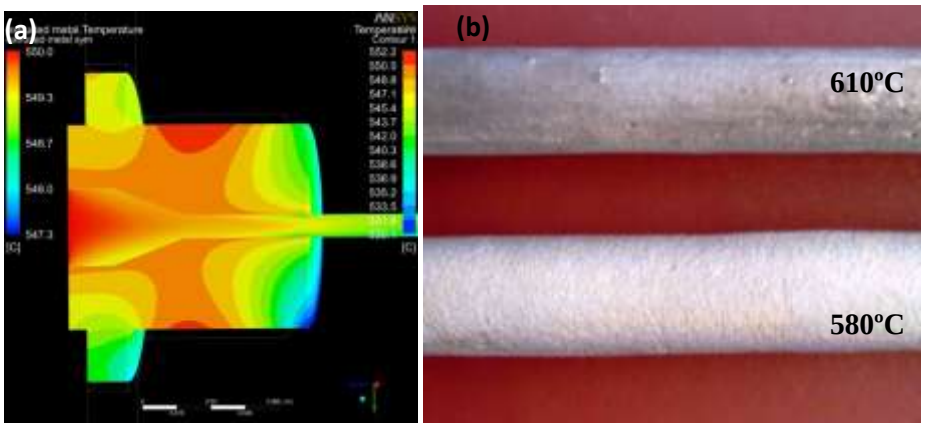

Figure 6.11: (a) Thermal profile at die with no cooling (b) Effect of die exit temperature on bar

It was observed experimentally that when the die exit is increased by partial re-melting of the bar we could create a thin film of liquid metal within the tube of the die along which the bar can slide allowing for a better surface and easier extrusion.

2) Methods used

Different cooling methodologies and the evolution of the final cooling system are detailed below. Initially the bar was quenched using a simple trough as detailed below in Figure 6.12. However the cooling it offered was not observed to be even.

Figure 6.12: Original trough for collecting bar

A) Inserts

To shift the position of the solidification transition point into the die, a variety of water cooled die ends inserts were used. However it was observed that this methodology caused a tremendous amount of heat to be sucked out of the system to the atmosphere at the die end through conduction even when water was not used. This was verified by simulated results as seen in Figure 6.13(c). Melt was observed to keep on jamming in the die. Therefore it was deemed that water cooling would be done outside the die assembly.

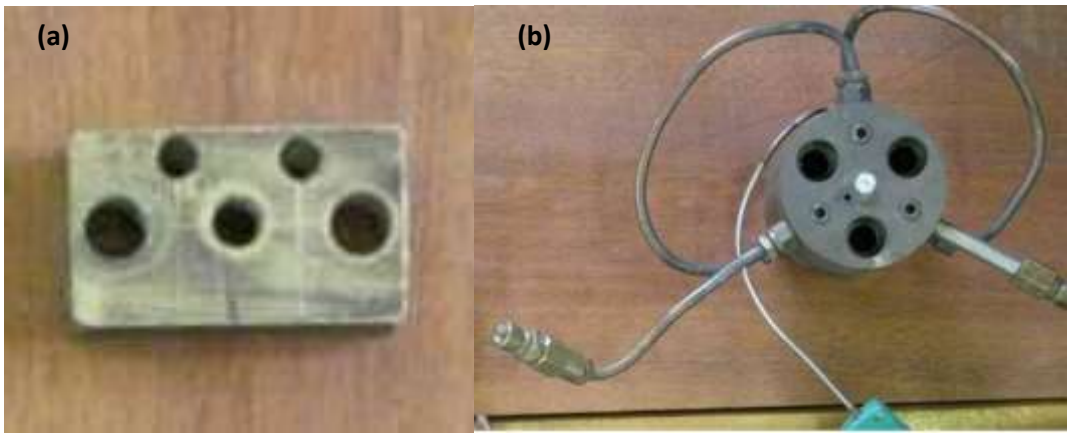

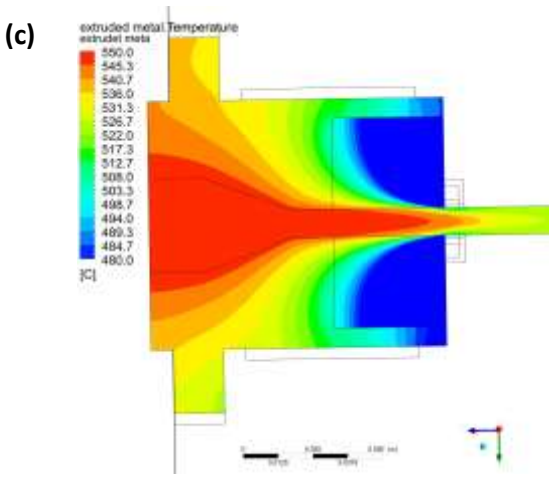

Figure 6.13 (a & b) examples of inserts used (c) Simulation results of using an insert

B) Water bath

To conduct the heat transfer outside the die a simple water bath was utilised to quench the alloy as it emerged from the die as detailed in Figure 6.14(a). However the extruded bar kept getting stuck in the outlet. This is because, as the bar was extruded the resistance friction from the trough against the soft semisolid prevented it from moving down the trough at a speed equal to that of the extrusion.

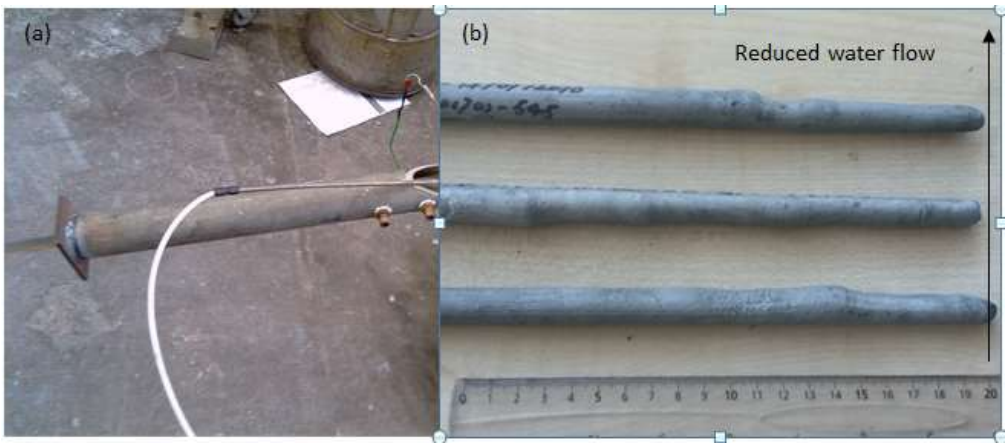

Figure 6.14: (a) Water bath system used (b) Gradual increase of diameter caused by friction from the trough

This caused a continuous build up of material at the die end causing the diameter to increase along the extrusion direction as seen in Figure 6.14(b) eventually jamming the exit of the water bath. Therefore it was realised that the friction factor needed to be eliminated. In accordance to fundamental theory it is seen that strength of the bar was directly proportional to the solid fraction and less material was observed to build up as the water flow was increased.

C) Water spray

To eliminate the friction exerted upon the bar, a simple top spray device was introduced as detailed schematically in Figure 6.15(a). However this led to the observation of uneven cooling on the top and bottom surfaces resulting in severe deformation of the bar and cracking of the outer skin. Other complications associated with such a methodology was to balance the water cooling amount against the strength of the quenched strand as excessive water flow is sufficient to break the soft semisolid strand before it solidifies enough whereas too little water would not cool the strand enough.

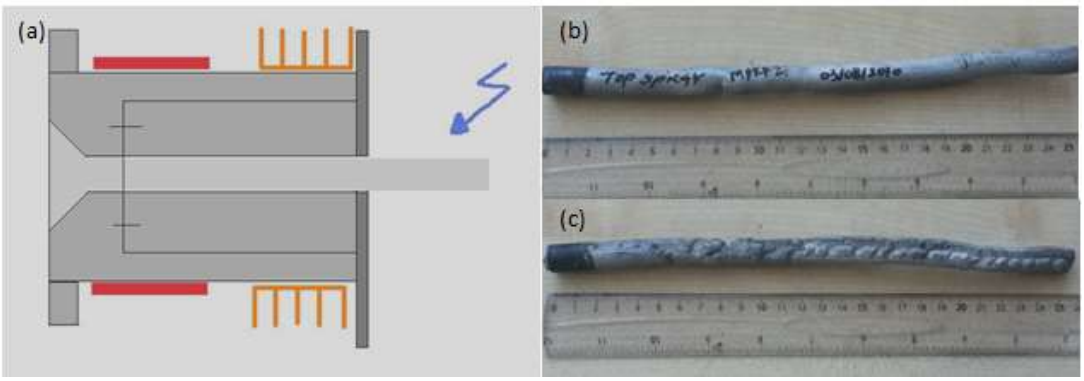

Figure 6.15: (a) Schematic of water spray system (b) Comparison of surfaces of bar obtained using water-spray top surface (c) Bottom surface

The sample shown in Figure 6.15 (b & c) was obtained at a flow rate of ~15l/min in order to achieve a strand that would not break. It can be observed from the sample, that there is a significant amount of deformation and skin cracking.

D) New trough

A new trough as seen in Figure 6.16(a) was designed to combine the understandings gained from trying the above concepts. Cooling was achieved outside the die by use of insulation. The Friction was reduced by providing a larger amount of cooling evenly around the bar using the inlet marked 'I' as seen in Figure 6.16(a). Bars were successfully extruded at flow rates of 4 and 8l/min. At 8l/min the bottom surface was still observed to display rub marks thereby signifying that friction was still prevalent when a long trough is used. This is seen in Figure 6.16 (e).

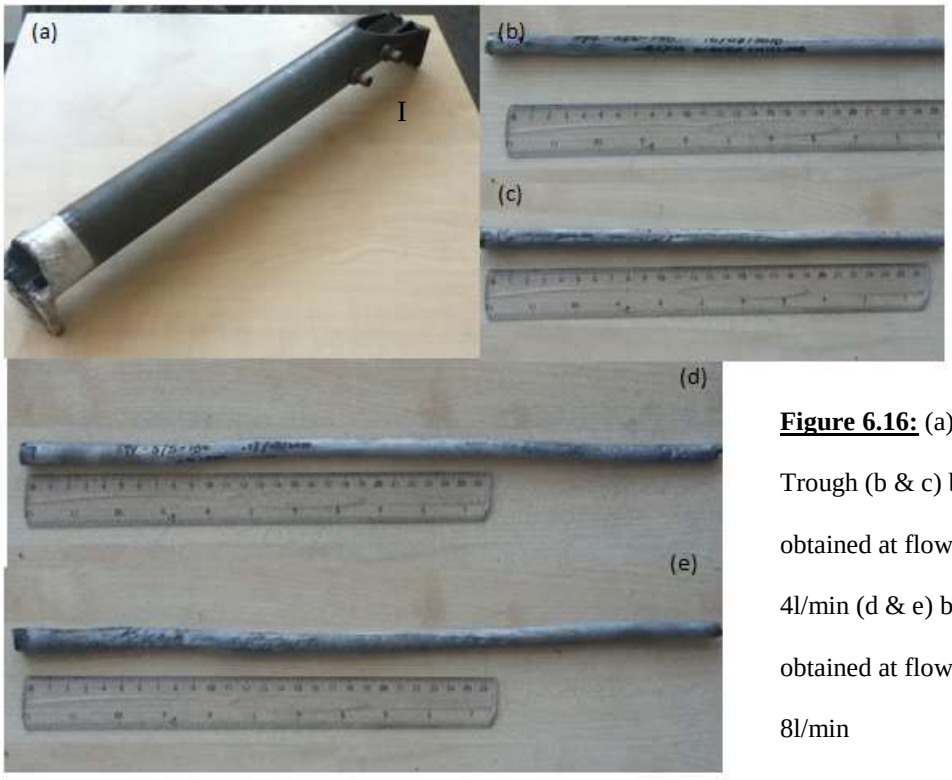

Figure 6.16: (a) New Trough (b & c) bar obtained at flow rate 4l/min (d & e) bar obtained at flow rate 8l/min

E) Brass cooling water ring (BCWR)

Based on the above understanding the BCWR was developed and is detailed in Figure 6.17(a–c). This is essentially a compacted version of the previous trough to eliminate friction. A favourable exit temperature gradient is created and the water is sprayed on the surface of the metal to strengthen it and the bar is cooled outside the die with minimal friction.

Figure 6.17(d & e) shows the simulations of using the BCWR to cool. Metal temperature was set at 580ºC, water inlet temperature was set to 25ºC and water flow rate was set to 4l/min. Based on the processing conditions the water flow rate can be varied to shift the solid/liquid interface so that it is at an optimal distance away from the die thereby creating a semisolid shell of sufficient integrity allowing the bar to be cooled as it is extruded. Figure 6.17(e) shows evolution of the bar using AZ91D.

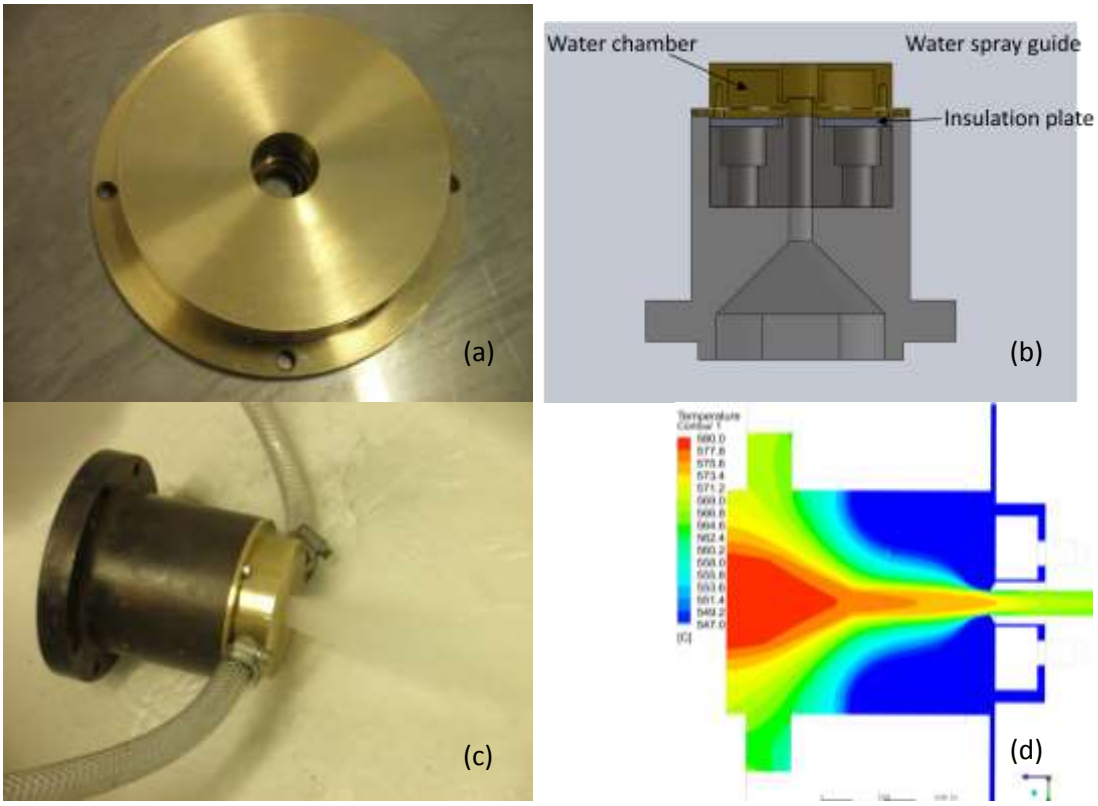

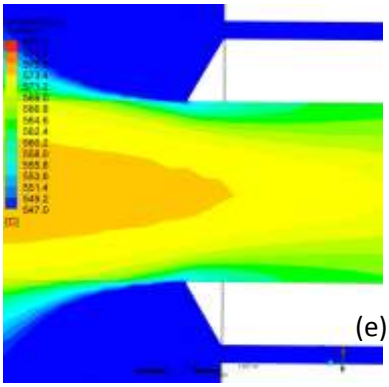

(e)

(f)

Figure 6.17: (a) BCWR (b) Schematic of BCWR (c) BCWR in operation (d & e) Simulated results using BCWR (f) Evolution of bar varying the flow rate using BCWR

6.5 Problems in Design-Inherent Aspects of the Screw Extruder

If the rheoextrusion process was to be looked at purely in functional terms, it can be broken down into a few steps.

- Shearing of slurry before the extruder
- Transport of the slurry using a screw pump
- External cooling
- Coiling

As discussed previously for the transport of the slurry a simple counter-rotating screw pump is used as it provides a positive displacement pump action and due to the high turbulence of the flow the melt can be further sheared. However using a screw pump for such purposes will always have some problems for the application due to the inherent nature of design of the screw pump.

- A small amount of air always being present behind the feed section leading to inherent porosity
- Nature of flow squeezing out of liquid phase causing segregation. Furthermore this liquid phase is known to travel backwards as the flight gap leak and is observed to collect around the bush causing additional wear of the graphite bush and reducing its life as seen in Figure 6.18(a)
- High wear of the screws leads to an increased molybdenum pickup thereby reducing the amount of aluminium alloy that can be processed within the available impurity tolerance. Furthermore the higher temperature of the input melt can increase the chemical attack of the aluminium as seen in Figure 6.18(b)
- Start up problems such as the possibility of melt jamming the machine on start up due to a small space for dendritic networks to grow in and waste of approximately 20m of extruded bar while steady state is being reached

Figure 6.18: (a) Wear of screw by liquid phase squeezed through screw bush (b) Additional wear near feed section

CHAPTER 7

DISCUSSION

7.1 Mechanisms of Grain Refinement in Primary Solidification

Extruded materials can display higher strength compared to the initial cast ingots due to the smaller grain size and elimination of casting defects such as segregation. Although the grain size and mechanical properties obtained so far by twin-screw rheoextrusion are not comparable to those carried out using methods such as ECAP and ECAE [Kubota et al., 1999; Mabuchi et al., 1997; Mohri et al., 1999] the process did demonstrate a good degree of controllability of properties. In the present investigation the slurry maker was able to create slurry with a desirable microstructure at an adequate speed. This was then transported down the extruder, and further refined before being extruded at the die where it was shaped into a rod of a predetermined diameter.

From the previously presented results it is seen that grain size is affected by several parameters. This section discusses in detail the various mechanisms involved that contribute to the overall grain refinement in TSRE at different points during the process. The solidification behaviour in TSRE is unique and is not readily seen in any of the existing technologies available to manufacture bars. Based on obtained results it is hypothesised that the microstructural refinement is governed by two distinct phenomena at different stages in the solidification process.

7.1.1 Nucleation under forced convection

In the process solidification starts to occur when the slurry is being prepared in the rotor stator slurry maker and during transport down the barrel of the extruder. In both these areas the conditions of the flow are characterised by high shear rate and high degree of turbulence. Such characteristics make for very powerful mixing. Consequently, the temperature and composition fields are uniform throughout the entire alloy melt during both the continuous cooling stage and the isothermal shearing stage.

Works by Fan and others show that the mixing power of the twin-screw mechanism can disperse any potential agglomerates of nucleation agents, and hence increases their potency for heterogeneous nucleation. In addition, the high turbulence of the twin-screw mechanism is an efficient means for heat transfer, reducing the chance for recalescence and re-melting [Fan, 2002].

In conventional casting processes to produce long profiles such a continuous casting or DC casting primary solidification of the process occurs by heterogeneous nucleation of the chilled liquid at the mould wall by a mechanism described as ‘big-bang’ [Chalmers, 1963]. The nuclei generally have a low survival rate as they are carried off by convection forces to overheated liquid zones within the alloy where they can re-melt and dissolve. It is observed that the majority of the crystal growth is columnar initiated at the mould wall and the few surviving nuclei contribute very unevenly to the resultant microstructure. The result of this is the typical coarse microstructure observed in cast products. A high nucleation rate on its own is not enough for a refined microstructure and the survivability of nuclei plays an important role in grain refinement, i.e. it is crucial that a higher number of nuclei survive as this can only refine the microstructure further.

To attain a high survival rate of nuclei at a given undercooling the following conditions need to be achieved

- Uniform temperature and chemical composition throughout the solidifying melt
- Quick thermal exchange to extract latent heat
- Well dispersed nucleation agents

When these conditions are met then what is coined as 'effective nucleation' [Fan and Liu, 2005; Ji and Fan, 2002] is obtained and all the nuclei have a good chance of survival and can contribute to microstructural refinement.

To understand the nature of the nucleation one must first understand the nature of the flow provided by the slurry maker and the twin-screw mechanism of the extruder. The contribution of high shear rate to effective nucleation in the TSRE process can be described by two mechanisms.

1) At the macroscopic level the flow within the slurry maker and twin-screw extruder is characterised by intense turbulence and high shear rate. This causes nuclei and other nucleation sites to be evenly distributed compared to conventional, DC or continuous casting processes. In addition to this, cyclic variations of flow are also encountered by the slurry due to the continuously changing flow direction within the twin-screw mechanism on route from hopper to die. The gaps within the machine are narrow and therefore this contributes to the shear level and heat exchange through thermal convection.

The uniform temperature and composition fields through dispersive mixing actions offer a higher nucleation survival rate and promote 'effective nucleation'. The result of this is a characteristic nucleation and growth phenomenon that differs from the conventional

casting processes and is more similar to the nucleation seen in the rheomoulding process [Fan, 2002].

This argument is well supported throughout the experimental results in micrographs such as Figure 5.9 presented in the previous section which shows a high number of close packed near-spherical grains with a small size distribution.

2) At the microscopic level the high intensity of shear is advantageous in dispersing oxide agglomerations. Although no oxide particles were observed in the course of the study, due to the volume of available text regarding the influence of shear dispersing oxides to promote heterogeneous nucleation it is not unreasonable to assume that similar mechanisms occur during TSRE.

It is reported that these agglomerations tend to be non-uniformly dispersed through the melt. Investigations by Fan [2009a] show that three morphologies of magnesium oxide occur in such non-sheared AZ91D melts. These are namely

a. Young oxide films formed during operations such as melt transfer and pouring
b. Old oxide films formed on top of the alloy in the crucible as it is melting
c. Oxide skins from the original alloy ingot

Findings from investigations by Fan [2009a] are presented in Figure 7.1. The figure shows SEM micrographs obtained by melt filtration where molten alloy is forced to flow through a micro-porous filter and the intermetallic particles and inclusions are collected by the filter.

The figure shows the particles collected by Fan using this technique and compares particles seen in the sheared and non-sheared alloy. Fan's findings show that after intense shearing

only intermetallic particles and old oxide films remain within the α-magnesium matrix and the size of the remaining old oxide agglomerations (darker spots) is severely reduced.

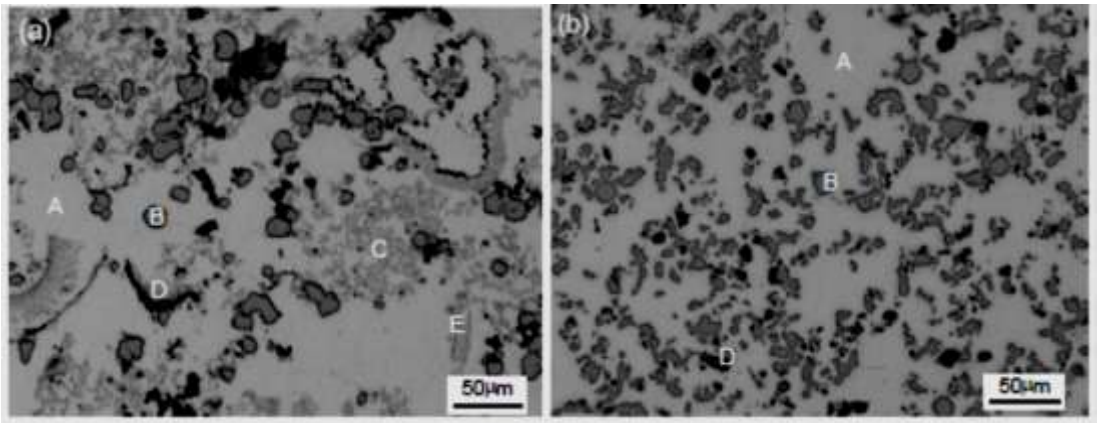

Figure 7.1: SEM micrographs showing the morphology of oxide and Al_8Mn_5 intermetallic particles from (a) non-sheared and (b) sheared AZ91D alloy melts. For the sheared sample, the shearing temperature, shearing speed and shearing time were 650ºC, 800rpm and 45s respectively. The following labels are used in the micrographs: A: α-Mg matrix; B: Al_8Mn_5 particle; C: young MgO films; D: old MgO films; E: MgO skins *[Fan et al., 2009a]*

On higher magnification the absence of the young oxide and oxide skin in Figure 7.1(b) are explained. Fan explained that upon intense shearing it is seen that oxide agglomerations were broken up and distributed evenly as single particles of 100-200nm in size in the sheared sample. These findings are shown in Figure 7.2.

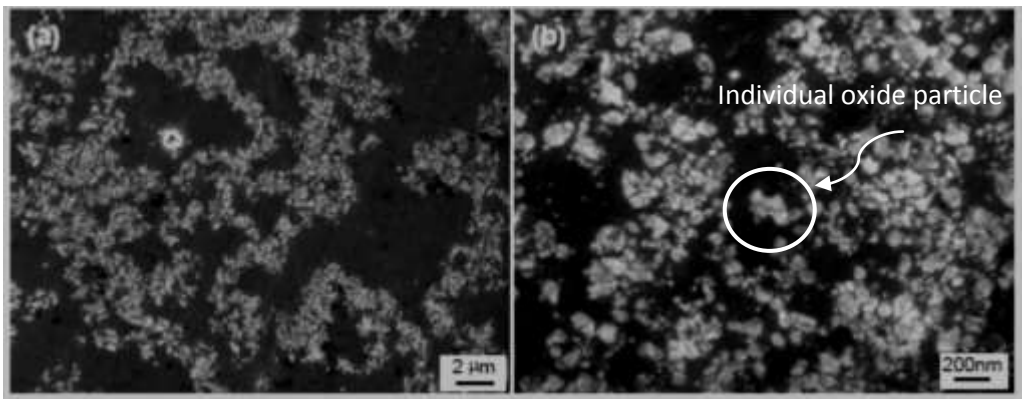

Figure 7.2: SEM micrograph showing (a) the oxide film from the un-sheared melt and (b) the morphology of the MgO particles of the sheared AZ91D alloy melt *[Fan et al., 2009a]*

Crystallography findings of Fan and co-workers [2009 a], show that some of the interfaces between MgO/α-Mg are semi-coherent with a small crystallographic misfit. The reported orientation relationship between the MgO/α-Mg phases is reported to be:

$<1\text{-}210>_{Mg}//<01\text{-}1>_{MgO}$ and $\{0002\}_{Mg}$-2°from$\{111\}_{MgO}$

Fan therefore concluded that the crystallographic matches of some of these MgO particles can further improve the viability of particles to act as potential sites for the nucleation and enhance heterogeneous nucleation.

On the other hand according to the free growth model proposed by Greer and co-workers [2000] the presence of potent nucleating particles does not necessarily result in effective grain refinement in the solidified structure.

For a given system containing nucleated particles that are wetted, the model predicts the free growth undercooling ΔT_{fg} which is inversely proportional to the nucleating particle size *d*.

$$\Delta T_{fg} = \frac{4\gamma}{\Delta S_V d} \tag{7.1}$$

Where γ is the interfacial energy between the liquid and nucleating solid phases and ΔS_V is the entropy of the fusion per unit volume. The above equation suggests that for heterogeneous nucleation, larger particles require a lower undercooling, whereas fine particles require larger undercooling. Accordingly grain growth should begin from larger particles and smaller particles will therefore be re-melted or will contribute much less to the final grain refinement. This suggests that the uniformity of structure is dependent on the size distribution of nucleating particles.

On observation of the uniformity of the highly refined structure presented in Figure 5.9(d) it is not unreasonable to assume that the size distribution of nucleation sites is narrow and these sites are well spread out by convection. The fine uniform structure further indicates that, assuming oxide is the key heterogeneous nucleant, the shear provided is adequate to distribute the majority of the oxide with a narrow size distribution and a favourable particle size; and that these particles contribute to refinement by acting as nucleating sites is in accordance to investigations available in literature [Greer et al., 2000; Quested and Greer, 2004].

7.1.2 Development of non-dendritic structures

It has been demonstrated by Men et al. [2010] that the rotor stator system provides high turbulence, convection and shear rates and this in turn can promote heterogeneous nucleation as discussed previously. This is considered to be the primary reasons for the achievement of the refinement of the slurry prior to feeding as seen in Figure 7.3.

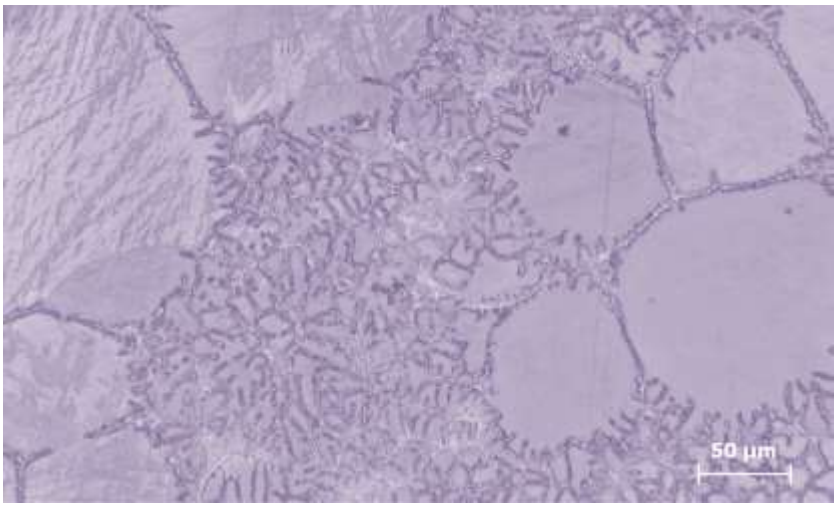

Figure 7.3: Detailed observation of slurry prepared at 590°C

However during solidification there are a number of routes by which further grain refinement can take place and non-dendritic structures can be formed. Furthermore in the TSRE process it is necessary that non-dendritic structures are produced as the continuous forming is dependent on high fluidity which is a rheological characteristic achieved when non-dendritic structures are present.

As the slurry passes through the twin-screw extruder there is a reported decrease in particle size as shown in Figure 5.21(a). This is detailed more in Figure 7.4 which shows the effect of grain refinement pictorially and evolution of the morphology of the structure (grain density and shape) during the extrusion of the slurry through the twin-screw extruder.

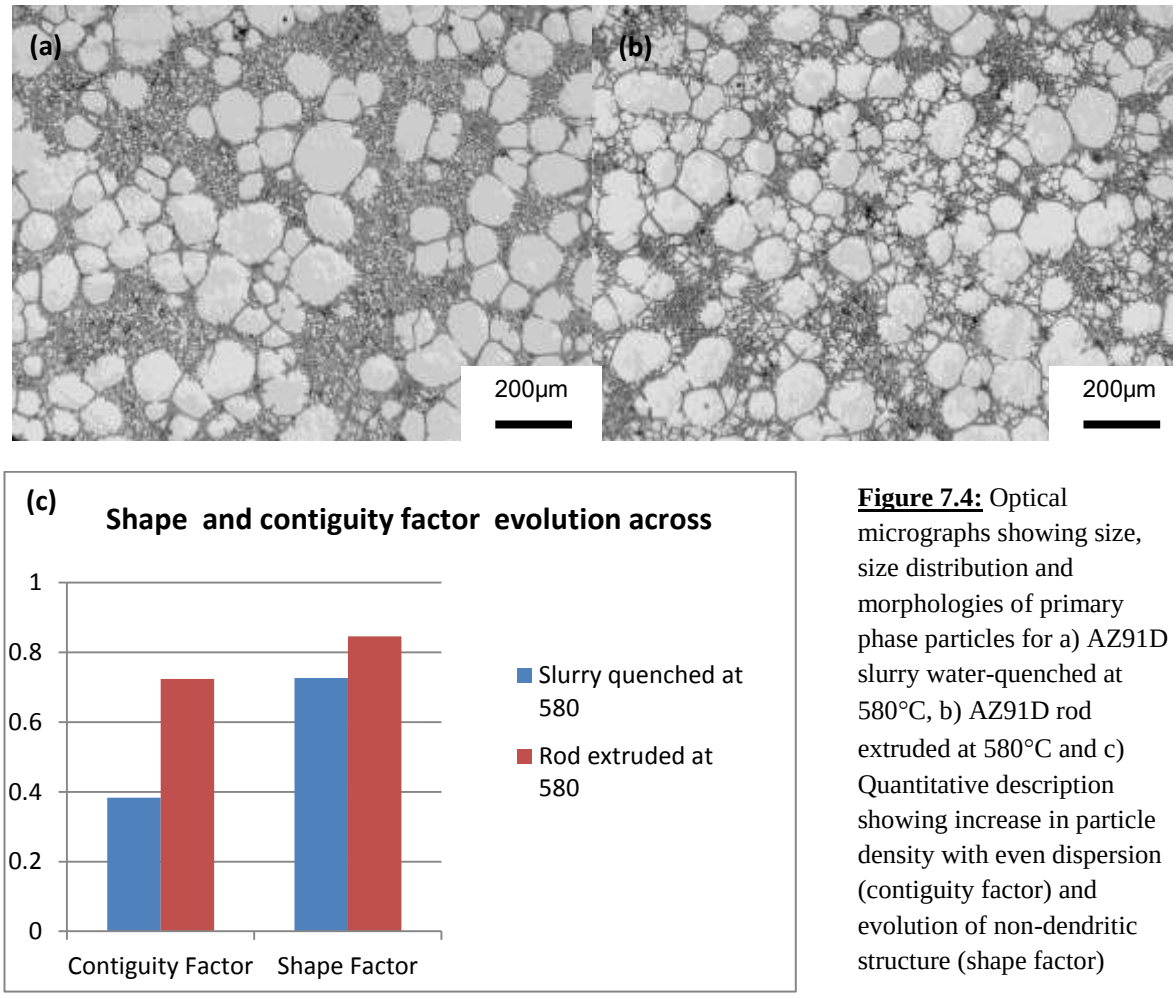

Figure 7.4: Optical micrographs showing size, size distribution and morphologies of primary phase particles for a) AZ91D slurry water-quenched at 580°C, b) AZ91D rod extruded at 580°C and c) Quantitative description showing increase in particle density with even dispersion (contiguity factor) and evolution of non-dendritic structure (shape factor)

From analysis of the results it is thought that there are three main contributing factors to the development of non-dendritic structures. These are discussed in detail in this section.

a) Fragmentation in the extruder

Theory suggests that during slurry making under forced convection, the initial dendrites would fragment through one of the mechanisms and the detached arms can then further undergo a coarsening process to provide the observed globular particles.

It is conventionally believed [Doherty et al., 1984; Flemings, 1991; Hellawell, 1996; Ji and Fan, 2002; Molenaar et al., 1985; Molenaar et al., 1986; Mullis, 1999; Vogel and Cantor, 1977] that in slurry the evolution of a spherical non-dendritic grain structure from a dendrite via rosette occurs through one or more of the following mechanisms.

1) Dendrite arms melting at the root [Hellawell, 1996] or by liquid penetration through high angle boundaries [Doherty et al., 1984]
2) Cellular growth and ripening effect [Molenaar et al., 1985; Molenaar et al., 1986]
3) Dendrite arms breaking due to thermal-solutal convection [Mullis, 1999]
4) Dendrite fragmentation by mechanical force [Flemings, 1991]

Since there are not many dendritic structures in the slurry it can be assumed that the majority of the globular spherical structure is due to the result of spherical growth under forced convection and this is detailed in the next section. This is in good agreement to research done by Ji and Fan [2002] as well as simulations carried out by Qin and Fan[2000].

b) Solidification under convection

The previous section may explain the reason for the fragmentation and solid particle multiplication of tiny dendrites but it does not explain why these particles would develop into more equiaxed globular structures rather than more dendrites as seen in Figure 7.3.

An explanation to this can be formed when considering recent experimental [Fan and Liu, 2005; Ji and Fan, 2002] studies on different materials conducted by Fan and co-workers which are supported by findings of Monte Carlo simulations conducted by Das et al. [Das et al., 2002] and phase field simulations conducted by Qin et al. [Quin and Wallach, 2003]. These studies suggest that in the presence of turbulent flows, high shear helps transport solute atoms away from the solid liquid interface and stabilises planar growth by restricting dendrite development. Therefore it is thought that the globular non-dendritic structure in the results is believed to be a direct consequence of spherical growth under forced convection. This is in accordance with the microstructures of sheared slurries prepared at various temperatures seen in Figure 5.1 and 5.2 suggesting that the convection causes the growth of spherical particles. The rise in particle density in Figure 5.21(b) may well be due to the increase in nucleation rate due to cooling in the barrel and potential additional nucleation sites brought about by the breakup of dendrites as discussed previously. The increase in particle number and particle size contributed to the increase of solid fraction.

The volume fraction of solid particles described in Figure 7.5 in the slurry was calculated from the measured particle size and density by the relationship detailed in Equation 4.3 assuming random particle distributions. The calculated results are given in Figure 7.5 and compared to theoretical predictions from the Scheil equation taking the partition coefficient of the alloy as 0.36) as shown in Figure 7.5.

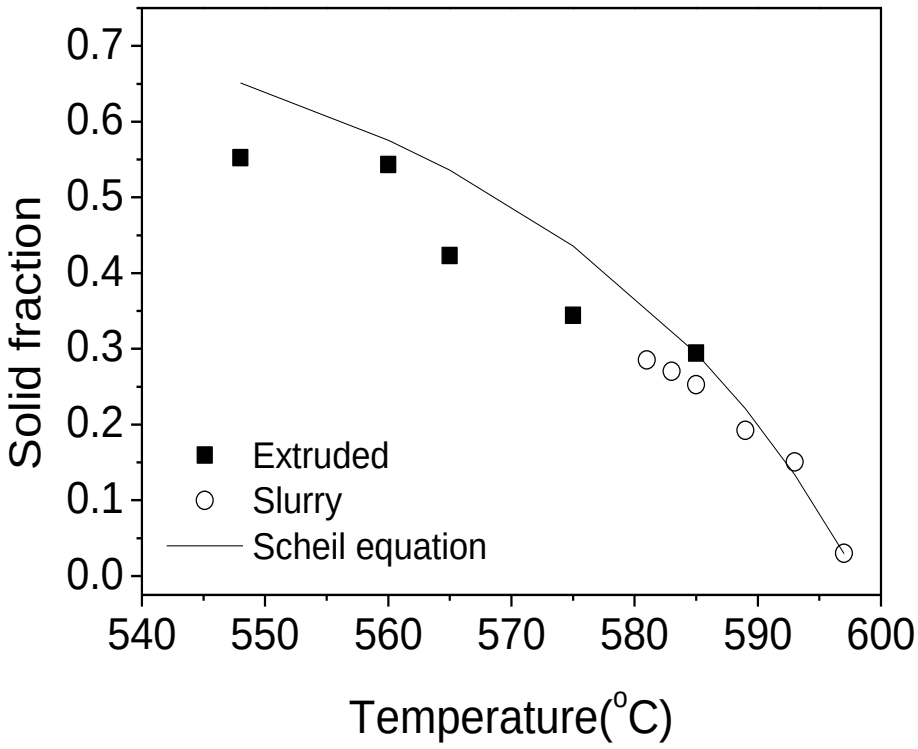

Figure 7.5: Microstructural parameters of the AZ91D slurry and extrusions as a function of temperature: Solid fraction of primary particles in comparison with predictions by the Scheil equation

The calculated volume fraction is in a good agreement with the theoretical predictions confirming the validity of particle size and density measurements and the findings in Figure 5.21.

Figure 5.21 also shows that while the particle density increased the average particle size quickly maximised and then stayed constant against decreasing temperature. The continuous trend up to this point in particle density increasing with respect to the process temperature suggests that there was no significant change in the mechanisms responsible for nucleation over the range of temperatures.

It is then difficult to explain why the average particle size remained constant, which resulted in a negative deviation of the measured solid fraction from the theoretical

predictions as shown in Figure 7.5. The size of the largest particles in the slurry was noted as almost constant from 593 to 585ºC. This indicates that the forced convection by intensive shearing restricted growth of particles once they had grown to a certain size.

This particle growth behaviour may be related to the solid particles coherency in the slurry, which is reported to be at about 592ºC for AZ91D magnesium alloy under low shear rate by Gourlay et al. [2008], although more investigations are required to understand the mechanisms behind this phenomenon.

Microstructural analysis revealed an increase in particle number density and nucleation rate during extrusion as shown in Figure 5.21(b). This is attributed to the difference in cooling rate experienced by the slurry when compared with the slurry making examination. In accordance with general theory when the slurry was introduced to the extruder, due to the increased cooling rate there was an increase in the undercooling and nucleation rate.

On average for AZ91D the cooling rate during slurry making was approximately 5ºC/min while as the slurry was poured into the rheoextruder it may have experienced a cooling rate of 40-140ºC/min. From Figure 7.3 it can be seen that in the extruded sample there are several newly formed alpha phase particles and their morphology is mostly dendrite- or rosette-like.

Figure 7.6 suggests at 580ºC the shear experienced by the melt was not sufficient to allow for spherical growth. However the shear was adequate to achieve granular non-dendritic structures at 560ºC. This is because the lower temperature corresponds to a higher solid fraction, higher viscosity and increased shear force that enhances the effect of shearing at lower temperatures.

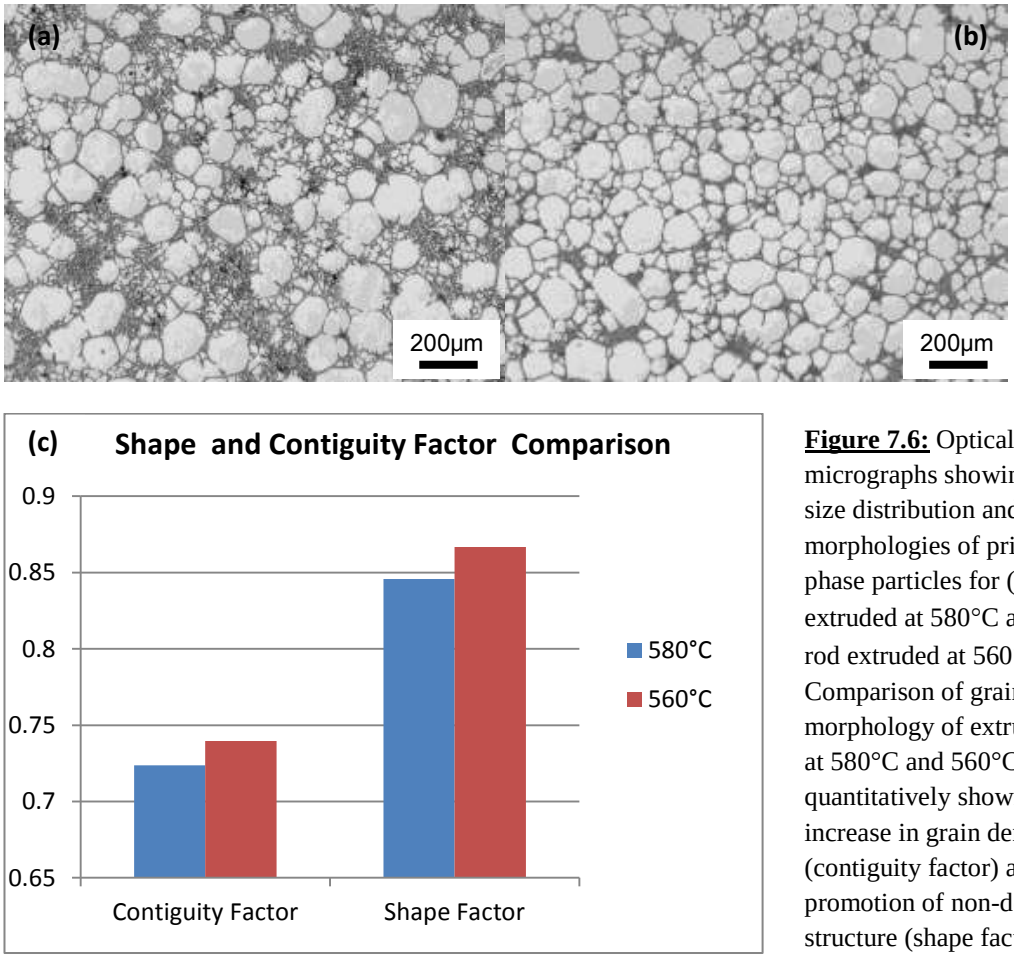

Figure 7.6: Optical micrographs showing size, size distribution and morphologies of primary phase particles for (a) a rod extruded at 580°C and (b) a rod extruded at 560°C. (c) Comparison of grain morphology of extrusions at 580°C and 560°C quantitatively showing increase in grain density (contiguity factor) and promotion of non-dendritic structure (shape factor)

In addition to this the lower temperature also provides a higher driving force for particles to grow and when this is coupled with the high level of turbulence it results in the formation of a non-dendritic structure under relatively low shear rates. At 150RPM the shear rate of the extruder is approximately 400/s and the results are in agreement with the findings of Ji and co-workers [2002].

c) Deformation and dynamic recovery

As the Zener-Hollomon parameter of the deformation is reduced, cross-slip is seen to become more favourable, [Couret and Caillard, 1985] and the reordering of dislocations leads

to the creation of low-angle boundaries (LABs). The rotation of these new substructures leads to a progressive rise in the number of misorientations and in the gradual appearance of high-angle boundaries (HABs) [Galiyev et al., 2001; Ion et al., 1982;Tan and Tan, 2003]. This process is also known as continuous dynamic re-crystallisation (cDRX) or extended recovery.

During severe compression and extensions, deformation by twinning has been observed in several studies. However this extent of twinning was not observed in the TSRE process. This shows that the stresses required to activate deformation by twinning were not observed and the deformation was essentially accommodated by slip. This indicates that the value of the Zener-Hollomon parameter is thought to be below the critical value of ~7x 10^{12} s^{-1}.

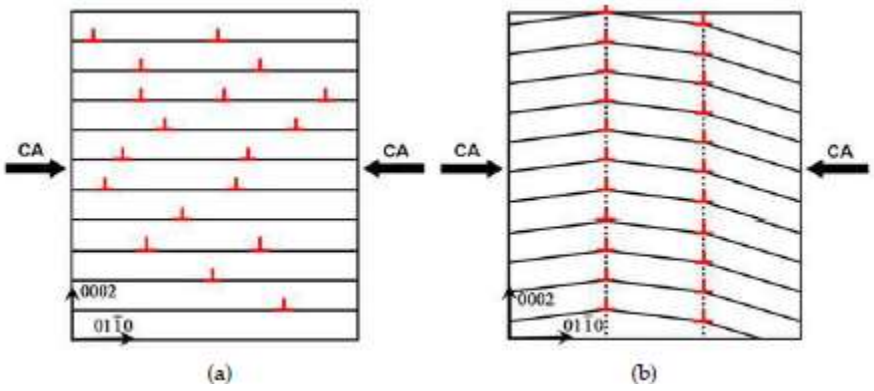

Figure 7.7: A schematic representation of the formation of microbands and their associated boundaries, and the associated changes in basal plane orientation. (a) Agrain deformed in compression, (b) the microbands originate from the rearrangement of basal dislocations (shown in red).The dotted lines correspond to the geometrically necessary boundaries

In such cases it is reported that during the early phase of deformation at high temperature grains of magnesium are fragmented by geometrically necessary boundaries (GNBs). These boundaries separate microbands (MBs) of material at different orientations. These

boundaries are seen to be straight, oriented perpendicular to the compression axis and transverse going into the grain. The formation of MBs is accredited to the mechanism of dynamic recovery and they are seen to increase with strain. This is depicted schematically in Figure 7.7.

Figure 5.22(a) which was a micrograph of a material attained at a higher temperature only depicts twins as deformation structures. Whereas the presence of MBs in Figure 5.22(b) indicates that stresses were below the critical level to activate twinning as the deformation was accommodated primarily by slip. Twins can also be easily introduced into the surface of magnesium specimens by grinding or polishing. It is therefore highly possible that the twins observed are artefacts induced by specimen preparation and not formed during the extrusion process where deformation temperature was well above where twinning is expected. However there seems to be a contradiction in this result as there would be a higher strain put on the material at lower temperatures due to an increase in shear stress corresponding to an increase in solid fraction and viscosity. Based on theory one would expect to see a higher presence of twins rather than MBs at lower temperatures as the Zenner-Hollomon parameter would be increased.

It is reported that as-cast magnesium structures can have twins of up to 12% of the entire volume [Kaibyshev and Sitdikov, 1994]. Therefore this result could be used as an indication that for higher temperature extrusions there is virtually no deformation and the twin structures observed are naturally occurring twins due to lowering the temperature to 545°C, and only a tiny amount of deformation that is accommodated by slip is observed. This would result in the observed microbands.

Although the high temperatures would inevitably mean there would be some level of recovery, the lack of evidence of dynamic recovery in samples extruded above 560°C may be evidence that there was effectively no deformation to begin with. This further indicates

that at such conditions there is practically no strain on the material and the process is more similar to the continuous rheocasting processes rather than the extrusion process.

If this is the case then it can be speculated that upon further reduction of temperature or changes in machine parameters that would increase strain, more MBs would be observed and eventually deformation by twinning would occur once the critical value of the Zener-Holloman parameter was achieved. Furthermore there is evidence in the literature that suggests that at extremely high temperatures and low strains, initially formed twins can transform into re-crystallised grains during deformation [Kaibyshev and Sitdikov, 2001]. This is depicted as region 'I' in Figure 7.8.At lower temperatures when the activation energy of the plastic flow approaches a critical level for volume self diffusion (~135kJ mol^{-1} in Mg [Frost & Ashby, 1982]) an increase in basal dislocations is seen to be the controlling mechanism of deformation. [Galiyev et al., 2001; Barnett, 2003]. Under these conditions recrystallisation by bulging of initial grain boundaries (also known as discontinuous dynamic recrystallisation) is also reported [Guo et al., 2005; Martin et al., 2008; Sitdikov and Kaibyshev, 2001]. The specific mechanisms of re-crystallisation in magnesium are dependent on strain and temperature and are depicted in Figure 7.8 [Kaibyshev & Sitdikov, 1994].

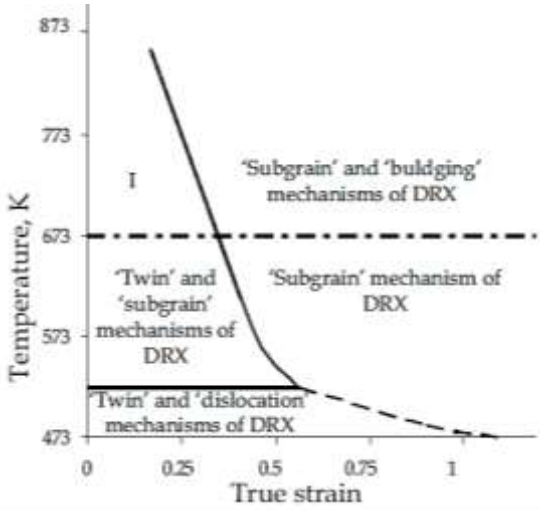

Figure 7.8: Dependence on factors for the mechanisms for re-crystallisation [*Kaibyshev and Sitdikov, 1994]*

7.2 Eutectics

In AZ91D at 431°C, secondary solidification starts to occur and the eutectic reaction occurs in the remaining liquid alloy. The morphology of these structures can be used to shed light on the solidification behaviour of the alloy and influence the mechanical properties and post operation heat treatment settings significantly.

The eutectic reaction is described by the following equation.

$$L \rightarrow \alpha + \beta(Mg_{17}(Al, Zn)_{12}) \tag{7.2}$$

The morphology of the eutectic in hypoeutectic Mg-Al alloys depends on the composition and cooling rate. For slow cooling rates and in alloys with high aluminium content regular lamellar or fibrous eutectic morphologies are seen. *[Dahle et al., 2001]*

In cases with low aluminium content such as AZ91D and in cases with a rapid cooling rate fully or partially divorced morphologies are reported i.e. the intermetallic phase takes a massive type of morphology as opposed to the fibrous or lamellar morphologies of normal eutectics. *[Dahle et al., 2001]*

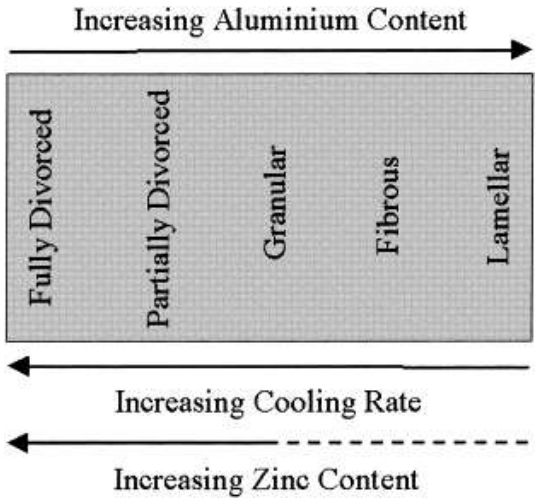

Figure 7.9: The effect of aluminium content, zinc content and cooling rate on eutectic morphology in permanent mould cast hypoeutectic Mg–Al alloys *[Dahle et al., 2001]*.

A fully divorced eutectic morphology consists of totally divided phases with single β-phase $Mg_{17}Al_{12}$ particles surrounded by eutectic α-magnesium existing in every inter-dendritic region where as partially divorced structures are described to be islands of eutectic α-magnesium within the β-$Mg_{17}Al_{12}$ phase [Dahle et al. 2001].

The effect of aluminium and zinc content as well as the cooling rate on the morphology of the eutectic are shown schematically in Figure 7.9. It can be seen that the eutectic tends towards a less divorced structure when aluminium content is increased but more divorced as the zinc content or the cooling rate is increased. These mechanisms are detailed by Nave [2000] and are dependent on the location of the coupled zone and undercooling during solidification.

After primary solidification at 560°C (f_s=0.6) and 580°C (f_s=0.4), one would expect the composition of the remaining liquid to have an increased composition of aluminium. In the sample at 580°C the composition of the remainder of the liquid phase after primary solidification will have lower aluminium % content as there is a higher quantity of liquid phase. Therefore again it should be observed that the sample at 580°C should have a more divorced eutectic structure as opposed to the sample at 550°C. This is not observed.

In addition, investigations show that zinc has a tendency to concentrate in the intermetallic phase [Guldberg, 1997] with a local content of up to 4%. Therefore at a lower process temperature it can be assumed that the eutectic liquid is compositionally richer in zinc causing a fully divorced structure at low process temperatures. This is in agreement with the obtained results at 550°C from Figure 5.24(a) which show a divorced eutectic. Therefore it can be concluded from our results that in the processing of AZ91D by rheoextrusion the content of aluminium in the secondarily solidified liquid does not affect the structure of the eutectic as much as the content of the zinc.

Another interesting morphology is observed in the eutectic across the range of process temperatures is the formation of magnesium ‘islands’ surrounded by thick deposits of eutectic. This can be seen in Figure 7.10. This can be accredited to the unique cooling process during rheoextrusion.

In the rheoextrusion process cooling occurs in two distinct manners. Initially, the slurry is cooled at a low cooling rate in the extruder and when it leaves the extruder it is quenched which corresponds to a higher cooling rate.

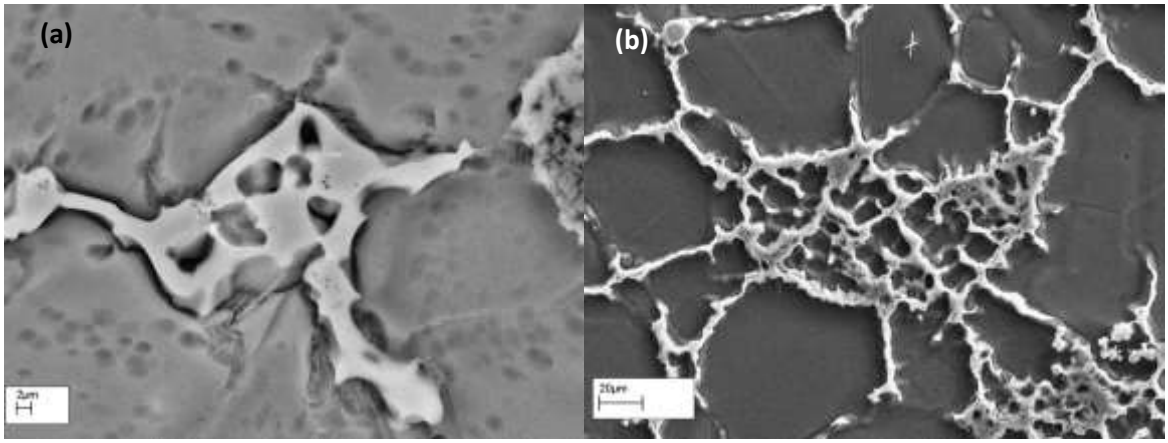

Figure 7.10: Island structures observed in eutectic pockets at a) 545°C b) 575°C

During the initial cooling it is assumed that the primary phase grows and the remaining liquid phase begins to get entrapped between formed grains.

The lowest explored process temperature was limited due to the limitations of the machinery. Even so at such temperatures the removal of 40-60% of magnesium as solid phase α-particles can disrupt the composition of the remaining liquid. The local increase in aluminium content in the composition in such pockets can shift the position of the liquid across the solvus line to a point on the phase diagram where larger undercooling would be required for solidification. This liquid phase would fill the spaces in between grains and pockets of aluminium rich liquid would be carried towards the die.

On quenching after the die, large undercooling provided causes the precipitation of the remaining magnesium within the pockets of this liquid phase creating a structure that should look like islands within the sea of liquid phase. The precipitation of magnesium rather than aluminium suggests that the phase composition has not shifted across the eutectic point.

Furthermore at higher temperatures there would be a higher content of liquid and magnesium content within this liquid. This would result in larger islands when compared to structures obtained at lower process temperatures. The morphology of these islands would be dependent on the cooling rate and in accordance with solidification theory a more dendritic morphology should be observed at higher undercooling. The results are seen to fit this trend. These large islands could act as areas for local stress concentrations thereby explaining the observed trend in mechanical properties with respect to the process temperature. This is discussed in section 7.6.

7.3 Intermetallics

The most prominent intermetallic compound observed was intermetallics formed with manganese. Manganese is added to Mg-Al alloys to improve the corrosion resistance. The most common manganese intermetallic particles found are the Al_8Mn_5 particles. Different morphologies of this intermetallic were found in the middle of grains and the grain boundary. This can be seen in Figure 5.28.

Particles formed at the centre of grains were observed to be larger and these particles could have acted as sites of heterogeneous nucleation as described by Ohno [2006] as they would have precipitated and started to grow at higher temperatures. Furthermore their position within the centre of grains seems to validate this.

Particles found at the grain boundary were observed to be smaller and less faceted. It is thought that these may be formed upon final solidification during quenching when the remaining liquid phase with low manganese content solidifies between primary grains.

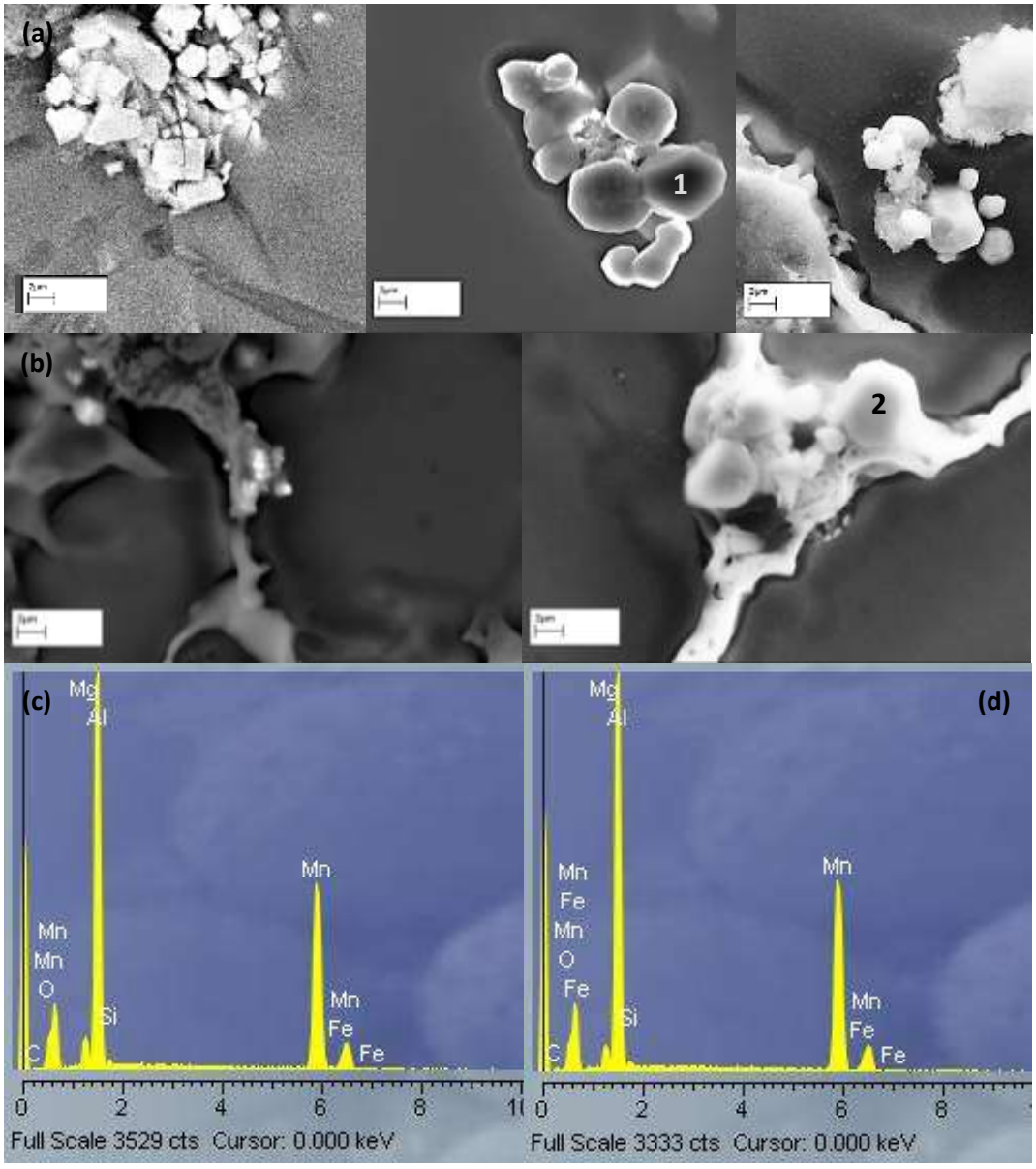

Figure 7.11: a) evolution of the manganese-rich intermetallic found a) within the grain at 545°C, 560°C and 575°C b) at the grain boundary at 560°C and 575°C c) Spectrometry results from point 1 in Figure 7.11(a) and d) Spectrometry results from point 2 in Figure 7.11(b)

The morphology of both these particles is affected by the process temperature. As the process temperature increases, the particles in the centre of grain appear to become smaller and more rounded as seen in Figure 7.11(a). Ohno suggested that the Al_8Mn_5 particle nucleates before magnesium. At a lower process temperature a higher level of undercooling may allow for a more developed crystal growth which can explain the larger more developed structures. This suggests that the level of undercooling plays a significant role on the morphology of these particles.

Contrary to this, the particles found at the grain boundary were observed to grow in size as the process temperature increased. At high temperatures fewer and smaller primary intermetallic particles are precipitated. Therefore the remaining eutectic liquid would have a higher content of manganese. Upon quenching this is precipitated into larger crystals at the grain boundary. This explains the trend seen in the results and is seen in Figure 7.11(b).

The trend of lower grain size at lower processing temperature suggests that the availability of suitable primary intermetallic particles may contribute to an increase in grain density by acting as sites for heterogeneous nucleation.

During the rheoextrusion of magnesium, iron was observed to be a picked up impurity. Spectrometry reveals that this iron has an affinity towards manganese and is generally found in or around the Al_8Mn_5 crystals. Figure7.11 (c & d) show that the iron will accumulate anywhere the manganese will.

This can be accredited to the high melting point of iron compared to magnesium and in a similar manner to manganese, iron will precipitate as an intermetallic before the solidification commences. Cao et al. [2004] suggests that these particles can act as suitable sites for heterogeneous nucleation in Mg-9%Al alloys. This is in agreement with work by

Byun et al. [2003] who showed that $Al_8(Mn, Fe)_5$ particles can act as effective nucleation agents in AZ91D.

7.4 Microstructural Defects

Twin-screw rheoextrusion is a new process and as expected there are still some defects that are found within the bar which reduce the overall quality of the rod .Even though TSRE is a future emerging technology it can be seen that a lot more work needs to be done to improve the quality of extruded bars. For now the most suitable applications for materials processed by this method are applications where mechanical properties are not critical such as welding rods and feedstock. These defects will be discussed in this section.

7.4.1 Segregation

Since rheoextrusion is performed in the semisolid state it is unavoidable that there will be both solid and liquid phase present. This is demonstrated by the presence of the secondarily solidified dendritic networks seen in all the microstructures. Segregation can be of two types: macro-segregation and micro-segregation.

Micro-segregation is defined as the non-uniform distribution of alloying elements within a volume and is a chemical non-uniformity that is seen and is measured on the scale of the dendrite spacing. It typically occurs when the partitioning and redistribution of the solute between solid and liquid phase that accompany the solidification of alloys do not reach equilibrium and uniform chemical potential is not obtained within all phases of the cast alloy. Due to the small and symmetrical dimensions of the extruded profile coupled with

the non-dendritic structure this sort of segregation is not readily observed in rheo extruded bars.

A macro-segregation model caused by volumetric deformation in a coherent mushy zone was suggested by Nicolli [2005]. Such investigations show that for Al-4 wt % Cu even a small strain (~2%) of the solid network can lead to macro segregation comparable to results of solidification shrinkage induced melt flow [Nicolli et al., 2005].

The mechanism of macro-segregation is well documented in the literature pertaining to reverse extrusion and is understood to be due to the relative movement of the liquid phase out of the solid skeletal network within the mushy zone of semisolid metal systems.

The literature reviewed in Section 2.1 describes Darcy's law which is used to understand the liquid flow through a porous medium (Equation 2.2). The law relates the dependence of the velocity of liquid phase flow relative to the solid phase on factors such as the permeability and the pressure gradient. The literature survey also describes the Carman-Kozeny model (Equation 2.3), [Bear, 1972] which shows the dependence of the permeability on factors such as the grain size and the fraction of liquid phase. From Equation 2.3 it can be seen that the value of the permeability is proportional to the square of the average grain size.

$$K \propto d_m^2 \tag{7.3}$$

Figure 5.21 shows that the grain size is dependent on the process temperature and that at higher process temperatures larger grains are observed. This in turn means that the permeability of structures obtained at higher process temperatures is higher and this results

in a larger value of the velocity of the liquid phase relative to the solid skeleton indicating more segregation.

In addition to this, higher temperatures indicate that there will be a higher fraction of liquid phase on analysis of the Carman-Kozeny model, [Bear, 1972] it can be seen that the permeability is also proportional to the value of the liquid phase which suggests that the structure is more susceptible to segregation at higher temperatures.

Results obtained and seen in Figure 5.12 and Figure 5.14 showing more segregation at higher process temperatures are in agreement with this.

The pressure built up by the extruder also plays a significant role in the segregation process as it is the driving force of the movement of the liquid phase relative to the solid phase. This is due to mushy metal being squeezed at the die end by the pressure built up by the rotating screws.

From calculations obtained processing magnesium at temperatures of 560°C, the built up pressure of the screws is found to be 6kPa. Calculations suggest that the theoretical output for the slurry should be 0.19m/s. The calculated fraction of solid and the viscosity was based on the same methods described in investigations by Ilinka [2008], whereas the shear rate was calculated by the methods detailed by Samoilov [1969]. The difference between the calculated value and measured value (~0.1m/s) can be attributed to the energy dissipated for overcoming the frictional forces within the die upon solidification. These forces in turn contribute to a pressure built up by the screws at the die.

This pressure can be useful as it can be used to compact the solid skeleton. However in the presence of a higher fraction of liquid phase, this pressure can be transferred to the fluid which finds its way back through the extruder by a means of a variety leakage flows. In

TSRE the most significant of these is the flight back leakage flow and as the liquid phase is squeezed in the outward direction at the die it is picked up by the flight gap leakage flow which conveys it backwards.

Figure 7.12: Segregated liquid squeezed through the flight gap

This phenomenon has been verified during the maintenance of the machinery. Figure 7.12 shows such solidified segregated liquid after it has been squeezed through the gap of the graphite bush causing the screws to jam.

It has been reported that the grain morphology and solid fraction play a significant role to minimise this sort of segregation. It was reported by Guo [2006] that electromagnetic vibration led to grain refinement and the equiaxed grains greatly reduced the segregation behaviour of as cast AZ80 magnesium billet.

During solidification under convection solute is continuously rejected into the liquid phase causing the liquid to become richer in solute. It has been shown by Kurz that the morphology of the solute rejected is significant [Kurz and Fisher, 1986] since the large

numbers of equiaxed grains reject solute evenly. As the solidification proceeds, the crystal growth then increases the solid fraction (f_s) evenly and at the dendrite coherency solid fraction (f_s^{ch}) the crystals impede each other's growth as shown by Gourlay and Dahle [2007]. It has been reported that the value of (f_s^{ch}) is dependent on size and shape of the crystals [Arnberg et al., 1993; Sumitomo et al., 2000; Veldman et al., 2001]. The value of (f_s^{ch}) is reported to range from ~0.15 for columnar and ~0.5–0.74 for equiaxed crystals as demonstrated in investigations by Arnberg [1993] and Dahle and St. John [1998]. This in turn means there is less available liquid phase to segregate for non-dendritic structures.

This confirms that the convection offered by the counter-rotating twin-screws as well as the feeding mechanism that play an important role in the formation of non-dendritic structures can effectively be used to reduce the overall segregation.

7.4.2 Porosity

Types of porosity in the rheoextruded samples are categorised based on their scale and are discussed below.

A) Micro-porosity – Hydrogen evolution and solidification shrinkage

Evidence of micro-porosity can be seen in Figure 5.25. The cause of micro-porosity in Mg-Al alloys has been a debated topic since early investigations conducted by Baker [1945] and a lot of argument has occurred over the contribution of various factors such as dissolved gas and solidification shrinkage to the formation of micro-porosity. Initial studies suggested that dissolved hydrogen was not a significant factor since the difference in solubility of hydrogen between solid state and liquid state is relatively small compared to aluminium alloys. It was instead believed that the solidification shrinkage was responsible

for the porosity formation. However this theory was soon dismissed and measurements of the dissolved hydrogen content in melt before solidification has suggested that it contributes to the formation of micro-porosity, [Baker, 1945; Liddard et.al., 1945; Whittenberger et al., 1952].

However, it is unlikely that the formation of micro-porosity is down to just one of the two mechanisms described above and it is known that shrinkage and evolution of dissolved gas occur simultaneously to form micro-porosity just as in any other alloy system [Whittenberger et al., 1952].

Compared to aluminium alloys, magnesium alloys have a lower thermal conductivity and solidify slower. As a result of the wide freezing range the inter-dendritic feeding is a very important stage during solidification. It has been reported [Øvrelid et al., 1997] that the solubility of hydrogen is dependent on the aluminium content of the Mg-Al alloy and that this content has a significant effect on the solubility levels [Schaffer et al., 2001]. Findings of these studies show that peak porosity occurs at 9 wt.% Al as seen in Figure 7.13.

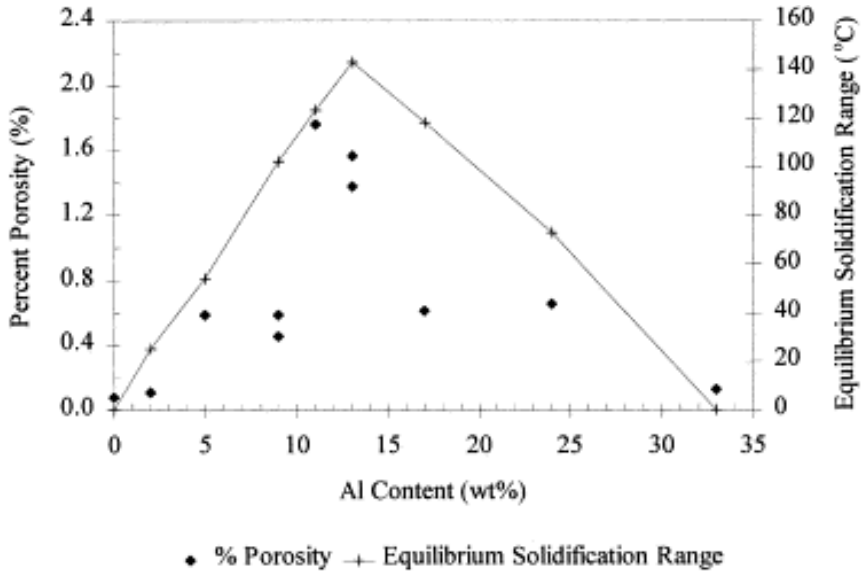

Figure 7.13: Percentage porosity versus aluminum content and freezing range versus aluminium content. Note that the large freezing range correlates with a greater incidence of porosity *[Dahle et al., 2001]*.

Pure magnesium and the eutectic alloy both display low levels of porosity and this is related to the relatively isothermal solidification of these alloys. In other alloys the volume fraction of the eutectic increases proportionally with the content of aluminium and this reduces porosity. Therefore the reason for the peak porosity at about 9% is thought to be due to a combination of various factors such as mushy zone size, inter-dendritic feeding, permeability and eutectic volume fraction [Dahle et al., 2001].

B) Macro-porosity– Entrapment of air

There are two major reasons for the presence of entrapped gas in the extruded melt. The first is due to the presence of air in the extruder when the melt is introduced to it. As the melt is mixed in the presence of air an amount of air gets entrapped within the viscous solidifying fluid and is observed as entrapped gas porosity. This however is a start-up problem that will only be encountered on the laboratory scale since with continuous running of the machinery all the air from within the barrel will be expelled.

Figure 7.14: Graphite screw bush

The second reason for the entrapment of air is a more inherent design flaw. This is because an inclined screw extruder will always have a volume of air trapped behind the feed section. As the metal is mixed in its presence this leads to the addition of gas porosity into the melt. Similar problems are also reported in other fields such as polymers and pharmaceuticals where twin-screw extruders are used [Cisneros et al., 2002; Crowley et al., 2007].

To overcome this, a graphite screw bush was inserted over the screw shafts to reduce the overall volume of air present thereby reducing the porosity levels in the extruded bar as seen in Figure 7.14.

7.4.3 Hot tearing

Hot tearing is not commonly observed in the rheoextrusion process and was only encountered while dealing with the aluminium alloy LM24. It is well documented that the reason for hot tearing is uneven rates of solidification shrinkage caused mostly due to uneven cooling rates [McCartney, 1989; Nadella et al., 2008] at different points of a solidifying structure especially when a large body is considered. However due to the small dimensions of the rheoextruded bar as small and one would not expect to find significantly different rates of cooling even on quenching.

Microstructural analysis of rheoextruded LM24 indicate severe separation of silicon from the matrix to the extent where unexpected large grains of primary silicon are observed. It is thought that due to such an uneven compositional structure the local stresses associated with uneven contraction rates of aluminium and silicon may lead to the formation of these

hot tears. The possible reasons for this solidification process are discussed further in Section 7.5.

7.5 Limited Applicability to Aluminium Alloys

7.5.1 Molybdenum pickup observation

Spark analysis reveals the content of impurities picked up by the melt at various settings of time and temperature and are alloy specific. A molybdenum pick up is observed in all the aluminium alloys. This erosion is due to the high wear environment of the screws in the presence of the chemical attack by aluminium.

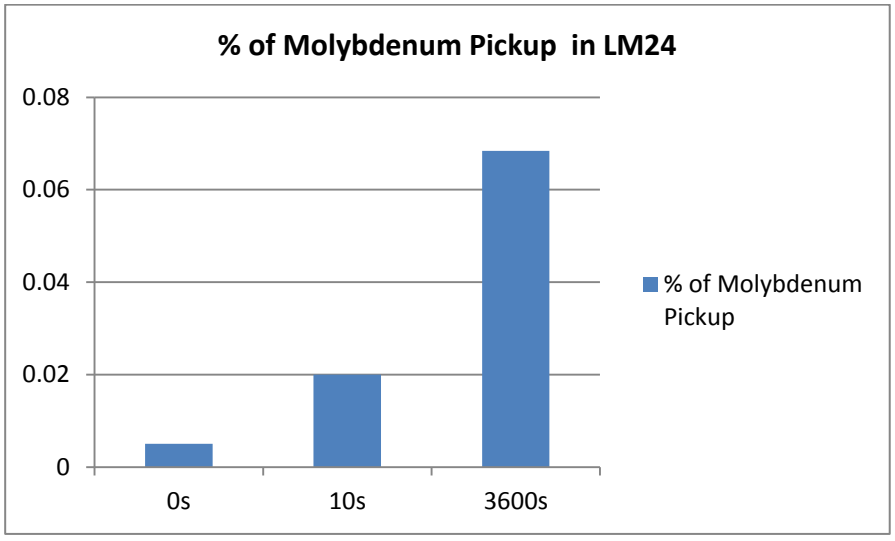

Figure 7.15: Comparison of molybdenum pickup over time

Aluminium alloy LM24 was sheared in the barrel for different lengths of time. Figure 7.15 compares the dissolution of molybdenum in LM24 over a period of time. Therefore it can

be assumed that over time the shear effect and transportation of the extruder will be reduced.

AA5356, LM24 and AA4043 were extruded and the composition of the extrudate revealed the level of molybdenum dissolution in the molten aluminium. Figure 7.16 compares the results. It is observed that a higher silicon-containing alloy will pick up less molybdenum. This is accredited to a layer of molybdenum silicide forming on the surface which gives protection from further chemical attacks. Therefore it is more feasible to extrude aluminium alloys with a high silicon-content using the twin-screw rheoextruder.

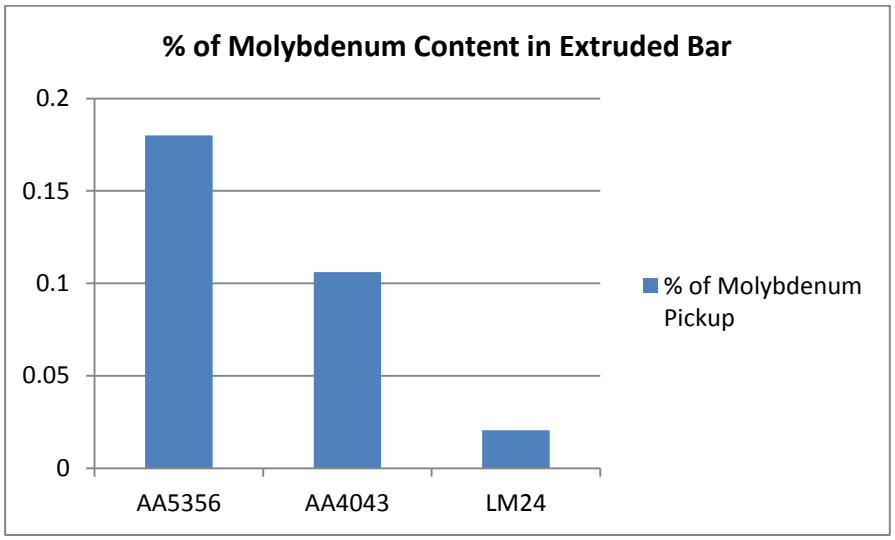

Figure 7.16: Comparison of molybdenum pickup by different aluminium alloys

This problem will always exist for non-silicon-containing alloys unless the material for the screws and barrel is changed to a material like sailon in which is observed not to corrode in aluminium. This is not a practical solution to the problem.

Continual washing with silicon-containing alloys is another solution however this again is not very feasible as the layer of $MoSi_2$ is barely 10 µm and in the high wear environment this can easily chip allowing for liquid aluminium to creep in under the coating causing pits.

It was also observed that the rate of molybdenum pickup is proportional to the process temperature. Therefore, perhaps there will be uneven erosion in areas of the extruder with higher temperature such as the feed section and die. AA4043 was extruded at a variety of processing temperatures. The composition of the extrudate revealed the level of molybdenum dissolution in the molten aluminium. Figure 7.17 compares the results.

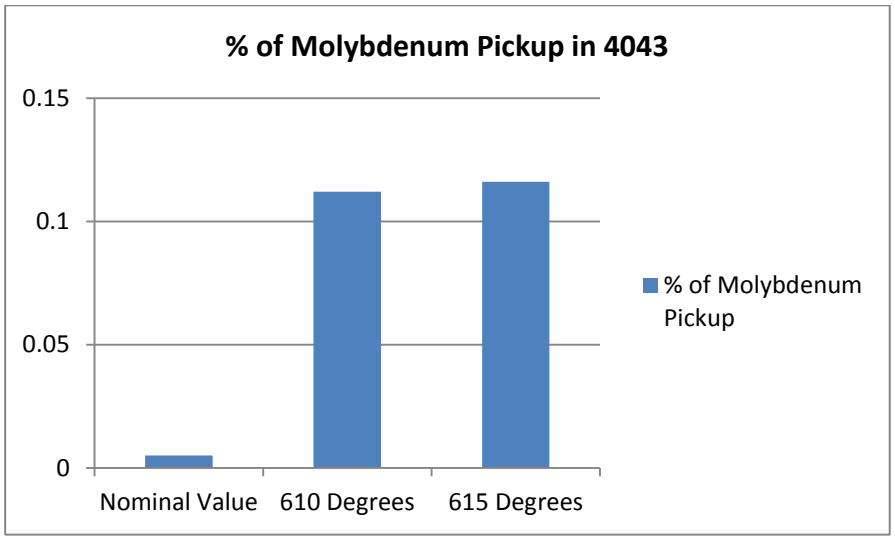

Figure 7.17: Comparison of molybdenum pickup at different process temperature

Another probable reason for the observation of such a high level of molybdenum content in the melt could possibly be from the formation of molybdenum oxide on the surfaces of the extruder as it is being heated up. However this is a condition that will only be observed in the laboratory experiments and will be eliminated if the machine is used continuously.

Therefore over prolonged use the observed molybdenum level should theoretically drop to a nominal value as this oxide layer is flushed out and the only remaining source of molybdenum contamination comes from direct dissolving in the chemical attack.

7.5.2 Phase separation and irregular eutectic in Al-Si alloys

Due to the nature of the aluminium-silicon system it is observed that alloys with a high silicon content do not respond well to the semisolid processing offered by rheoextrusion. This can be observed when comparing the solidified structures of the three tested alloys. As the silicon content is increased, large particles of primary silicon are observed as detailed in Figure 5.36.

This could be because when the hypoeutectic composition of LM24 is close to the eutectic point on the solidification of the primary alpha-aluminium the composition of the remaining liquid phase moves across the solvus line past the eutectic point and becomes hypereutectic in composition. Therefore on further cooling during quenching, primary silicon would form rather than primary aluminium. Similar findings were reported by Liao [2010] while studying eutectic solidification in near-eutectic Al-Si casting alloys.

When compared to results of Nikanorov et al. [2005] the structure of the primary silicon seen in some extrusions indicate that the local content of silicon can be close to 25%.

This solidification behaviour in high silicon-content alloys such as LM24 is thought to be the prime reason for the formation of hot tears because it is thought that the different solidification rates of the different elements would cause local stresses to build causing the formation of a tear.

Literature also shows that the cooling rate plays a significant role in the morphology of the eutectic in Al-Si alloys. Two morphologies are observed: course eutectic (CE) and fine eutectic (FE). During solidification the angular blocky silicon forms first and the CE nucleates from the preformed primary silicon particles.

Coarse silicon flakes are observed to nucleate and grow radially from primary silicon blocky particles. The microstructure supports this hypothesis on the formation of the course eutectic as detailed in Figure 7.18. This is in agreement with investigations carried out by Liao [2010].

The primary silicon can act as an efficient nucleation sites for the CE , it can nucleate and grow with little undercooling and can be precipitated at high temperatures. On the other hand, FE nucleates at other sites (not primary Silicon) and these are more difficult to form and require a higher undercooling.

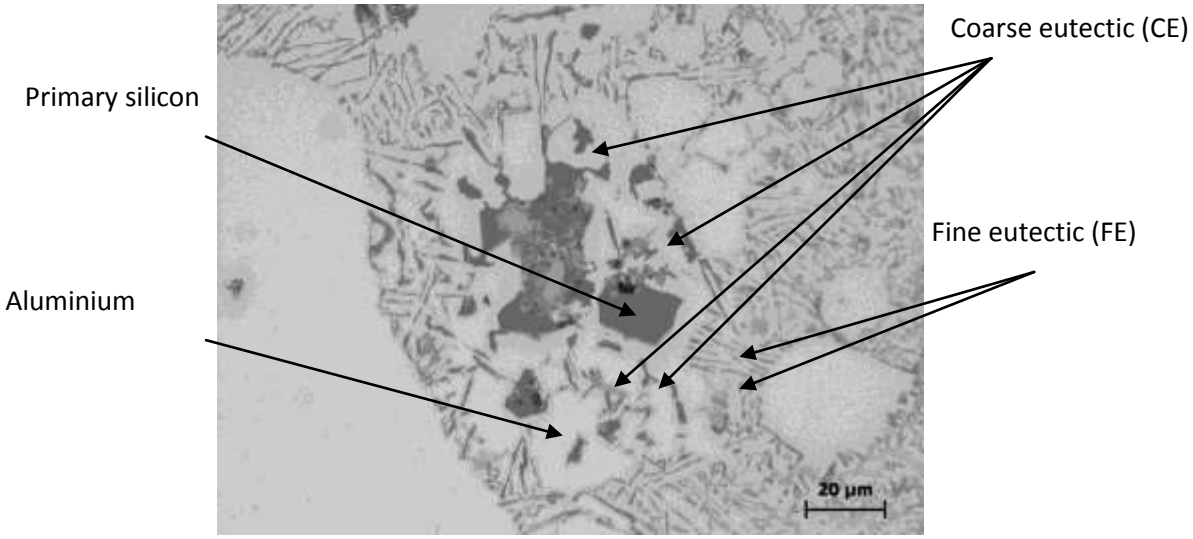

Figure 7.18: Non-uniform microstructure observed in LM24 extrusions

In the CE structure the aluminium is observed to form as dendritic crystals that nucleate on and envelop coarse silicon flakes. This hinders the growth of the silicon flake and further growth has to occur through diffusion of silicon atoms through the aluminium. This leads to the formation of short coarse flakes as coupled growth is impossible.

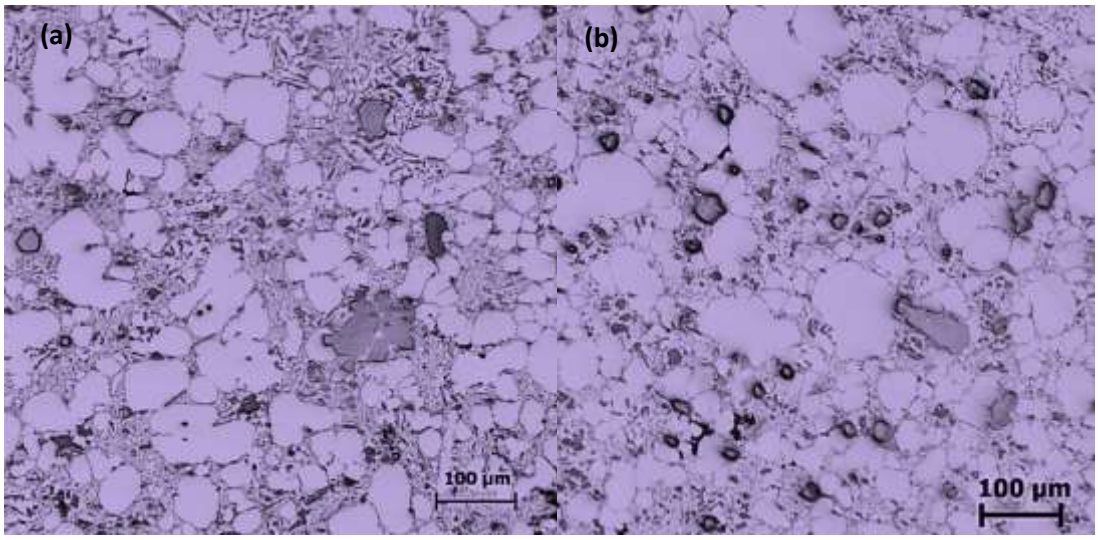

Figure 7.19: Primary silicon reduction between samples obtained at a) 565°C b) 554°C

Investigations by Ichikawa and Ishizuka [1987] show that rheocasting can help improve the microstructure by reducing the amount of blocky primary silicon because of the shearing effect. This trend is also observed in the samples observed in rheoextrusion and is demonstrated in figure 7.19. At lower temperature as discussed earlier a higher shear rate is achieved and therefore less primary silicon is observed. This could be because the additional shear effect redistributes the content of the silicon more effectively and this can lead to less primary silicon solidifying. Furthermore the formation of the FE is aided by a higher undercooling and this can lead to less silicon being available for primary solidification.

7.6 Mechanical Behaviour

It is a well-established fact that a fine microstructure results in improved mechanical properties and this is detailed by the Hall-Petch equation. Stress-strain curves obtained from tensile testing of AZ91D bars at different processing temperatures with a fixed pouring temperature of 590ºC were compared in Figure 5.40. The results show that at lower process temperature the smaller grain size seen is responsible for the improvement in mechanical properties. This is in accordance to the Hall-Petch equation and other investigations [Kubota et al., 1999]. However there are other factors that affect the mechanical behaviour of rheoextruded rods and these are discussed in this section.

7.6.1 Effect of porosity

Microstructural defects such as segregation and porosity can also be the root causes of the poor mechanical performance of rheoextruded bars. The main defect observed was the entrapment of gas during slurry making and feeding. Some of these pores were found to be as big as ~120μm as shown in Figure 5.34(b) and thence were detrimental to the structural integrity of the bar. Other types of porosity from secondary solidification were also observed 5.34(c & d). However these were not as widespread or as severe as the gas porosity. At lower temperatures porosity arising from segregation was avoided due to the lack of liquid phase as discussed in Section 7.4.1. This further enhanced the mechanical properties at lower temperatures if severe gas porosity was absent.

However porosity from entrapped air was mainly thought to be a start up problem of the system and hydrogen evolution is currently being tackled by degassing methods such as bubbling argon gas through the melt.

7.6.2 Quantity of eutectic phase

Eutectic phase in bars rheoextruded at lower temperature was only found as small sized eutectic cells. This is because high extrusion force squeezes the liquid phase into the cells during the extrusion as seen in Figure 5.23. Due to the high solid fraction at lower temperature, the eutectic phase and intermetallic phase was only discontinuously dispersed.

This is in agreement with previous studies by Czerwinski who pointed out that the interface between primary solid and the eutectic plays an important role on the fracture of the material with high primary solid content [Czerwinski et al., 2001].

It has been demonstrated in accordance with the findings of Czerwinski, Wang and others [Czerwinski et al., 2001; Ghosh et al., 1995; Wang et al., 2006; Zhang et al., 2009] that both the strength and the ductility increase with an increased solid fraction. This corresponds to decreasing extrusion temperatures and a reduced eutectic phase. Furthermore the enhanced shearing effect at lower temperatures can supress as well as breakup the dendritic eutectic structure and may enhance the mechanical properties. This can further help describe the observed trend in the results.

It was concluded that

- For alloys with a solid fraction below 20% the internal structure of the primary solid and the eutectic mixture controls the properties and
- for a large solid fraction, the interface between the primary solid and the eutectic mixture is a key factor which controlled the tensile properties of the material.

It is interesting to note that contrary to this, it was reported in a particular thixo moulding investigation performed by Zhang and co-workers [2009]. In this study an increase in solid fraction was found to tend to reduced tensile strength and ductility while lowering the

moulding temperature apparently improved mechanical properties. However an explanation for this phenomenon was not available.

At lower temperatures the reduced amounts of liquid phase resulted in a less amount of a eutectic phase that was found to be spread out more evenly in smaller pockets. It has been found that the secondarily solidified phase is generally weaker and more brittle and therefore a structure with a thick intermetallic is more likely to fail at lower loads because of this brittle character of the secondarily solidified phase as identified by Czerwinski et al. [2001], Yang et al. [2010] and Zhang et al. [2009].

In addition to this, results shown in Figure 5.25 show that the size of the eutectic cell greatly influences its structure. Larger pockets that are characteristic of high temperature extrusions are observed to be riddled with micro-porosity when compared to the structure of small pockets of eutectics observed in low temperature extrusions. Such a structure makes the eutectic phase of extrusions at higher process temperatures weaker, further explaining the trend in the results.

Therefore it can be concluded that the dependence of the mechanical properties on the solid fraction and processing temperature, and the amount and distribution of the eutectic phase is more important than the deviation of chemical compositions from equilibrium values.

7.6.3 Effect of heat treatment

Czerwinski and co-workers also suggested that the larger micro-chemical heterogeneity of Al and Zn segregation were to blame. $Mg_{12}Al_{12}$ precipitates and eutectic islands were

observed as seen in Figure 7.20(c) and these can play a significant role on the fracture mechanics.

It was observed that in as-cast structures, manganese-rich intermetallics embedded in the eutectic acted as points of stress concentration. This can be seen in Figure 7.20(a). Upon solutionising, the intermetallic phase is seen to dissolve and the cause of fracture was observed to change to smaller alpha-grains within eutectic as seen in Figure 7.20(b). It is thought that these grains within a eutectic are formed when intermetallic eutectic dissolves into alpha-islands described in Figure 7.10 causing them to form a single larger grain within the eutectic. After precipitation heat treatment the only cause of fracture was observed to be remaining areas of eutectic deposits acting as stress concentration points as seen in Figure 7.20(c).

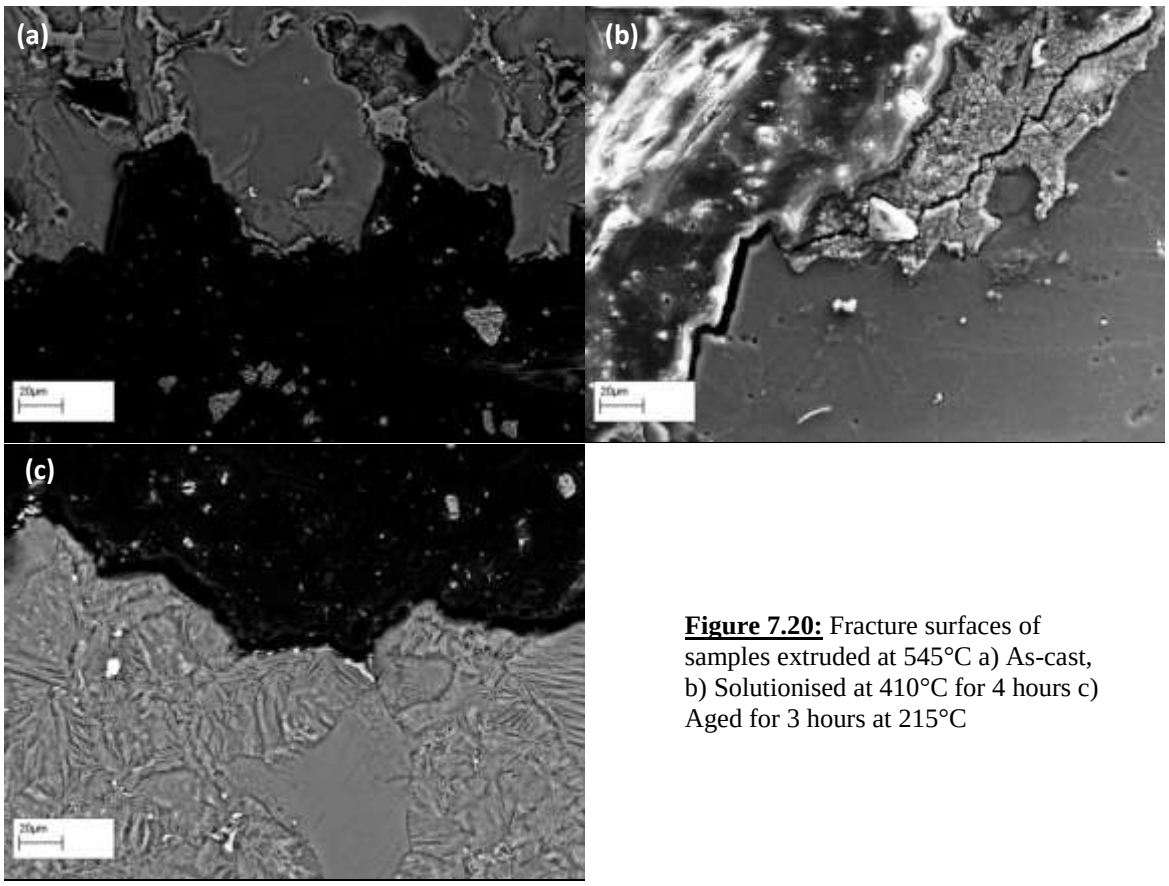

Figure 7.20: Fracture surfaces of samples extruded at 545°C a) As-cast, b) Solutionised at 410°C for 4 hours c) Aged for 3 hours at 215°C

CHAPTER 8

CONCLUSION & FURTHER WORK

A novel semisolid processing rheoextrusion technology based on a counter-rotating twin-screw extruder has been developed and tested in this study. Twin-screw rheoextrusion provides a true one-step process for producing a bar directly from the melt. It also has the potential to provide a way of reducing manufacturing costs by using lighter machinery and by eliminating billet casting and processing. Furthermore the microstructural refinement offered without chemical additives allows the extruded materials to be 100% recyclable. In addition the shortened manufacturing route and continuous nature of the process significantly improve the efficiency of the process compared to other available methods.

A continuous extruded bar was obtained with a smooth surface. The microstructure of the extrudate was fine and uniform along both transitional and longitudinal directions. Low processing temperatures compared to other semisolid processes suppressed the formation of the eutectic and intermetallic phase resulting in discontinuously distributed eutectic along the grain boundaries. Lower temperatures also improved the microstructure and allowed for better mechanical properties. The demonstration of such a rheoextrusion process has provided justifiable evidence for it to be a shortened process and a replacement for conventional hot extrusion technology as it promises a large potential reduction in both process cost and complexity.

8.1 Concluding Remarks

1. A continuous process for the extrusion of metal rods has been successfully developed by taking advantage of the semisolid metal phenomenon and the mechanism of counter-rotating twin-screw extrusion and several rods of both aluminium and magnesium alloys have been produced under various processing conditions.
2. The process is capable of producing wrought products from a large range of alloys. The twin-screw rheoextrusion process has proven itself to be a feasible process for shaping of bars using commercial magnesium alloys. Its feasibility to produce aluminium extrusions is limited to the use of alloys with high silicon-content due to cross contamination of molybdenum and aluminium.
3. The process offers low cost and high quality wrought products that are 100% recyclable. This can facilitate the penetration of eco-friendly materials into industry for reduction of fuel consumption and CO_2 emission which can eventually provide a better environment for sustainable development.
4. The process comprises several innovative features such as the *in situ* slurry making by the use of a high shear rotor stator mixer and continuous processing ability by the use of self-wiping counter-rotating twin screws which when employed together give the process the ability to be a true one-step melt to product technology for continuous metal production.
5. Compared to conventional processes the process is seen to display a shortened route to component manufacture which can reflect on savings in capital investment, raw materials, energy consumption, operating space and manpower. The overall cost saving is expected to be several hundred percent over the conventional route.

6. Several process parameters such as process temperature, extrusion speed and cooling were defined and explored indicative that the machinery is capable of a operating across a large window of process settings.
7. Innovative solutions to problems specific to the metal extrusion process were developed. These included the brass ceramic water ring for the specific requirements of the cooling process and the feeding system to continuously allow high viscosity melt to be introduced into the system.
8. The process offers advantageous features in microstructural refinement control. The high shear rotor stator produced slurry of a fine and uniform non-dendritic primary phase particles. This non-dendritic microstructure was maintained through the transport process and further refined by the shearing offered by the twin screws and some plastic deformation.
9. Liquid segregation was reduced due to intensive shearing being applied during the process thereby homogenising the melt producing continuous rods with a fine and uniform microstructure with reduced minimal chemical heterogeneity.
10. The extruded bars possessed moderate mechanical properties and these values were controlled by micro-scale properties such as particle size, morphology and volume of the secondarily solidified phases and defects.
11. Lowering extrusion temperatures showed a positive impact on microstructural refinement and tensile test performance due to the reduced volume of secondary solidification.
12. At low temperatures eutectic was squeezed into relatively tiny cells and secondarily solidified networks were seen to diminish after heat treatments validating instant inline solutionisation process downstream.

13. The formation of non-dendritic structures by the process is an effective means of reducing the segregation of liquid phase allowing the process to compete against continuous casting techniques.
14. Numerical analysis shows that a steady state thermal profile in which the slurry temperature is decreased within the extruder can be easily achieved. This allows for a smooth transition from pouring temperature to extrusion temperature to produce a sufficient solid fraction to be developed for the forming process.

8.2 Further Work to be done

8.2.1 Limitations of laboratory scale experiments

Due to the constraints posed by the available facilities, as mentioned above a steady state processing condition was not achieved. This was mainly due to the fact that enough melt could not be supplied to the machine that would be sufficient to extrude material for the required time of approximately 2 minutes. Furthermore there were always defects associated with start up conditions such as entrapped air and inclusions which would have significantly reduced if the machine was running continuously. Upon achievement of a continuous extrusion the defined parameters can be further optimised to produce rods with a more refined microstructure.

8.2.2 Reduction of porosity

Porosity can be reduced by several methods, the most prominent being establishing a continuously running process and flushing out all the entrapped air. Furthermore to

increase the packing of the material in the die it may also be feasible to increase the incline of the machine.

8.2.3 Optimising die profiles

The internal geometry of the die can be optimised with respect to conditions of the flow rate of the metal to the die in accordance to work done in the polymer industry to increase compaction and reduce surface instabilities such as the formation of sharkskin and surface tearing.

8.2.4 Reduction of molybdenum pickup to overcome limitations in processing aluminium

The chemical attack posed by aluminium alloys is a very persistent problem in metallurgy. It is due to this that the feasibility of the entire process is limited to only high silicon-containing alloys which have a very limited commercial potential. It is therefore imperative to create a solution to reduce the impact of this problem.

Some possible suggestions are as follows

A) *Coatings:* An inherent problem of using coatings is that the coating itself is a very thin layer and due to wear – if a small chip occurs in the coating – the liquid aluminium can start attacking the underlying substrate metal. However wear resistant coatings have come a long way in their performance over the last couple of years. One of the most inert coatings available for high temperature high wear applications is the diamond-like carbon (DLC) coating as used on turbine entry

blades in jet engines. Furthermore since the coating is of carbon it is inert to the chemical attack posed by aluminium.

B) *Use of a fully ceramic pumping system*: To fully circumnavigate this problem of chemical attack it may be a feasible idea to substitute the pumping mechanism used so that it is capable of incorporating ceramic components that are resistant to the chemical attack of aluminium in the first place as detailed in the previous section. A commercially available design is the Kubota ceramic pump used to transport molten aluminium.

8.2.5 Achievement of a fully integrated process

Optimisation of the process conditions for an extrusion that incorporates all the accessoryequipment that have been tested separately such as the slurry maker, feeding system and the coiler.

REFERENCES

Agnew and Duygulu 2005 S. Agnew , O. Duygulu , Plastic anisotropy and the role of non-basal slip in magnesium alloy AZ31[J], International Journal of Plasticity, 2005, 21:1161-1193.

Agnew et al. 2003 S Agnew, C Tome, D Brown, T Holden, S Vogel, Study of slip mechanisms in a magnesium alloy by neutron diffraction and modelling[J], Scripta Materialia, 2003, 48:1003 -1008

Anonumous 1945 Anonymous German Patent 750 509, 1945.

Arif et al. 2002 A Arif., A Sheikh , S Qamar ,M Raza , K Al-Fuhaid , Product defects in aluminium extrusion and their impact on operational cost The 6th Saudi Engineering Conference, KFUPM, Dhahran, December 2002

Armstrong et al. 1962 R Armstrong, I Cood, RM Douthwaite, NJ Petch Phil. Mag 7 (1962)

Arnberg et al. 1993 L. Arnberg, G. Chai, L. Bäckerud; Materials Science and Engineering A,Volume 173, Issue 1-2, December 1993, pp. 101-103

Baigent 1956 K Baigent, Trans. Plastics Inst., 1956, 134.

Baker 1945 Baker W A. Microporosity in magnesium alloy castings. Inst. Metals, 1945, 71: 165-204.

Barnett, 2003 A Taylor model based description of the proof stress of magnesium AZ31 during hot working. Metallurgical and Materials Transactions A, 34, 8.

Bear 1972 J. Bear; 'Dynamics of Fluid in Porous Media', Dover Publications, New York; 1972,pp. 764

Berezhnoy 2000 VL Berezhnoy, Non Traditional Process techniques of extrusion and Pressing. Int J Manf Technology (2000) 16 pp19-22

Bohlen et al. 2005 Y Bohlen, SB Yi, J Swiostek, D Letzig, HG Brokmeier, KU Kainer, Microstructure and Texture development during Hydrostatic extrusion of Magnesium Alloy AZ31. Scripta Materialia 53 (2005) 259-264

Brown and Flemings 1993 S Brown, MC Flemings, Adv Mater Process 143 (1993) 36-40

Burger 1978 F Burger, In 5th Leobener Kunststoffkolloquium Doppelscknecken-extruder, editedby Lorenz Verlag, Vienna, 1978, 46.

Burghauser et al. 1938 F Burghauser, U.S. Patent 2 115 006, 1938.

Burghauser et al. 1941 F Burghauser,, Erb, K. U.S. Patent 2 231 357, 1941; U.S. Patent 690 990, 1939.

Byun et al 3003 JY Byun, S Kwon, HP Ha, JK Yoon. In: Kainer KU, editor.Magnesium alloys and their applications. Wiley-VCH; 2003. p.713–8.

Cao et al. 2004 P. Cao, Ma Qian, , D.H. StJohn, Effect of iron on grain refinement of high-purity Mg–Al alloys,Scripta Materialia
Volume 51, Issue 2, July 2004, Pages 125–129

Cetlin et al. 2010 P Cetlin, M Teresa, P Aguilar, R Figueiredo, T Langdon, Avoiding cracks and inhomogeneities in billets processed by ECAP[J], Journal of Materials Science, in press.

Chalmers 1963 B. Chalmers; Journal of Australian Institute of Metals, Volume 8, 1963, pp. 225-263

Chen and Tsao 1999 C. P. Chen, C. -Y. A. Tsao; Materials Science and Technology, Volume15, Issue 9, September 1999, pp. 981-985

Cho and White 1995 J.W Cho , J.L White. SPE ANTEC Tech. Papers, 1995, 53, 1554.

Couret and Caillard, 1985 An in situ study of prismatic glide in magnesium - I: the An in situ study of prismatic glide in magnesium—I. The rate controlling mechanism, Acta Metallurgica Volume 33, Issue 8, August 1985, Pages 1447–1454

Czerwinski 2004 F Czerwinski.Semisolid extrusion moldingof Mg-9%Al-1%Zn alloys [J]Journal of material Science 39 (2004) 463– 468

Czerwinski and Zielinska-Lipiec 2005 F Czerwinski, A Zielinska-Lipiec, The microstructure evolution during semisolid molding of a creep-resistant Mg–5Al–2Sr alloyActa Mater 53 (2005) 3433-3444

Czerwinski et al. 2001 F Czerwinski, A Zielinska-Lipiec, PJ Pinet, I Overbeeke, Correlating the microstructure and tensile properties of thixomoulded AZ91D magnesium alloy[J]Acta mater. 49 (2001) 1225–1235

Dahle and StJohn 1998 A. K. Dahle, D. H. StJohn; Acta Materialia, Volume 47, Issue 1,December 1998, pp. 31-41

Dahle et al. 2001 A .K. Dahle, Y. C. Lee, M. D. Nave, P. L. Schaffer, D. H. StJohn; Journal ofLight Metals, Volume 1, Issue 1, February 2001, pp. 61-72

Das and Fan A. Das, Z. Fan; Materials Science and Technology, Volume 19, Issue 5, May2003, pp. 573-580

Das et al. 2002 A Das, S Ji, Z Fan, Morphological development of solidification structures under forced fluid flow: a Monte-Carlo simulation [J] Acta Materialia 50 (2002) 4571–4585

Dey and Biesenberger 1987 SK Dey, KA Biesenberger, SPE ANTEC Tech. Papers, 1987, 133.

Doboczky 1965 a Doboczky, Z. Plastverarbeiter, 1965, 16, 57.

Doboczky 1965 b Doboczky, Z. Plastverarbeiter, 1965, 16, 395.

Doherty et al. 1984 RD Doherty, HI Lee, EA Feest, Microstructure of Stir cast metals [j]Materials Science and Engineering, 65 (1984) 181-189

Du and Zhang 2007 X Du, E Zhang, Matter Lett, 61 (2007) 2333-2337

Ellias-Boyed et al.1988 L Ellias-Boyed, DH Kirkwood, MM Sellars, Proc 2nd World Basque Conf on New structural Materials eds AK BHASIN JJ MOORE KP YOUNG Midson Spain, Servico Central de Publicaiones del Gobierno Vasco, 1988, 285-295

Fan 2002 Z Fan. Semisolid metal processing, [J] Inter Mater Rev 47 (2002) 49-86

Fan 2005 Z Fan Development of the rheo-diecasting process for magnesium alloys, Mater Sci Eng A, 413/414 (2005) 72-78

Fan and Ji 2000 Z Fan S.Ji , M.J. Bevis PCTT Patent, WO 02/13993 A1, Priority date: 11/08/00.

Fan and Liu 2005 Z. Fan, G. Liu; Solidification behaviour of AZ91D alloy under intensive forced convection in the RDC process Acta Mater, 53, (2005), 4345

Fan et al. 2005 Z Fan X Fang. S Ji . Mater. Sci. Eng. A, 412 (2005), 298-306.

Fan et al. 2009 a Z Fan, M Xia, H Zhang, G Liu, JB Patel, Z. Bian, I Bayandorian, Y Wang, HT Li, G Scamans Melt conditioning by advanced shear technology (MCAST) for refining solidification microstructures [J] Int Journal of cast metl Research (2009) v22 pp1-4

Fan et al. 2009 b Z Fan, Y Wang, ZF Zhang, M Xia, HT Li, J Xu, L Granasy, G Scamans Shear enhanced heterogeneous nucleation in some Mg and Al-alloys [j] International Journal of Cast metals Research (2009) V22 pp 1-4

Findik, 1998 F Findik, Discontinuous Precipitation, Journal of Material Science Letters 17(1998) 79-83

Fink and Feenstra 2002 S Fink, F Feenstra Solid Freeform fabrication by extrusion and deposition of semisolid alloys [J] Journal of materials science 37 (2002) 3101-3106

Finke et al. S. Finke, M. Suéry, C. L. Wei; in: Proceedings of the 6th InternationalConference on semi-solid processing of alloys and composites, S2P 2000, Turin, Italy, pp. 169-174

Flemings 1974 MC Flemings, 'Solidification processing', McGraw-Hill; 1974, pp. 214-262

Flemings 1991 MC Flemings Behaviour of Metal Alloys in Semisolid state, Metall Trans A 22 (1991) 957-981

Flemings et al 1976 MC Flemings, R Reik, K Young Rheocasting[J], Materials Science and Engineering,1976, 25:103-117.

Flynn et al. 1961 P Flynn, J Mote, J Dorn, On the thermally activated mechanism of prismatic slip in magnesium single crystals[J], Transactions of the Metallurgical Society of AIME, 1961, 221:1148-1151.

Forn et al. 2010 A Forn, G Vaneetveld, TJ Pierre, S Menargues, M Baile, M Campillo, A Rassili Thixoextrusion of A357 aluminium alloy [J] Trans. Nonferrous Met. Soc. China 20(2010) s1005-s1009

Frost and Ashby 1983 H Frost, M Ashby, Deformation mechanism maps [M]. Oxford: Pergamon Press, 1983

Galiyev et al., 2001 Galiyev, A.; Kaibyshev, R. & Gottstein, G. (2001). Correlation of plastic deformation and dynamic recrystallization in magnesium alloy ZK60. Acta Materialia, 49, 8

Ganzeveld 1993 Ganzeveld, K.J., Janssen, L.P.B.M. Can J Chem Eng, 1993, 71, 411.

Ganzeveld et al. 1994 Ganzeveld, K.J., Capel, J.E., Vanderwal, D.J., Janssen, L.P.B.M. ChemicalEngineering Science, 1994, 49, 1639.

Ghosh et al. 1995 D Ghosh, K Kang, C Bach, JG Roemer, C Vanschilt in: Proc of Inter Symp on recent metallurcical advances in light metals Industries, Eds S. Macewen, J.P. Gilardeau, Vancouver, Canada, 1995, 473-479

Gourlay and Dahle 2007 C. M. Gourlay, A. K. Dahle; Nature, Volume 445, Issue 7123,January 2007, pp. 70-73

Gourlay et al 2008 CM Gourlay, B Meylan, AK Dahle Shear mechanisms at 0–50% solid during equiaxed dendritic solidification of an AZ91 magnesium alloy [J]Acta Materialia 56 (2008) 3403–3413

Greenfield 1972 P Greenfield 'Magnesium', Mills and Boon Limited, London, 1972, pp. 11

Greer et al. 2000	A.L. Greer, A. M. Bunn, A. Tronche, P. V. Evans, D. J. Bristow; Acta Materialia, Volume 48, Issue 11, June 2000, pp. 2823-2835
Guan etal. 2006	RG Guan, JL Wen, SC Wang, XH Liu Microstructure behavior and metal flow during continuously extending-extrusion forming of semisolid A20 17 alloy, [J] Trans Nonferrous Met Soc China, 16 (2006)
Guo et al. 2006	S. Guo, Q. Le, Y. Han, Z. Zhao, J. Cui; MetallurgicalandMaterialsTransactions A, Volume 37, Issue 12, December 2006, pp. 3715-3724
Guo et al., 2005	S. Guo, Q. Le, Z. Zhao, Z. Wang, J. Cui; Materials Science and Engineering A,
Haga and Kapranos 2002	Volume 404, Issue 1-2, September 2005, pp. 323-329
Haghayegh et al.2008	R Haghayeghi, Y Liu, Z FanMelt Conditioned Direct Chill Casting (MC-DC) of Wrought Al-alloysSolid State Phenomena (Volumes 141 - 143) pg 403-408
Hartner 1938	Hartner U.S. Patent 2 119 162, 1938.
Hellawell 1996	A Hellawell,., Proc of 4th Inter Conf on Semi solidProcessing of Alloys and Composites, eds D.H. KIRKWOOD, P. KAPRANOS. Sheffield UK, 1996, 60-66
Helstrup 1939	Helstrup, L.K.V. U.S. Patent 2 179 303, 1939.
Holdaway 1917	Holdaway, W.S. U.S. Patent 1 218 602, 1917.
Hu et al.1995	LIANXI H. SHOUJING L., WENCAN H., WANG Z.Development of the technique of extrusion directly followinginfiltration for the manufacturing of metal-matrix compositesJournal of Materials Processing Technology 49 (1995) 287 294
Ichikawa 1987	K IchiKawa, S Ishizuka Improvement in microstructure in hypereutectic Al-Si alloys by rheo casting Trans Japan Inst Metals V28, No.5 p 434-444 1987
Ilinka 2008	F. Ilinca, J. Hetu, J. Mosian, F. Ajersch, Three-dimensional injection molding simulation of AZ91D semi-solid magnesium alloy, Int. J Mater. Form, 1(2008), 3-12.
Janssen 1975	L Janssen, , L Mulders, , J Smith, Plastics and Polymers, 1975,43, 93.
Janssen 1978	L Janssen, Twin Screw Extrusion. Elsevier: Amsterdan, 1978.
Janssen and Ganzeveld 1996	L Janssen., K Ganzeveld, Handbook of Applied Polymer ProcessingTechnology. 31(619), 1996.

Janssen and Smith 1975	L Janssen, J Smith. In PRI/BSR Conf. on Polymer Rheology and PlasticProcess, edited by Loughborough(GB), 1975, 160.
Ji and Fan 2002	S Ji, Z Fan Solidification behaviour of Sn-15 Wt Pct Pb Alloy under a high shear rate and high intensity of turbulence during semisolid processing [j] Metallurgical and |Materials Transactions A Volume 33A Nov (2002) pp3511
Ji et al. 2001	S Ji, Z Fan, J Bevis, Semi-solid processing of engineering alloys by a twin-screw rheomoulding process [J] MaterSci Eng A299 (2001) 1225-1235
Ji et al. 2002	S Ji, A Das, Z Fan, Solidification behavior of the remnant liquid in the sheared semisolid slurry of Sn–15 wt.%Pb alloy Scripta Materialia 46 (2002) 205–210
Joly and Meherbian 1976	P. A. Joly, R. Mehrabian; Journal of Materials Science, Volume 11,Issue 8, August 1976, pp. 1393-1418
Kaibyshev and Sitdikov, 1994	RO Kaibyshev, OH Sitdikov The relation of crystallographic slip and dynamic recrystallization to the local migration of grain boundaries. I. Experimental results[[Previously Titled: Crystallographic gliding and dynamic recrystallization related to local grain boundary migration. I. Experimental results.Phys. Met. Metallogr.(Russia) 78 (4), 420-427`
Kaibyshev and Sitdikov 2001	R Kaibyshev ,O Sitdikov, Dynamic recrystallisation in Pure magnesium. Mater Trans, Vol 42 No 9 pg 1928-1937 2001
Kang et al. 2010	L Yang, Y Kang, F Zhang, J Xu, Microstructure and mechanical properties of rheo-diecasting AZ91D Mg alloy [J]Trans. Nonferrous Met. Soc. China 20(2010) s862-s867
Kattamis and Piccone 1991	TZ Kattamis, TJ PicconeMater sci Eng 1991 A13a 265-272
Keisskalt et al. 1937	Kiesskalt, S., Tampke, H., Winnacker, K., Weingaertner, E. German Patent 652 990,1937
Keisskalt et al. 1939	Kiesskalt, S., Tampke, H., Winnacker, K., Weingaertner, E. German Patent 676 045, 1939
Kiesskalt 1927	Kiesskalt, S. VDI Zeitschr, 1927, 71, 453.
Kiesskalt 1943	Kiesskalt, S., Borgwardt, E. U.S. Patent 739 278, 1943.
Kim et al. 2007	S Kim, Y Yoon, H Jo, Novel thixoextrusion process for Al wrought alloys[J], Journal of Materials Processing Technology, 2007,187-188:354-357.
Kiuchi and Kopp 2002	Mushy/Semi-Solid Metal Forming Technology –

	Present and FutureCIRP Annals - Manufacturing TechnologyVolume 51, Issue 2, 2002, Pages 653–670
Klenk 1971 a	Klenk, K. Plastverarbeiter, 1971, 22, 33.
Klenk 1971 b	Klenk, K. Plastverarbeiter, 1971, 22, 105.
Klenk 1978	Klenk, K.P. In 5th Leobener Kunststoffkilloquium Doppelschnecke-extruder, edited by Lorenz Verlag, Vienna, 1978, 39.
Koike 2005	J Koike Enhanced deformation mechanisms by anisotropic plasticity in polycrystalline Mg alloys at room temperature[J], Metallurgical and Materials Transactions A, 2005, 36:1689-1696.
Koike et al. 2003	J Koike, T Kobayashi, T Mukai, H Watanabe, M Suzuki, The activity of non-basal slip systems and dynamic recovery at room temperature in fine-grained AZ31B magnesium alloys[J], Acta Materialia, 2003, 51:2055-2065.
Kolpashnikov and Vyalov 1973	AI Kolpashnikov, VA Vyalov,Hydraulic Extrusion of Metals [In Russian], Metallurgiya, Moscow (1973)
Kopp et al. 1998	R Kopp, H Mertens, M Wimmer, G Winning Thixoextrusion of Aluminium Wrought Alloys [C],In: KUMAR BHASIN A, MOORE J, YOUNG K, MIDSON S, Editors, Proceedings of the 5th international Conference on Semi-solid Processing of Alloys and Composites, Colorado, USA, 1998:12.
Kopp et al. 1999	R Kopp, T Moller, D Neudenberger, G Winning, Thixoforging and thixoextrusion benefits of innovative forming tehnologyies [C], The 6th International Conference on Tchenology of Plasticity (ICTP), Nurnberg, Germany, 1999.
Kubota et al. 1999	K Kubota, M Mabuchi, K Higashi. Review Processing and mechanical properites of fine grained magnesium alloys [J] Journal of Materials Science 34 (1999) 2255-2262
Kurz and Fisher 1986	W. Kurz, D. J. Fisher; 'Fundamentals of Solidification', 2nd edition,Trans. Tech. Publications Ltd., Aedermannsdorf, 1986, Appendix 8, pp. 214-216
Laxmanan and Flemings 1980	V Laxmanan, MC Flemings Deformation of Semi solid Sn-15 Pct Pb Alloy Metallurjuical Transactions A 11A 1927-1937
Lee and White 2001	Lee, B.H., White, J.L. Int Polym Proc, 2001, 16, 172.
Lee and White 2002	Lee, B.H., White, J.L. Polym Eng Sci, 2002, 42, 1710.

Lee et al. 2005 B Lee, D Joo, M Kim, Extrusion behaviour of Al-Cu alloys in the semisolid state[J], Materials Science and Engineering A, 2005,402:170-176.

Leistritz et al. 1940 Leistritz, P., Burghauser, F. German Patent 699 757(1940); German Patent 682 787,1939.

Leuhy et al. 1985 H Leuhey, Masounave, J Blain J. Mater Sci 1985 20 105-113

Liao et al.2010 H.C. Liaoy, M. Zhang, J.J. Bi, K. Ding, X. Xi and S.Q. Wu Eutectic Solidication in Near-eutectic Al-Si J. Mater. Sci. Technol., 2010, 26(12), 1089-1097

Lim and White 1994 Lim, S., White, J.L. Int Polym Proc, 1994, 9, 33

Luo et al. 2010 S Luo, W Keung, Y Kang, Theory and application research development of semi-solid forming in China, [J]Trans Nonferrous Met Soc China, 20 (2010) 1805-1814

Ma et al. 2012 Ma, Q., Li, B., Oppedal, A.L., Whittington, W., Horstemeyer, S.J., Marin, E.B., Kadiri, H. El., Wang, P.T. and Horstemeyer, M.F. (2012) Effect of Strain Rate on Dynamic Recrystallization in a Magnesium Alloy under Compression at High Temperature, in Magnesium Technology 2012 (eds S. N. Mathaudhu, W. H. Sillekens, N. R. Neelameggham and N. Hort), John Wiley & Sons, Inc., Hoboken, NJ, USA. doi: 10.1002/9781118359228.ch56

Mabuchi et al. 1997 M Mabuchi, T Asahina, H Iwasaki Mater Sci. Technol 13 (1997) 1387

Mada and Ajersch 1996 M Mada , F Ajersch Mater Sci Eng. 1996 A212 171-177

Markhenkel 1965 H Markhenkel,. Kunststoffe, 1965, 55, 363.

Marshall 1939 Marshall, W.R. U.S. Patent 2 434 707, 1948.

Martin et al. 1994 C Martin, P Kumar S Brown Acta Metall Mater 1994 42 3603-3614

Martin et al., 2008 An EBSD study of the misorientations related to dynamic recrystallization in Mg AM30 deformed at high temperatures. Proceedings of 15th International Conference 577

Maschinenfabrik 1939 Handle, Maschinenfabrik, S. German Patent 670 670, 1939

Men et al. 2010 H Men, B Jiang, Z Fan Acta Mater 58 (2010) 6526-6534

Menges and Klenk 1966 Menges, G., Klenk, K. Der Plastverarbeiter, 1966, 17, 791.

Modigell and Koke 1999 M Modigell, J Koke Mech Time Depend. Mater 1999 3 15-30

Mohri et al.1999 T Mohri, M Mabuchi, N Saito, M Nakamura Mater Sci Eng A257 (1999) 287

Molenaar et al. 1985 J Molenaar, F Salemans, L Katgerman, The structure of stircast Al-6Cu J Mat Sci 20 (1985) 4335-4342

Molenaar et al. 1986 J Molenaar, , L Katgerman W Kool, R Smeulders. On the formation of the sitcast structure [J] Journal of Materials Science 21 (1986) 389-394

Montelius 1929 Montelius, C.O.J. U.S. Patent 1 698 802, 1929.

Montelius 1933 Montelius, C.O.J. Teknist Tidskaift, 1933, 6, 61

Montelius 1934 Montelius, C.O.J. U.S. Patent 1 965 557, 1934.

Mullis 1999 A.Mullis. Growth induced dendritic bending and rosette formation during solidification in a shearing flow Acta Mater 47 (1999) 1783-1782

Nadella et al. 2008 R Nadella, D Eskin, Q Du, L Katgerman [J] Progress in MaterialsScience, Volume 53, Issue 3, March 2008, pp. 421-480

Nagata et al. 2006 R Nagata, Y Uetani, H Takagi Rheo Extrusion of A7075 Aluminum alloy utilising semisolid slurry Manufacturedby simple method [j] Mat Sci For Vols 519-521 (2006) pp1847-1852

Nicolli et al. 2005 L. C. Nicolli, A. Mo, M. M'Hamdi; Metallurgical and MaterialsTransactions A, Volume 36, Issue 2, February 2005, pp. 433-442

Nikaronov et al.2005 S.P. Nikanorova, M.P. Volkova, V.N. Gurina, Yu.A. Burenkova,Structural and mechanical properties of Al–Si alloys obtained by fast cooling of a levitated melt Materials Science and Engineering: A Volume 390, Issues 1–2, 15 January 2005, Pages 63–69

Obara et al. 1973 T Obara, H Yoshinaga, S Morozumi{1122}<1123> slip system in magnesium[J], Acta Metallurgica, 1973, 21:845-853

Olier 1923 Societe Anonyme Des Establissements A. Olier, G.P. British Patent 180 638, 1923.

Øvrelid et al. 1997 E. Øvrelid, P. Bakke, T.A. Engh, Light Metals (1997) 141-154.

Pasquetti1952 Pasquetti, C. British Patent 677 945, 1952

Perlin and Raitbarg 1975 IL Perlin, G Raitbarg Theory of the extrusion of metals [in Russian], Metallurgiya Moscow (1975)

Pinsky et al. 1984 D Pinsky, P Charreyron, MC Flemings Compression of semisolid dendritic Sn-Pb alloys at low strain rates[J], Metallurgical Transactaions B, 1984, 15:173-181.

Polmear 2006 IJ Polmear 'Light Alloys: from traditional alloys to nanocrystals', 4th edition,Elsevier/Butterworth-Heinemann, Oxford, 2006

Porter and Eastering 1992 D. A. Porter, K. E. Easterling; 'Phase transformations in metals and alloys', 2nd edition, Chapman and Hall, London, 1992, pp. 139, 185

Qian 2007 M Qian Heterogenous Nucleation on Potent spherical substrates during solidifcation [J] Acta Materialia 55 (2007) 943-953

Qin and Fan 2000 R. S. Qin, Z. Fan; in: TMS 2000 Annual Meeting and Exhibition,Magnesium technology, Turin, Italy, 2000, pp. 819-824

Quested and Greer 2004 T. E. Quested, A. L. Greer; Acta Materialia, Volume 52, Issue 13,August 2004, pp. 3859-3868

Quin and Wallach 2003 RS QIN, ER Wallach Phase-field simulation of semisolid metal processing under conditions of laminar and turbulent flow [J] Materials Science and Engineering A357 (2003) 45 /54

Rattanochaikul et al. 2010 T Rattanochaikul, S Anudom, M Memongkol Development of aluminum rheo-extrusion process using semi-solid slurry at low solid fraction Trans. Non ferrous Met Soc. China 20(2010) 1763-1768

Rauwendaal 1986 C Rauwendaal, Polymer Extrusion. Hanser: Munich, 1986

Roberts and Fan 2002 KA Roberts,. "DEVELOPMENT OF TWIN-SCREW RHEO-EXTRUSION PROCESS." Proeeedings of the 7th Inter national Conference on Semi-solid Processing of Alloys and Composites, Tsukuba. 2002.

Sakai et al. 1987 T Sakai, N Hashimoto, N Kobayashi,SPE ANTEC Tech. Papers, 1987, 146.

Samilov 1969 A.V. Samoilov, Translated from Khimicheskoe I Neftyanoe Machinostroenie, 10(1969)6-9

Schenkel 1985 G Schenkel, in Kunststoffe-€in Werkstoffmack Karrier. edited by Glenz W, HanserVerlag: Munich, 1985.

Scherba 1999 VN Scherba, Classification of methods of extruding Aluminm alloys based on Process Charerecteristics [J] Metallurgist Vol 43 Nos 5-6 1999 221-227

Schmitz 1944 Schmitz, W.R. U.S. Patent 2 360 894, 1944.

Schneider 2005 Schneider, H. Kunststoffe, 2005, 44.

Schutz 1962 Schutz, F.C. Soc. Plast. Eng. J., 1962, 18, 1147.

Sitdikov and Kaibyshev, 2001 Dynamic recrystallization in pure magnesium. Materials Transactions, 42, 6, 1928.

Soda et al. 1995 H Soda, A Mclen, Z Wang, G Motoyasu Pilot-scale casting of single crystal copper wires by the ohno continuous casting process Journal of Material science 30 (1995) 5438-5448

Somekawa et al 2008 H Somekawa, A Singh, T Mukai Microstructure Evolution of Mg-Zn binary alloy During a direct Extrusion Process [j] Scripta Materialia 60 (2009) 411-414

Song et al.2008 R Song, Y Kang, A Zhao J Material Process technology 198 (2008) 291-299

Spencer et al. 1972 D Spencer, R Meherbian MC Flemings Rheological behaviour of Sn-15 pct Pb in the crystallization range[J], Metallurgical Transactions, 1972, 3:1925-1932.

Suery and Flemings 1982 M Suery, MC Flemings Effect of Strain Rate on Deformation Behaviour of Semi Solid Dendritic Alloys [J] Metallurgical Transactions A 1982 13 A 1809-1819

Sumitomo et al. 2000, T. Sumitomo, D. H. StJohn, T. Steinberg; Materials Sciene and Engineering A, Volume 289, Issue 1, September 2000, pp. 18-29

Taha et al. 1988 M Taha, N ElmaHallaway, N Assar J Mater Sci 1988 23 1379-1390

Tan and Tan, 2003 Dynamic continuous recrystallization characteristics in two stage deformation of Mg-3Al-1Zn alloy sheet. Materials Science and Engineering A, 339, 9.

Taylor 1938 G Taylor Plastic deformation of metals[J]. The Journal of the Institute of Metals, 1938, 62:307-324.

Tenner 1963 Tenner, R.I. J. Appl. Polym. Sci., 1963, 14, 129

Tenner and Kunststoffe 1987 Tenner, H. Kunststoffe, 1987, 102.

Tenner1956 Tenner, K. Kunststoffe, 1956, 46, 431

Thiele 2003 Thiele, W., in Pharmaceutical extrusion technology. edited by Dekker M, New York,2003.

Turng and Wang 1991 L Turng, K Wang J Mater Sci 1991 26 2173-2183

Tzimas and Zavaliangos 2000 S Tzimas, A ZavaliangosEvaluation of volume fraction of solid in alloys formed by semisolid processing JOURNAL OF MATERIALS SCIENCE 35 (2000) 5319 – 5329

Valer et al. 1998 J. Valer, F. Saint-Antonin, P. Menses, M. Suéry; in: Proceedings of the 5thInternational Conference on semi-solid processing of alloys and composites, S2P 1998, Colorado,USA, 1998, pp. 3-10

Veldman et al 2001 N. L. M. Veldman, A. K. Dahle, D. H. StJohn, L. Arnberg; Metallurgicaland Materials Transactions A, Volume 32, Issue 1, 2001, pp. 147-155

Vogel and Cantor 1977 A Vogel, B Cantor, Stability of a spherical particle growing from a stirred melt Crystal Growth 37 (1977) 309-316

Vogel et a. 1979 A. Vogel, R. D. Doherty, B. Cantor; in: 'Solidification of Casting of Metals',The Metals Society, London, 1979, pp. 518-525

Wang et al. 2006 Y Wang, G Liu, Z FanActa Mater 54 (2006) 689-699

Wannasin et al. 2008 J Wannasin, S Janudom, R Rattanochaikul Development of the gas induced semi-solid metal process for aluminum die casting application [J]. Solid State Phenomena, 2008, 141/142/143: 97−102.

White 1990 White, J.L., Twin Screw Extrusion: Technology and Principles. Hanser: Munich,

Wiegand 1879 Wiegand, S.L. U.S. Patent 155 602, 1879.

Yoo et al. 2001 M Yoo, S Agnew, J Morris Non-basal slip system in H.C.P. metals and alloys: Source mechanisms[J], Materials Science and Engineering A, 2001, 319-321:87-92

Young et al 1983 K Young, C Kyonka, J Courtois US Patent 4, 415, 374, 1983

Zhang et al. 2008 H Zhang, Q Yan, L Li, .Microstructures and tensile properties of AZ31magnesiumalloy by continuous extrusion forming process [J]Materials Science and Engineering: AVolume 486, Issues 1–2, 15 July 2008, Pages 295–299

Zhang et al. 2009 Y Zhang, Y Liu, Z Cao, Q Zhang, L Zhang, Mechanical properties of thixomolded AZ91D magnesium alloy [J]materials processing technology 2 0 9 (2 0 0 9) 1375–1384

Zhou et al. 2008 T Zhou, Z Jiang, J Wen Semi-solid continuous casting–extrusion of AA6201 feed rods Materials Science and Engineering A 485 (2008) 108–114